

**Development of Colorimetric and Fluorescent Antibiotic Biosensors and
Synthesis of Drug-Related Biomimetic Molecules for Calcium Carbonate
Polymorph Control and Stabilization**

by

SHAN HAZOOR

**Presented to the Faculty of the Graduate School of
The University of Texas at Arlington in Partial Fulfillment
of the Requirements
for the Degree of**

DOCTOR OF PHILOSOPHY

THE UNIVERSITY OF TEXAS AT ARLINGTON

December 2022

Copyright © by Shan Hazoor 2022

All Rights Reserved



Acknowledgment

I would like to express my deepest gratitude and thank to my supervisor and professor, Dr. Frank W. Foss for his continuous guidance, mentorship, and encouragement throughout my Ph.D. journey. He has been very kind and supportive at each step when I needed his help. He provided me with many different opportunities to excel in performing and carry out various projects and collaborations. I highly admire his broad knowledge and different approaches to teach and train me as an organic chemist, which certainly helped me in other areas of chemistry. He allowed me to work on various interdisciplinary projects, which broadened my knowledge to other areas of science. His continuous support in the lab and out of the lab to encouraging me and to present my work in many different national meetings have been extremely helpful for my personal growth. Dr. Foss and his wife's hospitality and encouraging comments always make me more confident in myself after achieving any milestone of my life during my graduate studies.

I would also show my sincere thanks to my committee members Dr. Carl J. Lovely, Dr. He Dong and Dr. Jongyun Heo always providing me with novel ideas and approaches in my research work. Their comments and suggestion always helped me to make continuous improvements in my research work. Also, I would like to thank Dr John C. Lang and Dr. Peter Kroll for their assistance in my research work.

I am truly indebted to my collaborators Dr. He Dong, Dr. Erika La Plante, Dr. Warda Ashraf, Dr. Su Yang, Dr. Weike Chen, Trinh Thao My Nguyen, Ian Shortt, Miranda W. for their continuous efforts in making the projects more significant for the scientific community, is very admirable.

I would like to thank my undergraduate students Vikramjeet S. Brar, Saiyara Baset, Carlos Waddle, and Ho Vicki; their effort in moving the projects forward is appreciable.

I also owe my gratitude to Dr. Nam, Dr. Kayunta Johnson-Winters, and Dr. Carl J. Lovely for teaching me chemistry knowledge when I took classes from them, those topics helped me later in my research work.

Also, I would like to offer my gratitude to my family, my dad, mom, brother and sister for their continuous encouragement and prayers that always motivated me. Also, my thanks to my lab mates Dr. Pawan Thapa, Dr. Alena Denisenko, Ryan Madigan, Thanh Vuoung, Reagan Miller, and Patrick Ho for their suggestions in our lab group meetings.

Moreover, my sincere gratitude for Mrs. Jill Howard, Mrs. Debbie Cooke, Ms. Nora Heverly, Mrs. Stephanie Henry, Dr. William Cleaver and Dr. Cynthia Griffith for always guiding me with necessary information to perform my duties. I am thankful to Dr. Roy McDougal and Dr. Brian Edward for training me on different instruments. I show my gratitude to the stockroom supervisor, Mrs. Beth Klimek for providing me with all the chemical supplies as necessary.

Abstract

Development of Modified Antibiotic Biosensors and Synthesis of Drug-Related Molecules

Shan Hazoor, Ph.D.

The University of Texas at Arlington, 2022

Supervising professor: Frank W. Foss, Jr.

Abstract:

Polydiacetylene (PDA) polymers are conjugated macromolecules with desirable sensing properties. The presence of alternate double and triple bonds (en-yne subunits) generates electron delocalization in the PDA backbone, yielding a characteristic blue color, which changes to red upon environmental perturbations to the conjugated backbone structure. In chapter 1 PDA polymers containing a functional monomer 10,12-pentacosadiynoic acid-vancomycin conjugate (PCDA-Van) were prepared. Syntheses of different monomers containing different polar head groups were carried out to investigate a compatible monomer with PCDA-van stability. Gram-positive bacterial cell wall sequencing oligopeptides (OP) *D*-Ala-*D*-Ala and *L*-Lys-*D*-Ala-*D*-Ala were synthesized as a model for bacterial sensing. The PCDA-Van provided rapid and direct detection of OP visibly through a blue to purple color transition upon the addition of OP. PCDA-Van containing liposomes became fluorescent in the presence of *S. aureus*.

In chapter 2, PCDA-peptide was synthesized for the detection of gram-positive bacteria *Methicillin-resistant Staphylococcus aureus* (MRSA). PDA-peptide stability was optimized by using three monomer system to prepare liposomal polymer. PDA-peptides were labelled with a dabsyl-labeled lipid to obtain fluorescent images to analyze the bacterial interaction with liposomes. Next, a diphenyl diacetylene (DA) linker was synthesized, coupled with peptides (Pep-DA-Pep), to prepare a PDA containing hydrogel with pH sensing applications. At acidic pH, antimicrobial agents were incorporated into the PDA hydrogel and upon elevated pH gel-to-sol transition delivered the drug to the target alkaline infection site.

In chapter 3, the ability of biomimetic molecules to control the carbonation and precipitation process of CaCO_3 in cementitious materials was investigated. The purpose of the study was to enhance the stability and function of cementitious material. A series of different bisphosphonate (BPs) molecules were synthesized, containing different alkyl chains and a distal functional group. Experiments were performed with CaCl_2 solution in the presence of different BPs moieties for CaCO_3 precipitations. BPs with longer alkyl chain molecules showed the enhanced formation of vaterite and amorphous calcium carbonate (ACC). Characterization of the precipitation was done with atomic force microscopy (AFM), thermogravimetric analysis (TGA), conductivity experiments, Fourier-transform infrared spectroscopy (FTIR) and was supported with computational studies.

In chapter 4, future work is described to further our study on the biosensing of infective species and the preparation of metal carbonate binding molecules to target bacterial species and effect on CaCO_3 precipitation respectively.

Table of Contents

Acknowledgment.....	iii
Abstract.....	v
Chapter 1.....	1
Synthesis of Pentacosadiyonic acid (PCDA) Derivatives to detect gram-positive bacteria	1
1.1. Introduction	1
1.1.1. Biosensor based on Pentacosadiyonic acid (PCDA)	2
1.1.2. PCDA biosensor for bacterial detection	3
1.1.3 Antibiotic vancomycin for selective detection of gram-positive bacteria	6
1.2. Synthetic approach toward gram-positive detection.....	7
1.2.1. Synthesis of PCDA-vancomycin for the detection <i>S. aureus</i>	7
1.2.2. PCDA-Vancomycin for the detection of oligopeptide.....	8
1.2.3. Preparation of liposomes	11
1.3. Results and discussion	12
1.3.1. Ultraviolet (UV) and fluorescent spectroscopy	12
1.3.2. Transmission electron microscopy (TEM) images of PCDA-Van interaction with <i>S. aureus</i> bacteria.....	17
1.3.3. Minimum inhibitory concentration (MIC) of PCDA-Van monomer and liposomes	21
1.3.4. Membrane localization assay	22

1.3.5. Size determination of PCDA and PCDA-Van liposomes with Dynamic Light Scattering (DLS).....	25
1.3.6. Thermal stability of PCDA-Van with PCDA derivatives as comonomers	27
1.4. Conclusion	29
Chapter 2.....	30
Coupling of PCDA with self-assembled peptide and synthesis of diacetylene molecules.....	30
2.1. Introduction	30
2.1.2. PCDA functionalized with LPRDA peptide via polyethylene glycol (PEG) linkers	31
2.1.3. Diphenyl and linear diacetylene linkers.....	32
2.2.1. Synthesis of Diphenyl DA linkers and coupling with oligopeptides	34
2.3. Results and Discussions.....	36
2.3.1. UV and fluorescent spectroscopy of PCDA-peptide modified liposomes for MRSA bacterial detection.....	36
2.3.2. Diphenyl DA linker synthesis	40
2.3.3. Diphenyl DA coupling with peptides.....	44
2.2.4. TEM characterization of peptide-DA-peptide hydrogel	45
2.4. Conclusion	47
Chapter 3.....	48

Synthesis of bisphosphonate molecules for calcium carbonate (CaCO₃)	
precipitation.....	48
3.1. Introduction	48
3.2. Biomimetic-Biomineralization by small organic molecules	49
3.3. Synthesis of bisphosphonate molecules and CaCO₃ precipitation	
characterization	52
3.3.1. Synthesis of bisphosphonate molecules	52
3.3.1. Atomic force microscopy (AFM) experiments.....	57
3.3.2. Conductivity experiment.....	58
3.3.4. Computational studies	58
3.3.5. Sample preparation for critical micelle concentrations (CMC).....	59
3.4. Results and discussions	59
3.4.1 Conductivity experiment of precipitates.....	59
3.4.2. Atomic force microscopy (AFM) studies	61
3.4.3. Thermogravimetric analysis (TGA)	65
3.4.4. Fourier transform infrared spectroscopy (FTIR) studies of precipitates	
and computational model	67
3.4.5. pKa and logP values from online source.....	73
3.4.6. Computational binding studies	74
3.4.7. Critical micelle concentration (CMC) results.....	78

3.5. Conclusion	80
Chapter 4.....	81
4.1. Future Directions	81
4.1.1. Synthesis of new PCDA derivatives.....	81
4.1.2. Stability of PCDA-peptide for detection of <i>MRSA</i>	82
4.2. Modification of DA linker.....	83
4.2.1. DA modification with maleimide ethylene amine linker	83
4.3. Calcium carbonate precipitation	84
4.3.1. Bisphosphonate with Amine functional group	84
Chapter 5 General experimental procedure-Biosensor	85
Chapter 6 General experimental procedure-Diphenyldiacetylene linker.....	97
Chapter 7 General experimental procedure-Biomimetic molecules	100
NMR and other characterization data.....	111
References.....	210
Biographical Information.....	228

List of Illustrations

List of Figures

Figure 1: 10, 12-Pentacosadiyonic acid (PCDA)	2
Figure 2: Ultraviolet photopolymerization of diacetylene	2
Figure 3: Rotation in en-yne backbone of PDA liposomes changes blue to red color	3
Figure 4: PCDA-based liposomes become fluorescent upon attachment with bio specie	3
Figure 5: Different composition of PDA with DPPC and DSPC liposomes exhibits different stability and color response	4
Figure 6: (a) Multiple bacterial species incubated with different compositions of PCDA and DSPC varying cholesterol per cent. (b) shows increasing cholesterol in the PCDA system increases the color transition from blue to pink.	5
Figure 7: Possible binding mode of vancomycin with dipeptide	6
Figure 8: (A) Model of Vancomycin binding to D-Ala-D-Ala sequence (B) UV spectra of 100 μ M 10% PCDA-Van: 90% PCDA with and without treating with dipeptide (C) UV absorption spectra of differ-ent mM conc. of dipeptide treating with 100 μ M 10% PCDA- Van: 90% PCDA (D) Fluorescent spectra of different mM conc. of di-peptide treating with 100 μ M 10% PCDA-Van: 90% PCDA	13
Figure 9: Colorimetric change of PCDA-Van liposomes when treated with different concentrations of dipeptide (A) and tripeptide(B)	14
Figure 10: Linearity of Fluorescent intensity at 540 nm for dipeptide	15
Figure 11: Linearity of Fluorescent intensity at 540 nm for Tripeptide	15

Figure 12: Control experiments of PCDA-Van liposomes with protected and non-protected amino acids 16

Figure 13: (A) Dipeptide colorimetric response calculated using CR% equations (B) Tripeptide colorimetric response calculated using CR% equation..... 17

Figure 14: (A) Fluorescent spectra of 100 μ M 10% PCDA-Van: 90% PCDA upon incubating with 100, 10^6 and 10^8 CFU bacterial conc. (B) TEM images of 10%PCDA-Van and 90% PCDA liposomes without bacteria (C) *S. aureus* bacteria only (D) TEM images of 10%PCDA-Van and 90 PCDA liposomes with *S. aureus* 19

Figure 15: PCDA-Van liposomes UV spectra with 108 CFU bacteria *S. aureus* bacteria in the presence of PCDA only liposomes 20

Figure 16: *S. aureus* bacteria in the presence of PCDA only liposomes 21

Figure 17: Structure of Dabsyl lipid 23

Figure 18: Liposomes synthesis with PCDA, PCDA-Van, and Dabsyl lipid 23

Figure 19: (A) Only 100% PCDA incubated with MRSA (B) PCDA-Van and Dabsyl incorporated PCDA incubated with MRSA (C) Mean fluorescent intensity..... 24

Figure 20: *E. Coli*. Bacteria in the presence of PCDA only liposomes (A) incubation with *E. Coli* bacterial (B) Mean fluorescent comparison of PCDA and PCDA-Van in presence of *E. Coli*..... 25

Figure 21: Size characterization of PCDA and PCDA-Van incorporated liposomes by dynamic light scattering (DLS), amount vs. size. The size distributions of the liposomes were weighted either by intensity of the scattering, an r^6 dependence vs. size, or by particle volume, an r^3 dependence vs. size. The intensity weighting emphasizes the particles of larger size disproportionately, but the volume weighting can obscure the

presence of the larger particles entirely. In this Figure, the small sizes are reasonably accurately represented in both alternatives..... 26

Figure 22: Liposome size comparison between PCDA and PCDA-Van incorporated liposomes, here weighted by volume, with the liposomes anticipated to have the larger charge density, the PCDA loaded liposomes, being smaller. The sizes for the smaller are centered at about 130 nm, and those for the larger centered at about 160 nm..... 27

Figure 23: Thermal stability of 10% PCDA-Van with 90% comonomer **4b** PCDA-OH (A), PCDA-NH₂ **4c** (B), and PCDA-Imidazole **4d** (C) at different temperatures for 5 min 28

Figure 24: PCDA bound with peptide sequence of anti-bacterial studies 30

Figure 25: Synthesis of PCDA modified with PEG and LPRDA peptide for detection of MRSA bacteria in Dr. He lab 32

Figure 26: Diphenyl DA acid linker 32

Figure 27: Peptides conjugated in Dieglmann et al studies..... 33

Figure 28: Atomic force microscopy (AFM) images of PDA nanofibers of DA-peptides in Dieglmann studies..... 34

Figure 29: Liposomes of composition 10%PCDA-pep, 30% PCDA, 57.5% PCDA-OH and 2.5% Dabsyl lipid. (A) Treatment of 10⁹ CFU E.Coli, MRSA, and blank solution with PCDA-pep liposomes at zero hour (B) Treatment of 10⁹ CFU E.Coli, MRSA and blank solution with PCDA-pep liposomes after 24 hour (C) Fluorescent intensity of 10⁷ and 10⁹ CFU E. Coli, MRSA, and control PCDA-pep 39

Figure 30: Chemical design of Pep-DA-Pep gel formation at acidic pH and transition solution in alkaline pH along with blue to purple color change (A) Structure of Pep-DA-

Pep (B) self-assemble amphilic Pep-DA-Pep transparent gel formation (in grey) forming 2D nano nanofiber exhibiting blue color when irradiated with 254 nm UV light. At alkaline pH, color change along with phase transition gel to solution and release of the drug on alkaline infection site 45

Figure 31: TEM images of Peptide-PDA-Peptide at acidic pH **(A)** pH 5.5, **(B)** pH 6.5, **(C)** slightly basic pH 7.5, and basic pH **(D)** pH 8.5. The conc. of Peptdie-PDA-Peptide was 10 mg/mL. NaOH was used to adjust the pH..... 46

Figure 32: Production of cement worldwide..... 48

Figure 33: Scanning electron microscopy (SEM) images showing the growth of ACC nanoparticles on the calcite crystal in the presence of 6% poly aspartic acid additive in calcium carbonate solution..... 50

Figure 34: (A) Structure of phytic acid (B) ACC polymorphs formation in the presence of phytic acid 50

Figure 35: (A) Structure of folic acid (B) Vaterite and calcite coexist..... 52

Figure 36: Bisphosphonate molecules with different alkyl chain lengths and functional groups 52

Figure 37: Bisphosphonate molecules with different alkyl chain lengths and functional groups 60

Figure 38: In situ atomic force microscopy (AFM) images of calcite surface in the presence of control solution (a) 0 min, (b) 12, and (c) 18 min. 61

Figure 39: In situ atomic force microscopy (AFM) images of calcite surface in the presence of C3 COOH at (a) 0 min, (b) 05, and (c) 42 min. 30 nm height of islands, and in the presence of C3 OH at (d) 0 min, (e) 03, and (f) 90 min 10 nm height of islands.. 62

Figure 40: In situ atomic force microscopy (AFM) images of calcite surface in the presence of C7 COOH at (a) 0 min, (b) 13, and (c) 40 min. 10 nm height of islands, and in the presence of C7 OH at (a) 0 min, (b) 02, and (c) 13 min. 2-6 nm height of islands 63

Figure 41: In situ atomic force microscopy (AFM) images of calcite surface in the presence of C11 COOH at (a) 0 min, (b) 13, and (c) 40 min. 350 nm height of islands, in the presence of C11 OH at (d) 0 min, (e) 02, and (f) 13 min. 420 nm height of islands, and in the presence of C11 non-functional at (g) 06, and (i) 23 min. 2-6 nm height of islands 64

Figure 42: TGA characterization of control, C3, C7, and C11 acid (COOH); C7 and C11 hydroxyl (OH) from conductivity experiments after 6 – 9 months. 67

Figure 43: FTIR results of pure C3, C7 and C11 acid (COOH) series and precipitates incorporated from conductivity experiments 68

Figure 44: FTIR results of pure C3 acid (COOH), control calcite and precipitates obtained from conductivity experiments for C3 acid (COOH)..... 69

Figure 45: FTIR results of pure C7 acid (COOH), control calcite and precipitates obtained from conductivity experiments for C7 acid (COOH)..... 70

Figure 46: FTIR results of pure C11 acid (COOH), control calcite and precipitates obtained from conductivity experiments for C11 acid (COOH)..... 71

Figure 47: In the presence base NaHCO₃, the possible resonating structures of phosphonate group. Model A: binding of calcium via top oxygen, Model B: binding of calcium via side arm oxygen 72

Figure 48: Different pKa values of bisphosphonate associated protons..... 73

Figure 49: (A) Overall charge -ve 3 (B) Overall charge -ve 4	75
Figure 50: Different modes of bisphosphonate C11 COOH binding with Ca ²⁺ . Mode A is the lowest energy	75
Figure 51: Different modes of bisphosphonate C03 COOH binding with Ca ²⁺ . Mode A is the lowest energy.....	76
Figure 52: Comparison of binding energies of longer chain bisphosphonate with Ca ²⁺	77
Figure 53: CMC calculations of C3, C7, and C11 acid (COOH) series of bisphosphonate	78
Figure 54: CMC calculations of bisphosphonate C11 acid (COOH) molecule.....	79
Figure 55: Proposed PCDA monomers	81
Figure 56: Different lengths of lipid monomers to stabilize PCDA-peptide	82
Figure 57: DA modification with maleimide	83
Figure 58: (A) short linear diacetylene (B) Long linear diacetylene molecules	83
Figure 59: (A) C07 chain length (B) C11 carbon chain length.....	84

List of Tables

Table 1 MIC values of PCDA, PCDA-Van monomer, PCDA-Van liposomes, and vancomycin	22
Table 2 Thermal stability of 10% PCDA-Van with 90% comonomer 4b PCDA-OH (Entry 1), PCDA-NH ₂ 4c (Entry 2), PCDA-Imidazole 4d (Entry 3), and PCDA (Entry 4) at different temperatures for 5 min	28
Table 3 PCDA-peptide stability with different comonomers composition	37
Table 4 Trials for Glaser coupling with different catalysts and base	41
Table 5 Hydrolysis of esters with different base equivalents.....	43
Table 6 Calcium carbonate polymorphs formation in the presence of bisphosphonate molecules	66
Table 7 pKa prediction of bisphosphonate molecules using ChemAxon online source	74

List of Scheme

Scheme 1: Synthesis of PCDA comonomers and PCDA-vancomycin monomer	8
Scheme 2: Synthesis of dipeptide D-Ala-D-Ala	10
Scheme 3: Synthesis of tripeptide L-Lys-D-Ala-D-Ala	11
Scheme 4: Synthesis of liposomes.....	12
Scheme 5: Synthesis of diphenyl DA linker (19).....	35
Scheme 6: Alternate scheme for the synthesis of (19) sequential Sonogashira and Glaser coupling	40
Scheme 7: Alternate scheme for the synthesis of (19) by performing stepwise Sonogashira and Glaser coupling	42
Scheme 8: Synthesis of bisphosphonate acid (COOH) series	54
Scheme 9: Synthesis of bisphosphonate alcohol (OH) series	55
Scheme 10: Synthesis of bisphosphonate amine (NH ₂) molecule.....	56
Scheme 11: Synthesis of bisphosphonate non-functional group molecule.....	57

Chapter 1

Synthesis of Pentacosadiyonic acid (PCDA) derivatives to detect gram-positive bacteria

1.1. Introduction

Bacterial infections are a serious threat to human health, causing various diseases, including infection to the pulmonary, endocarditis, pneumonia, skin, nasal tract, lung and elsewhere.¹⁻⁷ Bacterial resistance to many drugs causes a global threat as it involves a high risk of death. In 2018, studies by the World Health Organization (WHO) reported that such drug-resistant bacterial species contribute to the deaths of about seven hundred thousand people, with a prediction of reaching 10 million by the year 2050.⁸ While the infection rate for *Staphylococcus aureus* (*S. aureus*) declined between 2005 and 2012, a 2017 report suggests there is now an increase in its infection rate. Moreover, 2019 data from Center of Disease Control and Prevention (CDC) on *Methicillin-resistant S. aureus* (MRSA) shows 2.8 million people became infected and about 35,000 deaths occurred in that year. These life-threatening rates of bacterial infection need to be addressed quickly.^{9, 10}

Our efforts towards this issue revolved around building a biosensing system; to develop a selective and sensitive method that is readily available as a point of care (POC) device and can distinguish among various bacterial species. Some of the already existing methods for the detection of bacterial species performed in the laboratory include culture-based assays such as immunological analysis, enzyme-linked immunosorbent assays (ELISA), and genetic analysis; a more recently known method which is regularly been

employed is polymerase chain reaction (PCR), as costs for these assays decline over the years. These methods remain expensive, time consuming, require experts, and/or need a huge amount of samples for characterization and detection.¹¹⁻¹³ In some cases, patients may have to wait days to get the results, which only increases the cost of treatment and risk to patients.^{14, 15}

1.1.1. Biosensor based on Pentacosadiyonic Acid (PCDA)

Pentacosadiyonic acid (PCDA) is an amphoteric molecule consisting of 25 carbon units with a diacetylene (DA) functional group in the middle. The molecule can self assemble into various supramolecular structures in or on different environments. The DA functionality, being aligned between molecules, undergoes photopolymerization upon irradiation of 254 nm ultraviolet (UV) light (**Figure 2**).¹⁶ Formation of covalent polymer can be carried out on a solid surface such as glass by using Langmuir-Boldgett (LB) or Langmuir-Schaefer (LS) films.¹⁷⁻¹⁹

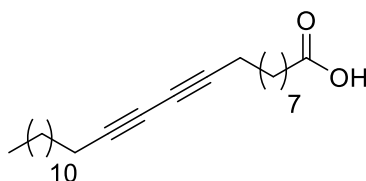


Figure 1: 10, 12-Pentacosadiyonic acid (PCDA)

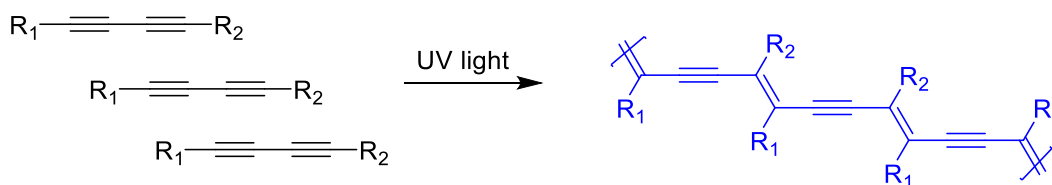


Figure 2: Ultraviolet photopolymerization of diacetylene

For more than a decade, PCDA has been used as a functional reporter in biosensors by many researchers due to its colorimetric and fluorescent properties.²⁰ PCDA in aqueous solution or, in some reports on solid surfaces,²¹ formed liposomes about 127 ± 58.3 nm in diameter.^{22,23} With well-optimized conditions, these blue colored but non-fluorescent liposomes change to purple or red colored fluorescent liposomes when perturbed by certain environmental factors such as pH, temperature, metals, bacteria, viruses, and other bio species.^{22, 24-30}

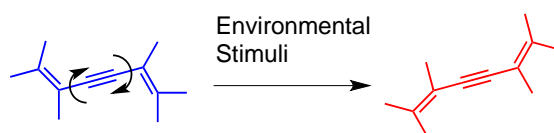


Figure 3: Rotation in en-yne backbone of PDA liposomes changes blue to red color.

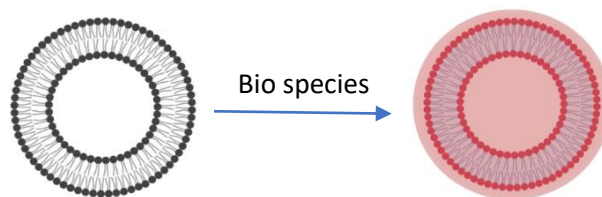


Figure 4: PCDA-based liposomes become fluorescent upon attachment with a bio species

1.1.2. PCDA biosensor for bacterial detection

Since its first use as a biosensor by Charych et al.,³¹ PCDA has been extensively used by many research groups.³²⁻³⁸

Recently, Zhou et al. reported a label-free colorimetric biosensor with PCDA to detect various bacterial species.³² Their detection method was based on sensing different toxins secreted by bacterial species for their direct distinguishable sensing. To achieve this goal,

use of PDA liposomes was designed by incorporating different phospholipids such as (1,2-dimyristoyl-*sn*-glycero-3-phosphocholine, 14:0) (DMPC), (1,2-dipalmitoyl-*sn*-glycero-3-phosphocholine, 16:0) (DPPC) and cholesterol into the PCDA liposomal system. The label-free detection mechanism depends on the lipid bilayer interaction between PCDA liposomes and lipid bilayer membranes of toxins secreted by biological species. PCDA liposomes were prepared with various ratios of different co-monomers, such as with above mentioned lipids and/or cholesterol molecules. In this study, after careful investigation of different phospholipids incorporation, the researchers found 1,2-distearoyl-*sn*-glycero-3-phosphocholine, 18:0 (DSPC) with PCDA more stable as intense blue color (**Fig. 5**)

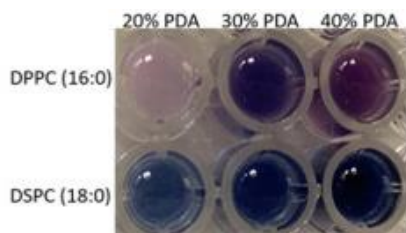


Figure 5³²: Different composition of PDA with DPPC and DSPC liposomes exhibits different stability and color response

Increased insertion of cholesterol into the PDA liposome greatly increased the sensitivity for *E.coli* and other bacterial species due to hydrophobic interaction between bilayer liposomes and toxin material. Different bacterial species presented different colors ranging from intermediate purple to pink (**Fig. 6**).

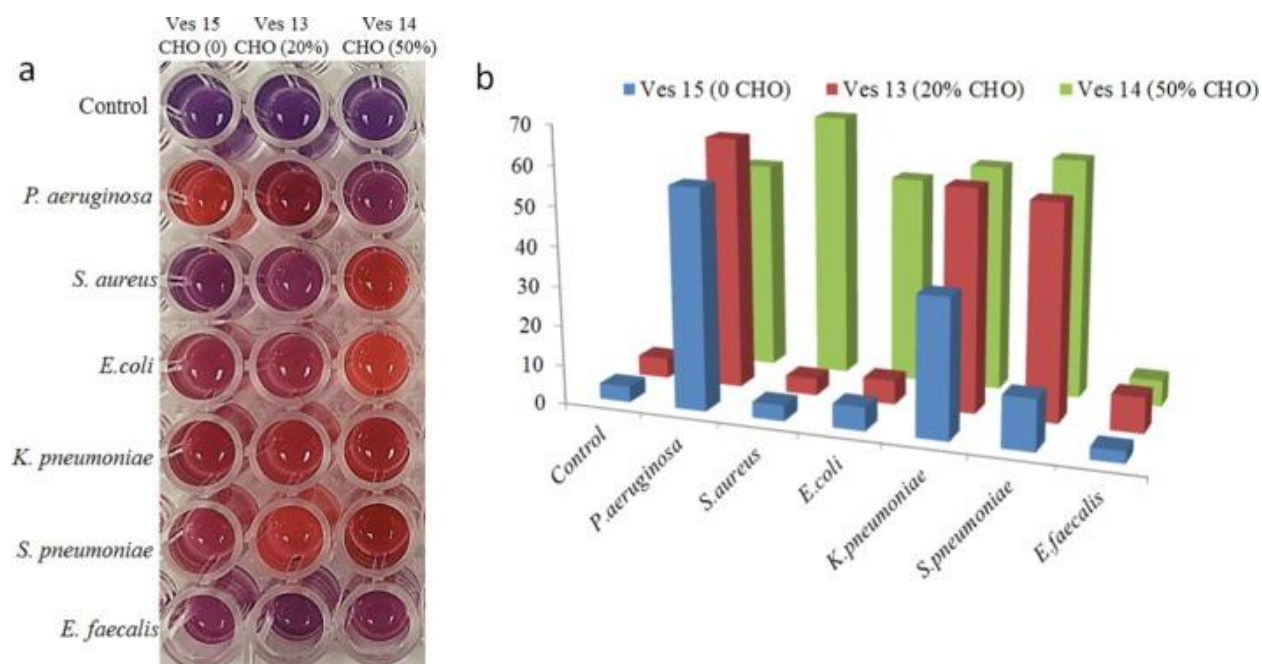


Figure 6³²: (a) Multiple bacterial species incubated with different compositions of PCDA and DSPC varying cholesterol per cent. (b) shows increasing cholesterol in the PCDA system increases the color transition from blue to pink.

In 2006, Jung et al. used ligand-receptor recognition technique to detect streptavidin (STA) by modifying PCDA with a small molecule, biotin.³⁹ The PCDA molecule was modified with 2-(ethylene oxide)diamine linkers for coupling with biotin for colorimetric detection of STA. For this purpose, different PCDA liposomes were prepared with different ratios of PCDA with PCDA-biotin monomer. Color transitions were calculated as $CR\% = [(PB_0 - PB_1)/PB_0] \times 100$ where $PB = A_{blue}/(A_{blue} + A_{red})$. Optical colorimetric transitions were measured spectroscopically, and the interaction was further confirmed with images obtained from transmission electron microscopy (TEM).

Using a specific biotin-streptavidin interaction STA was directly sensed, but very few reports have been presented in literature where the whole bacterial cell has been detected.^{40, 41} Our efforts here are to develop a method to detect the whole bacterial cell.

1.1.3 Antibiotic vancomycin for selective detection of gram-positive bacteria

The antibiotic vancomycin is a glycopeptide used for the treatment of gram-positive bacteria methicillin-resistant *S. aureus* (MRSA) infections.^{42, 43} It binds with bacterial cell wall sequence *D*-Ala-*D*-Ala or *L*-Lys-*D*-Ala-*D*-Ala through putative hydrogen bonding interactions (**Fig. 7**).^{44, 45}

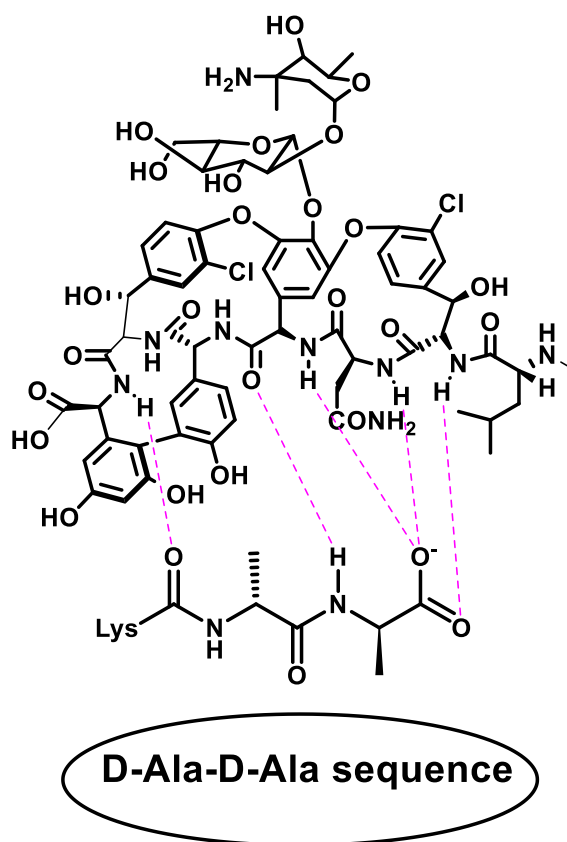


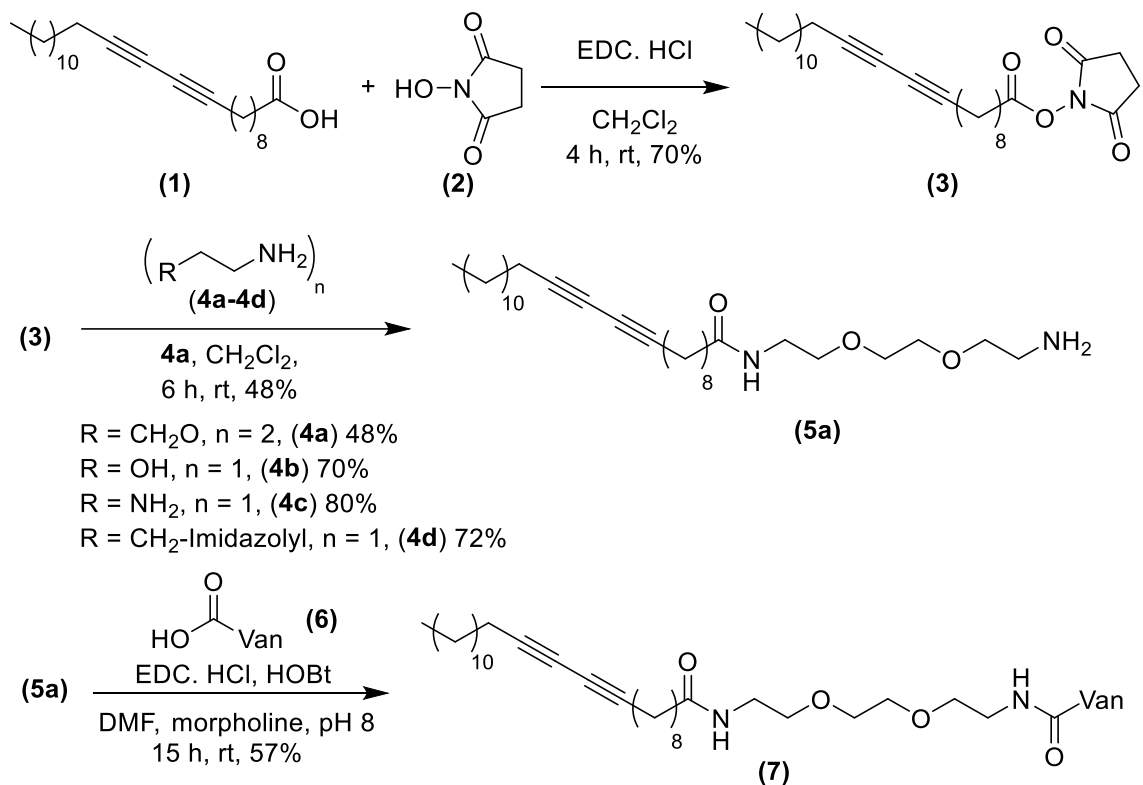
Figure 7: Possible binding mode of vancomycin with dipeptide

1.2. Synthetic approach toward gram-positive detection

1.2.1. Synthesis of PCDA-vancomycin for the detection *S. aureus*

For selective detection of gram-positive bacteria *S. aureus*, a PCDA biosensing molecule was used to couple with the carboxylic acid (COOH) group of vancomycin using a diamine linker. The synthesis started with PCDA (**Scheme 1**). PCDA's (**1**) carboxylic acid was activated with N-hydroxysuccinimide **2**, using N-ethyl-N'-(3-dimethylaminopropyl) carbodiimide hydrochloride (EDC•HCl) coupling reagent. PCDA-NHS ester **3** was treated with different co-monomers **4a-4d** to generate PCDA derivatives varying in its end group: ethanol amine **4b**, ethylene diamine **4c** and 3-aminopropyl imidazolyl **4d** to prepare PCDA-OH, PCDA-NH₂ and PCDA-imidazole respectively **5a-5d**.^{46, 47} The opposing end of the linker **4a** was reacted with a carboxylic acid residue of vancomycin using coupling reagents EDC•HCl and 1-hydroxybenzotriazole hydrate (HOBt) to effectively couple PCDA with vancomycin (**7**, PCDA-Van).⁴⁸

Scheme 1



Scheme 1: Synthesis of PCDA comonomers and PCDA-vancomycin monomer

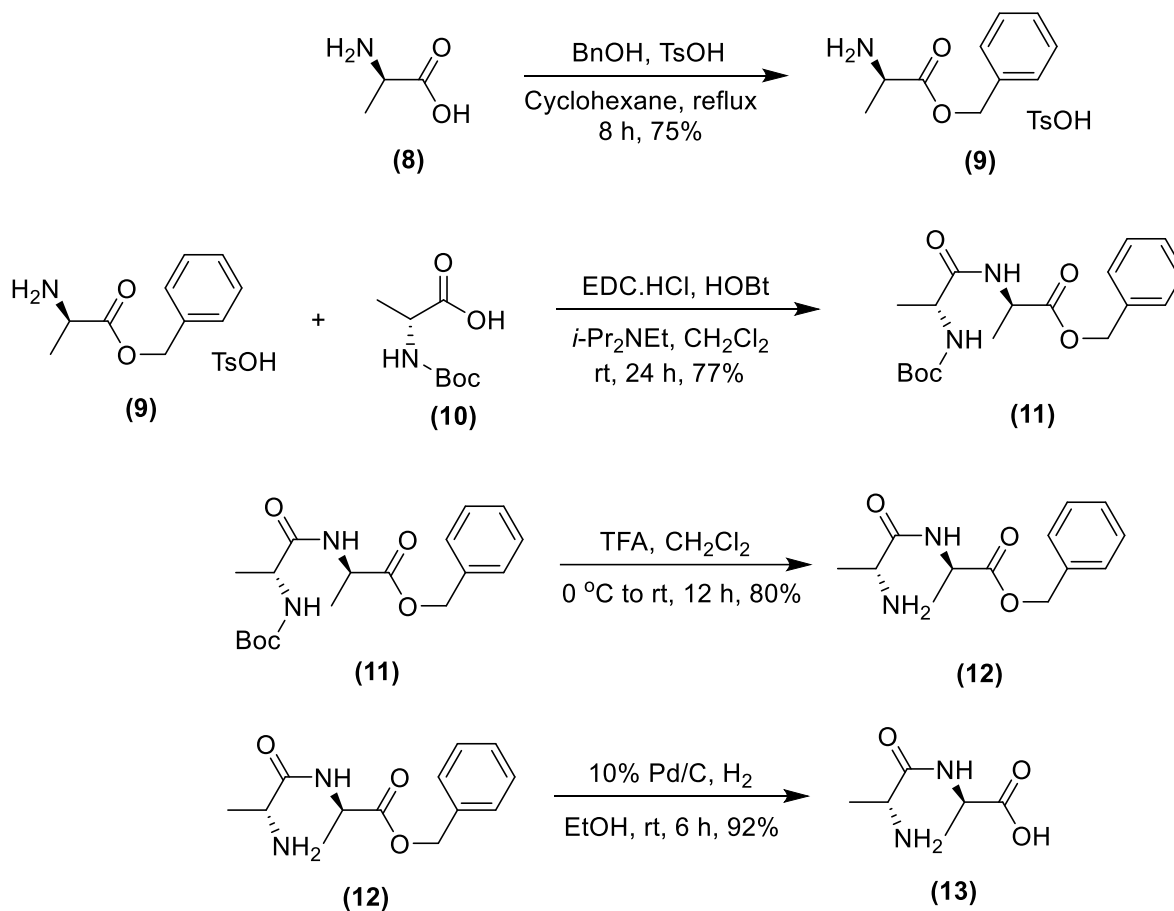
1.2.2. PCDA-Vancomycin for the detection of oligopeptide

PCDA liposomes have been reported to colorimetrically detect biomolecules,²⁸ It was planned to synthesize two small cell-wall mimetic peptide sequences: the dipeptide *D*-Ala-*D*-Ala and the tripeptide *L*-Lys-*D*-Ala-*D*-Ala, to serve as models for our bacterial detection system.⁴⁴

It was envisioned that titrating the PCDA-vancomycin liposomes with di- or tri-peptides would cause the PCDA-vancomycin to bind with them and change its blue color to purple or red with fluorescent enhancement in the system. For this purpose, synthesis of the

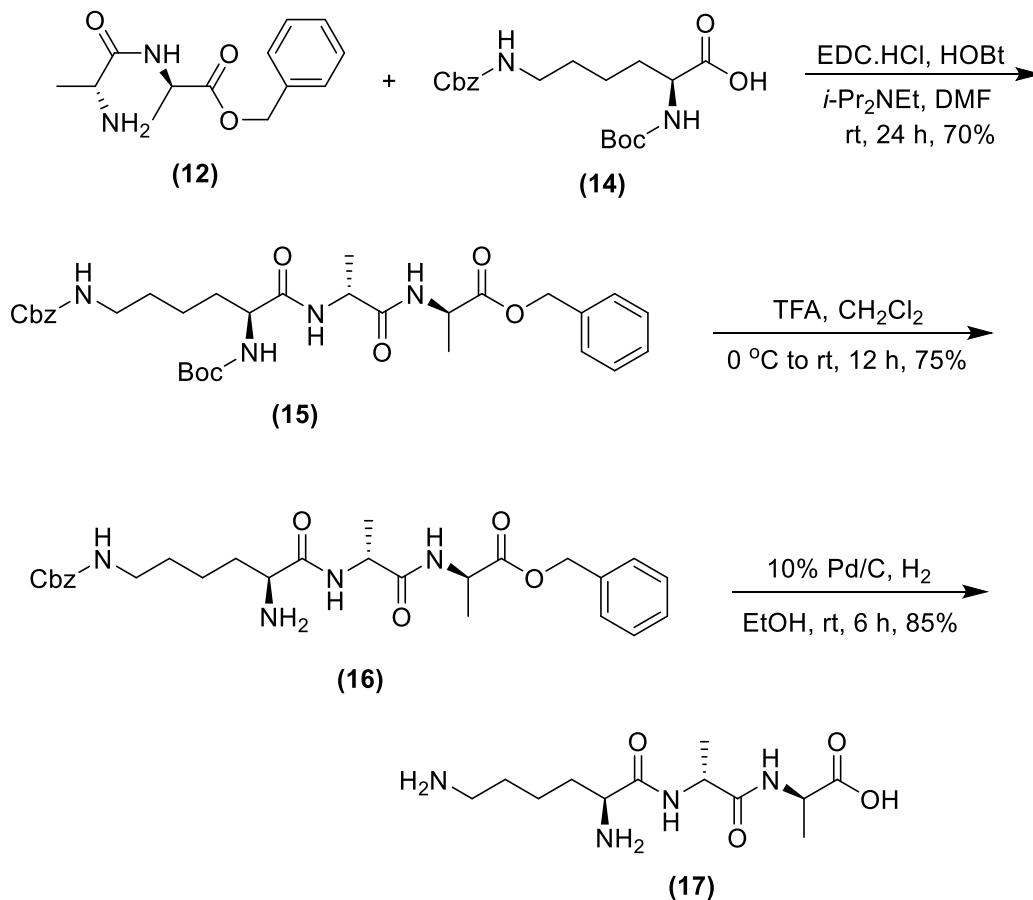
dipeptide was started with *D*-Ala **8** (**Scheme 2**) by treating it with benzyl alcohol to perform Fischer esterification in the presence of *p*-toluenesulfonic acid to synthesize molecule **9** as the toluenesulfonic acid salt. Next, **9** was reacted with *N*-protected *D*-Ala (**10**) after activating its COOH with EDC·HCl and HOBt coupling reagents to form a protected dipeptide (**11**). Furthermore, the Boc group was deprotected from **11** by treating it with trifluoroacetic acid (TFA) to get the product **12**. After that, the benzyl-protecting group was removed by hydrogenolysis treating **12** with 10%(w/w) Pd/C under hydrogen gas to prepare dipeptide **13**. To synthesize the tripeptide, **12** was reacted with *N,N*-protected lysine (**13**) to couple its free COOH group to prepare molecule **15**. Then a similar deprotection protocol was used to remove the Boc moiety to obtain **16**; then 10%(w/w) Pd/C was used for hydrogenolysis of both the OBn and Cbz groups to prepare the final tripeptide **17** in good yields.

Scheme 2



Scheme 2: Synthesis of dipeptide *D*-Ala-*D*-Ala

Scheme 3



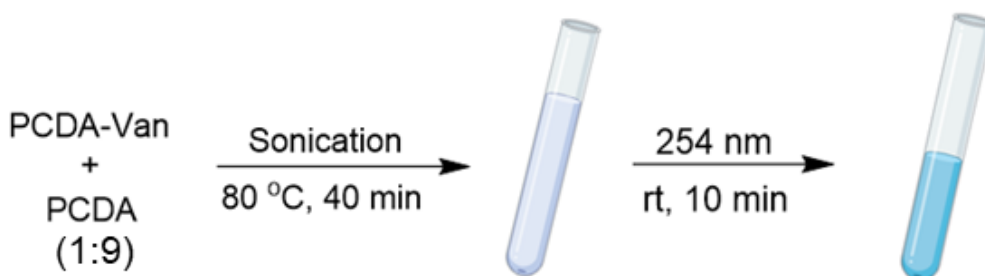
Scheme 3: Synthesis of tripeptide *L*-Lys-*D*-Ala-*D*-Ala

1.2.3. Preparation of liposomes

Liposomes of 0.1 mM concentration in total PCDA, with monomer PCDA-Van 10% and free PCDA 90%, were prepared as depicted in **Scheme 2**. Following the dissolution of both monomers in 1 mL of ethanol, the solvent was evaporated in vacuo. Then, 10 mL of Milli-Q water was added, and the mixture was sonicated for 40 min at 80 °C. The cloudy solution was filtered through 8 μm cellulose filter paper. The solution was stored at 4 °C overnight in a dark refrigerator. After that, a 4 W UV light (254 nm) was used to irradiate

the sample for 10 min, crosslinking a fraction of the liposomal PCDA's and converting the clear solution to blue.⁴⁹ Different compositions of liposomes were prepared by varying comonomers of PCDA-vancomycin with PCDA and other PCDA derivatives synthesized from linkers **4a-4d**.

Scheme 4



Scheme 4: Synthesis of liposomes

1.3. Results and discussion

1.3.1. Ultraviolet (UV) and fluorescent spectroscopy

10% PCDA-Van:90% PCDA liposomes at 100 μ M in Milli-Q water were treated with different concentrations of dipeptide or tripeptide. The effect of addition of the dipeptide on the visible absorption spectra is to increase the absorbance in the green, transmitting more of the complementary purple-red hues. (**Fig. 8 B**). Concentrations of dipeptide, ranged from 6.25 μ M to 100 μ M 12 mM to 80 mM. As the dipeptide or tripeptide concentrations were increased, the colorimetric transition from blue to purple was observed more intensely. (**Fig. 8C**). Notable increases of fluorescence intensity accompanied the increases in amount of dipeptide (**Fig. 8 D**).

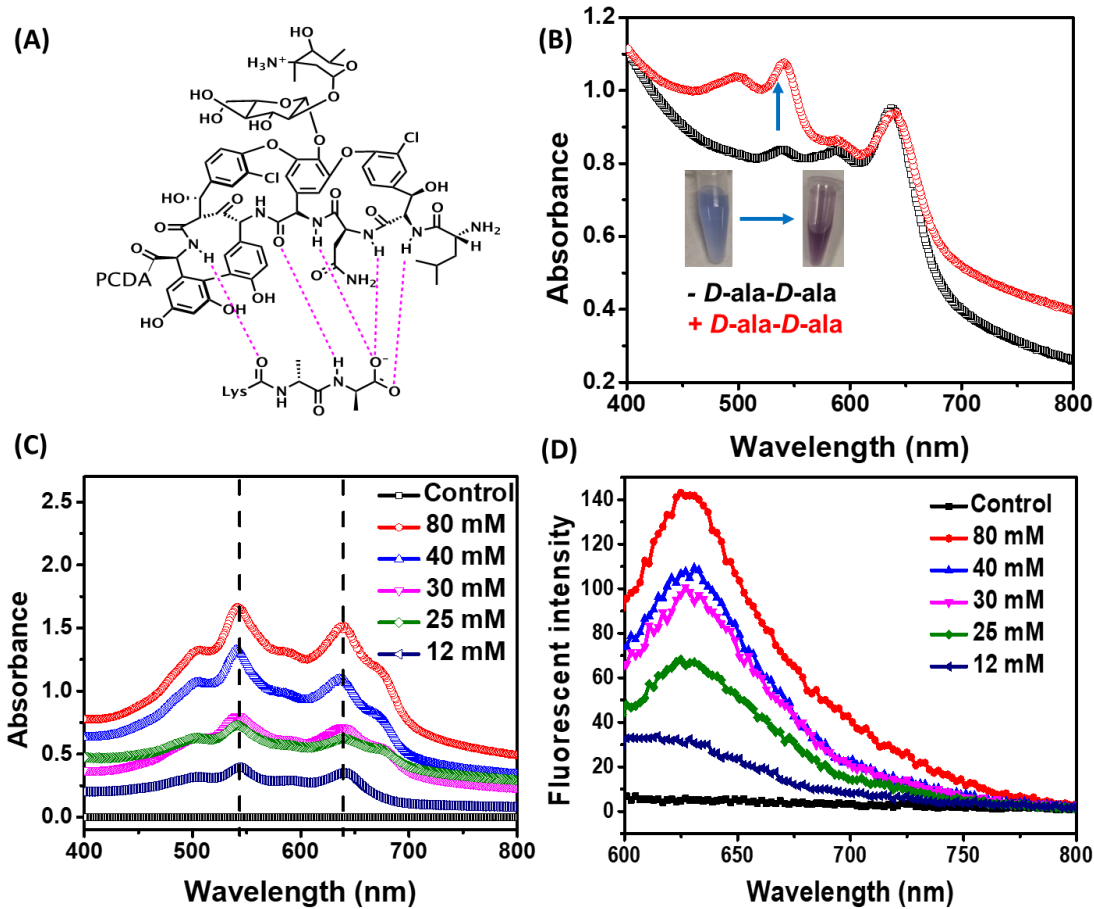


Figure 8: (A) Model of Vancomycin binding to D-Ala-D-Ala sequence (B) UV spectra of 100 μM 10% PCDA-Van: 90% PCDA with and without treating with dipeptide (C) UV absorption spectra of different mM conc. of dipeptide treating with 100 μM 10% PCDA-Van: 90% PCDA (D) Fluorescent spectra of different mM conc. of di-peptide treating with 100 μM 10% PCDA-Van: 90% PCDA

Limit of detection (LOD) for dipeptide and tripeptide was calculated based on a linear fitting curve using LOD formula ($LOD = 3\sigma k$; where σ is standard deviation, and k is the

slope for fluorescence intensity versus their concentrations.⁵⁰ LOD for dipeptide and tripeptide was found to be 4 mg/mL and 13 mg/mL respectively (**Fig. 9, 10, 11**). In case of tripeptide, at any conc. the liposomes precipitated out of the solution after 10 minutes.

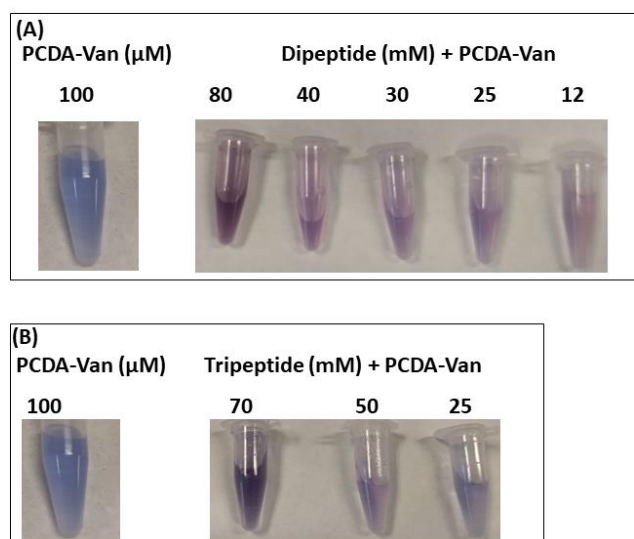


Figure 9: Colorimetric change of PCDA-Van liposomes when treated with different concentrations of dipeptide (A) and tripeptide(B)

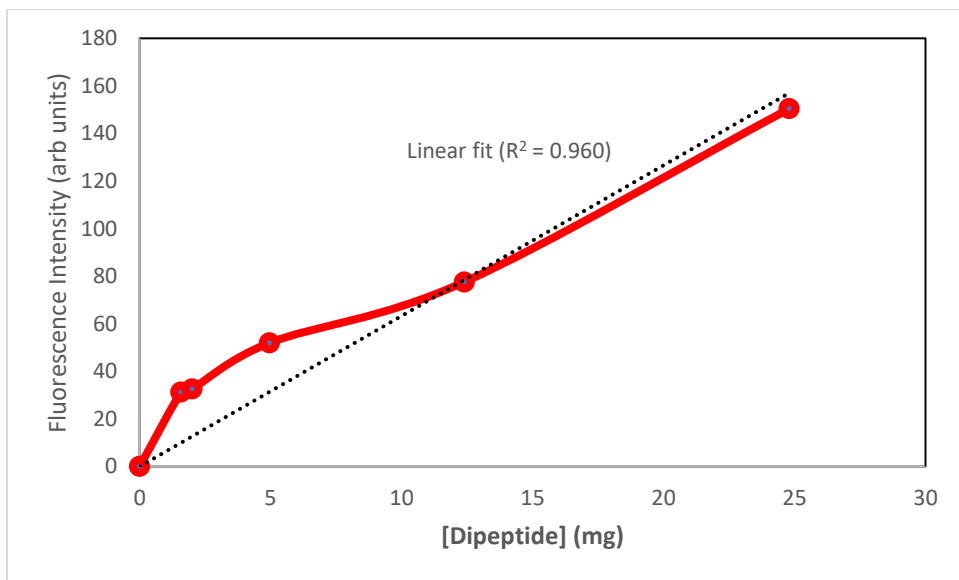


Figure 10: Linearity of Fluorescence intensity at 540 nm for dipeptide

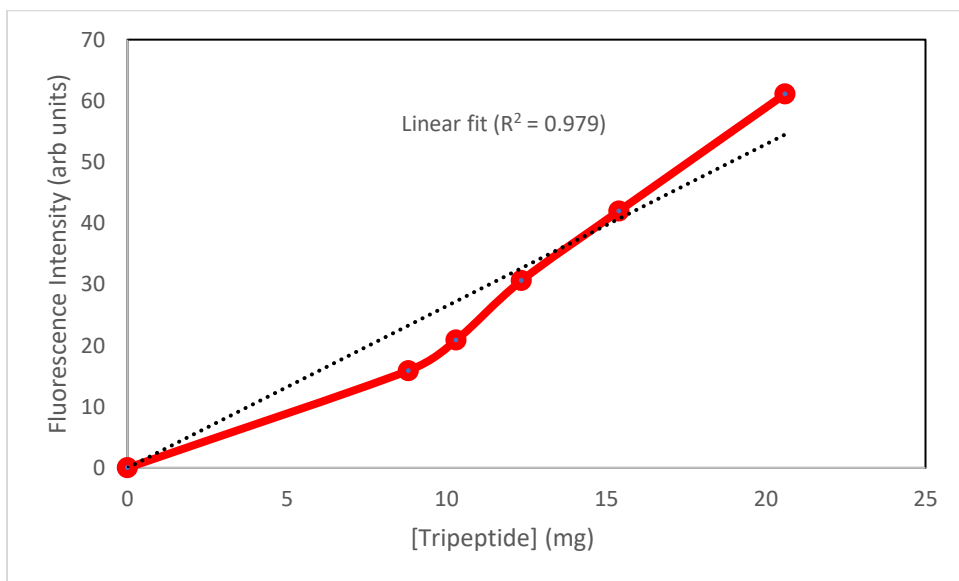


Figure 11: Linearity of Fluorescence intensity at 540 nm for Tripeptide

Control experiments revealed that a change in color was only observed in the presence of dipeptide or tripeptide. Protected amino acids Boc-*D*-Ala, H-Lys(Z)-OBn and non-protected *D*-Ala added to 10% PCDA-Van/PCDA liposomes in similar concentrations did not change color for up to 24 h, whereas, the addition of non-protected lysine (H-Lys-OH) changed color from blue to purple with UV absorption shift and presence of fluorescence in the system as well. This color change likely indicated charge interactions between lysine and PCDA-Van liposomes, observed at concentrations from 6 to 100 μM (**Fig. 12**).

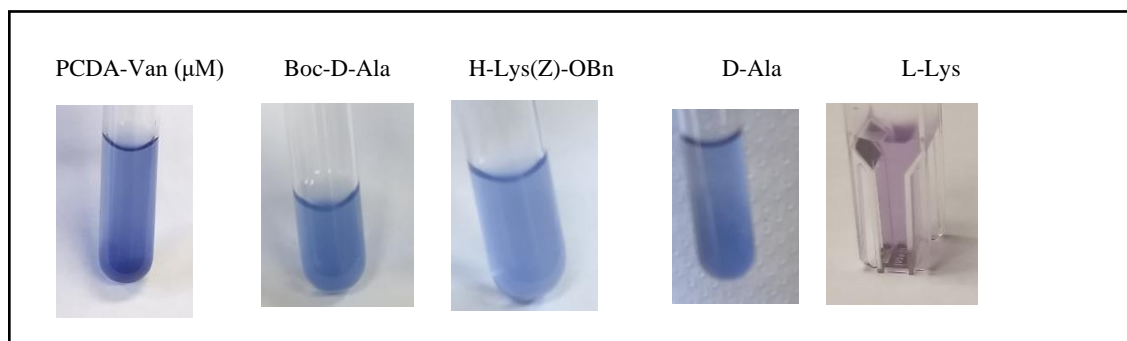


Figure 12: Control experiments of PCDA-Van liposomes with protected and non-protected amino acids

When liposomes generated from 100% PCDA were treated with dipeptide or tripeptide no color change was observed, confirming vancomycin's role in color change. The observable color change was accompanied by fluorescence when excited at the red absorption band. Fluorescence was observed to increase as the concentration of dipeptide or tripeptide was raised. Similarly, the absorbance was observed to shift from blue (640 nm) to purple (540 nm). Letting the relative blue response, $PB(i)$ at instance i , be defined as:

$$PB(i) = \frac{A_{642}(i)}{A_{545}(i) + A_{642}(i)} ,$$

the absorption-based colorimetric response to 78 mM di-peptide treated with 100 μM PCDA-Van as (purple color) solution, the change in relative blue response from baseline (0), could be computed as:⁵¹

$$CR(\%) = \left(\frac{PB(0) - PB(1)}{PB(0)} \right) \times 100$$

CR% was calculated in response to both dipeptide and tripeptide (**Fig. 13**).

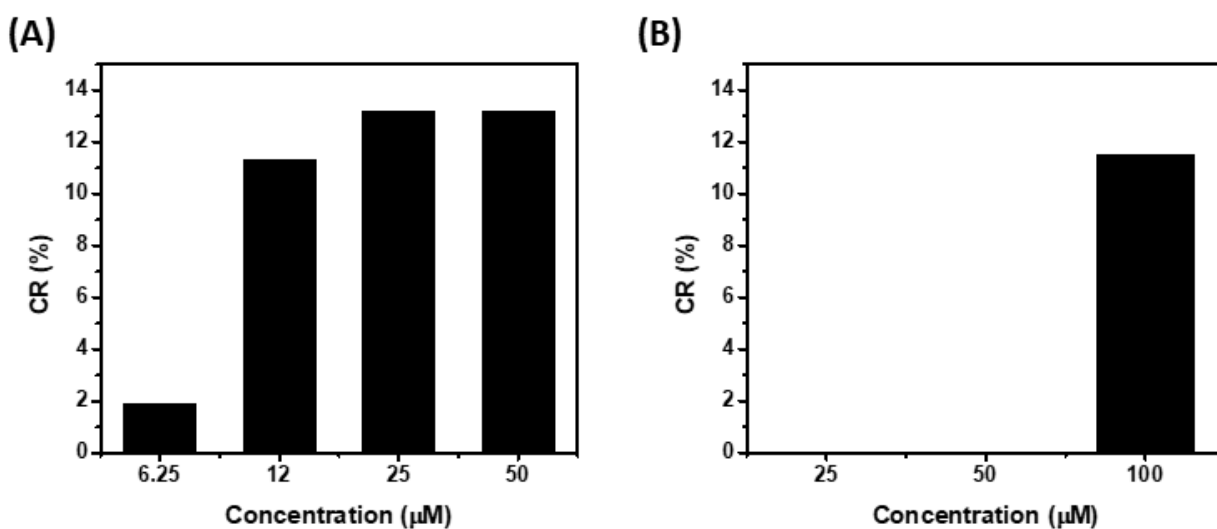


Figure 13: (A) Dipeptide colorimetric response calculated using CR% equations (B) Tripeptide colorimetric response calculated using CR% equation

1.3.2. Transmission electron microscopy (TEM) images of PCDA-Van interaction with *S. aureus* bacteria

Inspired by these results indicating the PCDA-bound antibiotic vancomycin's ability to detect bacterial cell wall terminal amino acid sequences, used as a model for bacteria, we next sought to validate the concept with live bacteria. PCDA-Van liposomes were used

to detect gram-positive bacteria *S. aureus*. For this purpose, liposomes of 0.1 mM concentration consisting of 10% PCDA-Van with 90% PCDA were synthesized after irradiating UV light for 20 min. Due to extended UV irradiation we obtained purple color liposomes with no fluorescence. Upon incubating these liposomes with different concentrations of bacteria for six hours, fluorescence was observed in the PCDA-Van liposomal system (**Fig. 14 A**). When the bacterial concentration was raised, the fluorescence emission at 642 nm increased. Especially at 10^8 CFU/mL bacterial concentration, the fluorescence emission increased by about 50% over the control, which demonstrated the increased interaction resulted in an elevated fluorescence response. Precipitation was observed in these liposomes in the presence of bacteria after only six hours; but without bacteria no precipitation was observed even after 24 hours.

The precipitation provides confirmatory evidence of an interaction between vancomycin vesicles and bacteria. UV spectra show that liposomes before and after treatment with bacteria are not altered significantly, simply retaining their purple color (**Fig. 15**).

We hypothesized that the interaction of vancomycin with the bacteria was the source of the precipitation/aggregation of liposomes whose increased association enhanced the PDA fluorescence. To directly observe the interaction between liposome and bacteria, Transmission Electron Microscopy (TEM) was used to visualize the liposome structure and this interaction between bacteria and PCDA-Van. Due to drying during sample preparation, the liposomes do experience collapse. The liposome alone is seen as a hollow round structure (**Fig. 14 B**). In the presence of bacteria, liposomal structures were observed at the bacterial membrane with some distortion of the bacterial cell wall, the

result suggested that the liposomes were binding to the bacterial membrane (Fig. 14 D). In the absence of liposomes whole bacteria were observed (Fig. 14 C).

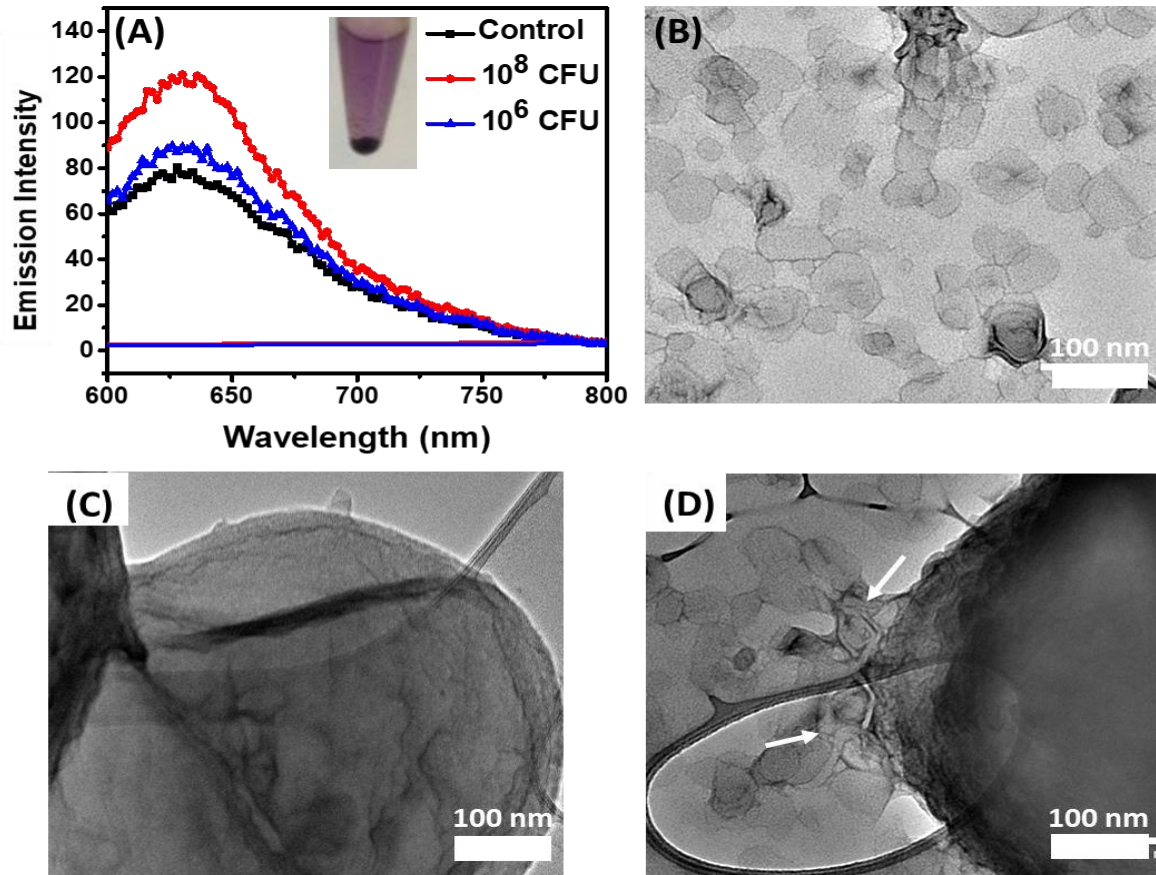


Figure 14: (A) Fluorescence spectra of 100 μ M 10% PCDA-Van: 90% PCDA upon incubating with 100, 10^6 and 10^8 CFU bacterial conc. (B) TEM images of 10% PCDA-Van and 90% PCDA liposomes without bacteria (C) *S. aureus* bacteria only (D) TEM images of 10 %PCDA-Van and 90% PCDA liposomes with *S. aureus*

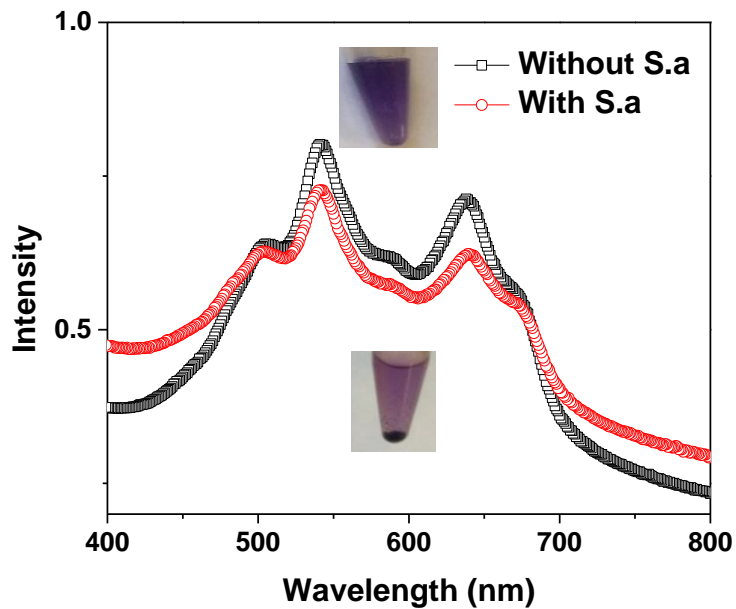


Figure 15: PCDA-Van liposomes UV spectra with 10^8 CFU bacteria *S. aureus* bacteria in the presence of PCDA only liposomes

To prove the binding was due to the presence of PCDA-Van, when 100% PCDA liposome were treated with bacteria, the bacterial membrane was smooth, and liposomes were rarely shown on site of bacterial membrane (**Fig. 16**).

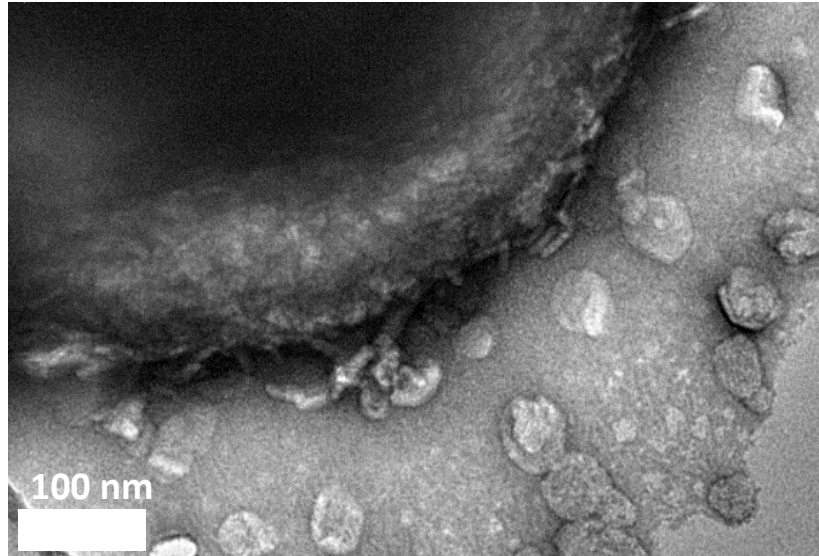


Figure 16: *S. aureus* bacteria in the presence of PCDA only liposomes

1.3.3. Minimum inhibitory concentration (MIC) of PCDA-Van monomer and liposomes

We investigated the potential anti-bacterial activity of vesicle-incorporated PCDA-vancomycin in a 10% PCDA-Van monomer in a 90% PCDA liposome preparation. This composition was compared against three other compositions: (i) 100% PCDA-Van monomer, a non-liposomal composition, (ii) 100% PCDA liposomal formulation with no vancomycin, and (iii) a preparation of pure vancomycin. The minimal inhibitory concentration (MIC) was determined for all four preparations. Vancomycin was consistent with the literature, about 300 ng/mL.⁴² The MIC value was greatly increased by simply conjugating the vancomycin with PCDA, the MIC was increased from 0.3 µg/mL to more than 37.8 µg/mL. Some of that loss of potency was retrieved by incorporating the PCDA-Van into the liposome, where the MIC was reduced by about 50%, to 18.8 µg/mL. The

control, 100% PCDA in the liposome, showed no inhibition. These results suggested the clustering of vancomycin in liposomes contributes to the reduction in MIC (**Table 1**).

Table 1: MIC values of PCDA, PCDA-Van monomer, PCDA-Van liposomes, and vancomycin

Compound		MIC Results ($\mu\text{g/mL}$)
1	Vancomycin	0.3
2	Monomer PCDA-Van	No inhibition
3	10% PCDA-Van: 90% PCDA liposome	18.8
4	100% PCDA liposome	No inhibition

1.3.4. Membrane localization assay

To elucidate whether the bacteria-induced conformational changes of PCDA within the liposomes which could be attributed to transient interactions or membrane binding of bacteria, we utilized fluorescence microscopy with intense fluorophore labeling of the liposomes.⁵² Liposomes were prepared as previously described, but now with incorporation of 5% dabsyl-labeled lipid (1,2-dioleoyl-sn-glycero-3-phosphoethanolamine-N-(dabsyl)) (**Fig. 17**) and either 10% or 0% vancomycin conjugated PCDA. It was envisioned that since dabsyl lipid has long alkyl chains, it can be incorporated into the PCDA-Van liposomes through hydrophobic interaction between PCDA-Van and dabsyl's

long chains (**Fig. 18**). Following incubation of 5% dabsyl liposomes with *E. coli* or MRSA fluorescence images were taken with a DAPI filter.

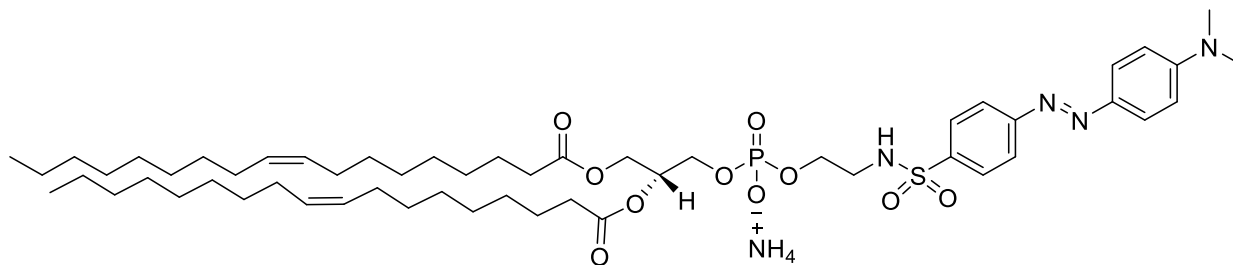


Figure 17: Structure of Dabsyl-lipid PE 18:1

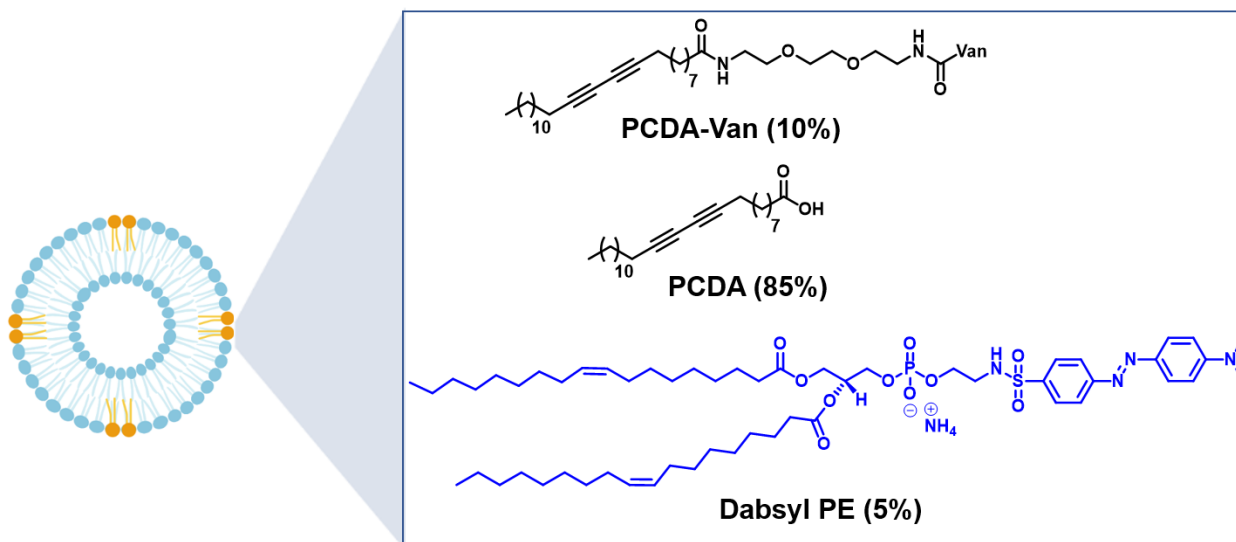


Figure 18: Liposomes synthesis with PCDA, PCDA-Van, and Dabsyl lipid

Images suggested there is increased binding towards MRSA with the addition of vancomycin, as PCDA-Van, in comparison to liposomes without vancomycin. Higher blue fluorescence was observed localized with MRSA cells. This targeting to MRSA was higher

than that for *E. coli*, indicating the specificity of Vancomycin in targeting gram-positive bacteria (Fig. 19).

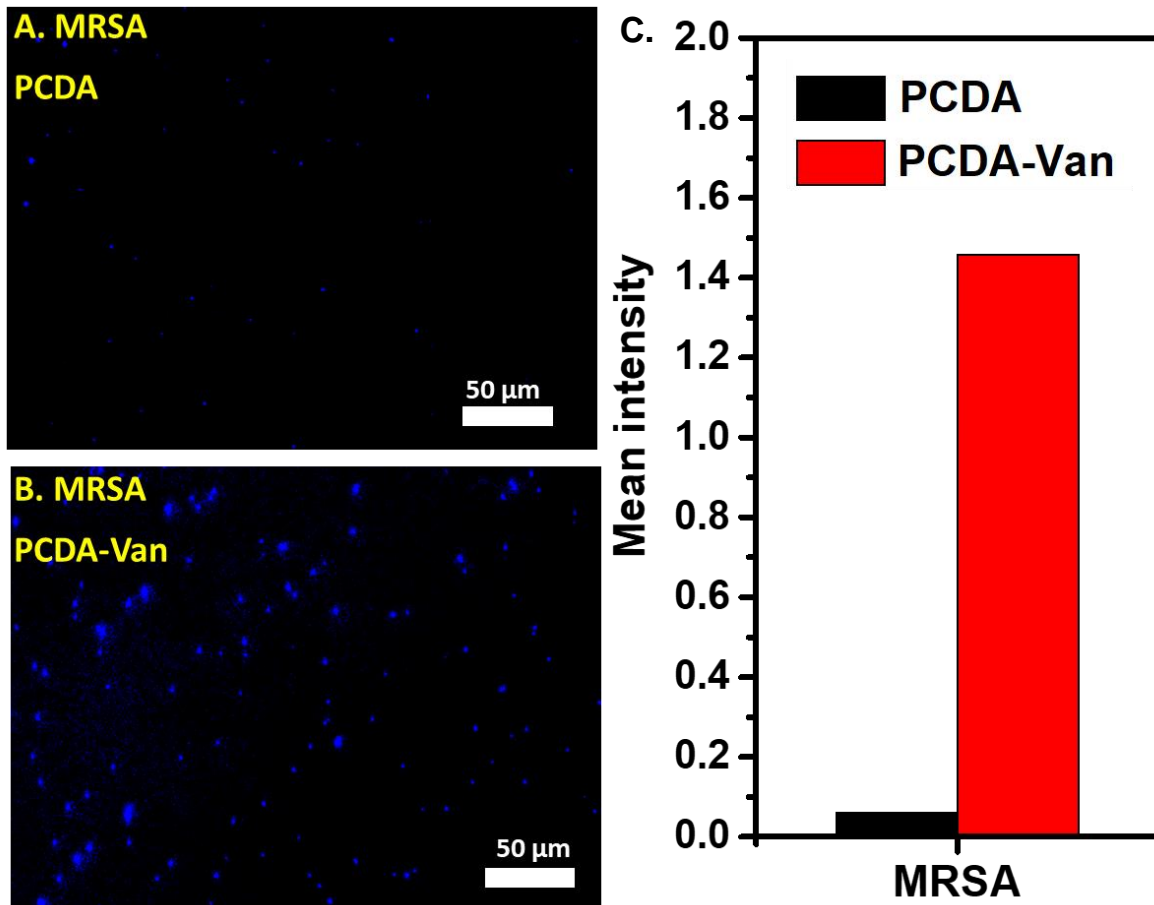


Figure 19: (A) Only 100% PCDA incubated with *MRSA* (B) PCDA-Van and Dabsyl incorporated PCDA incubated with *MRSA* (C) Mean fluorescence intensity.

PCDA-Liposomes have innate bacterial binding ability, however these binding assays lend evidence that vancomycin has preferentially enhanced the gram-positive binding ability of the liposomes relative to that of gram-negative bacteria (**Fig. 20**).

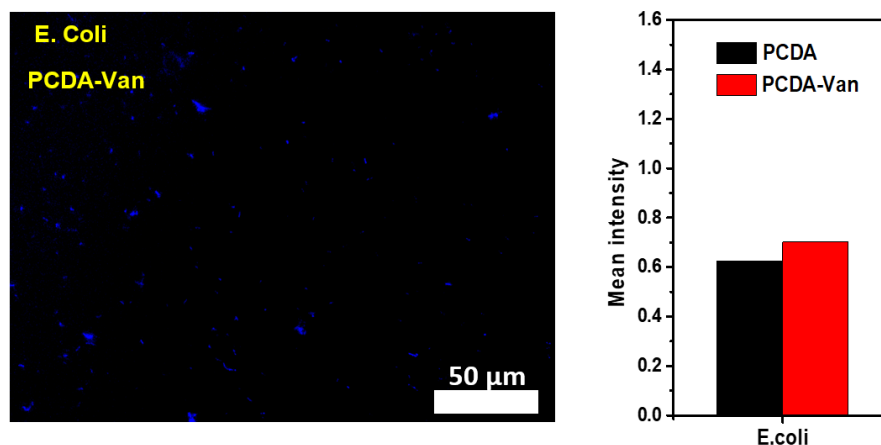


Figure 20: *E. coli*. Bacteria in the presence of PCDA only liposomes (A) incubation with *E. coli* bacterial (B) Mean fluorescence comparison of PCDA and PCDA-Van in presence of *E. coli*.

1.3.5. Size determination of PCDA and PCDA-Van liposomes with Dynamic Light Scattering (DLS)

For freshly prepared liposomes of PCDA-Van incorporated into PCDA, dynamic light scattering (DLS) was used to measure size distribution of vesicles. PCDA liposomes with 10% PCDA-Van were diluted 300-fold for DLS experiments. Intensity vs diameter shows polydisperse vesicles, with a minority of them being of small size with a mean of 164 ± 11.3 nm and a majority being of larger size ranging to a few microns. Particle volume vs diameter indicated only monodisperse vesicles with mean size 163 ± 8.25 (**Fig. 21, 22**). Samples were stored below 4 °C for four weeks and DLS experiments were performed

again to check the stability of liposomes. Initial experiments on these samples show mostly large vesicles (microns) and a diminished number, about 10% of them, were small. After centrifugation for 10 min at 4000 rpm about 67% were centered at 172 nm, indicating stability of these liposomes even after four weeks duration of storage.

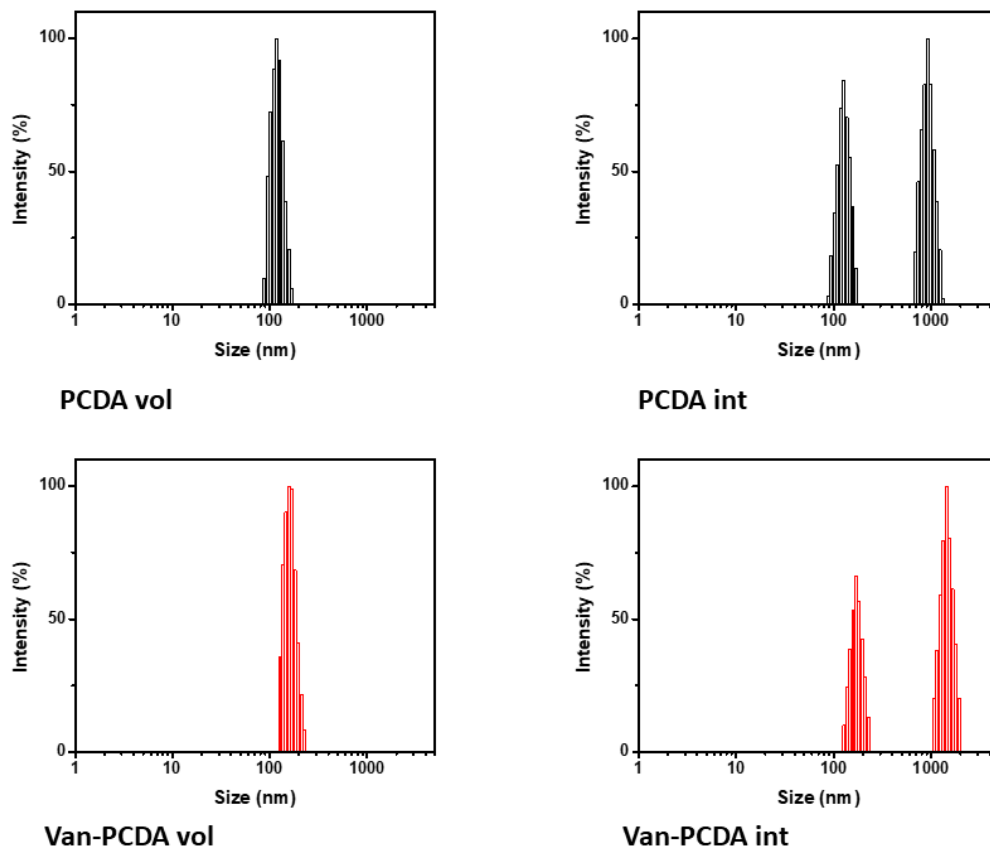


Figure 21: Size characterization of PCDA and PCDA-Van incorporated liposomes by dynamic light scattering (DLS), amount vs. size. The size distributions of the liposomes were weighted either by intensity of the scattering, an r^6 dependence vs. size, or by particle volume, an r^3 dependence vs. size. The intensity weighting emphasizes the particles of larger size disproportionately, but the volume weighting can obscure the presence of the larger particles entirely. In this Figure, the small sizes are reasonably accurately represented in both alternatives.

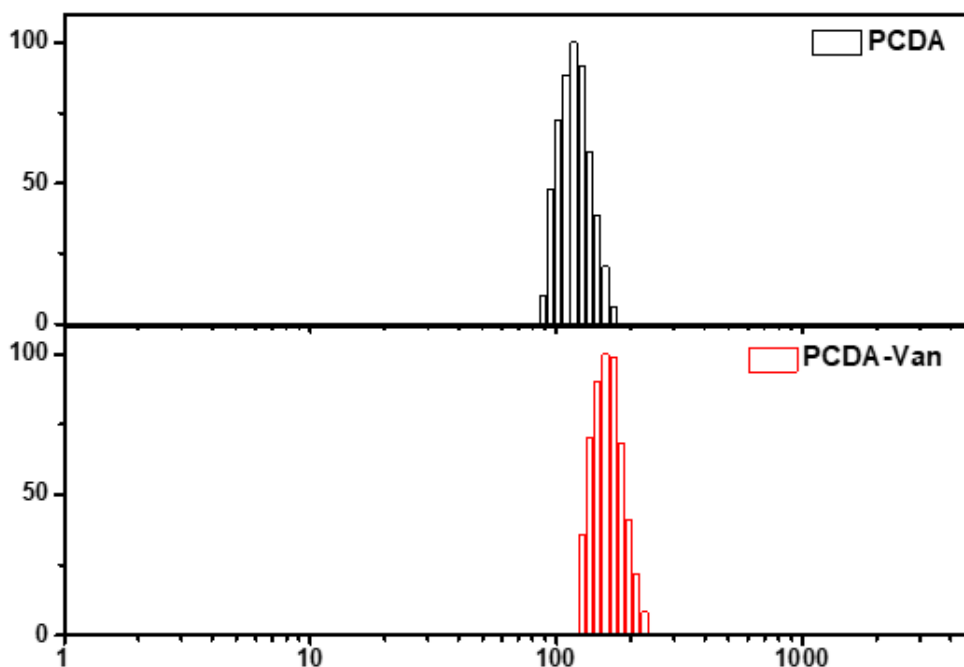


Figure 22: Liposome size comparison between PCDA and PCDA-Van incorporated liposomes, here weighted by volume, with the liposomes anticipated to have the larger charge density, the PCDA loaded liposomes, being smaller. The sizes for the smaller are centered at about 130 nm, and those for the larger centered at about 160 nm.

1.3.6. Thermal stability of PCDA-Van with PCDA derivatives as co-monomers

The thermal stability of PCDA monomers **4b**, **4c**, and **4d** by incorporating 10% PCDA-Van monomers was investigated. It was observed when 90% of **4b** was used with 10% PCDA-Van, after UV polymerization the liposomes generated were stable at room temp. with intense blue color. Whereas, in the presence of monomer **4c**, the liposomes immediately precipitated out of solution after 5 min UV irradiation but remained blue till

50 °C. Mixing of co-monomer **4d** in PCDA-Van produced purple-colored liposomes heavily precipitated at room temperature. (**Fig. 23, Table 2**)

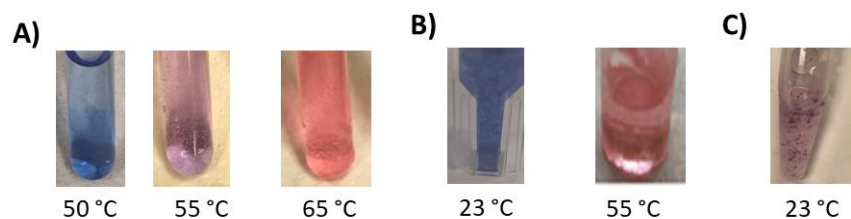


Figure 23: Thermal stability of 10% PCDA-Van with 90% comonomer **4b** PCDA-OH (A), PCDA-NH₂ **4c** (B), and PCDA-Imidazole **4d** (C) at different temperatures for 5 min

Table 2: Thermal stability of 10% PCDA-Van with 90% comonomer **4b** PCDA-OH (Entry 1), PCDA-NH₂ **4c** (Entry 2), PCDA-Imidazole **4d** (Entry 3), and PCDA (Entry 4) at different temperatures for 5 min.

Co-monomers (90%)		PCDA-Van monomer (%)	Room temp. Thermal stability	50 °C thermal stability	60 to 80 °C thermal stability
1	PCDA-OH	10	Stable Liposomes blue color	Stable liposomes blue color	Purple to pink color liposomes precipitates
2	PCDA-NH ₂	10	Blue color liposome precipitate	Pink color Liposome precipitate	Pink color Liposome precipitate
3	PCDA-Imidazole	10	Unstable Purple color liposome precipitate	Unstable pink color liposome precipitate	Unstable pink color liposome precipitate
4	PCDA	10	Stable Liposomes blue color	Unstable Purple color liposome precipitate	Purple to pink color liposomes precipitates

1.4. Conclusion

In conclusion, we successfully synthesized antibiotic-bound vancomycin-PCDA liposomes for rapid and direct detection of biomimetic small peptides of sequences *D*-Ala-*D*-Ala-, and *L*-Lys-*D*-Ala-*D*-Ala. Next, we used the same PCDA-Van liposomes to investigate the presence of *Staphylococcus aureus* bacteria. We observed a marked increase in fluorescence in the highly crosslinked PCDA-Van liposomal preparation. The binding of gram-positive bacteria with PCDA-Van was confirmed based on colorimetric and fluorescent responses, fluorescent microscopy, TEM, and by inhibition assay. Thermal stability of synthesized PCDA derivatives with PCDA-Van incorporation suggested the presence of positively charged head group on the co-monomer destabilize the inherent blue color nature of PCDA, whereas neutral or negatively charged monomers remained stable at room temp. Ongoing and future investigations in our laboratory are directed toward incorporating alternative antibiotics into the PCDA system to improve both detection and bactericidal activity.

Chapter 2

Coupling of PCDA with self-assembled peptide and synthesis of diacetylene molecules

2.1. Introduction

PCDA and other diacetylene monomers have been reported in many studies to bind covalently with self-assembled peptide amphiphiles for applications such as anti-bacterial, drug delivery, architectural investigation, and chemical or biosensing purposes.⁵³⁻⁶¹ Such moieties form secondary structures comprising β -sheets and/or 1D, 2D nanofibers.^{57, 58} Wu et al. reported the synthesis of polydiacetylene liposomes as a fluorescent probe for detection of gram-negative bacteria *E. coli*.⁶²

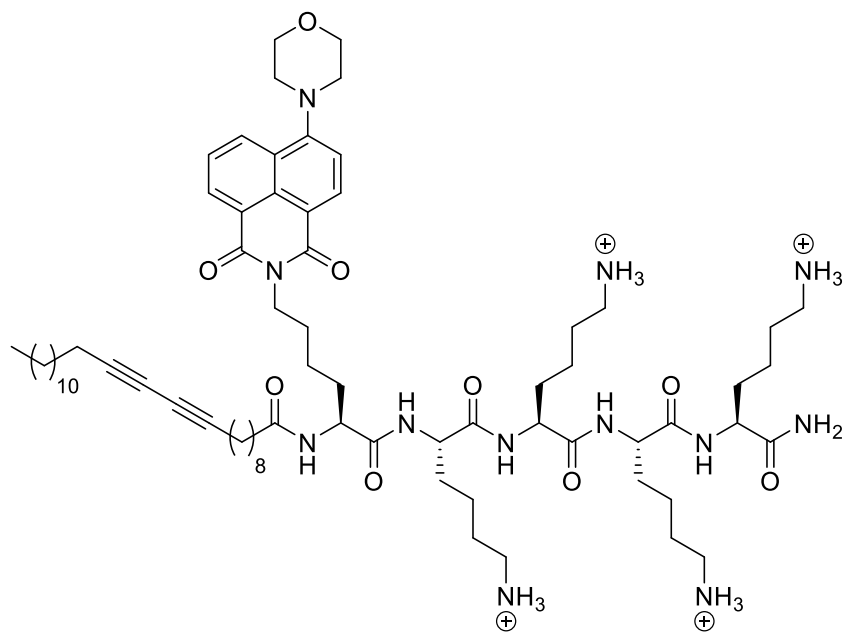


Figure 24: PCDA bound with peptide sequence of anti-bacterial studies

Solid-phase synthesis was done to prepare a PCDA-coupled pentalysine molecule in their studies with a naphthalic acid fluorophore attached to the N-terminus (**Fig. 24**). Liposomes were synthesized by mixing this PCDA-pentalysine derivatives and co-monomer tricosadiyonic acid (TCDA) after UV irradiation. Selective detection of gram-negative bacteria was achieved at concentration of 40 μM by the interaction of liposomes with the lipopolysaccharide (LPS) of the bacterial wall. The cytotoxicity assay revealed the liposomal system was non-toxic to human cells. ⁶²

2.1.2. PCDA functionalized with LPRDA peptide via polyethylene glycol (PEG) linkers

Inspired by these studies of Wu et al.,⁶² it was planned to modify PCDA with self-assembled peptide LPRDA linked through a polyethylene glycol unit to target gram-positive bacteria. LPRDA peptide targets sortases (SrtA) on the gram-positive bacterial cell wall.⁶³⁻⁶⁶ SrtA is an enzyme on *S. aureus* cell wall that helps it anchor to the host cell and cause infection.⁶⁷ By targeting the SrtA enzyme with LPRDA functionalized PCDA, we hoped to generate a selective biosensor for gram-positive bacteria *S. aureus* detection

PCDA was functionalized with PEG linker and LPRDA enzyme in Dr. He Dong's laboratory by Dr. Weike Chen and Ryan Madigan. (**Fig. 25**).

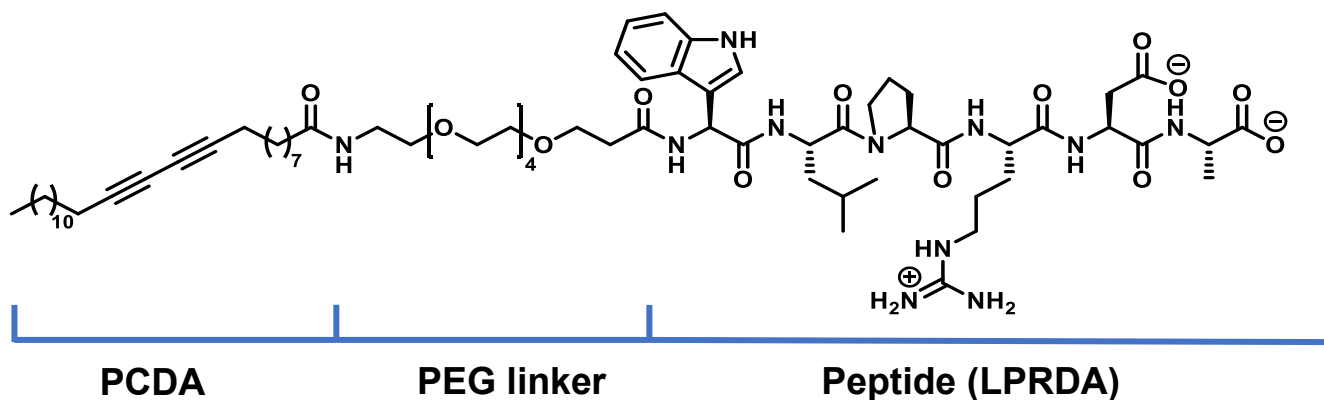


Figure 25: Synthesis of PCDA modified with PEG and LPRDA peptide for detection of *MRSA* bacteria in Dr. He lab

selectively target *MRSA*. Results were characterized with UV and fluorescent spectroscopy and discussed below.

2.1.3. Diphenyl and linear diacetylene linkers

The presence of phenyl rings in the diacetylene molecules have been reported to enhance the stability and results in reversibility back from red to blue color.⁶⁸ Very few reports exist in the literature where the use of diphenyl PDA (**Fig. 26**) type linkers have been used with another small molecule or oligopeptides for biosensor or drug delivery.⁶⁹⁻

72

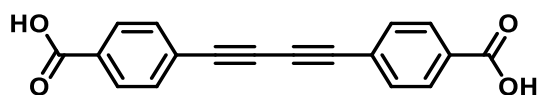


Figure 26: Diphenyl DA acid linker

Dieglmann et al.⁵³ used diacetylene diacids linker to couple to a desired peptide on both sides (**Fig. 27**) of it to produce PDA-nanostructure for biological purposes.

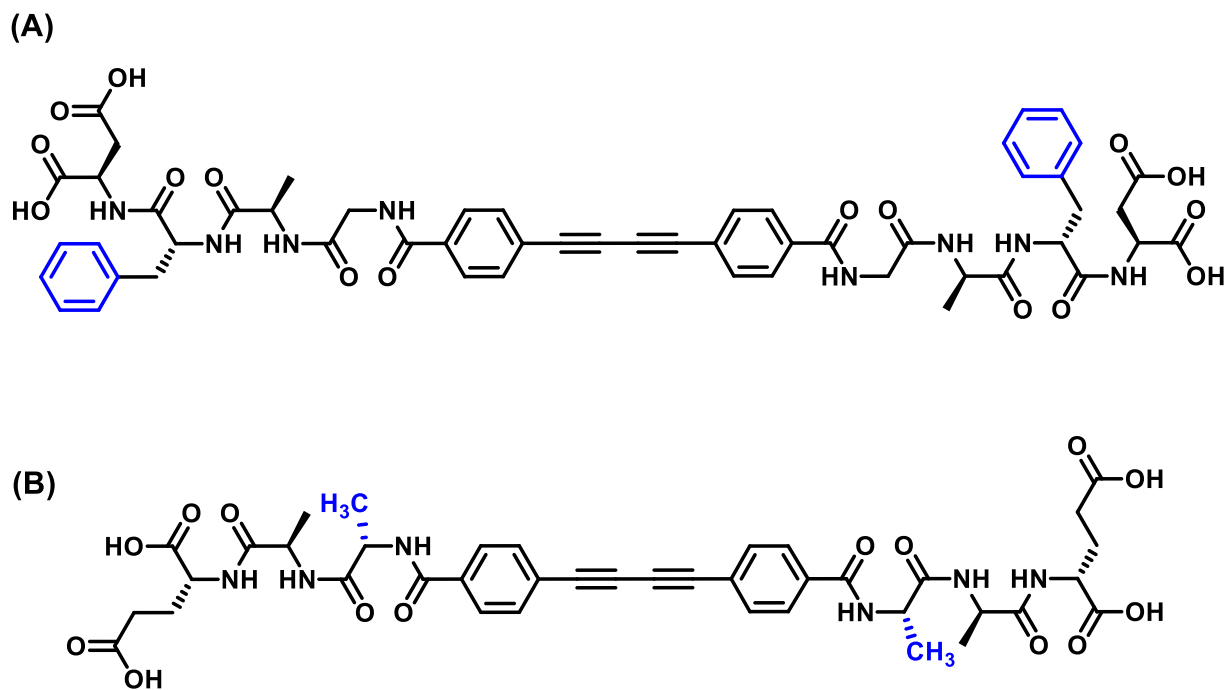


Figure 27: Peptides conjugated in Dieglmann et al. studies

The sequence of amino acids perfectly aligned the adjacent diacetylene for polymerization when irradiated with 254 nm UV light. Molecule (**B**), after polymerization, exhibited an interesting yellow color. Large nanofibers were observed with more hydrophobic amino acids sequence in (**B**) versus (**A**), in which small nanofibers were observed. 1D amyloid-like nanofibers formation was reported in this study (**Fig. 28**).

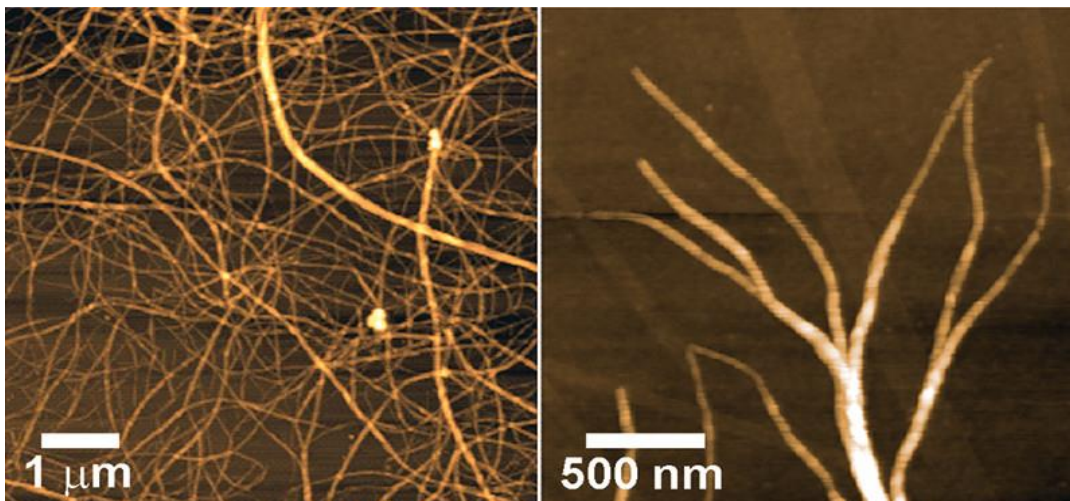
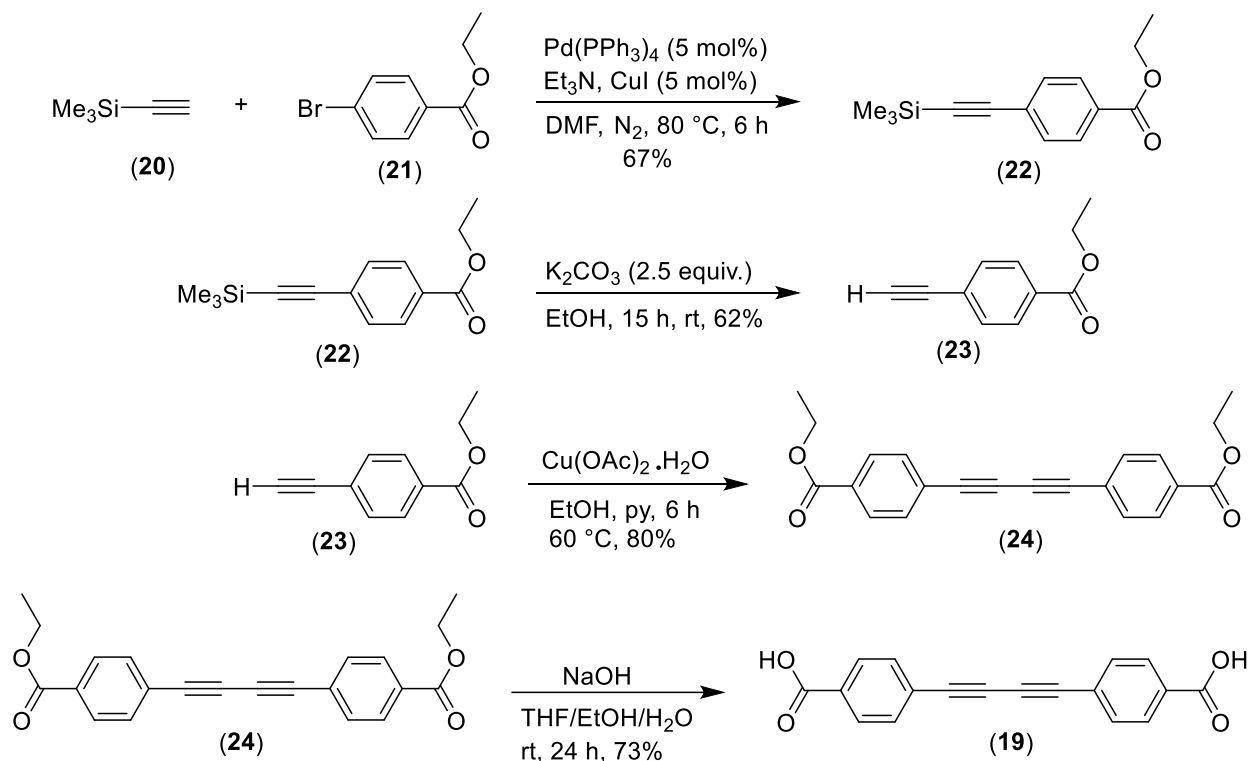


Figure 28⁵³: Atomic force microscopy (AFM) images of PDA nanofibers of DA-peptides in Dieglmann studies. Reproduce from Ref. 53.

2.2.1. Synthesis of Diphenyl DA linkers and coupling with oligopeptides

Inspired by the previous literature on the presence of diphenyl DA linkers with different functional groups giving rise to different types of PDA polymers, color transitions and primarily the formation of hydrogel,⁷³⁻⁷⁶ we planned to synthesize similar systems. With the development of such a system, it was planned to design it to be used as an antibacterial and/or drug-release system. First, we set out to prepare the diphenyl DA linker (**19**, **Scheme 5**).

Scheme 5



Scheme 5: Synthesis of diphenyl DA linker (**19**)

In general, Sonogashira cross-coupling was carried out between ethyl 4-bromobenzoate **21** and trimethylsilylacetylene **20** to acquire the aryl alkyne **22** in 67% yield. Deprotection of the trimethylsilyl group (TMS) was performed with K_2CO_3 in ethanol to provide terminal alkyne **23** with 62% yield. A Glaser coupling enabled construction of the diacetylene functional group of the DA linker. Copper acetate monohydrate $\text{Cu(OAc)}_2 \cdot \text{H}_2\text{O}$ was effective at generating the diacetylene compound (**27**) in 80% yield. Ester hydrolysis was accomplished with NaOH(aq) to obtain the final product as an off-white solid in 73% yield (**19**).

2.3. Results and Discussion

2.3.1. UV and fluorescent spectroscopy of PCDA-peptide modified liposomes for MRSA bacterial detection

The synthesized PCDA-PEG-peptide (PCDA-pep) (**Fig. 25**) with co-monomers PCDA (**Fig. 1**) and/or PCDA-OH (**4b**) was used against MRSA to determine the potential biosensing application. Initially PCDA-pep was used along with co-monomer PCDA, and the liposomes were synthesized using general procedure (**scheme 4**) with some modifications. Here, the dabsyl lipid was incorporated in the formation of liposomes to quantify fluorescence images upon binding with *MRSA*. Different concentrations of each monomer were used to optimize the system (**Table 3**), so liposomes stay blue at room temp. and only change in the presence of *MRSA* with fluorescence induced. Due to solubility issues, the liposomes were synthesized in the presence of 10% dimethyl sulfoxide (DMSO) solvent in water. (**Table 3**)

Table 3: PCDA-peptide stability with different comonomers composition

Liposome formulation of PCDA-pep with comonomers PCDA and PCDA-OH					
	PCDA-pep (%)	PCDA (%)	PCDA-OH (%)	Dabsyl lipid (%)	Liposomes stability (rt blue color; 6 hour)
1	10	87.5	0	2.5	Unstable
2	10	0	87.5	2.5	Stable
3	10	48.75	48.75	2.5	Unstable
4	10	30	57.5	2.5	Stable

In the presence of PCDA comonomer, the liposomal system was not stable at room temp., rather, the blue transition to purple was observed even in the absence of MRSA (Entry 1). It was planned to use PCDA-OH as a co-monomer, the newly formed liposomes were very stable and remained a blue color even in the presence of MRSA as no color change was observed (Entry 2). Based on these results, a three monomer system was used next where PCDA-peptide was used with PCDA and PCDA-OH (1:1) both as co-monomers (Entry 3). This composition produced unstable liposomes. Further increase in the percent of PCDA-OH gave the stable liposomes at room temp. (Entry 4).

In collaboration with Dr. Dong's lab, Ryan Madigan performed antibacterial experiments with 10^7 and 10^9 CFU of *MRSA* and *E. coli*. Since LPRDA is specific to *MRSA* so *E. coli* was used as a negative control (**Fig. 29**).

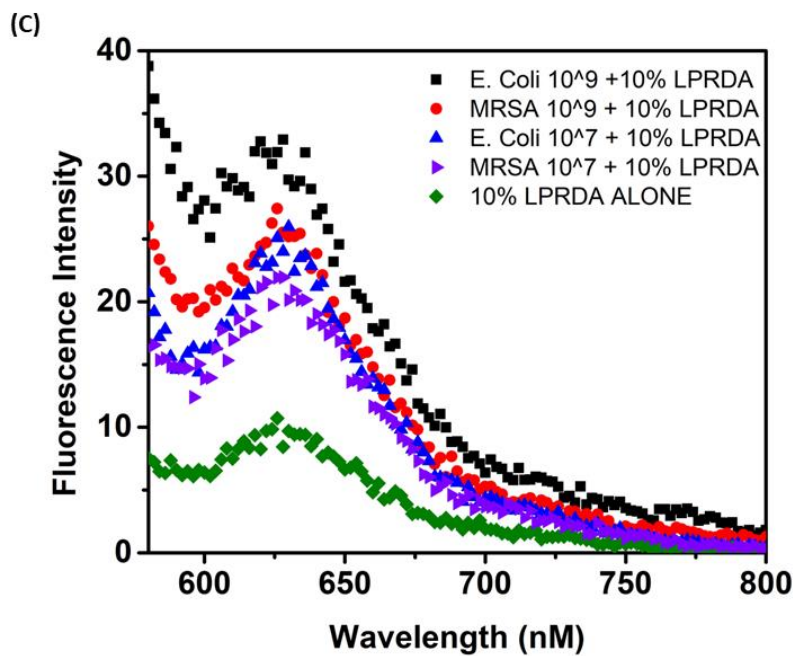
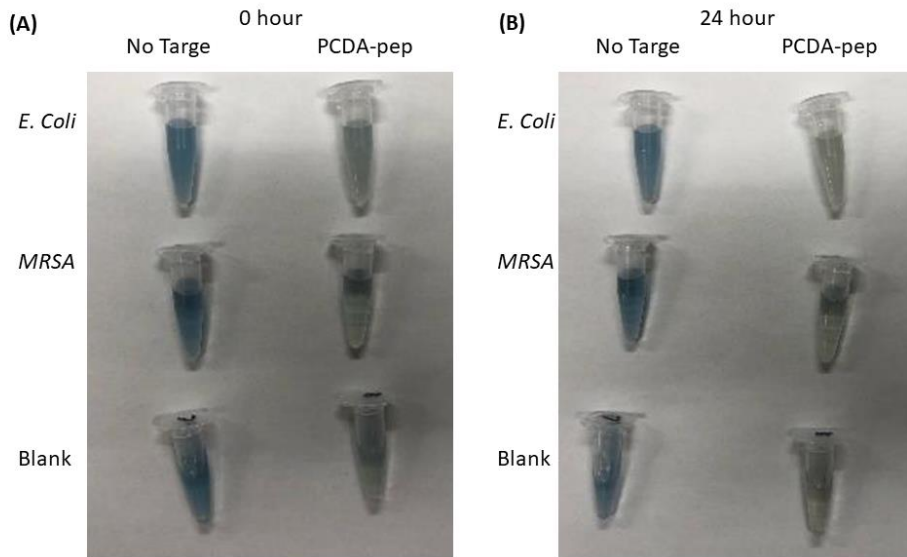


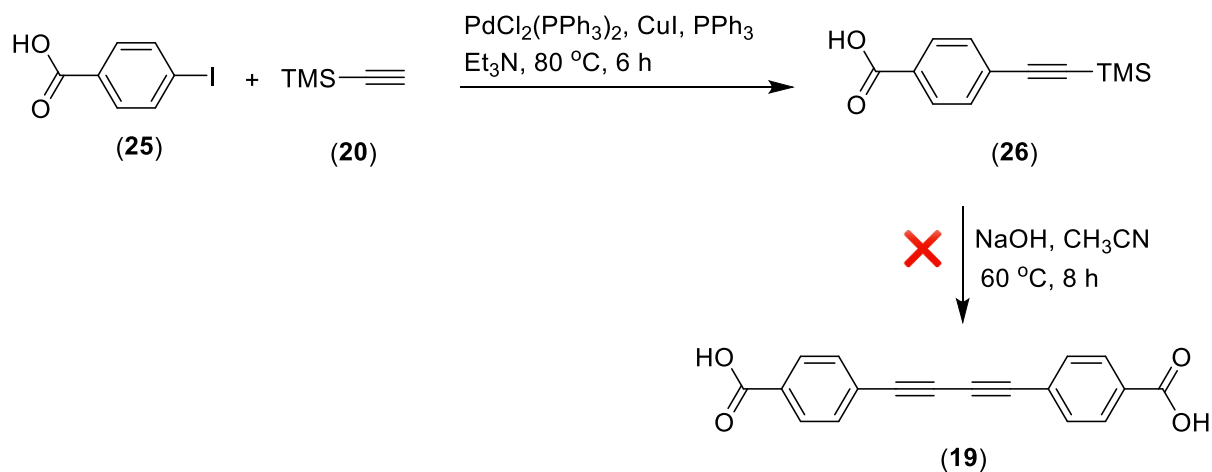
Figure 29: Liposomes of composition 10%PCDA-pep, 30% PCDA, 57.5% PCDA-OH and 2.5% Dabsyl lipid. (A) Treatment of 10^9 CFU *E.Coli*, *MRSA*, and blank solution with PCDA-pep liposomes at zero hour (B) Treatment of 10^9 CFU *E.Coli*, *MRSA* and blank solution with PCDA-pep liposomes after 24 hour (C) Fluorescent intensity of 10^7 and 10^9 CFU *E. Coli*, *MRSA*, and control PCDA-pep

At zero hour, all the samples with or without the presence of bacteria show a blue color solution indicating the stability of synthesized liposomes. After six hours, all the samples containing bacterial culture started changing color (**Fig. 29 A, B**). After 24 hours, the solution of all the samples was characterized with fluorescent spectroscopy. Results show no selectivity with the prepared composition of PCDA-pep. The fluorescent response was observed more in *E. coli* than *MRSA* suggesting no binding of LPRDA with gram-positive bacteria, PCDA-pep showed inherent fluorescent in them, indicated by the small intensity in the absence of any bacteria.

2.3.2. Diphenyl DA linker synthesis

Initial trials were conducted with iodobenzoic acid to perform sequential Sonogashira and Glaser coupling (**Scheme 6**).⁷⁷ This reaction scheme did not work as initially reported. After the workup, NMR of reaction mixture shows related peaks of coupling product (**29**), but after that, for Glaser coupling literature reported conditions for formation of (**19**) were unsuccessful, the NMR was uninterpretable and clearly contained multiple degradants.

Scheme 6



Scheme 6: Alternate scheme for the synthesis of (**19**) sequential Sonogashira and Glaser coupling

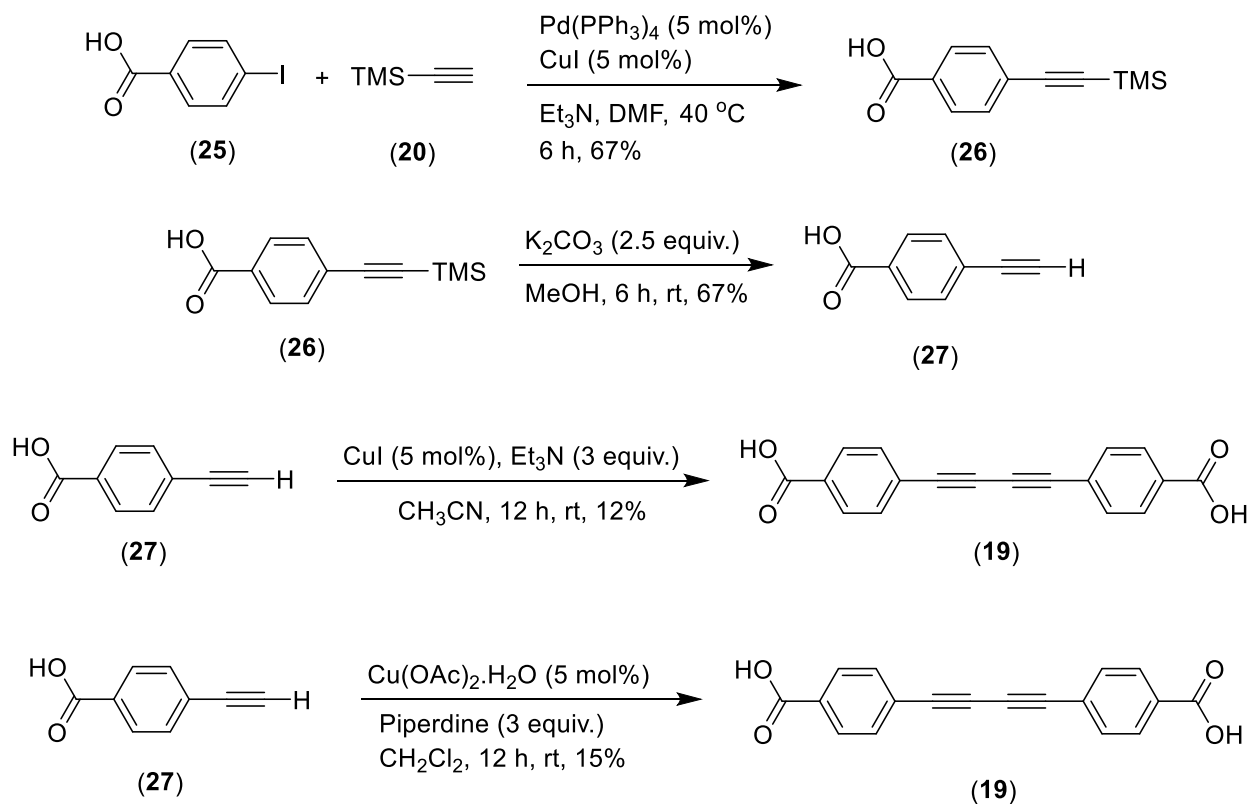
Table 4 Trials for Glaser coupling with different catalysts and base

Solvent (Distilled)	Base	Catalyst (5 mol%)	Product
CH ₃ CN	NaOH	CuI	Not Observed
CH ₃ CN	KOH	CuI	Not Observed
CH ₃ CN	NaOH	Cu(OAc) ₂ .H ₂ O	Not Observed

A possible reason was thought to be the loss of cross-coupling catalyst during the workup while passing the mixture through celite. Although the catalyst was additionally transferred in the reaction flask, still no product formation was observed. Switching the catalyst from CuI to Cu(OAc)₂.H₂O for Glaser coupling did not make any difference in getting the target molecule (**Table 4**).

After that, it was planned to do stepwise synthesis to make (**19**), first Sonogashira and then performing Glaser coupling (**Scheme 7**)

Scheme 7



Scheme 7: Alternate scheme for the synthesis of (19) by performing stepwise Sonogashira and Glaser coupling

Following the new route, we successfully obtained the Sonogashira product (**29**), TMS deprotection was successfully done and then the Glaser coupling was performed using CuI as well $\text{Cu}(\text{OAc})_2 \cdot \text{H}_2\text{O}$. However, the yields of last reaction was not satisfactory. It was thought to perform the Glaser coupling with ester protected substrate. So, the new scheme (**Scheme 5**) was followed, and Glaser coupling gave better yield of this time. In this **scheme 5**, many trials were done to hydrolyze the ethyl ester groups, but most of them did not work (Entry 1-4).

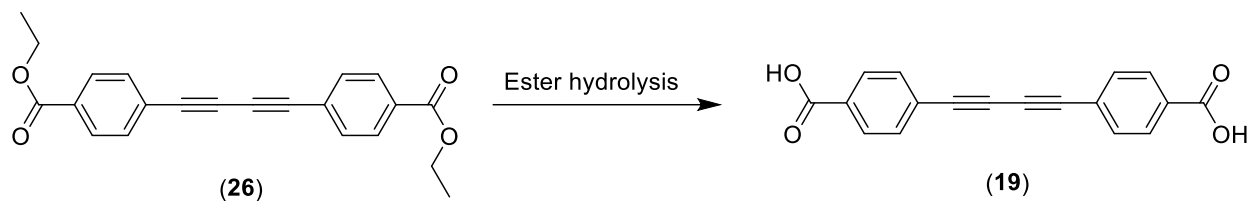


Table 5 Hydrolysis of esters with different base equivalents

Trials	Base (equiv.)	Solvent	Product (yield%)
1	KOH (2)	THF:H ₂ O (2:1)	SM*
2	KOH (5)	Ethanol, H ₂ O (cat.)	SM
3	KOH (10)	Ethanol, H ₂ O (cat.)	SM
4	NaOH (2)	Ethanol, H ₂ O (cat.)	SM
5	NaOH (5)	Ethanol, H ₂ O (cat.)	Mono acid
6	NaOH (10)	Ethanol, H ₂ O (cat.)	Mono acid
7	KOH (10)	Butanol	SM
8	NaOH (10)	MeOH/THF/H ₂ O	73%

By increasing the equivalence of base initially from 5 to 10, the mono-acid formation was observed (Entry 5 and 6). Furthermore, the increase in base equivalence did not make any change in another ester group. A helpful literature reference suggested a 1:1:1 mixture of three solvents for ester hydrolysis, which was tried on **(26)** to eventually give the expected product **(19)** at room temp. (Entry 8).⁷⁸

2.3.3. Diphenyl DA coupling with peptides

Dr. Chen from Dr. Dong's lab used solid phase synthesis to couple different peptides on both sides of our prepared DA linker.⁷⁹ He coupled following peptide sequences to couple with the DA linker to investigate hydrogel formation and polymerization: GQFQFEGGGLPRDA, GQFEGGGLPRDA, GSFEGGGLPRDA and GQIEGGGLPRDA. The final product was purified with HPLC and characterized by electrospray ionization (ESI) mass spectrometry (MS). After many trials and errors, it was decided to attach QF (Glutamine Q; Phenylalanine F) sequence with LPRDA to couple with DA linker for proper pH dependent hydrogel formation and colorimetric biosensing response along with drug release system on alkaline surface.

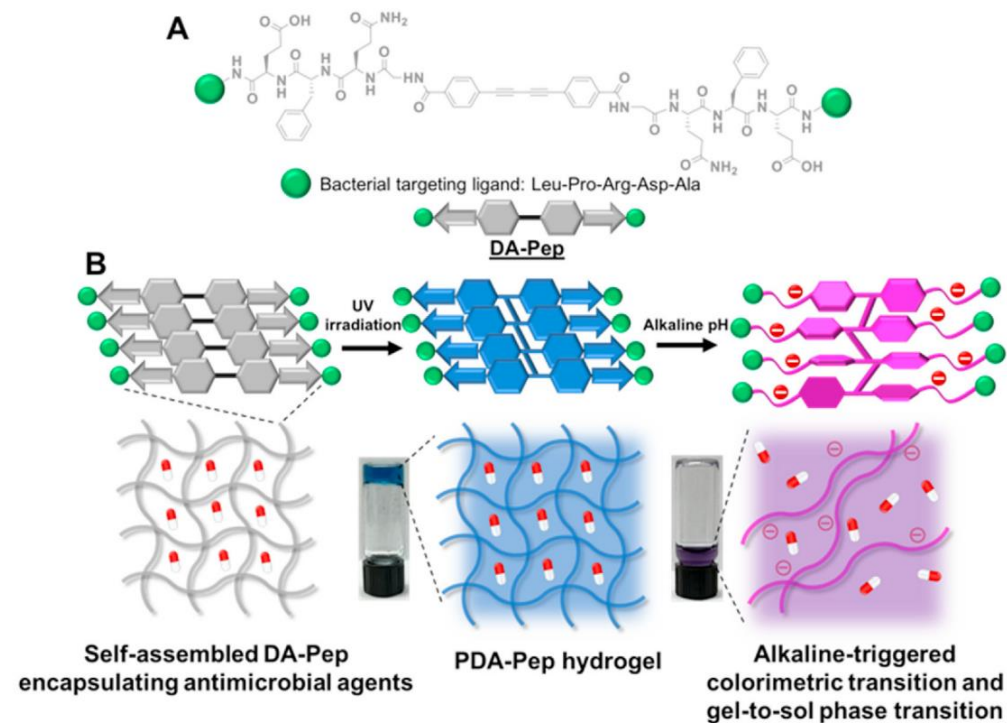


Figure 30¹³¹: Chemical design of Pep-DA-Pep gel formation at acidic pH and transition solution in alkaline pH along with blue to purple color change (A) Structure of Pep-DA-Pep (B) self-assemble amphiphilic Pep-DA-Pep transparent gel formation (in grey) forming 2D nano nanofiber exhibiting blue color when irradiated with 254 nm UV light. At alkaline pH, color change along with phase transition gel to solution and release of the drug on alkaline infection site

2.2.4. TEM characterization of peptide-DA-peptide hydrogel

To visualize the nanofiber formation, TEM images were taken at different pHs (**Fig. 31**). At acidic pH of 5.5 and 6.5, densely packed nanofiber structures were observed (**Fig 30 C, D**). Whereas, close to alkaline pH 7.6 and 8.5 dispersed nanofibers were observed (**Fig 30 C, D**). The color transition from blue to purple and gel to sol phase transition explains the structural changes in the DA linker, which might be due to protonation/deprotonation of the self-assembled peptides causing changes in the macroscopic structure.

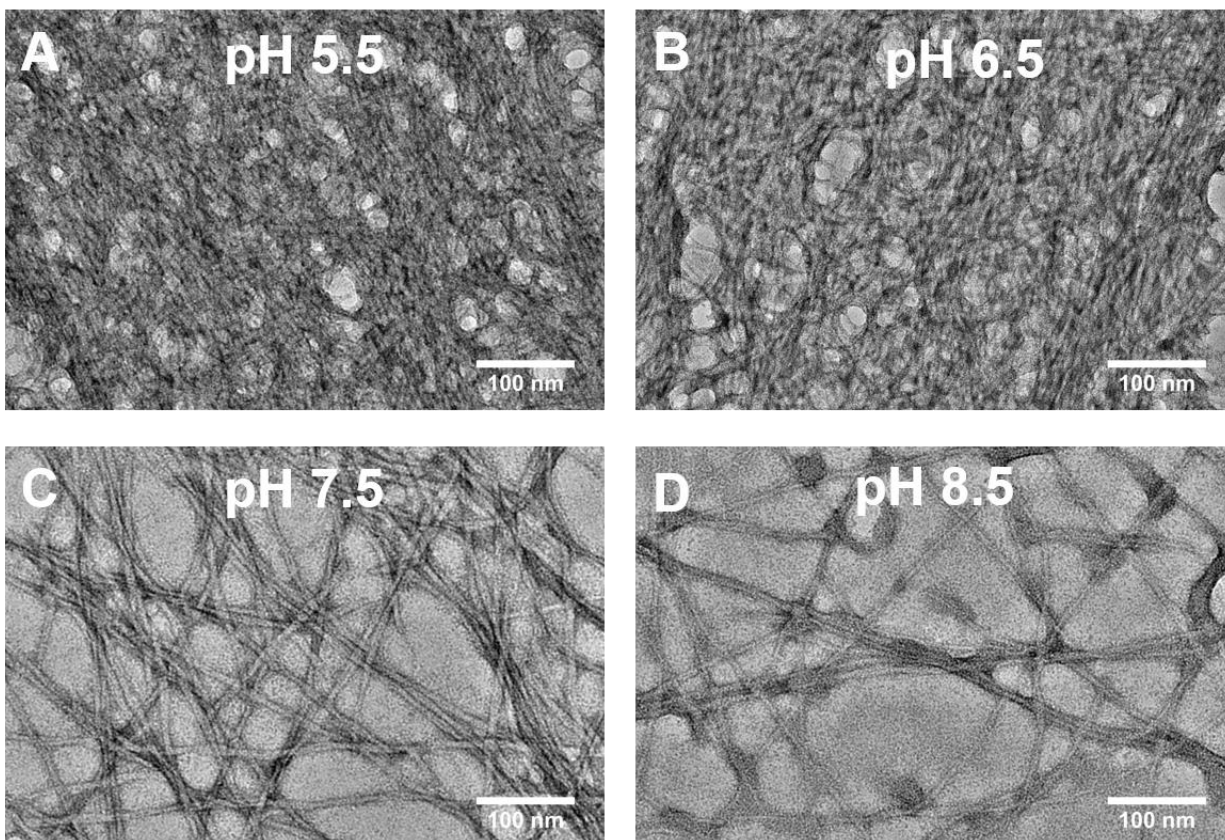


Figure 31 ¹³¹: TEM images of Peptide-PDA-Peptide at acidic pH **(A)** pH 5.5, **(B)** pH 6.5, **(C)** slightly basic pH 7.5, and basic pH **(D)** pH 8.5. The conc. of Peptide-PDA-Peptide was 10 mg/mL. NaOH was used to adjust the pH

2.4. Conclusion

In conclusion, the LPRDA peptide was coupled with the PCDA molecule to target selectively *MRSA* bacteria and was characterized with fluorescence spectroscopy. Results suggested no selectivity rather, *E. coli* shows more fluorescent response than *MRSA*. This response might be due to the inherent fluorescence present in *E. coli*. Giving the observed results. Working towards the synthesis of next generation diacetylene molecules, the synthesis of diphenyl DA linker was completed using Sonogashira and Glaser coupling reactions. The synthesized DA molecule was used with various peptide sequences to determine the desired peptide sequence for hydrogel formation and alkaline responsive system for sensing infectious sites and drug release system. In collaboration with Dr. Dong's lab, the antimicrobial activity and drug release on the alkaline infection site were investigated. Blue to purple color change was observed as the pH goes to alkaline due to gel-to-sol phase transition, simultaneously release of drug killing the onsite bacteria as determined by antimicrobial activity. Cytotoxicity results show good hemocompatibility of the synthesized PDA peptide system. This pH-responsive material was an effort towards building a biosensor as well as a drug release system. Future endeavors will be to explore other peptides and modify DA linkers to build a system for other chronic diseases.

Chapter 3

Synthesis of bisphosphonate molecules for the control of calcium carbonate (CaCO₃) precipitation

3.1. Introduction

During the production of cement, huge amounts of carbon dioxide (CO₂) is emitted, with a yearly release of 100,000,000 Kg which counts for 6% of the total emission from all the sources emitting CO₂.⁸⁰⁻⁸² The goal of this study was to investigate the impact of organic additives to control the interaction between CO₂ and cementitious material as an approach towards the production of greener cement. Ordinary Portland Cement (OPC) has been used extensively in construction worldwide. (Fig. 31) Currently global yearly production of cement is about 4 billion metric tons and is expected to increase to 5 billion by 2030.⁸³⁻⁸⁵

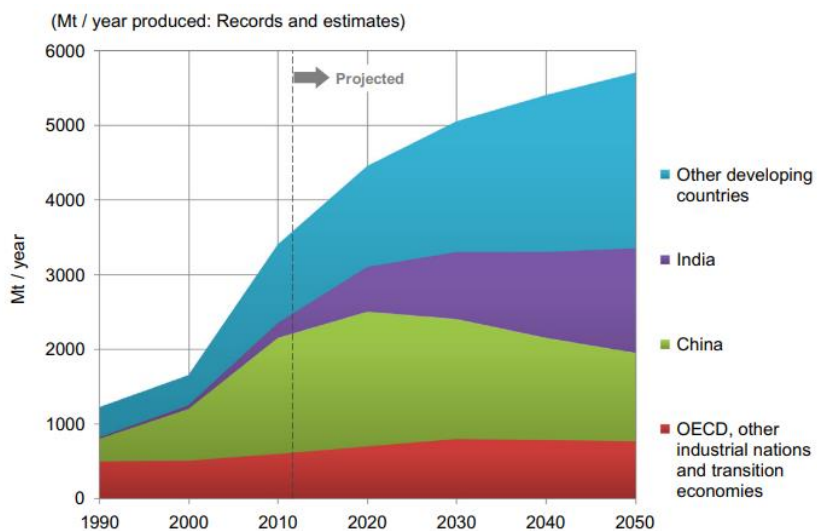


Figure 32⁸⁵: Production of cement worldwide

Cement based on calcium carbonate (CaCO_3) material have been developed and investigated by many researchers due to their ability to sequester carbon dioxide (CO_2), such cements are more biodegradable.⁸⁶⁻⁸⁸ CaCO_3 exists in six different polymorphs, the most commonly found polymorphs are calcite, amorphous calcium carbonate (ACC), vaterite and aragonite. Calcite is crystalline in nature and thermodynamically stable, whereas kinetic polymorphs ACC, vaterite, and aragonite are often unstable.⁸⁹ These polymorphs are present in both hydrate and anhydrous forms.⁸⁹⁻⁹² Biomineralization is a process in living organisms used for the formation of hard bioinorganic structures such as bones, teeth, eggshells, exoskeletons, and other mineral structures.⁸⁰ All these polymorphs can coexist simultaneously in different organisms or can be present as solely single form.^{91, 92} ACC polymorphs, while thermodynamically less stable than calcite, are desirable compared to their crystalline polymorphs, as crystalline structures suffer from anisotropic mechanical properties.

Binding of phosphorus species to Ca^{2+} is stronger than other metals such as Mg^{2+} or Na^+ .⁹³ In this study we propose to synthesize a series of small bisphosphonates (BPs) molecules with acidic (COOH), basic (NH_2), neutral (OH) and non-functional end group containing different chain lengths. Observation of the precipitation of CaCO_3 was planned in the presence of these bisphosphonate molecules.

3.2. Biomimetic-Biomineralization by small organic molecules

Aspartic acid and polyaspartic acid have been reported to control the formation of the amorphous calcium carbonate (ACC) polymorph in many studies.⁹⁴⁻¹⁰⁰ In biological systems, proteins rich with monomer aspartic acid or polyaspartic acid are known to

stabilize ACC over other polymorphs (**Fig. 33**). Studies show a possible explanation for this phenomenon might be the interaction between the negatively charged aspartic acid, which hinders the dissolution of ACC.¹⁰¹⁻¹⁰³

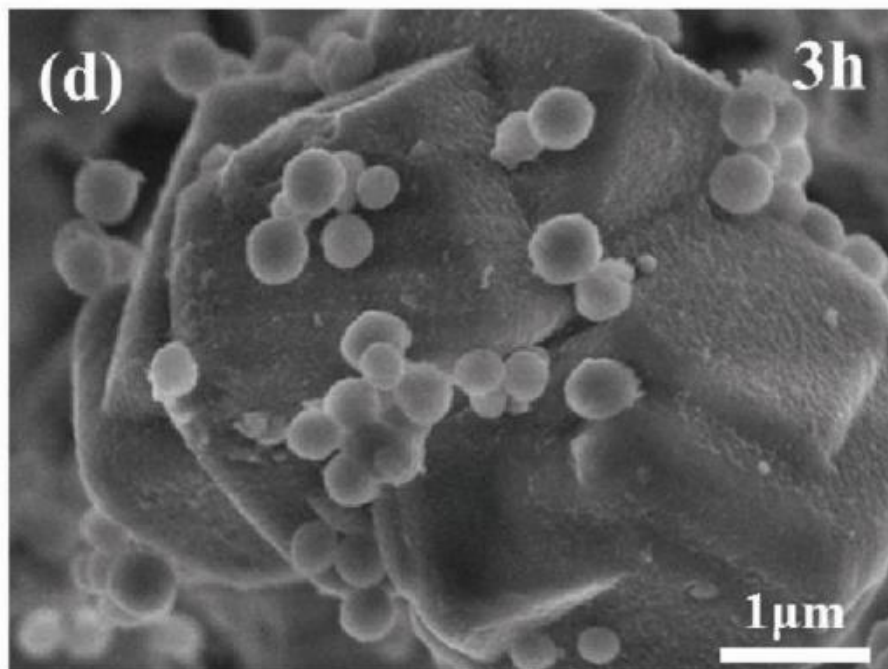


Figure 33⁹⁴: Scanning electron microscopy (SEM) images showing the growth of ACC nanoparticles on the calcite crystal in the presence of 6% poly aspartic acid additive in calcium carbonate solution

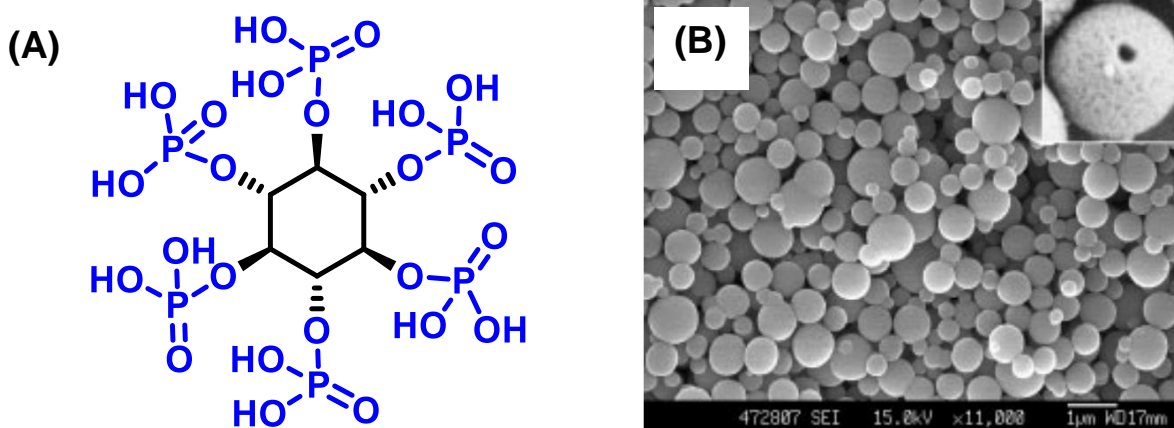
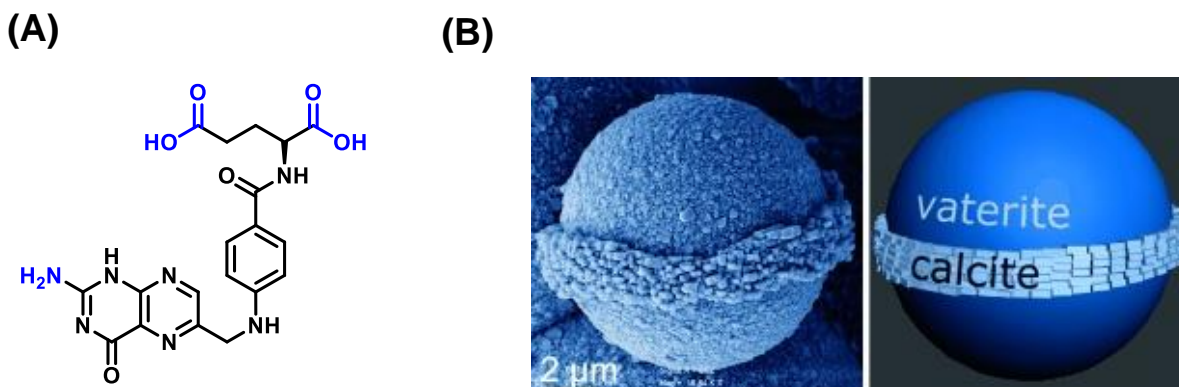


Figure 34¹⁰⁷: (A) Structure of phytic acid (B) ACC polymorphs formation in the presence of phytic acid

At calcite nucleation, the aspartic acid binding to the nucleation site is stronger than ACC, which renders its formation contributing to the stabilization and formation of ACC polymorphs.¹⁰²

Other than naturally occurring amino acids, some organic additives have also been reported to stabilize ACC polymorph of CaCO₃. One of such examples is the organic additives containing phosphorus compounds.¹⁰⁴⁻¹⁰⁶ Xu et al. in 2005 reported the use of phytic acid to stabilize the amorphous CaCO₃ microparticles.¹⁰⁷ ACC was precipitated as a hollow sphere by passing carbon dioxide gas into the solution of calcium chloride in the presence of phytic acid. X-ray diffraction and thermogravimetric analysis of the precipitates suggest the presence of ACC (**Fig. 33 B**). Phytic acid is an environment friendly organic compound used in many food additives,¹⁰⁸ it has six phosphorus atoms and twelve acidic protons (**Fig. 33 A**).

Wang et al. in 2013 conducted a study with organic additive poly(sodium 4-styrenesulfonate) and folic acid (**Fig. 34 A**) to for the formation of heterostructure where calcite and vaterite coexist.⁹² The ratio of organic additives were 1:2 (folic acid to polymer of sulfonate) used in the presence of CaCl₂ by passing carbon dioxide through the solution. Uniform microsphere formation was observed with scanning electron microscopy (SEM). Calcite crystals were equatorial on the microsphere of vaterite (**Fig. 34 B**).



3.3. Synthesis of Bisphosphonate molecules and CaCO₃ Precipitates

Characterization

3.3.1. Synthesis of bisphosphonate molecules

From literature precedence, our synthetic approach was to design bisphosphonate molecules bearing various functional groups at the distal end with different alkyl chain lengths (Fig. 36).

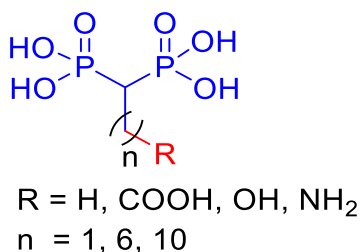
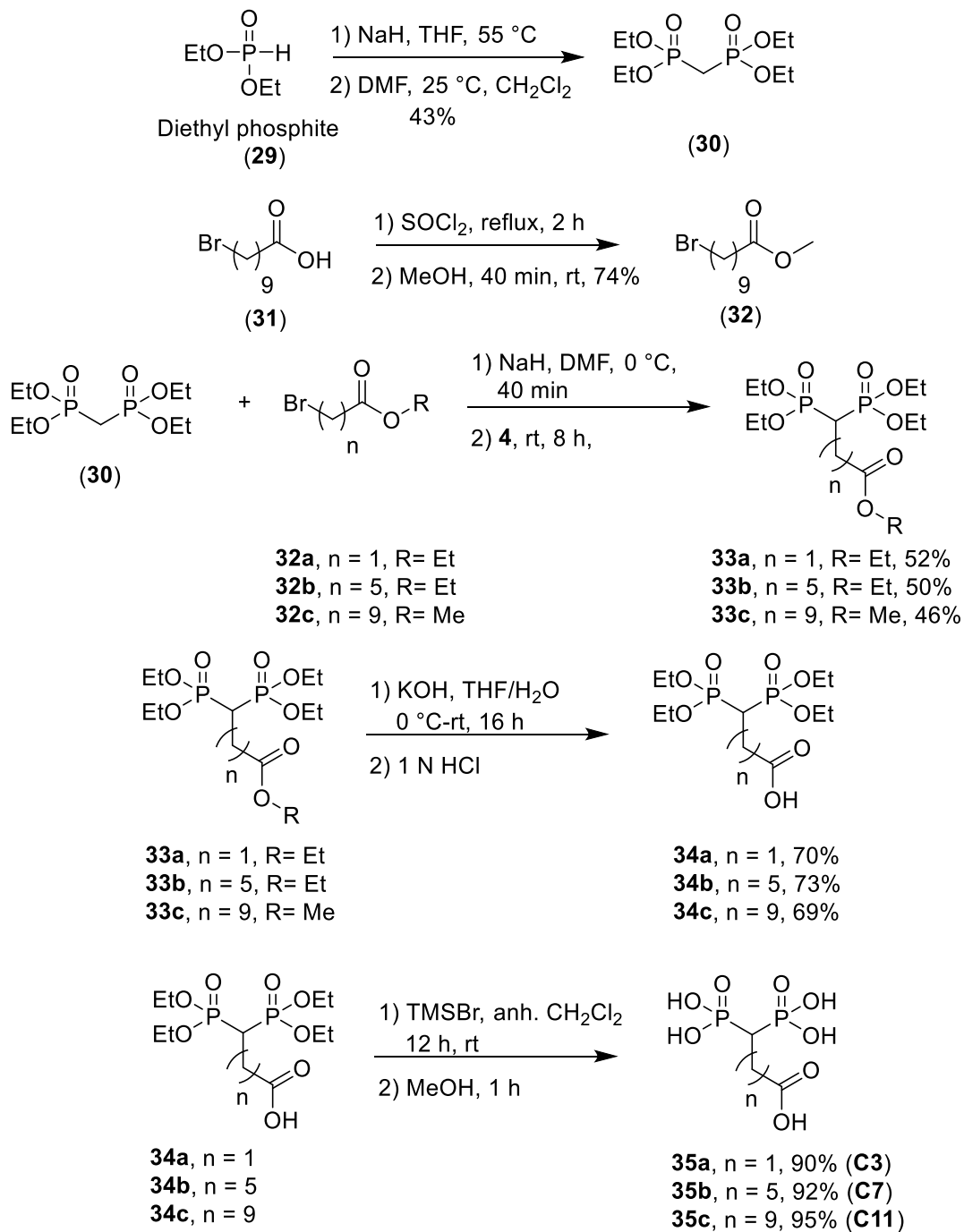


Figure 36: Bisphosphonate molecules with different alkyl chain lengths and functional groups

Commercially available, tetraethyl methylenebisphosphonate **30** was used for discovery scale synthesis but was eventually prepared from inexpensive dichloromethane and

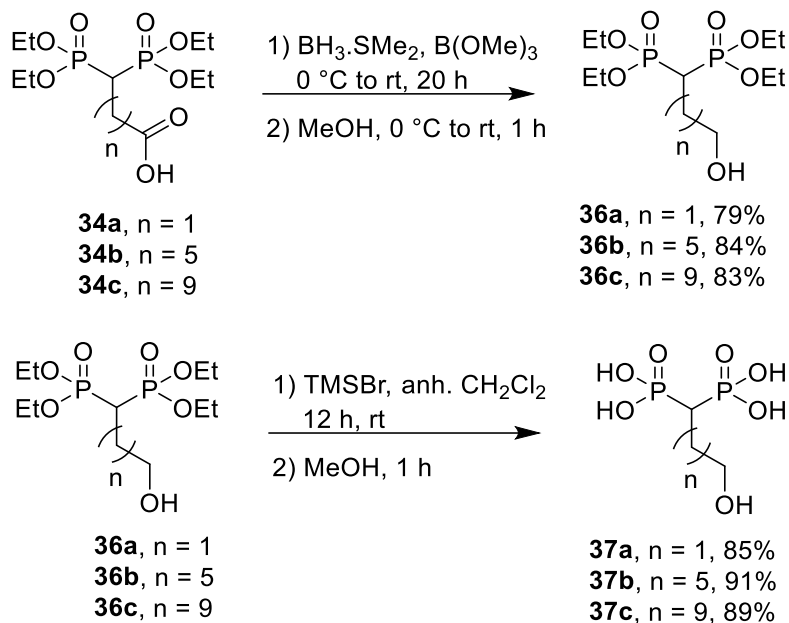
diethylphosphite **29** (**Scheme 8**) building blocks with 43% yield.¹⁰⁹ Different lengths of alkyl halides carrying acid functional groups were used to prepare alkyl substrates. Acid groups were protected as methyl ester formation. Then, the synthesized methylene bisphosphonate **30** was alkylated under basic conditions to prepare side chains of either three, seven, or eleven carbons. The method of preparation was altered based on the desired functional group incorporated at the end of the molecule. For the preparation of the acid series, after alkylation of bisphosphonate, the ester groups were hydrolyzed with KOH, lastly the ethoxy groups of phosphonate ester were deprotected using Bromotrimethylsilane (TMSBr) reagent to synthesize the final products. Towards the synthesis of the alcohol series, the acid molecules **34a-34c** were reduced using borane chemistry to set up a hydroxy group. Furthermore, the use of TMSBr gave the desired products containing hydroxy functional groups (**Scheme 9**).

Scheme 8



Scheme 8: Synthesis of bisphosphonate acid (COOH) series

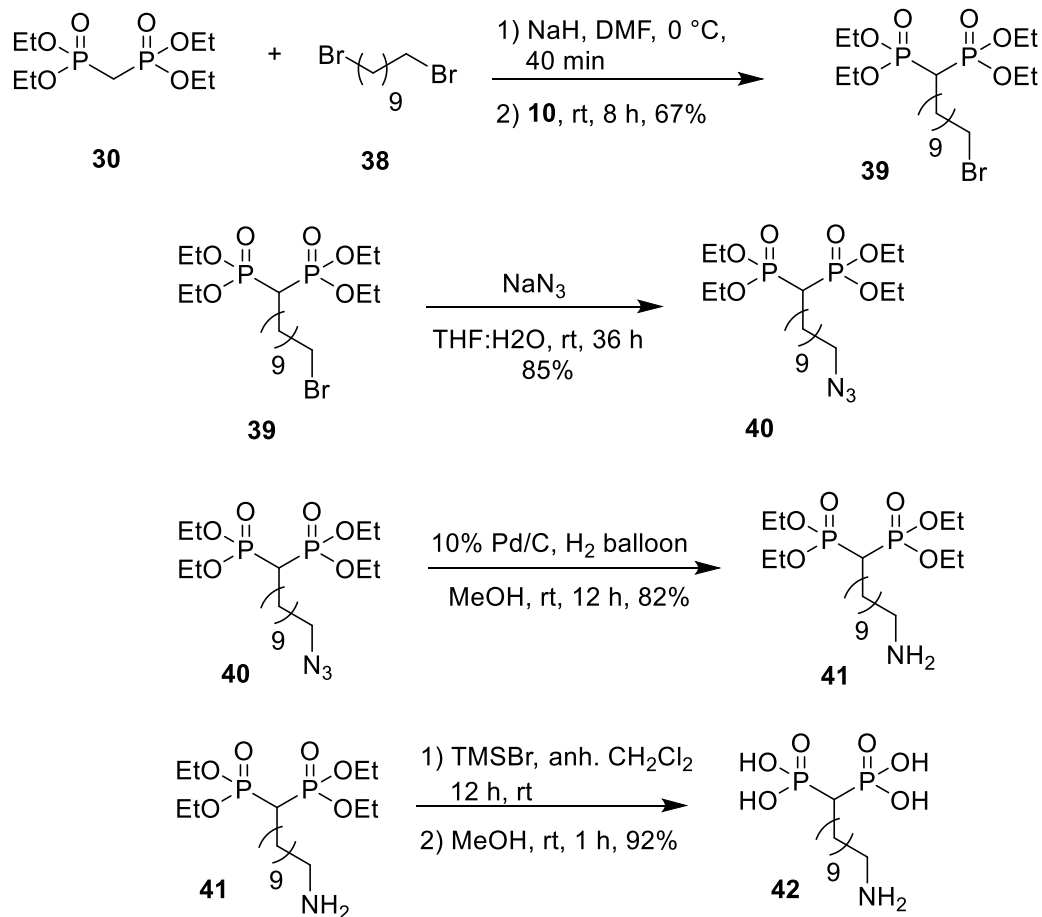
Scheme 9



Scheme 9: Synthesis of bisphosphonate alcohol (OH) series

To prepare the amine series (**Scheme 10**), bisphosphonate **30** was treated with 1,6-dibromohexanoate **38a** and 1, 10-dibromodecanoate **38b** for the synthesis of bromo bisphosphonate moieties. The bromide was then substituted by an azide group by reacting with sodium azide. Next, the azide was reduced with 10% Pd/C using hydrogen gas, which was followed by the deprotection of the bisphosphonate esters with TMSBr/MeOH to synthesize the desired molecules.

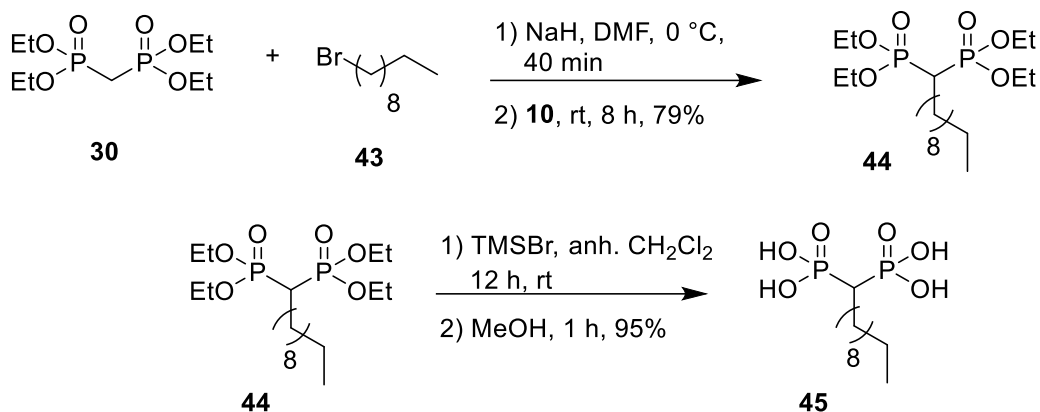
Scheme 10



Scheme 10: Synthesis of bisphosphonate amine (NH_2) molecule

In a similar manner, a bisphosphonate with no functional group at the end of the alkyl chain was also prepared. Bisphosphonate **30** was reacted with 10-bromodecane after deprotonation. Deprotection of the ethoxy groups gave the desired product with 93% yield (**Scheme 11**).

Scheme 11



Scheme 11: Synthesis of bisphosphonate non-functional group molecule

The functional groups vary by polarity and charge, whether an alcohol (polar-neutral), alkyl (non-polar, neutral), amine (polar, cationic), or carboxylic acid (polar, anionic). In all cases, the bisphosphonates were revealed by ultimate deprotection by the classic bromotrimethylsilane and methanol dealkylation method, which avoids charge build up on the deprotected bisphosphonate, leading to efficient pan-deprotection

3.3.1. Atomic force microscopy (AFM) experiments

In Situ AFM experiments were performed by Nguyen T. from Dr. La Plante's lab on calcite substrates. These were prepared by cleaving a single crystal calcite (Iceland Spar, Brazil) into plates having approximate dimensions of 1 cm × 1 cm × 1 mm (l × w × h) using a razor blade. Freshly cleaved calcite substrates were mounted on magnetic AFM discs using double-sided carbon tape to expose the calcite (104) surface. Surface was cleaned with ultra-high purity (UHP) N₂ gas to remove dust particles. For in situ experiments, the reaction solution was exposed to the AFM probe. The calcite surface was equilibrated with deionized water (Milli-Q, >18.2 MΩ·cm²) for 1 hour. After that, the calcite surface was exposed to the growth solutions by injecting a solution of CaCl₂ with a solution of NaHCO₃

and bisphosphonate molecules. The preparation of growth solutions were carried out by mixing the solution of NaHCO_3 and $\text{CaCl}_2 \cdot \text{H}_2\text{O}$ in DI water. Next, the Stock solutions of bisphosphonate molecules bearing various distal functional groups were made by simply dissolving them in deionized water. Then, this solution was transferred to NaHCO_3 . Overall solution concentration was adjusted with DI water before injecting them in the AFM instrument.

3.3.2. Conductivity experiment

T. Nguyen from Dr. Ericka La Plante's lab performed conductivity experiments with bisphosphonate additives. Super saturated growth solution of CaCl_2 and NaHCO_3 , each with a concentration of 50 mM prepared and mixed with 10 mM solution of bisphosphonate molecules. The solutions were mixed at 400 rpm for six hours contained in polypropylene centrifuge tubes. The conductivity of solutions was measured immediately after mixing the solutions after every 30 sec for a period of six hour. PuTTY software was used to collect and analyze the data. Calibration curves were used to convert the conductivity results into Ca^{2+} concentration and were plotted versus time. The precipitates were analyzed by Fourier-transform infrared spectroscopy (FTIR) and thermogravimetric analysis (TGA).

3.3.4. Computational studies

Computational Modeling of bisphosphonate molecules with calcium ions was carried out by Thanh Vuong. Density Functional Theory was used to predict the low energy conformation of various bisphosphonates with Ca^{2+} . The energy-minimized geometries and frequency analysis were computed at the ground state using M06-2X¹¹⁰ exchange-correlation functional with the 6-31G(d) basis set.¹¹¹ This basis set function 6-31G(d) was

supplemented with polarization function (d), which had one set of d functions on heavy atom.¹¹² PCM (Polarizable Continuum Model) solvation model was the default SCRF method which was applied to incorporate the aqueous solvation effect with water as the solvent.¹¹³ These functional keywords were specified in the route section to generate the low-energy molecular structure, oscillation frequency, and IR intensity. All DFT calculations were implemented in the gaussian 09 programs, and the results were visualized using Gaussview.

3.3.5. Sample preparation for critical micelle concentrations (CMC)

For CMC measurements using Du Nuoy ring the stock solution of each bisphosphonate containing acid and alcohol groups were prepared in DI water.¹¹⁴ Stock solution of 50 mM was prepared and diluted with different concentrations of 1 mM, 0.5 mM, and further down to 1 μ M. The samples were run in triplicate, and the average value was considered for CMC calculations.

3.4. Results and discussions

3.4.1 Conductivity experiment of precipitates

Conductivity experiments were performed with different chain lengths (C07 and C11) of bisphosphonate with acid (COOH) and alcohol (OH) functional groups at the other end. In the presence of bisphosphonate molecules, the rate of precipitation of calcium carbonate (CaCO_3) was higher leading to insufficient rate measurements. Calcium concentrations curves show a higher rate of precipitation in the presence of longer chain; presence of acid longer chain leads to higher rate of precipitation compared to longer chain alcohol functional group (**Fig. 37**). A relatively slow rate of precipitation was observed with C7 molecules; here, the same trend was observed, acid (COOH)

containing bisphosphonate leads to higher precipitation compared to alcohol (OH) (Fig. 37). Further experiments with short chain (C03) showed similar trends to C7 on rate of precipitation of CaCO_3 . For the control experiment, the equilibrium was achieved at about 35 mM calcium concentration over 4 hours. In the presence of bisphosphonates, the Ca^{2+} concentration lowered than the equilibrium implying the insolubility of precipitate in the presence of these additives.

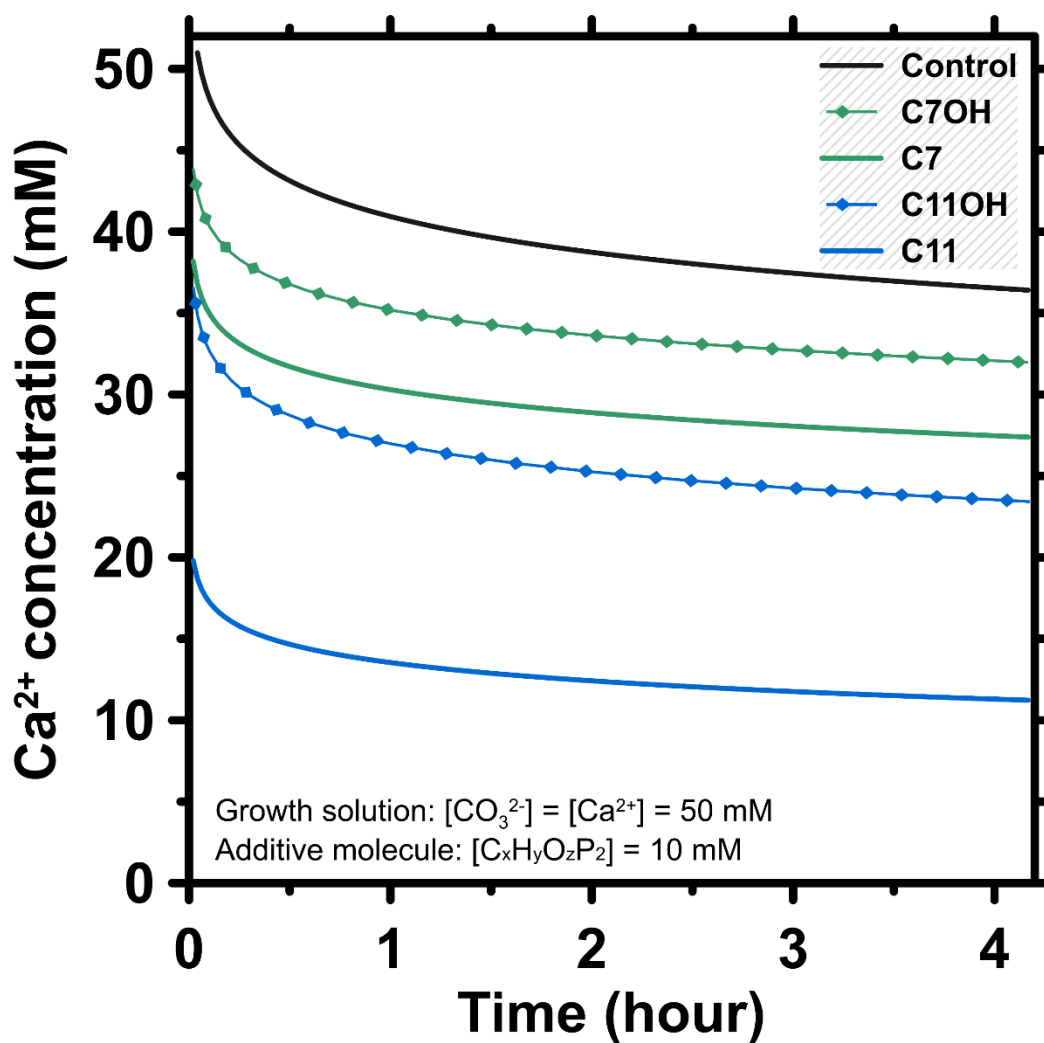


Figure 37: Bisphosphonate molecules with different alkyl chain lengths and functional groups

3.4.2. Atomic force microscopy (AFM) studies

AFM experiments were performed to investigate the effect of bisphosphonate molecules on the morphology of calcium carbonate (CaCO_3) precipitates. Step advance growth of CaCO_3 was observed on calcite substrate in the absence of bisphosphonate molecules (Fig. 38).

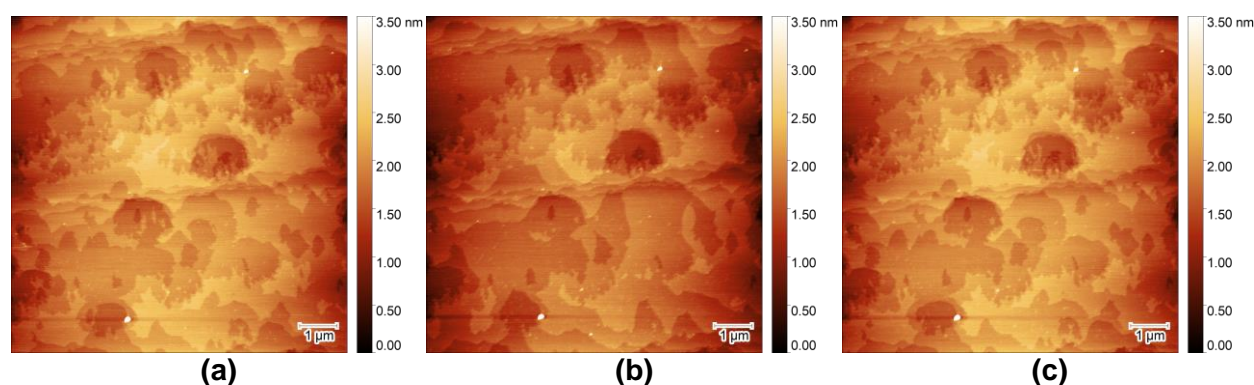


Figure 38: In situ atomic force microscopy (AFM) images of calcite surface in the presence of control solution (a) 0 min, (b) 12, and (c) 18 min.

When the bisphosphonate solution was introduced into the growth solution, rapid dissolution of calcite surface was observed with C03 and C07 chain length molecule, as the solution becomes more undersaturated suggesting the possible coordination of Ca^{2+} with the bisphosphonate moieties. During this process of calcite dissolution random nucleation was observed. Upon the introduction of C11 bisphosphonate series, rapid precipitation of CaCO_3 was observed covering the calcite surface.

AFM images presented different morphology appearances in the presence of C3, C07 series as compared to C11 regardless of distal functional groups. In the presence of short chain (C03 and C07) 2-dimensional islands/layers were observed consisting of 2-4 nm of height with COOH groups and about 10 nm in height with OH groups (**Fig. 39, 40**).

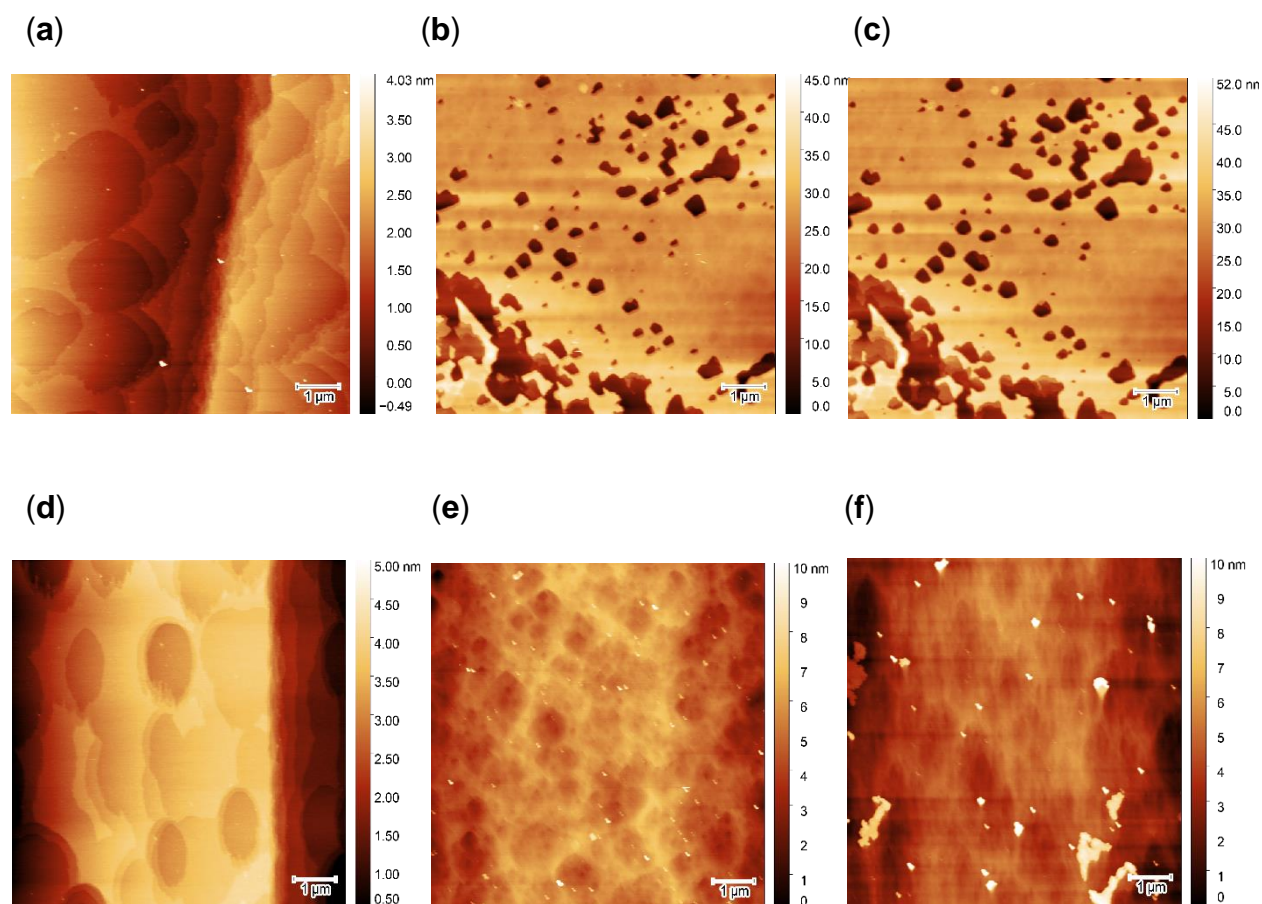


Figure 39: In situ atomic force microscopy (AFM) images of calcite surface in the presence of C3 COOH at (a) 0 min, (b) 05, and (c) 42 min. 30 nm height of islands, and in the presence of C3 OH at (d) 0 min, (e) 03, and (f) 90 min 10 nm height of islands

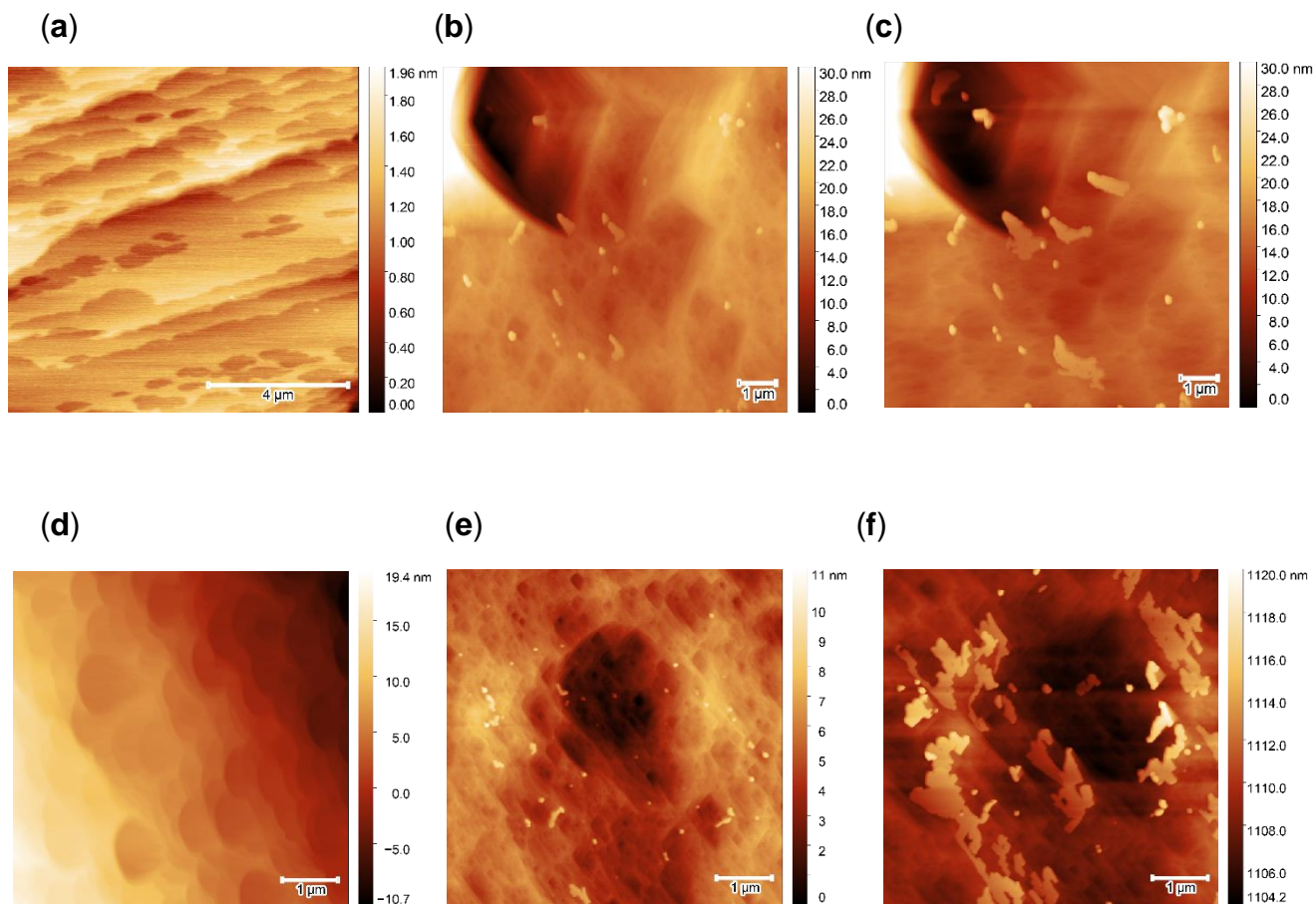


Figure 40: In situ atomic force microscopy (AFM) images of calcite surface in the presence of C7 COOH at (a) 0 min, (b) 13, and (c) 40 min. 10 nm height of islands, and in the presence of C7 OH at (a) 0 min, (b) 02, and (c) 13 min. 2-6 nm height of islands

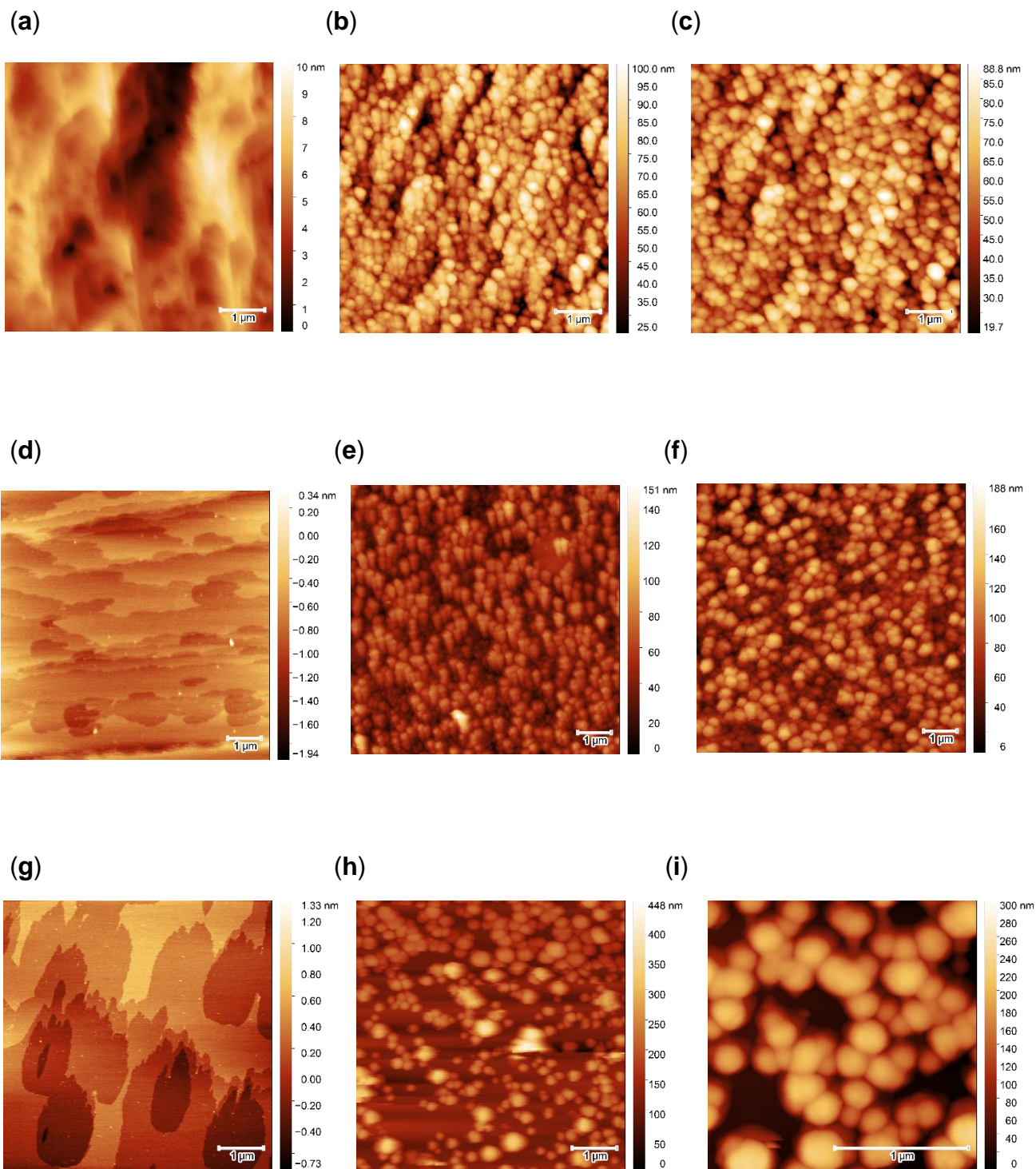


Figure 41: In situ atomic force microscopy (AFM) images of calcite surface in the presence of C11 COOH at (a) 0 min, (b) 13, and (c) 40 min. 350 nm height of islands, in the presence of C11 OH at (d) 0 min, (e)

02, and (f) 13 min. 420 nm height of islands, and in the presence of C11 non-functional at (g) 06, and (i) 23 min. 2-6 nm height of islands

A different type of CaCO_3 morphology was observed in the presence of longer chain bisphosphonate was treated. The formation of 3-dimensional islands was observed in all C11 series (COOH, OH, and non-functional) (**Fig. 41**). It suggests that the morphology of the precipitates was assigned by the chain length of bisphosphonate molecules. Short chain length (C3 and C7) give rise to 2D island, whereas longer chain length shows the formation of 3D islands.

3.4.3. Thermogravimetric analysis (TGA)

To elucidate the specific polymorph of CaCO_3 , TGA experiments were performed on the precipitates obtained after mixing of growth solution with bisphosphonate molecules. During the TGA experiments temp. range of 30 °C to 1000 °C was used for the decomposition of precipitates. Different decomposition rates were observed, indicating the presence of different polymorphs in the CaCO_3 precipitates (**Table 6**).

Table 6 Calcium carbonate polymorphs formation in the presence of bisphosphonate molecules

Content	C3 COOH		C07 COOH		C11 COOH	
	Temp. (°C)	Mass percent (%)	Temp. (°C)	Mass percent (%)	Temp. (°C)	Mass percent (%)
Water *	30 – 240	18.68	30 – 240	20.70	30 – 240	14.45
ACC/Vaterite	375 – 480	2.84	320 – 480	15.74	300 – 550	58.75
Calcite	475 – 700	37.64	475 – 700	32.68	570 – 800	16.27

(evaporable + non-evaporable) *

The presence of thermodynamic calcite, as well as kinetic polymorph ACC and/or vaterite, was observed in the formed precipitates of CaCO₃. ACC and vaterite share the same decomposition rate, so using TGA, each polymorph was indistinguishable. TGA results shows the presence of ACC/vaterite with longer chain bisphosphonate C11 COOH and C11 OH as major polymorphs and calcite as minor (**Fig. 42**). Whereas with shorter chain length, the formation of calcite was the major polymorph, and ACC/Vaterite was the minor.

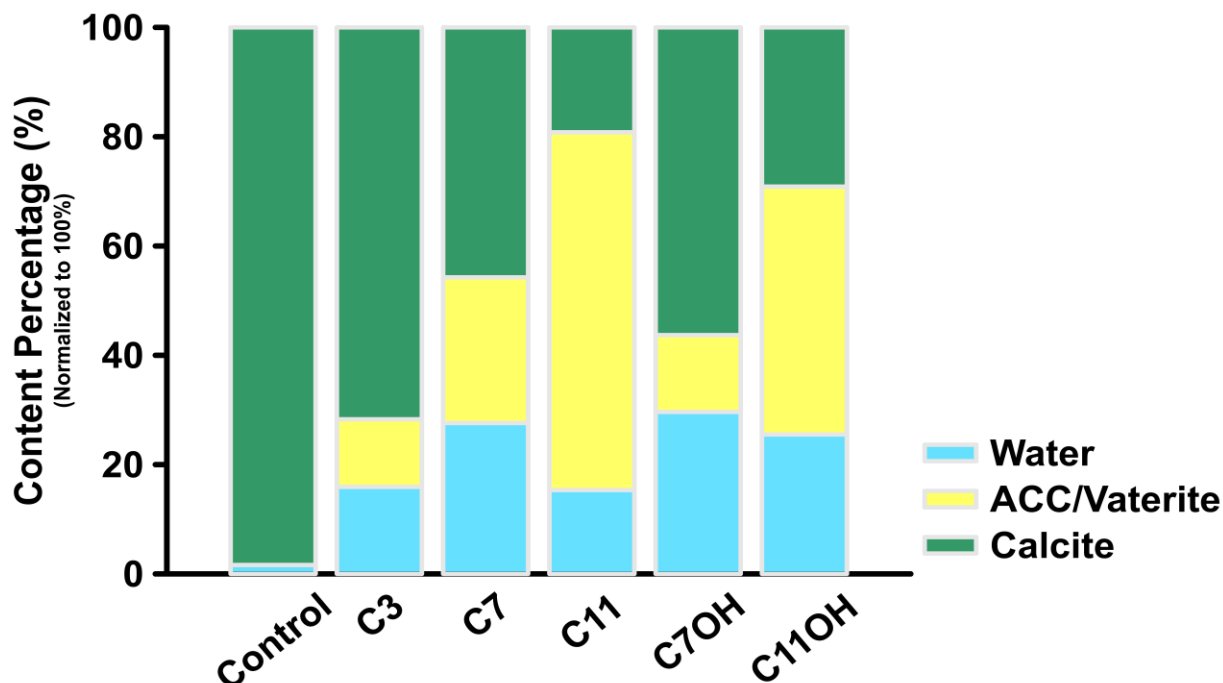


Figure 42: TGA characterization of control, C3, C7, and C11 acid (COOH); C7 and C11 hydroxyl (OH) from conductivity experiments after 6-9 months.

3.4.4. Fourier transform infrared spectroscopy (FTIR) studies of precipitates and computational model

FTIR analysis of precipitates was done to understand the binding of bisphosphonate molecules with the CaCO_3 . For this purpose, FTIR of pure molecules was compared with the solid precipitates (**Fig. 43**). A detailed study of FTIR comparison revealed expected changes in the bisphosphonate molecules upon interaction with CaCO_3 . The possible explanation could be the binding of Ca^{2+} ions with molecules, some interesting observations were the presence of C–H stretch (sp^3) around 2950 cm^{-1} in the precipitates suggesting the presence of bisphosphonate molecules. Similarly, weakening of P=O

double bond was observed as the stretching frequency moves to lower wavenumber from 1138 cm^{-1} to 1059 cm^{-1} in case of C11 COOH (Fig. 44)

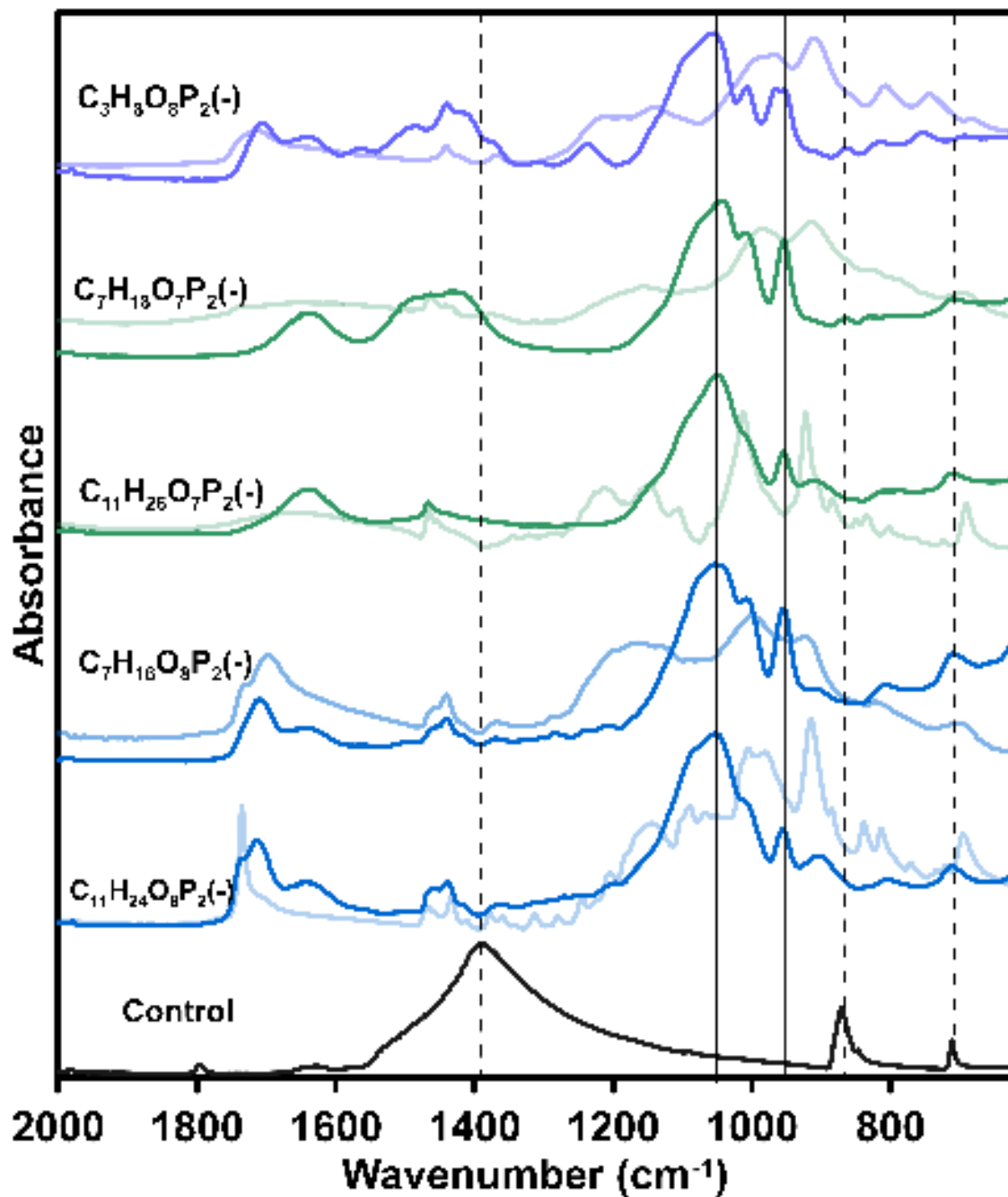


Figure 43: FTIR results of pure C3, C7 and C11 acid (COOH) series and precipitates incorporated from conductivity experiments

Figure 42. FTIR results of pure C3, C7 and C11 acid (COOH) series and precipitates incorporated from conductivity experiments

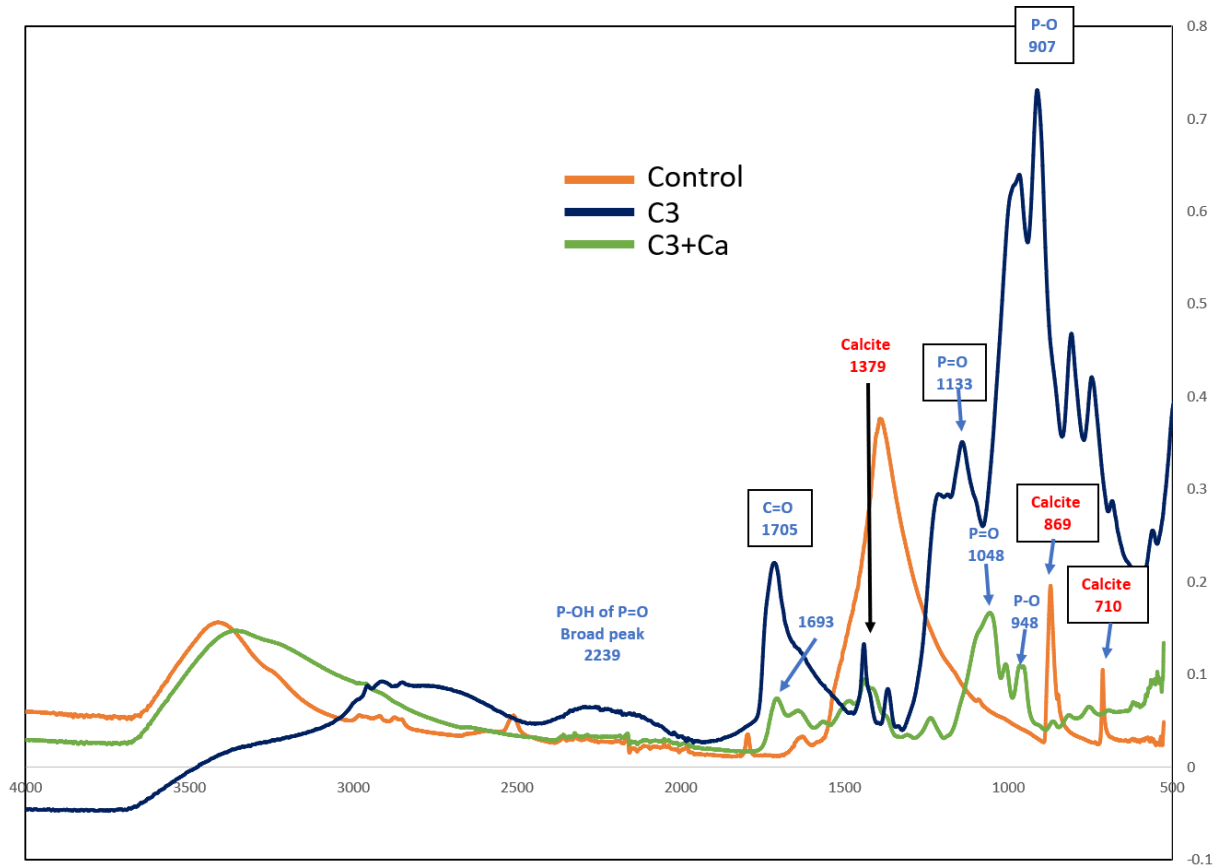


Figure 44: FTIR results of pure C3 acid (COOH), control calcite and precipitates obtained from conductivity experiments for C3 acid (COOH)

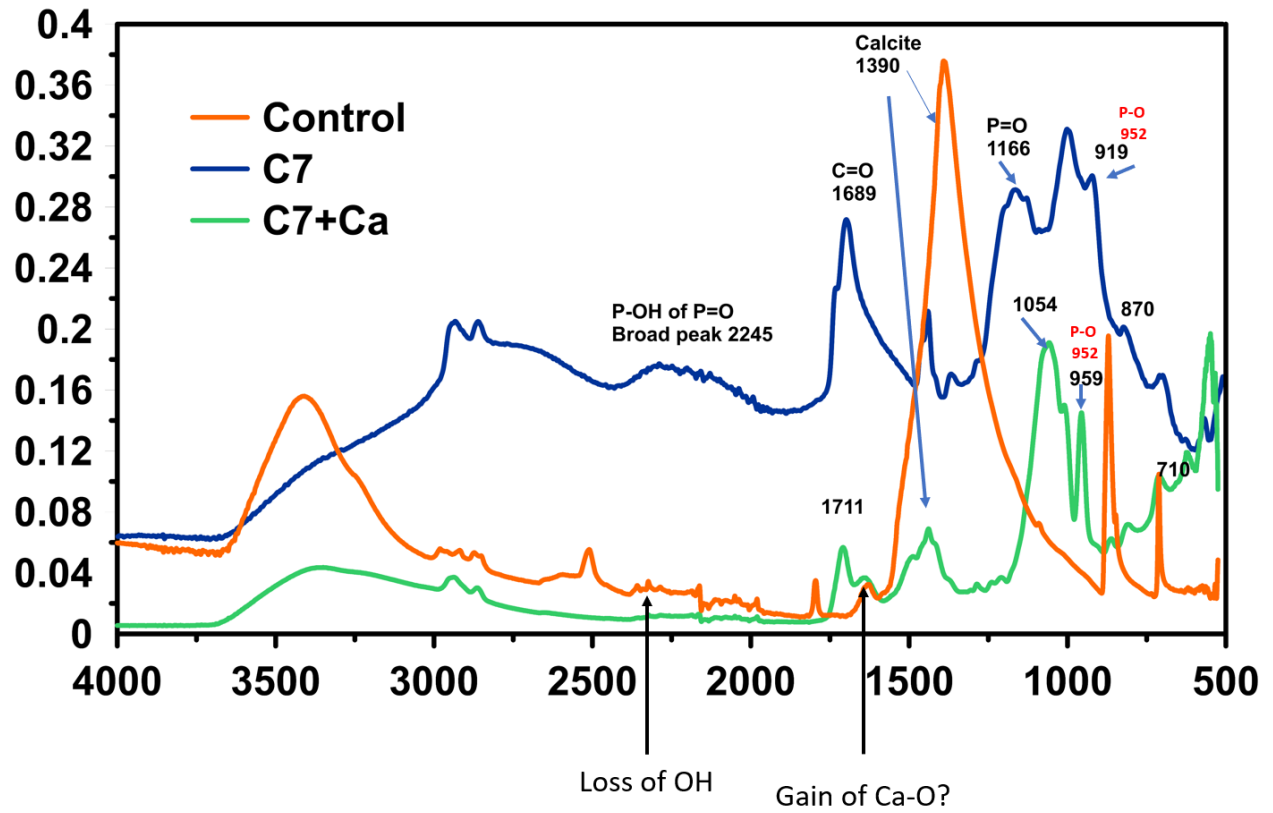


Figure 45: FTIR results of pure C7 acid (COOH), control calcite and precipitates obtained from conductivity experiments for C7 acid (COOH)

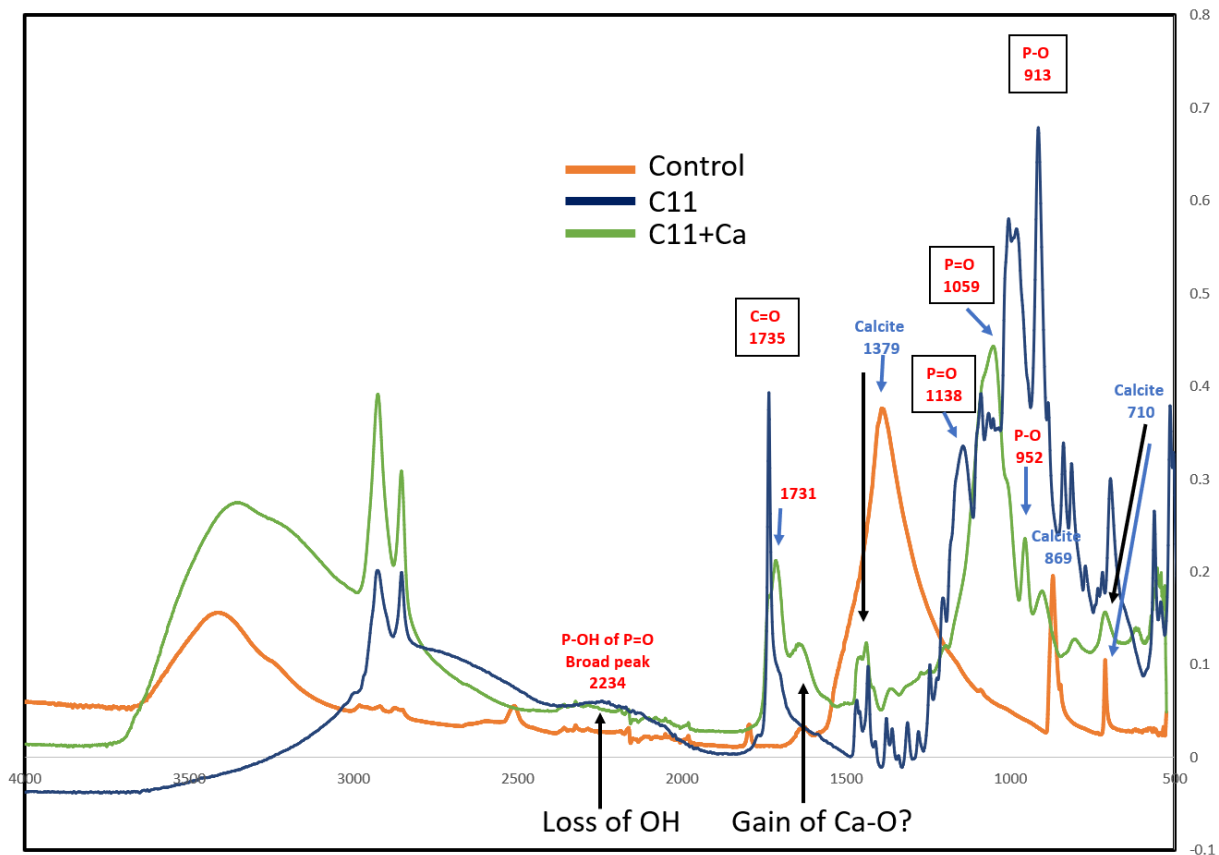


Figure 46: FTIR results of pure C11 acid (COOH), control calcite and precipitates obtained from conductivity experiments for C11 acid (COOH)

Also, strengthening of P–O single bond was observed as the corresponding peak shifts to higher wavenumber such as in case of C11 from 913 cm⁻¹ to 952 cm⁻¹. Results were similar in all the bisphosphonate-incorporated precipitates of CaCO₃ (**Fig 45, 46**). Bisphosphonate with distal COOH group, there was no change observed in the FTIR frequency of carbonyl, it remained unchanged, evident of its inability to participate in binding with Ca²⁺ ions.

Based on these observations it was hypothesized that the binding of Ca^{2+} with the bisphosphonate might possibly be occurring via model **A** instead of **B** (Fig. 47)

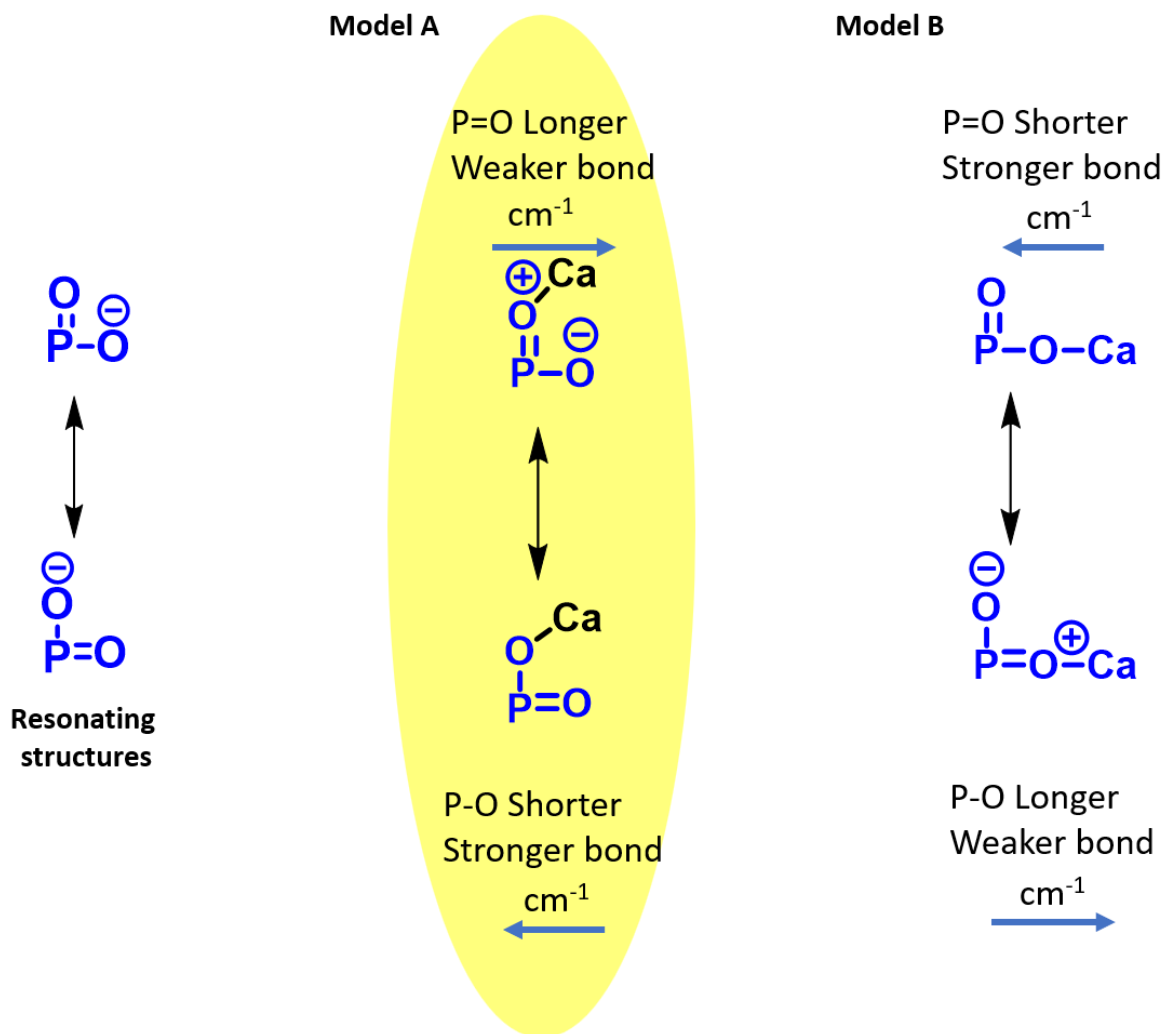
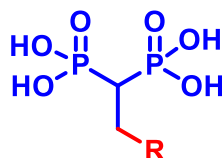


Figure 47: In the presence base NaHCO_3 , the possible resonating structures of phosphonate group. Model A: binding of calcium via top oxygen, Model B: binding of calcium via side arm oxygen

3.4.5. pKa and logP values from online source

Bisphosphonate molecules contain four acidic protons, and the pKa of standard bisphosphonates has been reported as seen in **Fig. 48**.¹¹⁵ Certainly, the 1st and 2nd dissociation occur on alternating phosphonate (PO₃H₂) subunits.



1st pKa = 1.35
2nd pKa = 2.87
3rd pKa = 7.03
4th pKa = 11.3

R = COOH, pka about 4.7

Figure 48: Different pKa values of bisphosphonate associated protons

Since pKa greatly influences different physical parameters such as solubility, lipophilicity, and binding of molecules, ChemAxon –an online available source –was used to estimate the pKas of all bisphosphonate molecules (**Table 7**).¹³²

ChemAxon predicted the pKa values of molecules within the range of literature values for all possible states. Negative lipophilicity (LogP) values indicate the high solubility in aqueous media compared to the organic phase.

Table 7 pKa prediction of bisphosphonate molecules using ChemAxon online source

Functional group		1 st pKa	2 nd pKa	3 rd pKa	4 th pKa	5 th pKa	Lipophilicity logP
COOH	C03	1.2	1.96	4.54	7.99	8.7	-3.03
	C07	1.21	1.97	6.55	7.98	8.68	-1.79
	C11	1.21	1.97	4.95	7.87	8.58	-2
OH	C03	1.21	1.97	7.87	8.58	15.99	-3.25
	C07	1.21	1.97	7.87	8.58	-1.99 (strongest basic pKa)	-2.00
	C11	1.21	1.97	7.87	8.58	-1.99 (strongest basic pKa)	-0.42
CH ₃	C11	1.21	1.97	7.87	8.58	N/A	1.03

3.4.6. Computational binding studies

Computational binding studies was done by Thanh Vuong of our laboratory. Density functional theory was used to identify the possible binding modes of all the synthesized molecules with Ca²⁺ ions. Considering the pka values from the literature¹¹⁵ and calculated from online sources, it was assumed that the overall charge state of bisphosphonate bearing acid (COOH) functional groups as -ve 4 and with all others as -ve 3 in the presence of base NaHCO₃ (**Fig. 49**).

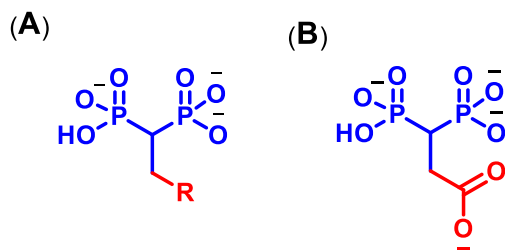


Figure 49: (A) Overall charge -ve 3 (B) Overall charge -ve 4

First trials were done by placing the Ca^{2+} at different special locations around C11 COOH and C3 COOH molecules to calculate the minimum binding energy (**Fig. 50, 51**). For longer chain C11 different binding modes suggest the preferred binding via mode A (**Fig. 50**).

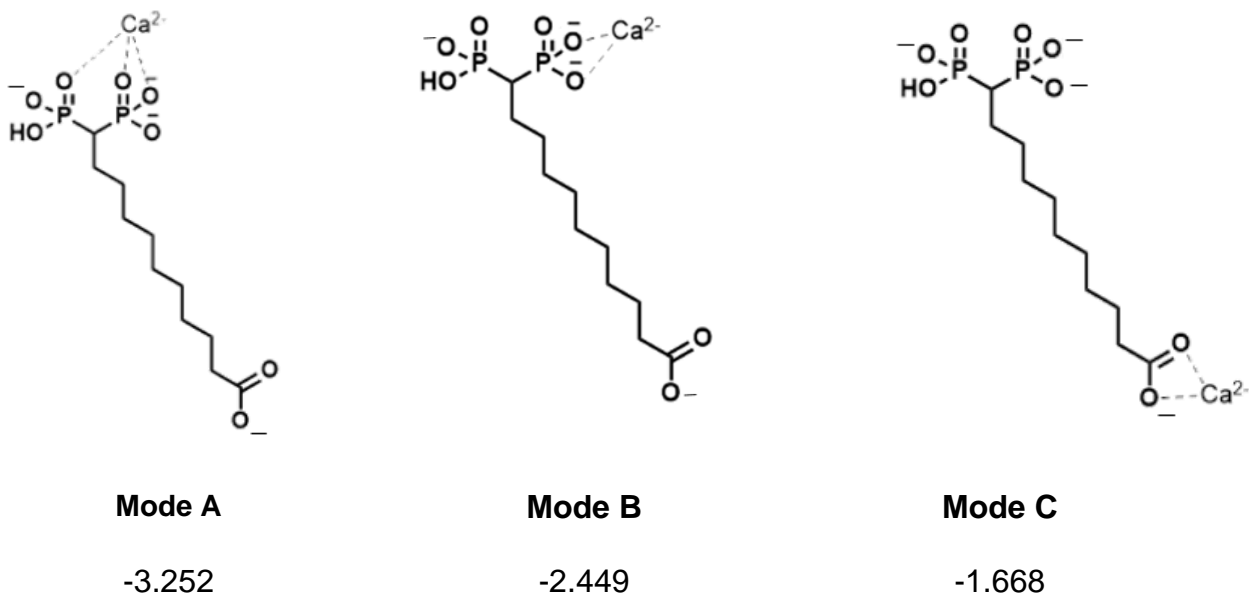


Figure 50: Different modes of bisphosphonate C11 COOH binding with Ca^{2+} . Mode A is the lowest energy

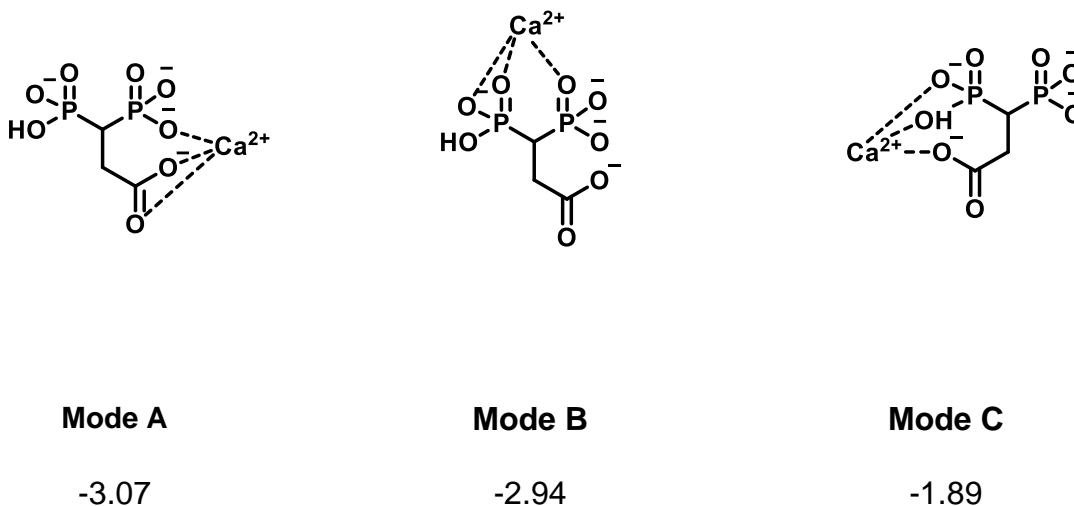


Figure 51: Different modes of bisphosphonate C03 COOH binding with Ca^{2+} . Mode A is the lowest energy

With a longer chain, mode A was preferred so further calculations with C11 OH and non-functional group molecule were done in a similar fashion. The computed values of all the longer chain molecules are comparable with no significant change in values (**Fig. 52**).

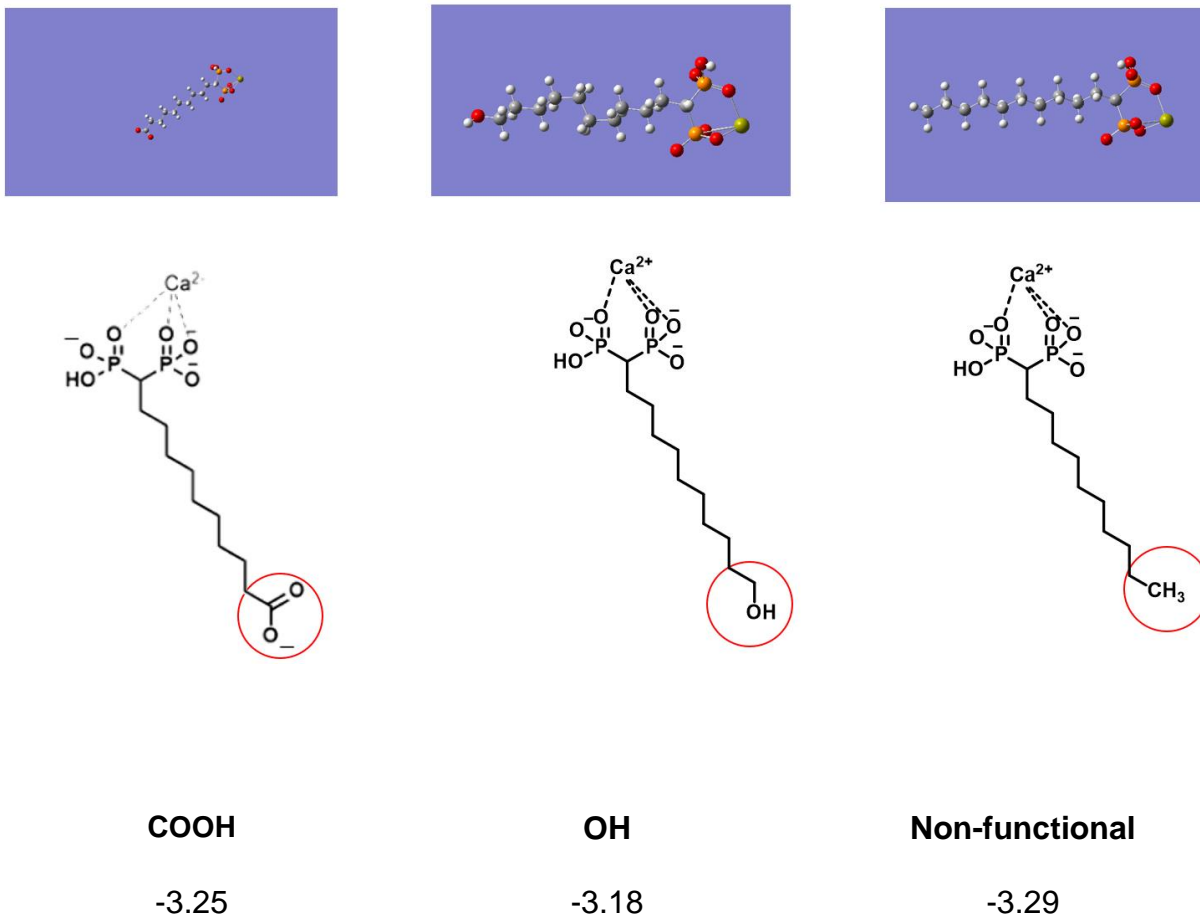


Figure 52: Comparison of binding energies of longer chain bisphosphonate with Ca^{2+}

Different modes of binding of longer chain versus shorter chain could presumably be the reason for the formation of major ACC polymorphs with longer alkyl chain as compared to calcite formation with shorter chain regardless of functional group presence.

3.4.7. Critical micelle concentration (CMC) results

A longer alkyl chain could form micelle in aqueous media. To determine this property of bisphosphonate molecules, Du Nuoy ring method was applied to determine CMC of all the bisphosphonate molecules. Initially, C3, C7 and C11 acid (COOH) of bisphosphonate series was used to determine their CMC values (Fig. 53).

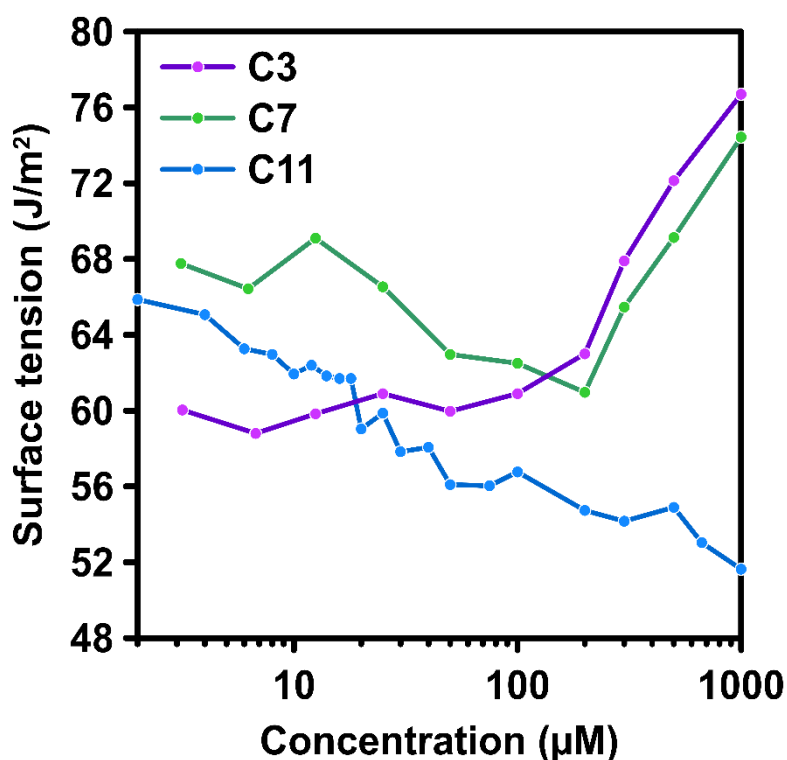


Figure 53: CMC calculations of C3, C7, and C11 acid (COOH) series of bisphosphonate

For C3 molecule it was observed that the surface tension is increasing as the concentration of the solution was increasing. Same effect was observed when the surface tension of sodium chloride solution was measured. This reflects that C3 is more behaving like an electrolyte. Whereas, for C11 (longer alkyl chain) it was observed that the surface

tension of the solution decreases as the concentration of the solution was increasing (Fig. 54). After the solution hits CMC the surface tension remains almost uniform. The CMC for C11 molecule was calculated as 39 μM , comparable with the literature CMC values of bisphosphonate molecules giving rise of micelle formation.¹¹⁵

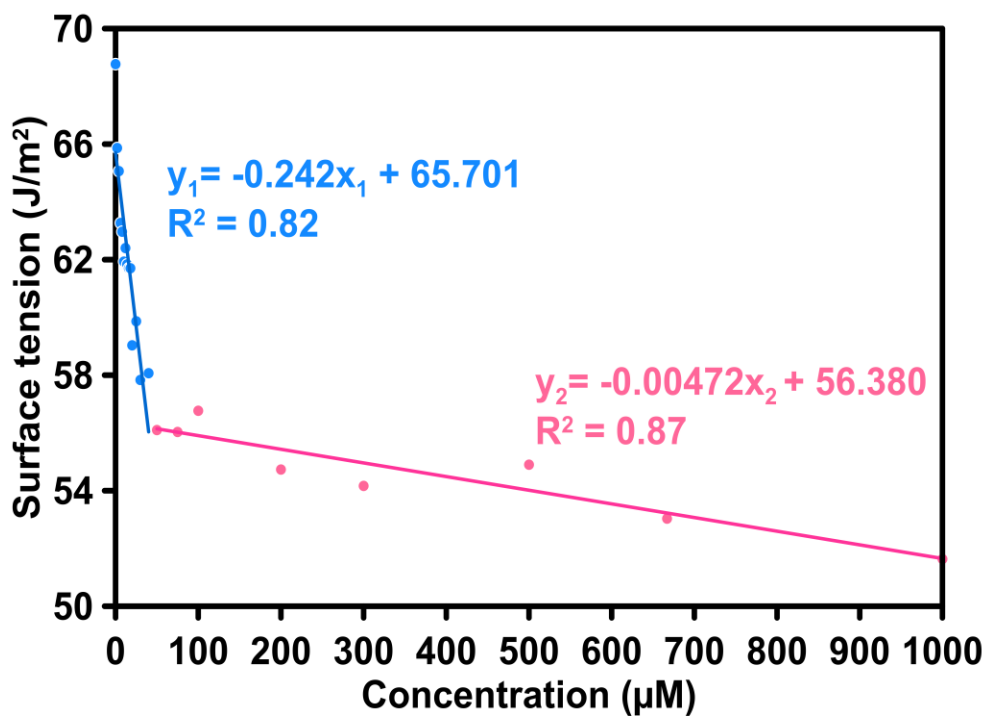


Figure 54: CMC calculations of bisphosphonate C11 acid (COOH) molecule

3.5. Conclusion

The synthesis of bisphosphonate molecules was done bearing a distal functional groups acid (COOH), alcohol (OH), and non-functional groups. These molecules were used for the precipitation of calcium carbonate to stabilize its kinetic polymorph ACC/Vaterite. Conductivity experiments were performed to obtain the precipitates and for quantification of calcium ions present in the solution. Characterization of precipitates was done with different techniques. *In situ* AFM experiments revealed the formation of different morphology with short chain as compared to bisphosphonate molecules with longer chain. Further characterization of precipitates with FTIR TGA presents the formation of kinetic polymorph ACC/Vaterite with longer alkyl chain and thermodynamic calcite formation with short alkyl chain (C3, C7). The computational binding model correlated with FTIR suggesting different binding modes of short and long alkyl chain molecules with CaCO₃. CMC results evidently indicated the micelle formation assisting the formation of kinetic polymorph. In this study, longer alkyl chain bisphosphonate molecules were able to stabilize kinetic polymorph ACC/Vaterite over calcite.

Chapter 4

4.1. Future Directions

4.1.1. Synthesis of new PCDA derivatives

In some reports it has been observed that PCDA colorimetric property can be reversible, first changing to purple or red in the presence of an analyte, then returning to blue as the analyte is washed away.¹¹⁶ From literature, it's observed that modifying the PCDA carboxylic head group with phenyl rings or with linear linker consisting of a number of heteroatoms in it, have the potential for reversibility in the system.¹¹⁷⁻¹²² Presumably, these ester/amide substituents provide a compensating series of intramolecular forces that can return the PDA sensor to its original configuration.

Synthesis of these new biosensor monomers into our PCDA-antibiotic system could make it reversible. This reversibility is of great importance as it can help to reduce the usage of material as the biosensing material would have the ability to reuse giving the possibility of greener biosensor. Some of the PCDA monomers we plan to synthesize are presented in (Fig. 55)

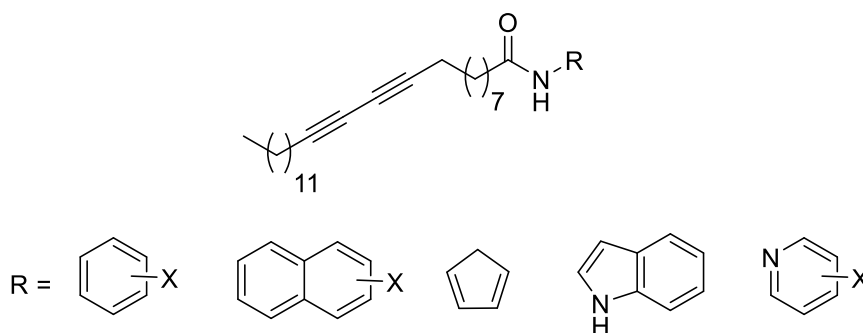


Figure 55: Proposed PCDA monomers

4.1.2. Stability of PCDA-peptide for detection of *MRSA*

The developed PCDA-peptide system, while functional, suffers from some stability issues, as the color change and precipitation were observed in the presence of non-target bacteria and sometimes even in the control system at certain temperatures and lengths of time. Mechanistically the color change in the PCDA is because of the tilt in the backbone in the presence of target ligand.¹¹⁶⁻¹¹⁸ This tilt can be delayed by the incorporation of lipid molecules (additional monomers) in the system.³² Possible lipids used to incorporate into the system are in **Fig. 56**.

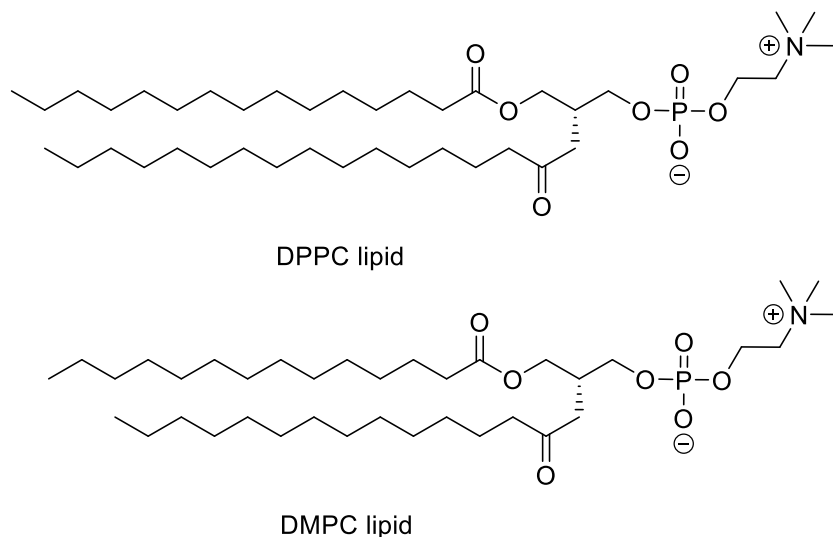


Figure 56: Different lengths of lipid monomers to stabilize PCDA-peptide

Introduction of these lipid monomers into the PCDA-peptide system can enhance the stability of the entire system by making the backbone of en-yne in the PDA more rigid.

4.2. Modification of DA linker

4.2.1. DA modification with maleimide ethylene amine linker

To create some flexibility in the gelation and to assist DA linker coupling with peptide having thiol group at the end, we planned to modify DA linker with maleimide linker on both sides (**Fig. 57**). From Dieglmann⁵³ and Dr. Chen's studies⁷⁹ it was observed that in some studies with Peptide-DA-peptide forming gelation was giving hard gel and/or the colorimetric response was not observed. So, with the modified DA molecule there might be a possibility to create gel with desired properties by attaching short spacer/linker in it.

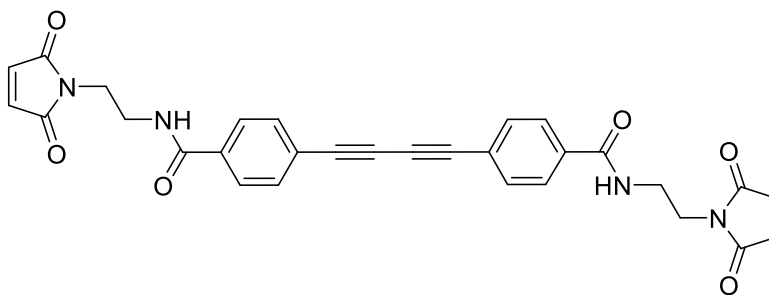


Figure 57: DA modification with maleimide

With the similar goal, we planned to synthesize linear DA linkers and investigate their polymerization and other associated properties (**Fig. 59**).

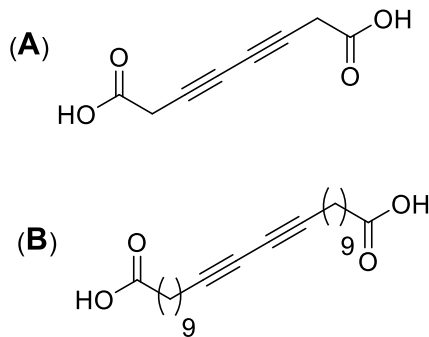


Figure 58: (A) short linear diacetylene (B) Long linear diacetylene molecules

4.3. Calcium carbonate precipitation

4.3.1. Bisphosphonate with Amine functional group

Bisphosphonate with acid (COOH) and alcohol (OH) functional group have been investigated for calcium carbonate precipitation. Next, bisphosphonate with NH₂ at the other end have been synthesized (**Fig. 57**) their rate of precipitation on CaCO₃ needs to be tested.

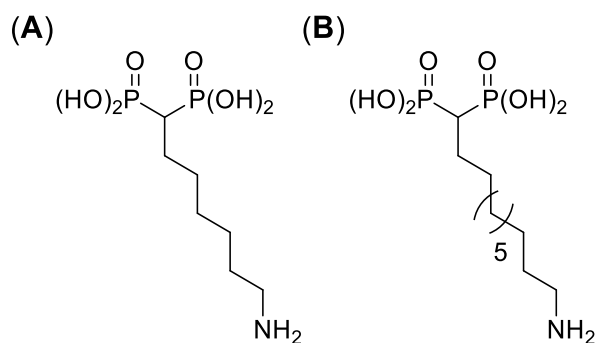


Figure 59: (A) C07 chain length (B) C11 carbon chain length

Chapter 5

General Experimental Procedure - Biosensor

All reagents were used as purchased from Alfa Aesar, Acros Organics and Sigma-Aldrich. 10, 12-Pentacosadiyonic acid was purchased as 98% grade from Alfa Aesar. Vancomycin hydrochloride, Molecular Biology Grade Powder was purchased from Alfa Aesar. All reactions were carried out under nitrogen atmospheric conditions unless otherwise stated. ^1H NMRs were recorded on 300 and 500 MHz spectrometers and referenced to the internal solvents (7.26 ppm in CDCl_3 or 2.5 ppm in $\text{DMSO-}d_6$ or 3.3 ppm in CD_3OD or 4.65 ppm D_2O). ^{13}C $\{^1\text{H}\}$ NMRs were recorded on 75 and 125 MHz spectrometers and referenced to the internal solvent signals (central peak 77.00 ppm CDCl_3 or 39.5 $\text{DMSO-}d_6$ 39.0 CD_3OD). NMR data are reported as: chemical shift (in ppm, δ), integration, multiplicity (s = singlet, d = doublet, t = triplet, q = quartet, m = multiplet, br = broad), coupling constant (in Hz, J). Thin layer chromatography was performed in silica gel coated aluminum plates (EMD Merck F254, 250 mm thickness). Also, TLC silica gel 60 RP-18 F254S was used for polar compounds. 254 nm ultraviolet light and ninhydrin stain (for amine containing molecules) and phosphomolybdic acid (PMA) used for general chemical stain. Flash column chromatography was performed over Silicycle SilicaflashP60 silica gel (mesh 230-400) or standard grade activated Alumina (mesh 50-300). C18-Reversed phase silica gel (fully end capped) was used for column chromatography of polar compounds. HRMS (high resolution MS) data were collected by time-of-flight mass analysis in the Shimadzu Center for Advanced Analytical Chemistry at UT Arlington. LC/MS-8080 triple quadrupole LC/MS/MS was also used from Shimadzu Center for Advanced Analytical Chemistry at UTA Arlington to acquire the mass. For

photospectroscopy characterization UV-Vis experiments were carried out in a Cary 50 Scan Spectrometer from Varian at 25 °C and Fluorescence experiments were performed in a Cary Eclipse Fluorescence Spectrophotometer from Agilent Technologies (Product Number G8800A) at 25 °C. Unless otherwise specified, instrumental set up includes: PMT detector voltage = High, Excitation filter = Auto, Emission filter = Open. All UV-Vis and Fluorescence measurements were taken using Buck Scientific type 18 quartz micro cuvette with 10 mM path length.

Synthesis of 10,12-Polydiacetylene N-hydroxysuccinimide (NHS-PCDA) ester (3)¹²³

376 mg (1 mmol) of 10, 12-pentacosadiionic acid (PCDA **1**) was dissolved in 5 ml of dichloromethane. In the stirred solution of PCDA **1**, 129 mg (1.12 mmol) *N*-hydroxysuccinimide (NHS **2**), and 224 mg (1.17 mmol) 1-ethyl-3-(3-dimethylaminopropyl) carbodiimide (EDC·HCl) were added. The solution was stirred under nitrogen gas for 4 hours at room temperature. The solvent was evaporated under vacuo and the product was extracted using 13 mL ethyl acetate and it was washed with water four times. The organic layer was dried over magnesium sulfate and filtered [16]. The product obtained was white powder 329 mg 70% yield. ¹H NMR (500 MHz, CDCl₃) δ 2.82 (s, 4H), 2.58 (t, *J* = 7.4 Hz, 2H), 2.22 (t, *J* = 6.8 Hz, 4H), 1.82 – 1.65 (m, 2H), 1.59 – 1.45 (m, 4H), 1.40 – 1.14 (m, 25H), 0.86 (t, *J* = 6.8 Hz, 3H); ¹³C NMR (125 MHz, CDCl₃) δ 169.3, 168.7, 77.7, 77.5, 65.4, 65.3, 32.0, 31.0, 29.7, 29.7, 29.7, 29.5, 29.4, 29.2, 28.9, 28.9, 28.8, 28.8, 28.4, 28.4, 25.7, 24.6, 22.8, 19.3, 19.2, 19.2, 14.2

Synthesis of N-(2-(2-(2-aminoethoxy)ethoxy)ethyl)pentacosa-10,12-diyamide (PCDA-EDEA) (5a)¹²⁴:

In an oven dried round bottom flask containing 40 mL of anhydrous dichloromethane 0.95 g (6.4 mmol) EDEA (2,2-(ethylenedioxy)-bis-(ethylamine **4a**)) was added. In a separate flask, 300 mg (0.64 mmol) of PCDA-NHS (**3**) was dissolved in 5 mL methylene chloride. This solution was added dropwise into the stirred solution of **4a** and the reaction mixture was stirred for 6 hours at room temp. The solvent was evaporated under vacuo to obtained white precipitates. The product was purified with silica column chromatography using a gradient solvent system (3-10% methanol/ dichloromethane). Product was obtained 168 mg (57% yield) as a blue precipitates as compared with literature. ^1H NMR (500 MHz, CHLOROFORM-*D*) δ 6.57 (t, J = 5.7 Hz, 1H), 3.61 (d, J = 5.0 Hz, 4H), 3.55 – 3.47 (m, 3H), 3.42 (h, J = 4.9 Hz, 2H), 2.96 (t, J = 7.6, 5.1 Hz, 2H), 2.19 (dt, J = 18.6, 7.4 Hz, 6H), 1.59 (t, J = 7.5 Hz, 2H), 1.48 (pd, J = 7.0, 3.8 Hz, 4H), 1.41 – 1.14 (m, 27H), 0.85 (t, J = 6.9 Hz, 3H). ^{13}C NMR (126 MHz, CDCl_3) δ 173.7, 77.7, 77.6, 71.3, 70.3, 70.2, 70.2, 65.4, 65.3, 41.1, 39.3, 36.7, 32.0, 29.4, 29.7, 29.7, 29.5, 29.4, 29.4, 29.3, 29.2, 29.1, 28.9, 28.9, 28.4, 28.4, 25.8, 22.8, 19.3, 19.3, 14.2.

Synthesis of N-(2-hydroxyethyl)pentacosan-10,12-diyamide (PCDA-OH) (5b**):**

In a dried round bottom flask containing solution of 0.23 mL (3.8 mmol) ethanolamine **4b** in 10 mL of anhydrous methylene dichloride was added 0.1 g (0.21 mmol) of PCDA-NHS solution in 5 mL methylene dichloride. The reaction mixture was stirred for 16 hours. The solvent was evaporated in vacuo and solid was subjected to flash chromatography, the product was purified with 2% MeOH in methylene dichloride solvent system. 38 mg (70%) yield of product was obtained as white solid as compared with literature. ^1H NMR (301 MHz, CDCl_3) δ 5.99 (s, 1H), 3.72 (t, J = 5.0 Hz, 2H), 3.42 (q, J = 5.3 Hz, 2H), 2.84 (s, 1H), 2.22 (dt, J = 11.7, 7.2 Hz, 6H), 1.78 – 1.13 (m, 32H), 0.88 (t, J = 6.4 Hz, 3H). ^{13}C NMR (126

MHz, CDCl₃) δ 175, 77.7, 77.5, 65.3, 62.6, 42.5, 36.7, 32.0, 30.1 – 29.4 (m), 29.4 – 29.1 (m), 29.1 – 28.6 (m), 28.4, 25.7, 22.8, 19.3, 14.2.

Synthesis of *N*-(2-aminoethyl)-10,12-pentacosadiynamide (5c):

In a 50 mL RBF containing 1 mL (15 mmol) solution of ethylene diamine **4c** in anhydrous methylene dichloride at 0 °C was added 0.15 g (0.31 mmol) PCDA-NHS (**3**) dropwise and the mixture was stirred for 8 h, at room temp. The solvent was rotary evaporated and the solid obtained was redissolved in dichloromethane. The solution was washed with saturated sodium chloride and water multiple times to get rid of excess ethylene diamine. The solution was dried over anhydrous MgSO₄. The solvent evaporated in vacuo and the crude product was purified with 10% methanol in dichloromethane. Product isolated as white solid 0.12 g 80% yield compared with literature. ¹H NMR (500 MHz, CDCl₃) δ 3.30 (dd, *J* = 11.7, 5.8 Hz, 2H), 2.83 (t, *J* = 5.9 Hz, 2H), 2.31 – 2.18 (m, 4H), 2.19 (dd, *J* = 18.2, 10.7 Hz, 2H), 1.62 (m, 2H), 1.56 – 1.45 (m, 12H), 1.41 – 1.18 (m, 28H), 0.88 (t, *J* = 6.9 Hz, 3H). ¹³C NMR (126 MHz, CDCl₃) δ 174.3, 77.7, 77.5, 65.4, 65.3, 40.7, 36.7, 32.0, 29.7, 29.7, 29.7, 29.6, 29.5, 29.4, 29.3, 29.2, 29.1, 29.1, 29.0, 28.9, 28.9, 28.5, 28.4, 25.7, 22.8, 19.3, 14.2.

Synthesis of *N*-(3-(1H-imidazol-1-yl)propyl)pentacosa-10,12-diynamide (5d)

In 10 mL anhydrous methylene dichloride was added 0.5 mL (4.2 mmol) of **4d**, to the above stirred solution was slowly added 0.30 g (0.64 mmol) solution of PCDA-NHS (**3**) at room temp. The reaction was stirred for 16 h then solvent was evaporated in vacuo and the precipitate was subjected to flash chromatography 5% methanol in dichloromethane solvent. 0.22 g of white solid product was obtained with 72% and was compared with

literature. ^1H NMR (500 MHz, CDCl_3) δ 7.47 (s, 1H), 7.05 (s, 1H), 6.94 (s, 1H), 3.99 (t, $J = 7.0$ Hz, 2H), 3.26 (q, $J = 6.6$ Hz, 2H), 2.23 (t, $J = 7.0$ Hz, 4H), 2.17–2.11 (m, 2H), 2.03–1.96 (m, 2H), 1.60 (p, $J = 7.3$ Hz, 2H), 1.50 (dhept, $J = 11.3, 4.1$ Hz, 4H), 1.40–1.19 (m, 27H), 0.88 (q, $J = 8.0, 7.1$ Hz, 3H). ^{13}C NMR (126 MHz, CDCl_3) δ 173.9, 137.1, 129.3, 119.1, 77.7, 77.4, 65.4, 44.6, 36.5, 31.9, 31.3, 29.8 – 29.6 (m), 29.5, 29.3 (dd, $J = 21.4, 9.8$ Hz), 29.1 – 28.7 (m), 28.4, 25.8, 22.7, 19.2, 14.17.

Synthesis of vancomycin monomer from N-(2-(2-(2-aminoethoxy)ethoxy)ethyl)pentacosanoic acid (PCDA-EDEA) and vancomycin (7) ⁴⁸:

Vancomycin.HCl (**6**) 235 mg (0.158 mmol), EDC·HCl 31 mg (0.2 mmol) and 1-hydroxy-7-azabenzotriazole 27 mg (0.2 mmol) all dissolved in dimethylformamide (DMF) and were stirred for 10 minutes. In this stirred solution, PCDA-EDEA (**5**) 80 mg (0.19 mmol) dissolved in 2 mL DMF was added. *N*-methyl morpholine was added to pH 8 and the resulting solution was stirred overnight at room temperature. The reaction was monitored with reverse phase C18 end capped silica gel glass thin layer chromatography (60% ACN/H₂O, 0.1 % formic acid). The solvent was evaporated in vacuo. The product was purified with reverse phase C18 flash chromatography (20% ACN/H₂O, 0.1% formic acid) followed by (50% ACN/H₂O, 0.1% formic acid). The obtained product was yellowish solid powder with 45% yield. HR-MS m/z : calcd for $\text{C}_{97}\text{H}_{129}\text{Cl}_2\text{N}_{11}\text{O}_{26}$ $[\text{M}+2\text{H}]^+$ - 969.4330, found 969.5349.

Esterification of D-Ala ¹²⁵(9):

In a 250 mL RBF 2.3 g (13 mmol) of *p*-toluenesulfonic acid, 1 g (11 mmol) of *D*-Ala (**8**) and 6.0 g (56 mmol) of benzyl alcohol were added in 30 mL of cyclohexane. The mixture was stirred for 8 hours under reflux using Dean Stark apparatus. Then, 20 mL of diethyl ether was added to the mixture and mixture was stirred for another hour at room temp. The product precipitated out of solution and were collected by filtration, it was further dried on high vacuo for 4 hours. The product was obtained as white solid 2.9 g with 77% yield. Compared with literature, ¹H NMR (500 MHz, D₂O) δ 7.56 – 7.48 (m, 2H), 7.31 – 7.27 (m, 5H), 7.20 – 7.15 (m, 2H), 5.15 – 5.07 (m, 2H), 4.71 – 4.61 (m, 5H), 4.04 (q, *J* = 7.3 Hz, 1H), 2.21 (s, 3H), 1.39 (d, *J* = 7.3 Hz, 3H). ¹³C NMR (126 MHz, D₂O) δ 170.6, 142.5, 139.4, 134.7, 129.5, 128.9, 128.5, 125.4, 68.5, 63.9, 48.8, 20.5, 15.1.

Synthesis of Dipeptide Boc-D-Ala-D-Ala-OBn (11):

In round bottom flask with 15 mL of anhydrous DMF, Boc-*D*-Ala-OH (**10**) 0.95 g (4.9 mmol), EDC.HCl 1.436 g (7.5 mmol), HOBt 1.11 g (8.2 mmol) were added, and the reaction mixture was stirred for 30 min at 0 °C. In a separate flask, TsOH. *D*-Ala-OBn (**9**) 1.76 g (4.9 mmol) and 4.3 mL (5 equiv.) of *N,N*-diisopropylethylamine were added along with 5 mL of DMF solvent and the mixture was stirred for 30 min at 0 °C. This mixture was transferred to activated acid of **10** and the reaction was stirred for 24 h at room temp. The product was extracted with 30 mL of ethyl acetate and was washed three times with NH₄Cl, saturated NaCl and deionized water. The organic solution was dried over anhydrous MgSO₄. The solvent evaporated and was purified with column chromatography using a gradient solvent (3-8% MeOH/DCM). The product was obtained as a white solid 2.06 g with 77% yield. Compared with literature, ¹H NMR (500 MHz, CDCl₃) δ 7.38 – 7.28 (m, 5H), 6.84 – 6.74 (m, 1H), 5.18 – 5.08 (m, 3H), 4.59 (p, *J* = 7.3

Hz, 1H), 4.19 (s, 1H), 1.42 (s, 9H), 1.39 (d, $J = 7.2$ Hz, 3H), 1.32 (d, $J = 7.1$ Hz, 3H). ^{13}C NMR (126 MHz, CDCl_3) δ 172.7, 172.4, 155.6, 135.4, 128.7, 128.5, 128.2, 80.1, 67.2, 53.5, 50.0, 28.4, 18.5, 18.3.

Synthesis of 12 by TFA Boc deprotection (12):

In an oven dried round bottom flask compound (**11**) 1.35 g (3.8 mmol) was stirred with trifluoroacetic acid (TFA) 4.5 mL (10 equiv.) and 15 mL of anhydrous dichloromethane at 0 °C for an hour. Then the mixture was stirred at room temp. overnight. The solvent was evaporated in vacuo three times with solvents benzene, ethyl acetate and diethyl ether. The product was purified with column chromatography using solvent system 5% MeOH/DCM followed by 10% MeOH/DCM. The product was obtained as yellow precipitates 0.76 g with 80% yield. Compared with literature, ^1H NMR (301 MHz, CDCl_3) δ 8.03 (s, 3H), 7.66 (d, $J = 6.9$ Hz, 1H), 7.39 – 7.19 (m, 5H), 5.23 – 4.95 (m, 2H), 4.45 (q, $J = 7.1$ Hz, 1H), 4.29 – 4.03 (m, 1H), 1.37 (dd, $J = 17.9, 6.8$ Hz, 6H). ^{13}C NMR (76 MHz, CDCl_3) δ 172.3, 169.9, 135.1, 128.7, 128.7, 128.2, 67.5, 66.0, 49.5, 48.9, 16.9, 16.8.

Synthesis of 13 by deprotection of OBn group with Pd/C hydrogenolysis ¹²⁶:

In a flask equipped with stirrer bar 350 mg (1.39 mmol) of dipeptide (**12**) was added 35 mg of 10% Pd/C powder. 15 mL of anhydrous ethanol was transferred into the flask covered with rubber septum; a hydrogen gas filled in balloon was attached on the closed flask. Mixture was purged for 5 minutes followed by stirring at room temp. for 6 h. The mixture was passed through a celite to remove the catalyst and the filtrate was evaporated to give yellow solid of product 236 mg with 92% yield. ^1H NMR (500 MHz, D_2O) δ 4.26 (q, $J = 7.3$ Hz, 1H), 3.95 (q, $J = 7.1$ Hz, 1H), 1.41 (d, $J = 7.1$ Hz, 3H), 1.30 (d, $J = 7.4$ Hz, 3H).

^{13}C NMR (126 MHz, DMSO- D_6) δ 174.1, 169.7, 48.4, 48.2, 17.2, 17.2. LC/MS calculated mass 160, found 161 $[\text{M}+\text{H}]^+$.

Synthesis of 15:

In 100 mL round bottom flask, 15 mL of anhydrous DMF was transferred with Boc-Lys(Z)-OH (**14**) 0.5 g (1.3 mmol), EDC·HCl 0.38 g (1.9 mmol), HOBt 0.29 g (2.2 mmol). The reaction mixture was stirred for 30 min at 0 °C. In a separate flask, H-*D*-Ala-*D*-Ala-OBn (**12**) 0.33 g (1.3 mmol) and 1.2 mL (5 equiv.) of base *N,N*-Diisopropylethylamine were added along with 5 mL of DMF solvent. The mixture was stirred for 30 min at 0 °C. This mixture of **12** was transferred to activated acid **14** and the reaction was stirred for 24 h at room temp. The product was extracted with 20 mL of ethyl acetate and was washed three times with NH_4Cl , saturated NaCl and deionized water. The organic layer was dried over anhydrous MgSO_4 . The solvent evaporated and was purified with column chromatography using solvent system 5% methanol / dichloromethane. Product obtained as white solid 0.56 g with 70 % yield. ^1H NMR (500 MHz, CDCl_3) δ 7.42 (d, $J = 7.6$ Hz, 1H), 7.34 – 7.23 (m, 10H), 5.61 (d, $J = 7.8$ Hz, 1H), 5.25 (s, 2H), 5.16 – 5.05 (m, 2H), 4.57 (dt, $J = 7.4$ Hz, 2H), 4.17 – 4.04 (m, 1H), 3.12 (q, $J = 6.7$ Hz, 2H), 1.79 – 1.65 (m, 1H), 1.59 (dtd, $J = 13.5, 8.6, 5.5$ Hz, 1H), 1.52 – 1.20 (m, 19H). ^{13}C NMR (126 MHz, CDCl_3) δ 173.1, 172.3, 172.1, 156.6, 156.2, 136.8, 135, 128.6, 128.5, 128.5, 128.3, 128.2, 128.1, 127.8, 80.7, 67.0, 66.5, 52.1, 51.0, 49.3, 40.3, 30.9, 28.3, 22.3, 18.0, 17.9

Synthesis of 16:

In an oven dried round bottom flask compound (**15**) 0.56 g (0.91 mmol) was stirred with trifluoroacetic acid (TFA) 1.5 mL (15 equiv.) in 15 mL of anhydrous dichloromethane at 0 °C for an hour. Then, the mixture was stirred at room temp. over night. Solvent was evaporated in vacuo and the mixture was high vacuo three times with benzene, ethyl acetate and diethyl ether. The product was separated with column chromatography using solvent system 10% methanol/dichloromethane Product obtained as white solid 0.35 g with 75% yield. ^1H NMR (500 MHz, METHANOL- D_3) δ 7.38 – 7.20 (m, 10H), 5.13 (q, J = 12.3 Hz, 2H), 5.03 (d, J = 2.9 Hz, 2H), 4.42 (q, J = 7.3 Hz, 1H), 4.34 (q, J = 7.1 Hz, 1H), 3.42 (t, J = 6.6 Hz, 1H), 3.09 (t, J = 6.9 Hz, 2H), 1.73 – 1.55 (m, 2H), 1.48 (q, J = 7.2 Hz, 2H), 1.40 – 1.33 (m, 5H), 1.30 (d, J = 7.2 Hz, 3H). ^{13}C NMR (126 MHz, METHANOL- D_3) δ 174.0, 173.4, 172.5, 157.6, 137.1, 135.9, 128.2, 128.1, 128.0, 127.9, 127.6, 127.4, 66.6, 66.0, 54.1, 53.5, 40.1, 33.4, 29.3, 22.3, 16.9, 15.8.

Synthesis of Tripeptide 17:

In a flask equipped with stirrer bar 50 mg (0.1 mmol) tripeptide (**16**) was added along with 5 mg of 10% Pd/C in 10 mL of anhydrous ethanol. The flask covered with a stopper and hydrogen balloon was attached on the flask. Reaction mixture was purged for 5 minutes and stirred for 6 h at room temp. The mixture was passed through celite and the solvent evaporated to give white solid tripeptide 23.6 mg with 85% yield. Compared with literature, ^1H NMR (500 MHz, METHANOL- D_3) δ 4.37 (q, J = 7.1 Hz, 1H), 4.24 (q, J = 7.2 Hz, 1H), 4.02 – 3.89 (m, 1H), 2.92 (tt, J = 7.5, 3.8 Hz, 2H), 1.67 (ddtd, J = 10.7, 8.3, 6.0, 2.6 Hz, 2H), 1.42 (s, 7H), 1.36 (dd, J = 11.0, 7.2 Hz, 5H). ^{13}C NMR (126 MHz, METHANOL- D_3) δ 176.1, 173.6, 172.8, 79.4, 48.9, 47.5, 47.3, 39.1, 27.4, 26.8, 22.4, 16.9, 16.7. LC/MS calculated mass 288 found 289 $[\text{M}+\text{H}]^+$.

Liposomes preparation:

For the preparation of 10% liposomes of PCDA-Van with 90% PCDA monomer 2 mg of PCDA-Van **7** was mixed with 6.7 mg of monomer PCDA **1** in a small vial and were dissolved in 10 mL of Ethanol. The solvent was evaporated in vacuo, the precipitates were mixed with ultrapure water (10 mL) to give 0.1 mM concentration of liposomes. The suspension was bath sonicated for 40 min at 80 °C. The hot cloudy suspension was immediately filtered through 0.8 μm cellulose filter paper to get rid of undispersed lipids aggregates. The solution was stored below 4 °C for 12 h. After that photopolymerization was done using handheld 254 nm Ultraviolet (UV) lamp (1mW cm^{-2}) at room temperature for 10 minutes. The blue liposomes were stored below 4 °C and were stable enough to work for 4 weeks.

Preparation of dipeptide and tripeptide for UV absorption and fluorescent study

5 mM solution of dipeptide and tripeptide was prepared by dissolving each peptide in ultra-pure water. In each experiment 200 μL of each solution was treated with different concentrations of liposomes. The pH of the peptide solution was 6.9. UV and fluorescent spectra were taken after 10 min of mixing peptide with liposomes. UV absorption for blue liposomes before and after treating with peptide gave maximum absorption about 640 nm whereas purple liposomes maximum absorption was observed around 540 nm. Fluorescent spectra were taken by exciting samples at 540 nm. For all experiments the excitation and emission slit width was 5 nm.

TEM characterization of liposome alone and liposome treated bacterial cells

TEM was used to analyze liposome and liposome treated bacterial cells. Liposome were diluted in water to reach a final concentration of 100 μM . 10 μL of liposome peptide solution was dropped onto a holey carbon grid. After 2 mins, excess solution was carefully removed using a filter paper. 10 μL of 2 wt% uranyl acetate solution was added on the grid for staining. After 2 mins, excess solution was carefully removed using a filter paper and the TEM sample was allowed to dry for at least 8 hrs before imaging. *S. Aureus* was washed with water for three times follow the exactly same procedure as fluorescence responsive experiment. For liposome treated bacterial cells, 50 μL of 10% PCDA-Van: 90% PCDA liposome solution (200 μM) was mixed with 50 μL of bacterial suspensions (10^8 CFU/mL). After 8 hrs of incubation at room temperature, 10 μL of mixed bacterial suspension was dropped onto a holey carbon grid for 5 mins. Excess solution was removed, and the sample was stained with 10 μL of 0.5 wt% uranyl acetate solution. After 3 mins, excess staining solution was removed and the TEM sample was left in air for at least 8 hours before imaging.

Minimal inhibitory concentration (MIC) determination

S. Aureus was cultured in MHB media under constant shaking at 100 rpm at 37 $^{\circ}\text{C}$ to reach their mid-exponential growth phase. The bacterial solution was plated on an agar plate for colony forming unit (CFU) counting. Bacterial suspensions were diluted to approximately 10^5 CFU/mL in MHB media as the initial CFU for inoculation. MIC was estimated based on the 2-fold serial broth microdilution method using PCDA concentrations ranging from 25 to 800 μM or vancomycin concentration from 25 to 800 μM (three replicates for each concentration). 50 μL of each sample solution was mixed with 50 μL of bacterial solution in a 96-well plate. The plates were incubated at 37 $^{\circ}\text{C}$

under constant shaking at 100 rpm for 18 hrs and the optical density (OD) at 600 nm was measured. The MIC was determined at the peptide concentration in which OD reading is below 0.06 and no cloudiness was visible to naked eyes.

Membrane localization assay:

Bacterial suspensions in MHB (*E.coli* and *MRSA*, 10^9 CFU/mL) were added to a confocal dishes and incubated overnight. Following incubation, bacterial suspensions were removed and dishes were washed with DI water three times to remove any non-adherent bacteria. Next, 200 μ L of 100 μ M liposome solution containing 5% 1,2-dioleoyl-sn-glycero-3-phosphoethanolamine-N-(dabsyl) and either 10% vancomycin conjugated PCDA or no target was added to the bacteria treated dishes and incubated for 2 hours. After 2 hours, bacteria plates were washed three times with DI water to remove unbound liposomes and 200 μ L of glycerol was added to fix cells. Images were captured using fluorescence microscopy with an excitation wavelength of 359 nm and an emission wavelength of 457 nm and processed using ImageJ software.

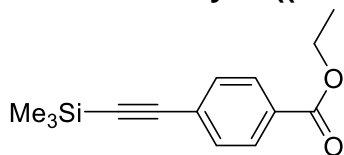
Dynamic Light Scattering spectrum

Liposomes at about 0.1 mM concentration were prepared and diluted to 1/300 fold for DLS experiment. A NonNegative Least-Squares (NNLS) analytical method was performed on these data to glean the most reliable assessments. Particle sizes were determined as either intensity- or volume-weighted diameters.

Chapter 6

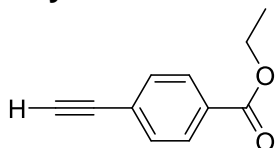
General Experimental Procedure-Diphenyl Diacetylene Linker

Synthesis of Ethyl 4-((trimethylsilyl)ethynyl)benzoate (22)



In an oven dried round bottom flask (RBF), 15 mL of anhydrous DMF and 8.0 mL of triethylamine were put together and nitrogen was bubbled through it for 30 min. Then, 5 mol% of Pd(PPh₃)₄ and CuI were added in the purged solvent followed by the addition of reagent 0.37 mL (2.6 mmol) of **1** and 0.5 g (2.2 mmol) of **2**. The mixture was heated to 80 °C for 6 h. The solvent was concentrated on rotary evaporation and oily mixture was taken up in 50 mL of ethyl acetate. The organic layer was washed three times with NH₄Cl, brine and water and dried over anhydrous MgSO₄. Organic layer was evaporated, and flash chromatography was performed with 5% EtOAc in hexane to get pure product. 0.3 g yellow oily product was obtained with 67% yield. ¹H NMR (500 MHz, CDCl₃) δ 7.98 – 7.93 (m, 2H), 7.52 – 7.47 (m, 2H), 4.35 (q, *J* = 7.1 Hz, 2H), 1.37 (t, *J* = 7.1 Hz, 3H), 0.25 (s, 9H). ¹³C NMR (126 MHz, CDCl₃) δ 166.2, 131.9, 130.1, 129.4, 127.7, 104.2, 97.6, 61.2, 14.4, -0.08.

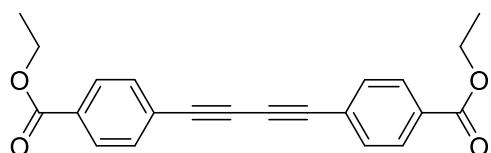
Synthesis of Ethyl 4-ethynylbenzoate (23)



In a RBF 0.1 g (0.4 mmol) of **3** was dissolved in anhydrous ethanol, 0.17 g of (1.2 mmol; 3 equiv.) of K₂CO₃ were added in the solution and the mixture was stirred for 18 h at room temperature under nitrogen environment. It was filtered off and solvent was evaporated in vacuo. The residues were taken up into 40 mL of 1:1 ethyl acetate and 1 M HCl solution. The organic layer was separated and washed with brine and DI water twice before rotary evaporated to get

yellow precipitates. Flash chromatography was performed with 2% EtOAc in hexane to get 44 mg of product with 62% yield. The product was yellow solid. ^1H NMR (500 MHz, CDCl_3) δ 8.03 – 7.96 (m, 2H), 7.58 – 7.51 (m, 2H), 4.37 (q, $J = 7.1$ Hz, 2H), 3.23 (s, 1H), 1.39 (t, $J = 7.1$ Hz, 3H). ^{13}C NMR (126 MHz, CDCl_3) δ 165.8, 131.9, 130.4, 129.3, 126.5, 82.7, 79.8, 61.1, 14.2.

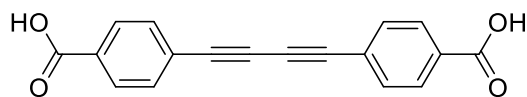
Synthesis of Diethyl 4,4'-(buta-1,3-diyne-1,4-diyl)dibenzoate (24)



1.0 g (5.8 mmol) of compound **4** was added into the RBF equipped with stirrer bar containing solution of 2 g (10 mmol) copper acetate monohydrate

($\text{Cu}(\text{OAc})_2 \cdot \text{H}_2\text{O}$) in 10 mL methanol and pyridine solvents (1:1). The reaction mixture was stirred for 6 h at 60 °C. The mixture was brought to room temperature followed by addition of 50 mL ice cold water in it. Solid precipitation was observed and filtered off. The precipitated were collected after filtration and were washed many times with water. The solid was suspended in hexane and filtered off, it was washed multiple times with hexane to get rid of impurities and let it air dry overnight. The obtained product was off white solid 1.6 g as 80% yield. ^1H NMR (500 MHz, CDCl_3) δ 8.02 (dt, $J = 7.8, 0.9$ Hz, 4H), 7.61 – 7.50 (m, 4H), 4.39 (qd, $J = 7.2, 0.9$ Hz, 4H), 1.40 (td, $J = 7.2, 0.9$ Hz, 6H). ^{13}C NMR (126 MHz, CDCl_3) δ 165.9, 132.6, 131.1, 129.7, 126.1, 82.0, 76.3, 61.5, 14.4.

Synthesis of 4,4'-(buta-1,3-diyne-1,4-diyl)dibenzoic acid (19)



In a 250 mL RBF 0.80 g (20 mmol) of NaOH were dissolved in solvent system THF/EtOH/ H_2O

(25/25/25 mL) solvent system followed by 0.85 g (2.5 mmol) of **5** was added. The mixture was stirred for 24 h, the solvent was evaporated in vacuo. The solid obtained was

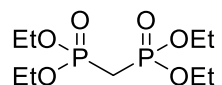
dissolved in 50 mL water and the pH was brought to 2 with 1 M HCl. Solid was filtered and washed with water; it was set to air dry overnight on a running high vacuum. 0.52 g of final product was collected as white solid with 73% yield. ^1H NMR (500 MHz, $\text{DMSO-}D_6$) δ 7.97 (d, $J = 8.0$ Hz, 4H), 7.75 (d, $J = 8.0$ Hz, 4H). Due to insufficient solubility of product in DMSO the Carbon NMR was not practicable, addition of few drops of base (DIPEA) solubilize the compound.

NMR with DIPEA: ^1H NMR (500 MHz, $\text{DMSO-}D_6$) δ 7.88 (d, $J = 7.9$ Hz, 4H), 7.54 (d, $J = 7.9$ Hz, 4H). ^{13}C NMR (126 MHz, $\text{DMSO-}D_6$) δ 168.5, 140.7, 131.9, 129.6, 121.2, 82.6, 74.4.

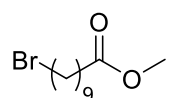
Chapter 7

General experimental procedure-Biomimetic molecules

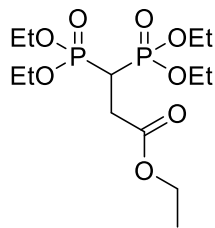
Synthesis of 30

 $^1\text{H NMR}$ (500 MHz, CDCl_3) δ 4.04 – 3.82 (m, 8H), 2.39 – 1.96 (m, 2H), 1.29 – 0.88 (m, 12H). $^{13}\text{C NMR}$ (126 MHz, CDCl_3) δ 62.4 (q, $J = 3.8, 3.1$ Hz), 25.1, 16.1 (q, $J = 3.5$ Hz). $^{31}\text{P NMR}$ (122 MHz, CDCl_3) δ 19.6.

Synthesis of 32

 To an oven dried round bottomed flask (RBF) at room temperature, was added acid **31** (3 g, 12 mmol), then thionyl chloride (1.3 mL, 18 mmol) was added by slow addition. The reaction mixture was heated to reflux at 80 °C for 2 h. After stirring for two hours, the reaction mixture was allowed to cool to room temp and methanol (0.8 mL, 20 mmol) was added dropwise. This mixture was stirred for another 40 minutes. The solution was condensed using rotary evaporator. DCM (30 mL) was added to the left-over mixture and washed two times each with 5% sodium bicarbonate, brine, and then deionized water. The organic layer was concentrated by rotary evaporator then dried by high vacuum to get 2.3 g (95%) of a brown oily product. $^1\text{H NMR}$ (500 MHz, CDCl_3) δ 3.57 (s, 3H), 3.31 (t, $J = 6.8$ Hz, 2H), 2.21 (t, $J = 7.5$ Hz, 2H), 1.76 (p, $J = 7.0$ Hz, 2H), 1.57 – 1.49 (m, 2H), 1.37 – 1.30 (m, 2H), 1.22 (s, 8H). $^{13}\text{C NMR}$ (126 MHz, CDCl_3) δ 174.0, 51.3, 33.9, 33.8, 32.7, 29.1, 29.1, 28.9, 28.6, 28.0, 24.8.

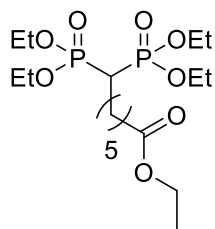
Synthesis of 33a¹²⁷



In an oven dried 100 mL RBF, was added tetraethyl methylenebisphosphonate (4.6 g, 16 mmol) and anhydrous DMF (15 mL). The solution was cooled to 0 °C, then, NaH (60% suspension in mineral oil) 0.43 g (18 mmol) was transferred in portions over a period

of 10 min. Reaction mixture was stirred at 0 °C for an hour before transferring neat ethyl bromoacetate **32a** 3 g (18 mmol) in it. The reaction mixture was stirred over night at room temp. To quench NaH, 4 mL of saturated solution of NH₄Cl was transferred in it and stirred for additional 5 min. The product was extracted three times with ethyl acetate, the organic layer was washed with NH₄Cl, brine and de-ionized water three times to get rid of DMF. It was dried over anhydrous magnesium sulfate and filtered. The solvent was evaporated in vacuo and flash chromatography was performed with 5% MeOH/Ethyl acetate solvent system to get the 3.2 g of product as colorless oil with 52% yield. ¹H NMR (500 MHz, CDCl₃) δ 4.10 – 3.83 (m, 10H), 2.99 – 2.76 (m, 1H), 2.62 (ddd, *J* = 15.2, 8.5, 6.3 Hz, 2H), 1.27 – 0.92 (m, 15H). ¹³C NMR (126 MHz, CDCl₃) δ 170.7 (t, *J* = 9.1 Hz), 62.7 (dd, *J* = 18.7, 6.5 Hz), 61.0, 32.7, 30.5 (d, *J* = 4.7 Hz), 16.1 (d, *J* = 6.1 Hz), 14.0. ³¹P NMR (122 MHz, CDCl₃) δ 22.6. IR. (neat) (ν̄) 964, 1014, 1240, 1736, 2983 cm⁻¹.

Synthesis of **33b**¹²⁸

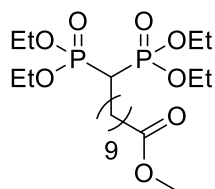


Synthesis of **33b** was done using the same procedure as **33a**, 3.4 g of colorless product was obtained with 50% yield. ¹H NMR (500 MHz, CDCl₃) δ 4.12 – 3.94 (m, 10H), 2.24 – 2.07 (m, 3H), 1.86 – 1.70 (m, 2H), 1.49 (dq, *J* = 23.9, 7.7 Hz, 4H), 1.23 (t, *J* = 7.1 Hz, 14H), 1.14 (t, *J* = 7.1

Hz, 3H). ¹³C NMR (126 MHz, CDCl₃) δ 173.5, 62.3 (dd, *J* = 18.9, 6.7 Hz), 60.0, 36.6, 34.1, 28.6 (d, *J* = 4.7 Hz), 28.6 (d, *J* = 6.6 Hz), 25.2 (t, *J* = 5.0 Hz), 24.4, 16.3 (dd, *J* = 6.2, 3.2

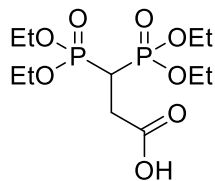
Hz), 14.1. ^{31}P NMR (122 MHz, CDCl_3) δ 24.4. IR. (neat) ($\tilde{\nu}$) 963, 1013, 1238, 1735, 2989 cm^{-1} .

Synthesis of 33c



Synthesis of **33c** was done using the same procedure as **33a**, 3.5 g of brown product was obtained with 46% yield. ^1H NMR (500 MHz, CDCl_3) δ 4.08 – 3.91 (m, 8H), 3.47 (t, J = 1.8 Hz, 3H), 2.19 – 1.99 (m, 3H), 1.79 – 1.63 (m, 2H), 1.40 (dt, J = 26.8, 7.4 Hz, 4H), 1.27 – 0.98 (m, 22H). ^{13}C NMR (126 MHz, CDCl_3) δ 173.9, 62.1 (dd, J = 19.9, 6.7 Hz), 51.1, 36.4, 33.7, 29.0 (d, J = 4.0 Hz), 28.9 (d, J = 6.4 Hz), 28.8, 25.2 (t, J = 5.2 Hz), 24.6, 16.1 (dd, J = 6.4, 3.4 Hz). ^{31}P NMR (122 MHz, CDCl_3) δ 24.5. IR. (neat) ($\tilde{\nu}$) 962, 1018, 1244, 1736, 2981, cm^{-1} .

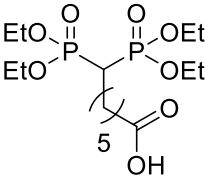
Synthesis of 34a



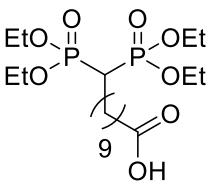
In 100 mL RBF equipped with magnetic stirrer bar 2 g (5.3 mmol) of **33a** was dissolved with 30 mL mixture of THF/ H_2O 2:1 ratio and kept at 0 $^\circ\text{C}$. To that mixture was added dropwise KOH 0.9 g (16 mmol) dissolved in 30 mL of above solvent mixture. The reaction mixture was warm to room temp. and stirred over night. 30 mL of ethyl acetate was used to extract the product. Aqueous layer was acidified with 1 N HCl to pH 1 and extracted again with fresh ethyl acetate. The aqueous layer was saturated with brine and the product extracted one last time with fresh ethyl acetate. All organic layers were combined and dried over anhydrous MgSO_4 . The organic layer was filtered off and evaporated. The product was purified with flash chromatography using 8% MeOH/Ethyl acetate. About 1.3 g colorless oily product was obtained with 70% yield. ^1H NMR (500 MHz, CDCl_3) δ 8.96 (s, 1H), 4.09 (qdd, J = 7.1,

5.5, 4.0, 2.3 Hz, 8H), 3.06 (tt, $J = 24.0, 6.0$ Hz, 1H), 2.74 (td, $J = 16.2, 6.1$ Hz, 2H), 1.24 (td, $J = 7.1, 2.6$ Hz, 12H). ^{13}C NMR (126 MHz, CDCl_3) δ 172.4 (d, $J = 9.0$ Hz), 63.1 (d, $J = 6.7$ Hz), 32.4, 30.2, 16.2 (d, $J = 6.1$ Hz). ^{31}P NMR (122 MHz, CDCl_3) δ 22.9. IR. (neat) ($\tilde{\nu}$) 967, 1014, 1234, 1725, 2983, 3399 cm^{-1} .

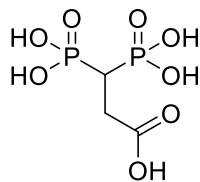
Synthesis of 34b


 Synthesis of **34b** was done using the same procedure as **34a**, 1.3 g of colorless oily product was obtained with 73% yield. ^1H NMR (500 MHz, CDCl_3) δ 4.20 – 4.03 (m, 8H), 2.34 – 2.15 (m, 3H), 1.94 – 1.79 (m, 2H), 1.67 – 1.45 (m, 4H), 1.28 (td, $J = 7.0, 1.0$ Hz, 14H). ^{13}C NMR (126 MHz, CDCl_3) δ 177.0, 62.7 (dd, $J = 18.2, 6.7$ Hz), 36.5, 34.0, 28.8, 28.7 (t, $J = 6.4$ Hz), 25.3 (t, $J = 5.1$ Hz), 24.5, 16.4 (dd, $J = 6.2, 3.1$ Hz). ^{31}P NMR (122 MHz, CDCl_3) δ 24.5. IR. (neat) ($\tilde{\nu}$) 972, 1021, 1213, 1722, 2932, 3480 cm^{-1} .

Synthesis of 34c


 Synthesis of **34c** was done using the same procedure as **34a**, 1.3 g of colorless oily product was obtained with 69% yield. ^1H NMR (500 MHz, CDCl_3) δ 4.18 – 4.01 (m, 8H), 2.32 – 2.14 (m, 3H), 1.89 – 1.73 (m, 2H), 1.59 – 1.41 (m, 4H), 1.22 (dt, $J = 25.5, 5.0$ Hz, 22H). ^{13}C NMR (126 MHz, CDCl_3) δ 178.1, 62.7 (dd, $J = 17.4, 6.7$ Hz), 36.5, 34.1, 29.2, 29.1 (d, $J = 2.8$ Hz), 29.0, 25.4, 24.8, 16.4 (dd, $J = 6.1, 2.8$ Hz). ^{31}P NMR (122 MHz, CDCl_3) δ 24.7. IR. (neat) ($\tilde{\nu}$) 972, 1018, 1204, 1740, 2982, 3496 cm^{-1} .

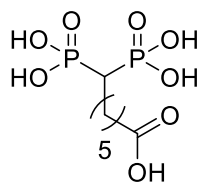
Synthesis of 35a¹²⁸ (C3)



In an oven dried RBF **34a** 0.3 g (0.87 mmol) was transferred in 10 mL anhydrous dichloromethane. Trimethylsilyl bromide 0.6 mL (4.4 mmol) was added, and the reaction was stirred at room temp. for 12 h. The

reaction mixture was concentrated on rotary evaporator and 2 mL of methanol was added in it and mixture was stirred for additional 1 hour. Methanol was evaporated to dryness to get 0.18 g of brown oily liquid product with 90% yield. ^1H NMR (500 MHz, METHANOL- D_3) δ 3.04 – 2.67 (m, 3H). ^{13}C NMR (126 MHz, METHANOL- D_3) δ 172.1, 34.4, 30.3. ^{31}P NMR (122 MHz, METHANOL- D_3) δ 21.5. IR. (neat) ($\tilde{\nu}$) 907, 981, 1132, 1705, 2948 cm^{-1} .

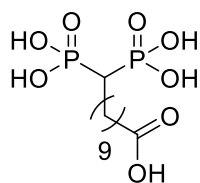
Synthesis of 35b (C7)



Synthesis of **35b** was done following the same procedure as **35a**. 0.23 g of brown oily product was obtained with 92% yield. ^1H NMR (500 MHz, METHANOL- D_3) δ 2.34 – 2.11 (m, 3H), 1.87 (tdt, J = 16.7, 9.6, 6.2 Hz,

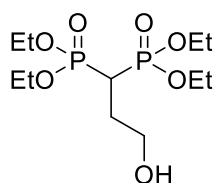
2H), 1.58 (qq, J = 7.4, 4.1, 3.6 Hz, 4H), 1.39 – 1.22 (m, 2H). ^{13}C NMR (126 MHz, METHANOL- D_3) δ 174.6, 50.8, 37.6, 33.3, 28.6 (d, J = 6.2 Hz), 25.1 (d, J = 5.5 Hz), 24.3. ^{31}P NMR (122 MHz, METHANOL- D_3) δ 21.5. IR. (neat) ($\tilde{\nu}$) 901, 995, 1134, 1725, 2951 cm^{-1} .

Synthesis of 35c (C11)



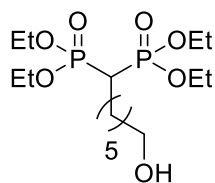
Synthesis of **35c** was done following the same procedure as **35a**. 0.28 g of brownish oily product was obtained with 95% yield. ^1H NMR (500 MHz, D_2O) δ 2.36 (t, $J = 7.5$ Hz, 2H), 2.27 – 2.10 (m, 1H), 1.84 (s, 2H), 1.65 – 1.44 (m, 4H), 1.25 (s, 10H). ^{13}C NMR (126 MHz, $\text{METHANOL-}D_3$) δ 174.6, 37.7, 33.4, 29.2, 29.2, 29.0 (d, $J = 5.7$ Hz), 28.8, 25.4 (d, $J = 4.8$ Hz), 24.7. ^{31}P NMR (122 MHz, D_2O) δ 23.0. IR. (neat) ($\tilde{\nu}$) 913, 1002, 1138, 1735, 2923 cm^{-1} .

Synthesis of 36a¹²⁹



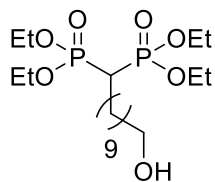
In an oven dried RBF **34a** 0.12 g (0.52 mmol) was transferred at 0 °C in 10 mL of anhydrous THF solvent under nitrogen. Borane dimethyl sulfide 43 μL (0.44 mmol) and trimethyl borate 50 μL (0.44 mmol) was added into the reaction mixture. The reaction was stirred at room temperature for 20 h. The reaction was brought to 0 °C and 0.25 mL of methanol was added and reaction was stirred for 1 h at room temp. The solvent was rotary evaporated, and the colorless oil was dissolved in methanol again and stirred for another 1 h. The solvent evaporated and the product was purified with 5% methanol in ethyl acetate. Product obtained as colorless oil 0.14 g with 79% yield overall. ^1H NMR (500 MHz, CDCl_3) δ 4.15 – 4.03 (m, 8H), 3.71 (t, $J = 5.9$ Hz, 2H), 2.55 (tt, $J = 24.1, 6.2$ Hz, 1H), 2.08 (ddq, $J = 17.4, 12.0, 6.0$ Hz, 2H), 1.27 (dd, $J = 7.7, 6.5$ Hz, 12H). ^{13}C NMR (126 MHz, CDCl_3) δ 62.8 (dd, $J = 11.2, 6.8$ Hz), 60.5 (t, $J = 7.1$ Hz), 33.3, 28.4 (t, $J = 4.8$ Hz), 16.3 (d, $J = 4.9$ Hz). ^{31}P NMR (122 MHz, CDCl_3) δ 24.4. IR. (neat) ($\tilde{\nu}$) 966, 1014, 1222, 2983, 3391 cm^{-1} .

Synthesis of 36b



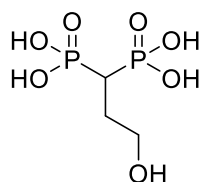
Synthesis of **36b** was done following the same procedure as **36a**. 0.17 g with 84% yield of product obtained as transparent colorless oil. ¹H NMR (500 MHz, CDCl₃) δ 3.94 – 3.74 (m, 8H), 3.25 (t, *J* = 6.7 Hz, 2H), 1.95 (tt, *J* = 24.4, 6.0 Hz, 1H), 1.59 (dtd, *J* = 17.2, 10.6, 4.9 Hz, 2H), 1.24 (tq, *J* = 15.5, 8.8, 8.2 Hz, 4H), 1.02 (t, *J* = 7.2 Hz, 16H). ¹³C NMR (126 MHz, CDCl₃) δ 62.2 (dd, *J* = 22.9, 6.7 Hz), 61.9, 36.3, 32.4, 28.9, 28.8, 25.2, 25.2, 16.1 (dd, *J* = 6.2, 3.3 Hz). ³¹P NMR (122 MHz, CDCl₃) δ 24.4. IR. (neat) (ν̄) 964, 1012, 1233, 2983, 3390 cm⁻¹.

Synthesis of 36c



Synthesis of **36c** was done following the same procedure as **36a**. 0.19 g (83% yield) of product was obtained as transparent colorless oil. ¹H NMR (500 MHz, CDCl₃) δ 4.05 – 3.91 (m, 8H), 3.40 (t, *J* = 6.7 Hz, 2H), 2.08 (tt, *J* = 24.2, 5.9 Hz, 1H), 1.79 – 1.60 (m, 2H), 1.36 (h, *J* = 6.9, 6.2 Hz, 4H), 1.23 – 1.00 (m, 24H). ¹³C NMR (126 MHz, CDCl₃) δ 62.5, 62.3, 36.5, 32.7, 29.4, 29.3 (d, *J* = 5.1 Hz), 29.2 (d, *J* = 11.5 Hz), 28.9 (t, *J* = 6.5 Hz), 25.7, 16.3 (dd, *J* = 6.4, 3.2 Hz). ³¹P NMR (122 MHz, CDCl₃) δ 24.6. IR. (neat) (ν̄) 967, 1014, 1223, 2981, 3392 cm⁻¹.

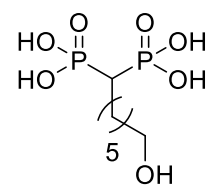
Synthesis of 37a



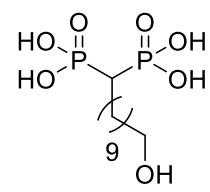
Synthesis of **37a** was done following the same procedure as **35a**. 0.16 g of brown oily product was obtained with 85% yield. ¹H NMR (500 MHz, METHANOL-*D*₃) δ 3.75 (t, *J* = 6.6 Hz, 2H), 2.42 (ddt, *J* = 47.9, 23.7, 5.3 Hz, 2H), 2.13 (tq, *J* = 17.4, 6.4 Hz, 2H). ¹³C NMR (126 MHz, METHANOL-*D*₃) δ 60.3,

34.4, 28.0. ^{31}P NMR (122 MHz, METHANOL- D_3) δ 23.5. IR. (neat) ($\tilde{\nu}$) 909, 1003, 1129, 2988 cm^{-1} .

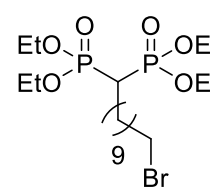
Synthesis of 37b

 Synthesis of **37b** was done following the same procedure as **35a**. 0.22 g of brown oily product was obtained with 91% yield. ^1H NMR (500 MHz, METHANOL- D_3) δ 3.53 (td, $J = 6.6, 1.0$ Hz, 2H), 2.34 – 2.18 (m, 1H), 1.97 – 1.79 (m, 2H), 1.55 (dt, $J = 34.2, 7.6$ Hz, 4H), 1.41 – 1.28 (m, 4H). ^{13}C NMR (126 MHz, METHANOL- D_3) δ 61.6, 38.4, 37.4, 36.3, 32.0, 28.9 (d, $J = 6.6$ Hz), 25.2. ^{31}P NMR (122 MHz, METHANOL- D_3) δ 23.4. IR. (neat) ($\tilde{\nu}$) 910, 1001, 1130, 2980 cm^{-1} .

Synthesis of 37c

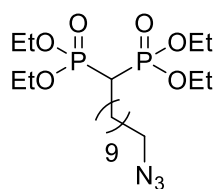
 Synthesis of **37c** was done following the same procedure as **35a**. 0.26 g of dark brown oily product obtained with 89% yield. ^1H NMR (500 MHz, METHANOL- D_3) δ 3.52 (t, $J = 6.7$ Hz, 2H), 2.30 – 2.10 (m, 1H), 1.99 – 1.79 (m, 2H), 1.53 (ddt, $J = 40.9, 13.8, 6.8$ Hz, 4H), 1.39 – 1.20 (m, 12H). ^{13}C NMR (126 MHz, METHANOL- D_3) δ 61.8, 37.6, 32.2, 29.4, 29.3, 29.3, 29.1, 25.5 (d, $J = 32.0$ Hz). ^{31}P NMR (122 MHz, METHANOL- D_3) δ 23.8. IR. (neat) ($\tilde{\nu}$) 913, 1005, 1135, 2983 cm^{-1} .

Synthesis of 39

 Tetraethyl methylenebisphosphonate **30** 0.15 g (0.51 mmol) was transferred to 100 mL RBF in 15 mL anhydrous DMF at 0 °C. NaH was added in it portion wise over a period of 10 min. The mixture was stirred for 40 min. In a separate flask 1,10-dibromodecane **38** was taken in 5 mL anhydrous DMF at 0 °C. Mixture of **30** was transferred dropwise into **38** and reaction was stirred overnight.

3 mL of NH_4Cl was added and the product was extracted twice with 30 mL ethyl acetate and washed three times with brine and de-ionized water. The organic layer was dried over anhydrous MgSO_4 and evaporated to get crude oily product which was subjected to flash chromatography 3% MeOH/ethyl acetate to obtained 0.17 g of colorless oily product 67% yield was recovered. ^1H NMR (500 MHz, CDCl_3) δ 3.96 (p, $J = 7.0$ Hz, 8H), 3.17 (t, $J = 6.8$ Hz, 2H), 2.11 – 1.94 (m, 1H), 1.65 (ddt, $J = 35.1, 14.4, 6.9$ Hz, 4H), 1.39 – 1.26 (m, 2H), 1.24 – 0.91 (m, 24H). ^{13}C NMR (126 MHz, CDCl_3) δ 62.0 (dd, $J = 20.8, 6.6$ Hz), 37.4, 36.4, 35.3, 33.5, 32.4, 29.1 – 28.5 (m), 28.3, 27.8, 25.2 (t, $J = 5.1$ Hz), 16.1 (dd, $J = 6.4, 3.2$ Hz). ^{31}P NMR (122 MHz, CDCl_3) δ 24.5.

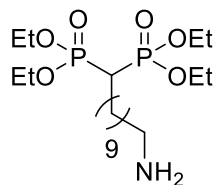
Synthesis of **40**¹³⁰



In a 100 mL RBF compound **30** 0.2 g (0.39 mmol) was dissolved in solvent mixture ethanol/water (10mL v/v) at room temp. Sodium azide 0.13 g (2 mmol) was added into the solution and the reaction mixture

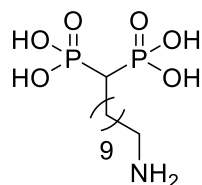
was stirred at room temp. for 36 h. Solvent was evaporated and chloroform was added into the white powder. The organic layer was washed three times with brine and water. Organic layer was evaporated and 0.16 g of colorless oily product was collected 85% yield. ^1H NMR (500 MHz, CDCl_3) δ 4.05 – 3.87 (m, 8H), 3.10 – 2.99 (m, 2H), 2.15 – 1.98 (m, 1H), 1.71 (tdd, $J = 16.8, 10.8, 6.3$ Hz, 2H), 1.37 (dp, $J = 14.7, 6.8$ Hz, 4H), 1.24 – 0.99 (m, 24H). ^{13}C NMR (126 MHz, CDCl_3) δ 62.2 (dd, $J = 21.0, 6.6$ Hz), 51.3, 36.6, 29.2, 29.1, 29.0 (t, $J = 6.0$ Hz), 28.7, 26.5, 25.4 (d, $J = 5.0$ Hz), 16.2 (dd, $J = 6.2, 3.4$ Hz). ^{31}P NMR (122 MHz, CDCl_3) δ 24.7.

Synthesis of 41



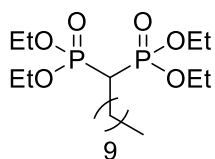
In an oven dried RBF compound 0.15 g (0.3 mmol) of **40** was added followed by 10% Pd/C w/w reagent under nitrogen in 15 mL anhydrous methanol. Hydrogen balloon was attached to the RBF and the reaction was run for 12 h. Reaction mixture was passed through celite, the solvent was rotary evaporated and the oily product was obtained as 82% yield 0.11 g. ^1H NMR (500 MHz, CDCl_3) δ 4.05 (ddd, $J = 12.6, 9.4, 6.2$ Hz, 8H), 2.50 (dtd, $J = 46.0, 7.3, 2.9$ Hz, 2H), 2.20 – 1.96 (m, 3H), 1.76 (tt, $J = 13.8, 7.3$ Hz, 2H), 1.48 – 1.01 (m, 28H). ^{13}C NMR (126 MHz, CDCl_3) δ 62.3 (dd, $J = 19.5, 6.8$ Hz), 42.0, 36.7, 29.5, 29.4 (d, $J = 3.5$ Hz), 29.2, 29.1, 29.0 (d, $J = 6.4$ Hz), 26.8, 25.5 (d, $J = 5.3$ Hz), 16.3 (dd, $J = 6.4, 3.3$ Hz). ^{31}P NMR (122 MHz, CDCl_3) δ 24.6.

Synthesis of 42



Synthesis of **42** was done following the same procedure as **35a**. 0.034 g of dark brown oily product obtained with 92% yield. ^1H NMR (500 MHz, METHANOL- D_3) δ 2.93 (dt, $J = 31.3, 7.9$ Hz, 2H), 2.16 (tt, $J = 23.7, 6.0$ Hz, 1H), 1.89 (dh, $J = 23.1, 7.6$ Hz, 2H), 1.74 – 1.52 (m, 4H), 1.33 (d, $J = 14.2$ Hz, 14H). ^{13}C NMR (126 MHz, METHANOL- D_3) δ 39.4, 37.8, 29.2, 29.1, 29.1, 29.0, 28.8, 27.2, 26.1, 25.9, 25.4. ^{31}P NMR (122 MHz, METHANOL- D_3) δ 23.5.

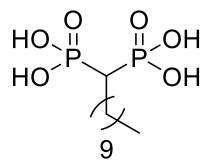
Synthesis of 44



Synthesis of compound 44 was done following the same procedure as **33a**. 3.2 g of the product was obtained as colorless oil with 79% yield. ^1H NMR (500 MHz, CDCl_3) δ 3.95 – 3.83 (m, 8H), 1.99 (tt, $J = 24.2, 6.0$

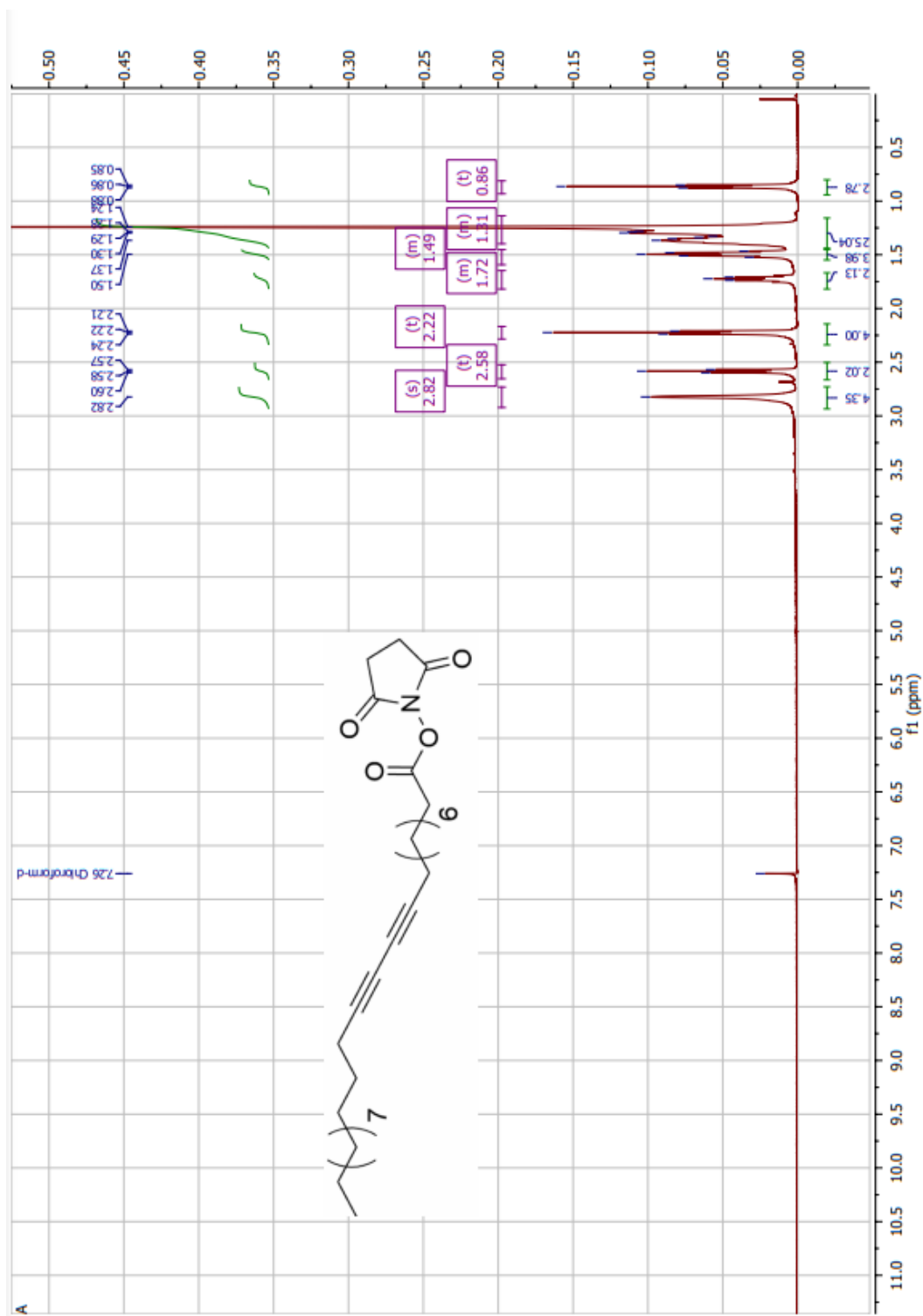
Hz, 1H), 1.72 – 1.52 (m, 2H), 1.34 – 1.22 (m, 2H), 1.11 – 0.89 (m, 26H), 0.59 (t, $J = 6.9$ Hz, 3H). ^{13}C NMR (126 MHz, CDCl_3) δ 62.2 (dd, $J = 19.5, 6.7$ Hz), 36.5, 31.7, 29.3 (d, $J = 4.0$ Hz), 29.1, 29.0, 28.8 (d, $J = 6.5$ Hz), 25.3, 22.4, 16.1 (dd, $J = 6.5, 3.3$ Hz), 13.8. ^{31}P NMR (122 MHz, CDCl_3) δ 24.7.

Synthesis of 45

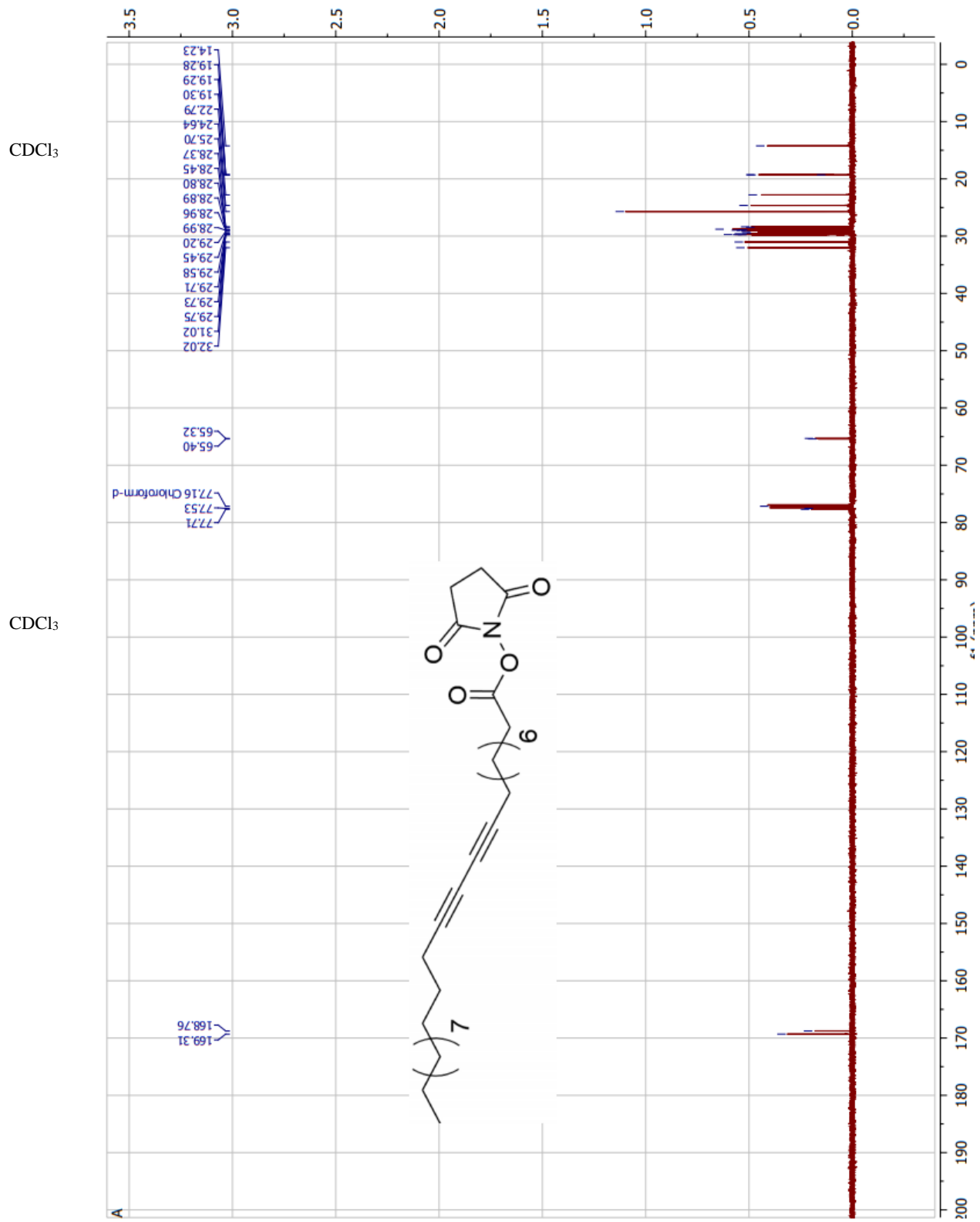


Synthesis of **45** was done following the same procedure as **35a**. 0.6 g of the product was obtained as yellow oily with 95% yield. ^1H NMR (500 MHz, $\text{METHANOL-}D_3$) δ 2.17 (t, $J = 20.5$ Hz, 1H), 1.87 (s, 2H), 1.64 – 1.44 (m, 2H), 1.26 (d, $J = 17.6$ Hz, 14H), 0.84 (t, $J = 6.8$ Hz, 3H). ^{13}C NMR (126 MHz, $\text{METHANOL-}D_3$) δ 37.6, 31.7, 29.4, 29.3, 29.2, 25.3, 22.4, 13.2. ^{31}P NMR (122 MHz, $\text{METHANOL-}D_3$) δ 25.0.

NMR and other characterization data

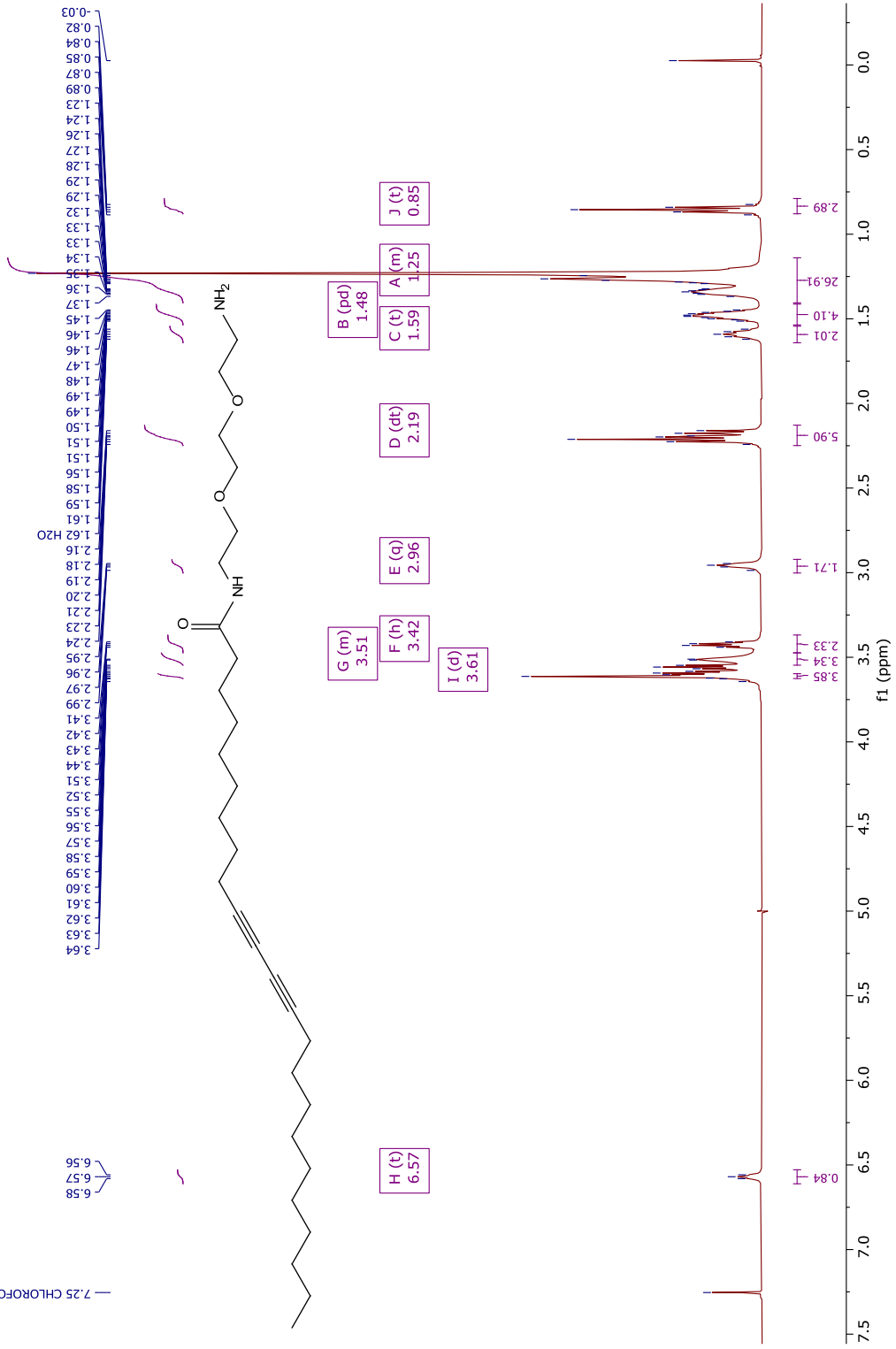


CDCl₃

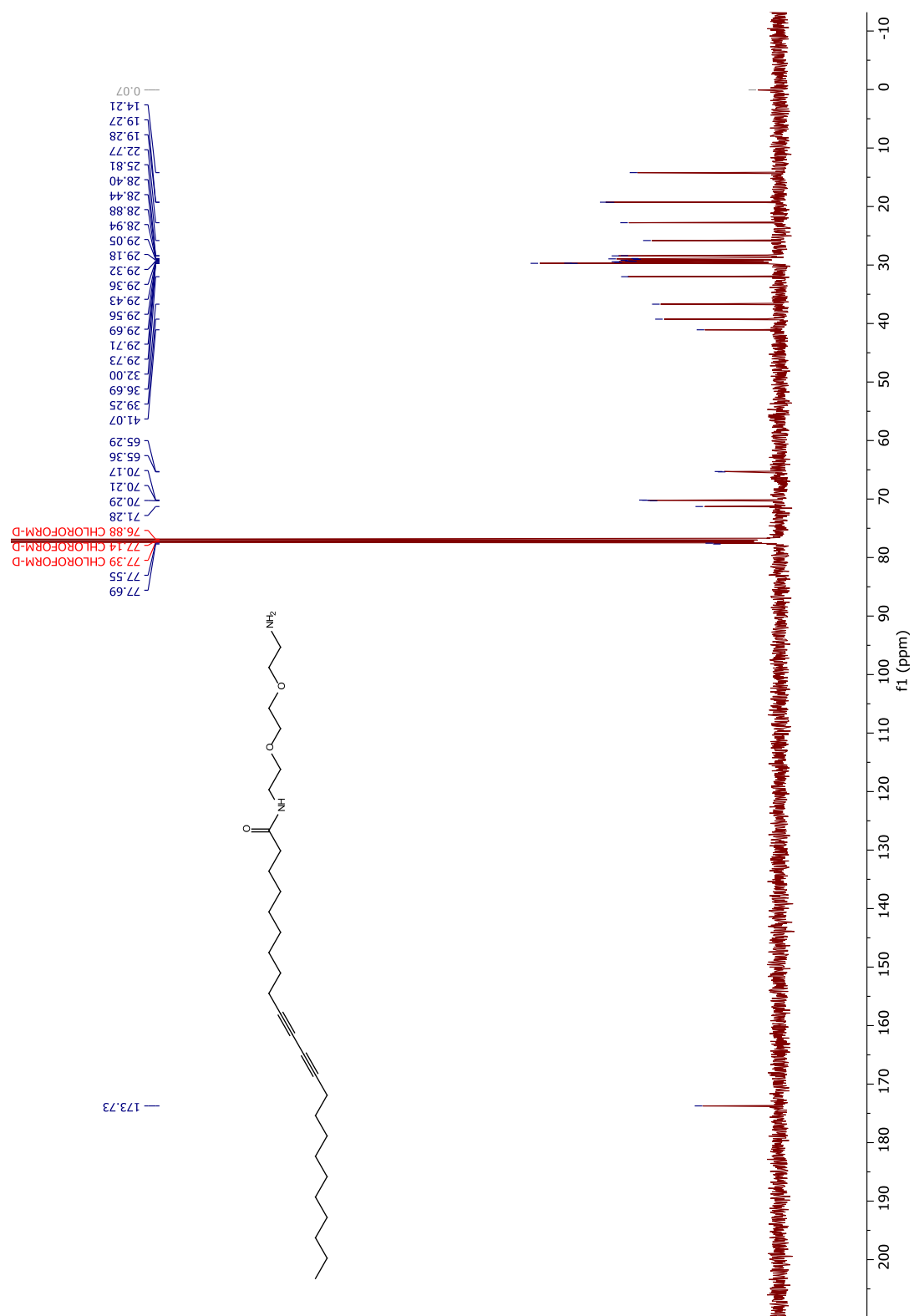


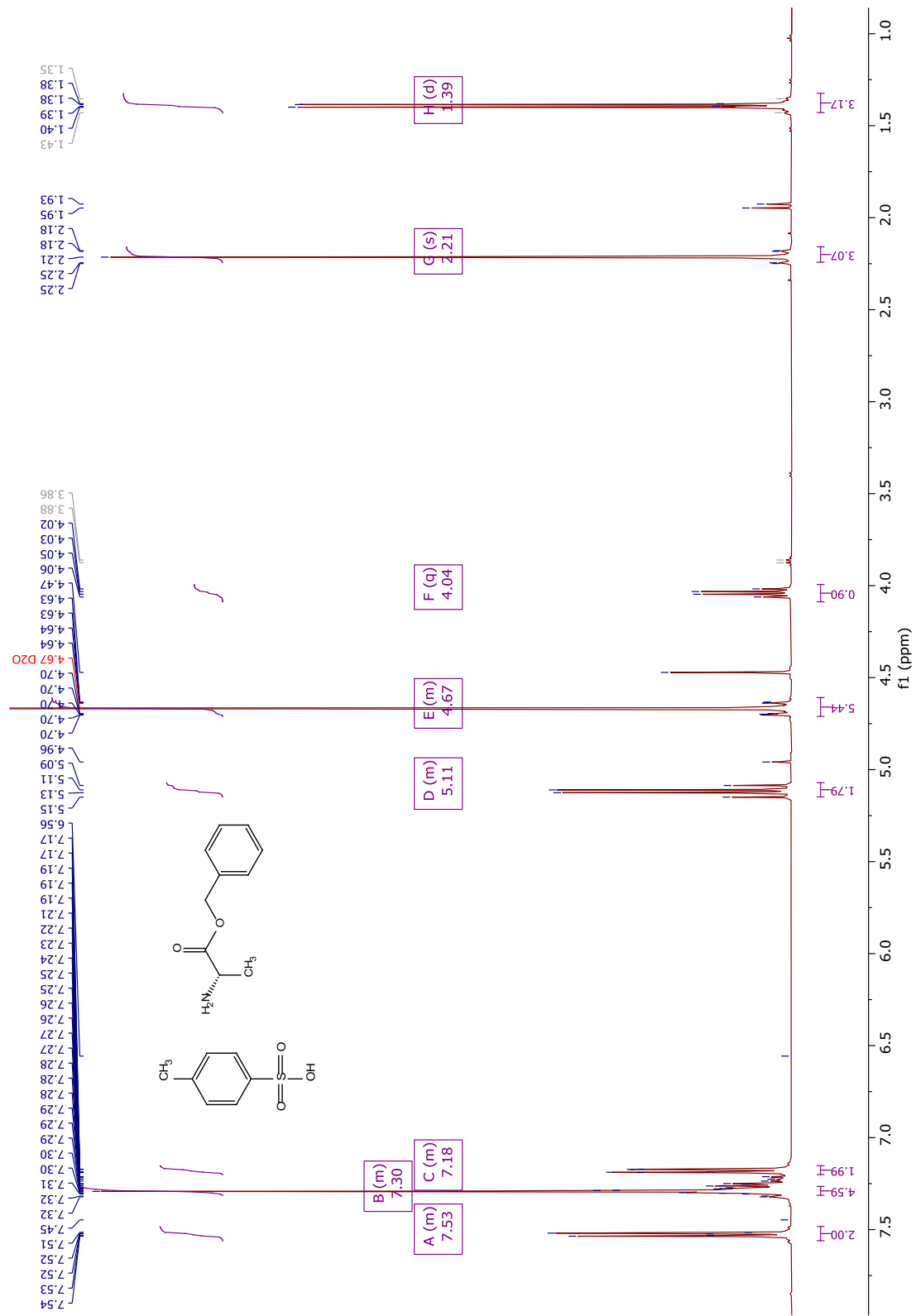
CDCl₃

7.25 CHLOROFORM-D

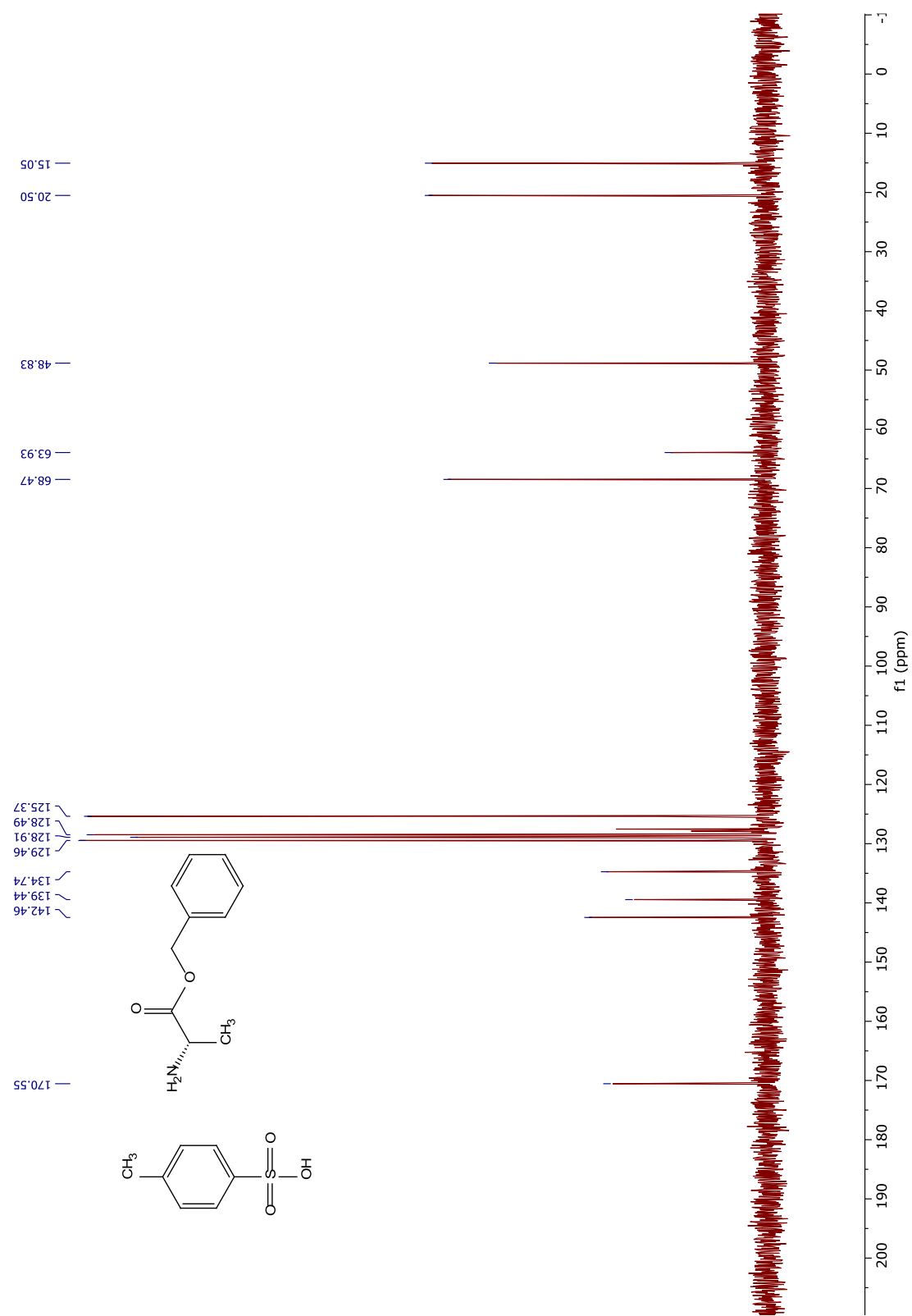


CDCl₃

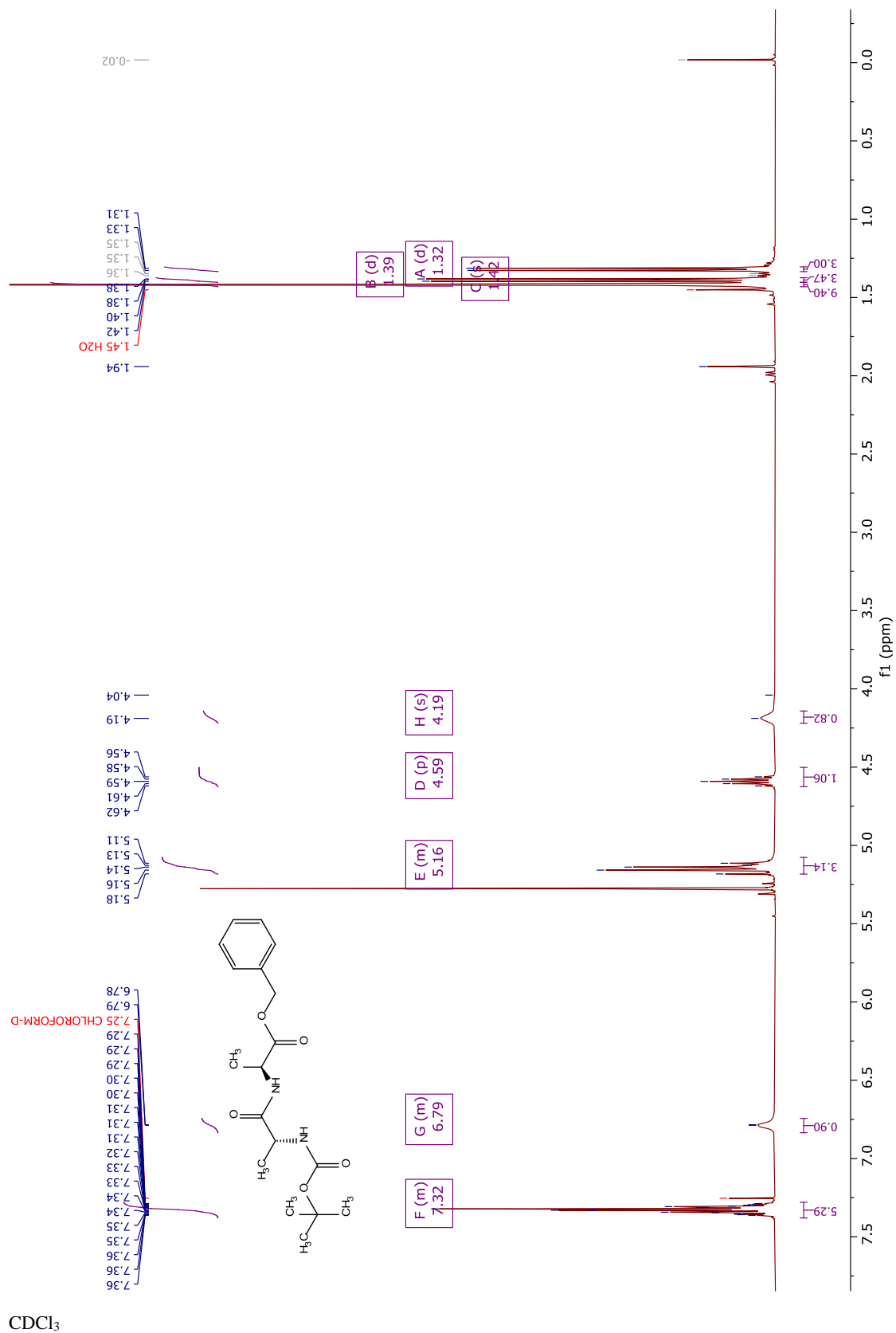




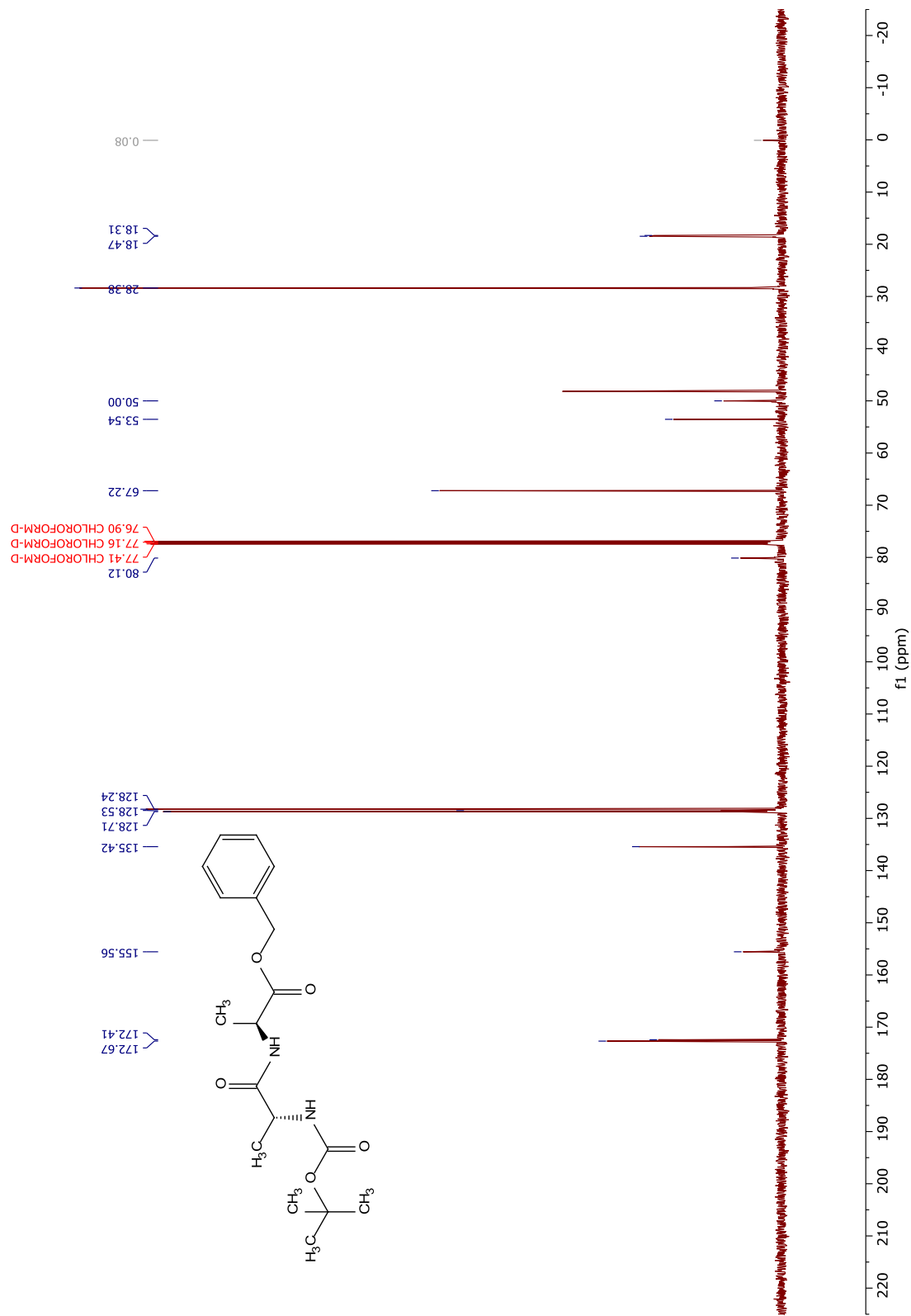
D₂O



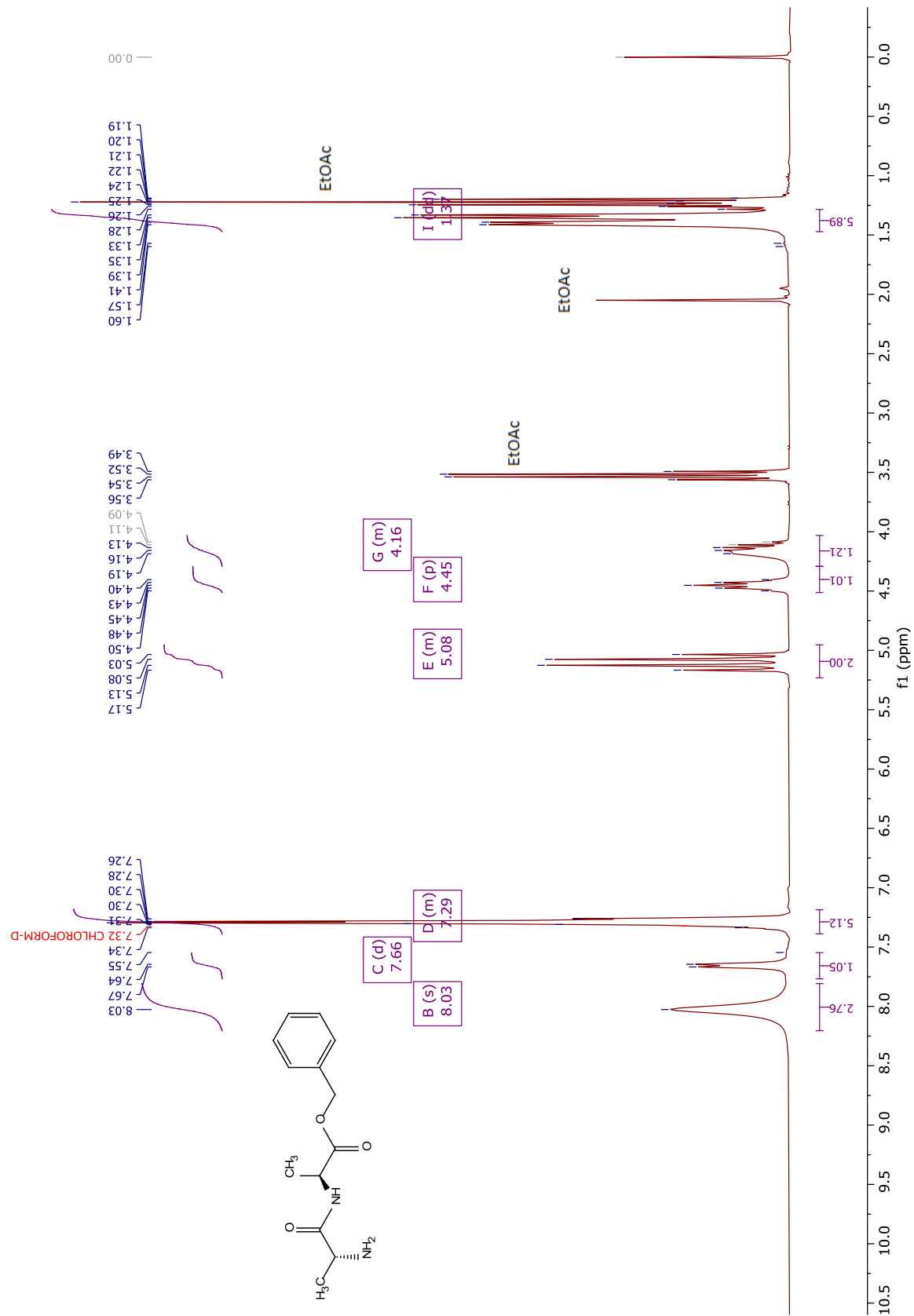
D₂O



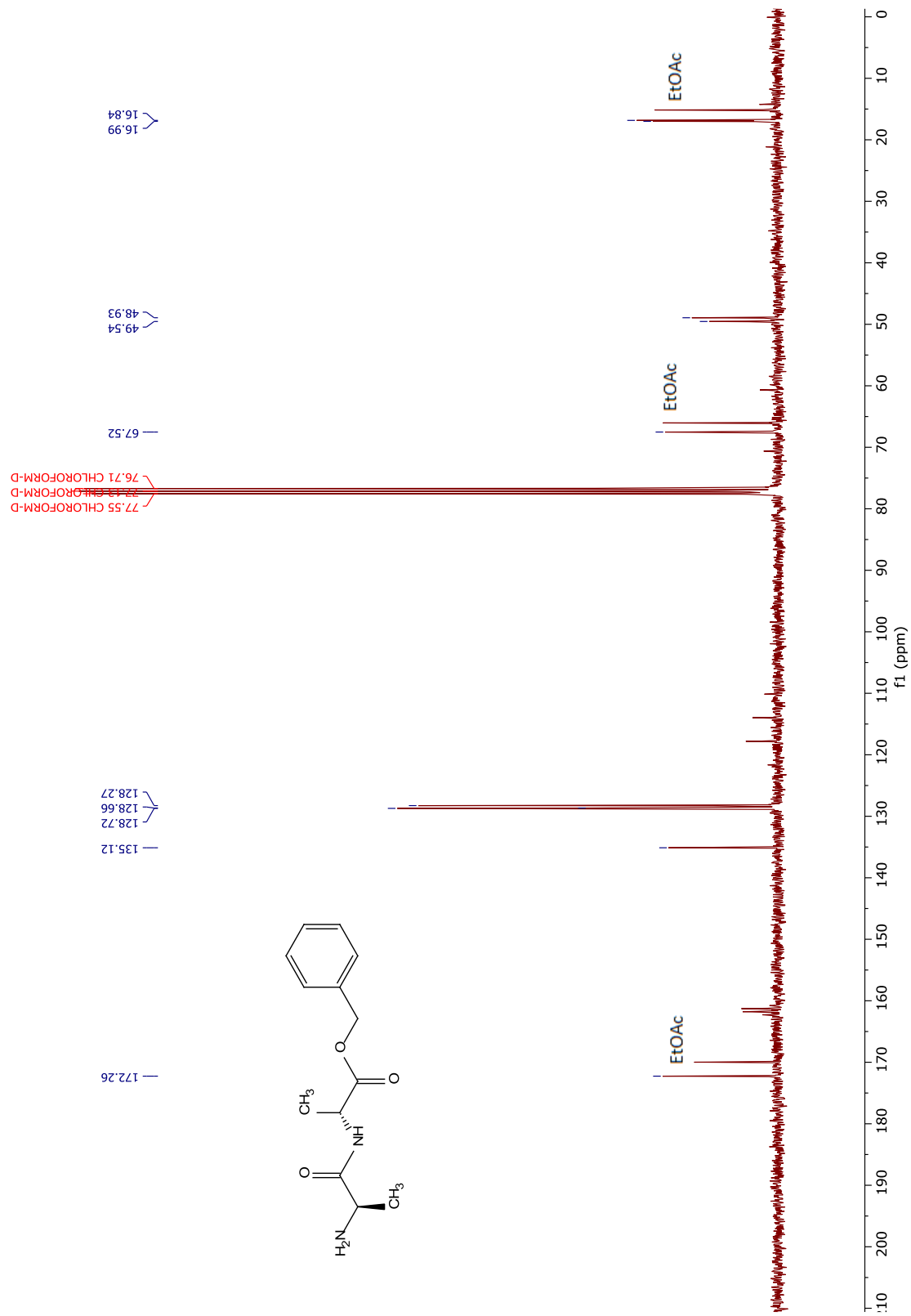
CDCl₃



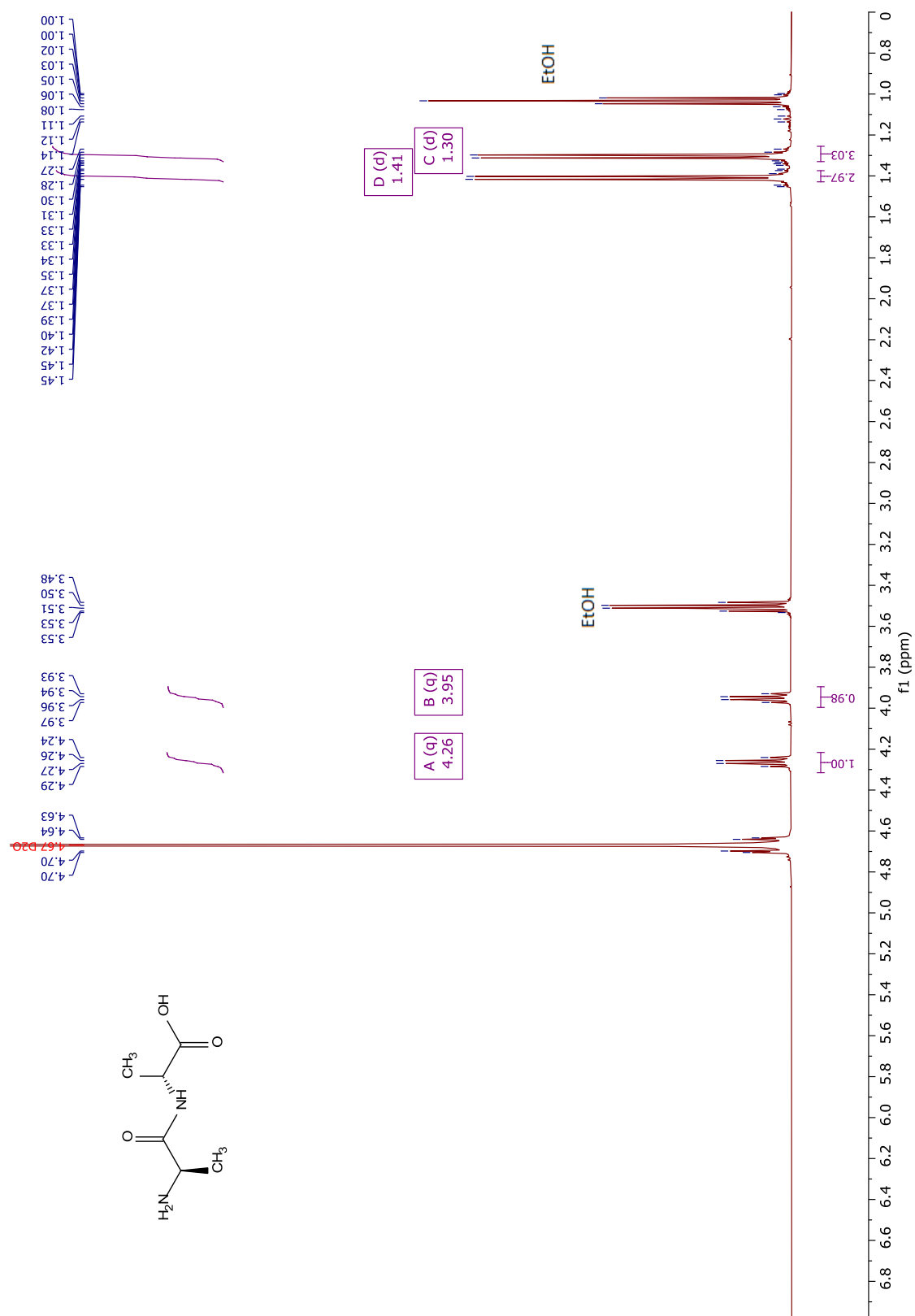
CDCl₃



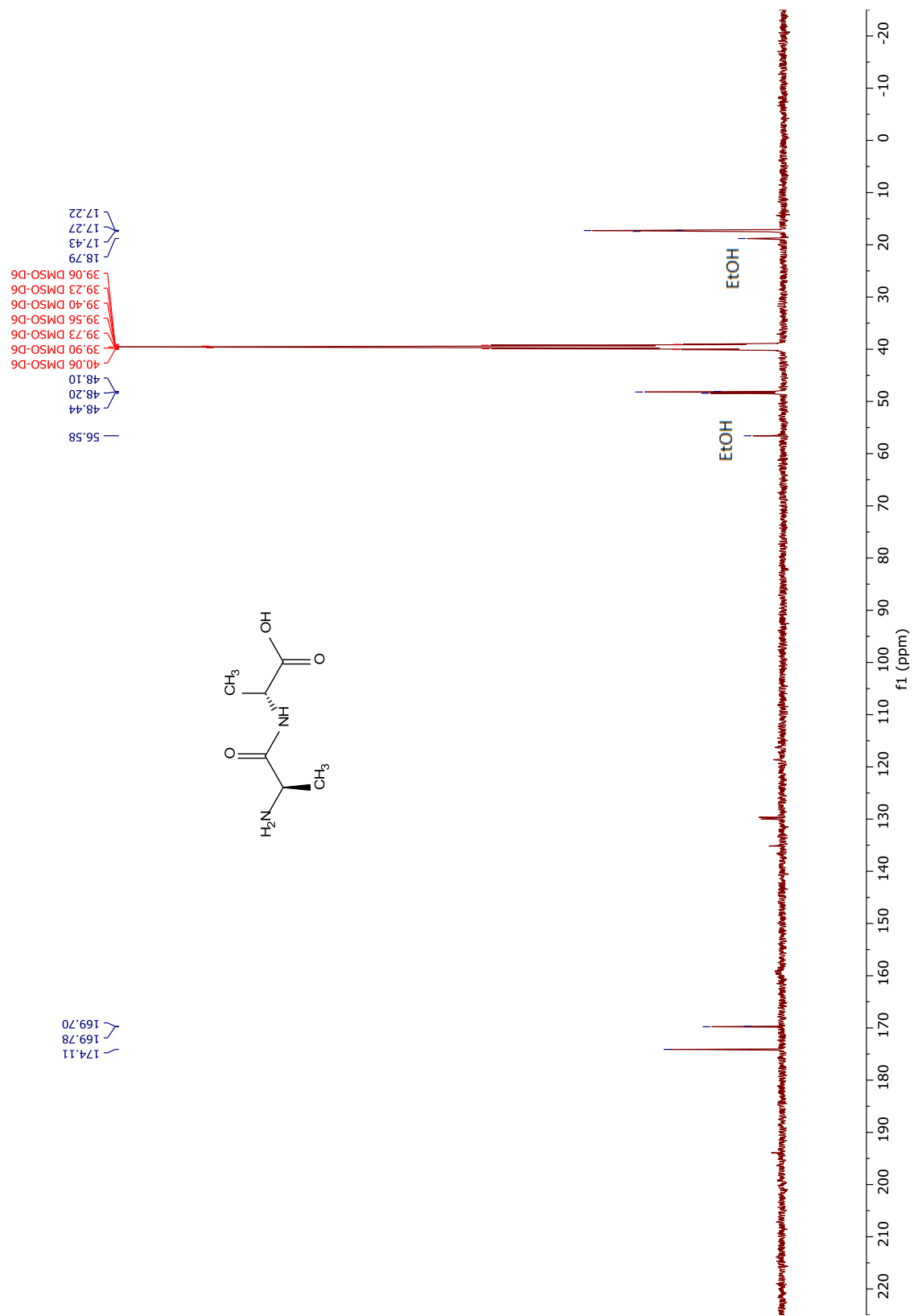
CDCl₃

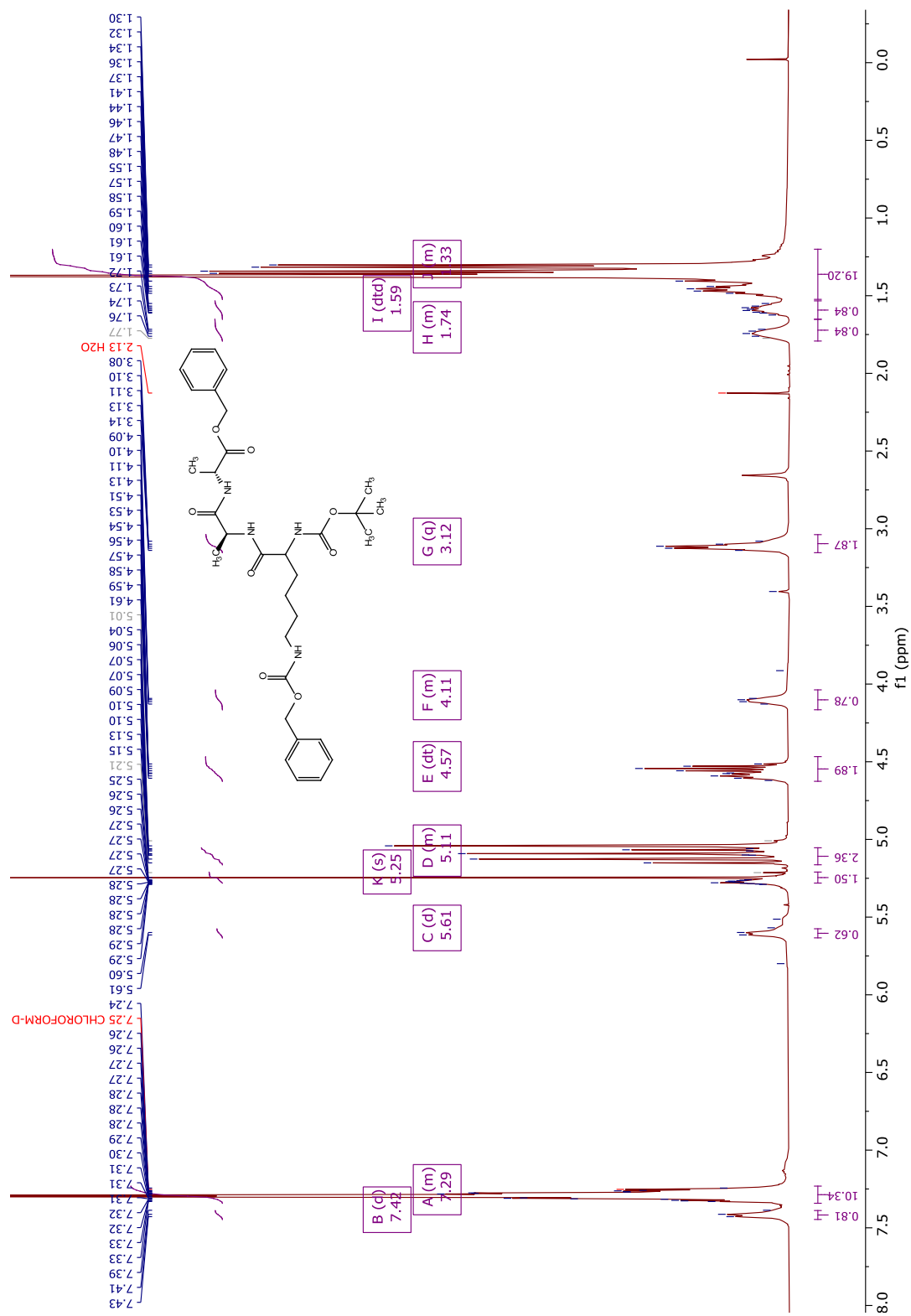


D2O

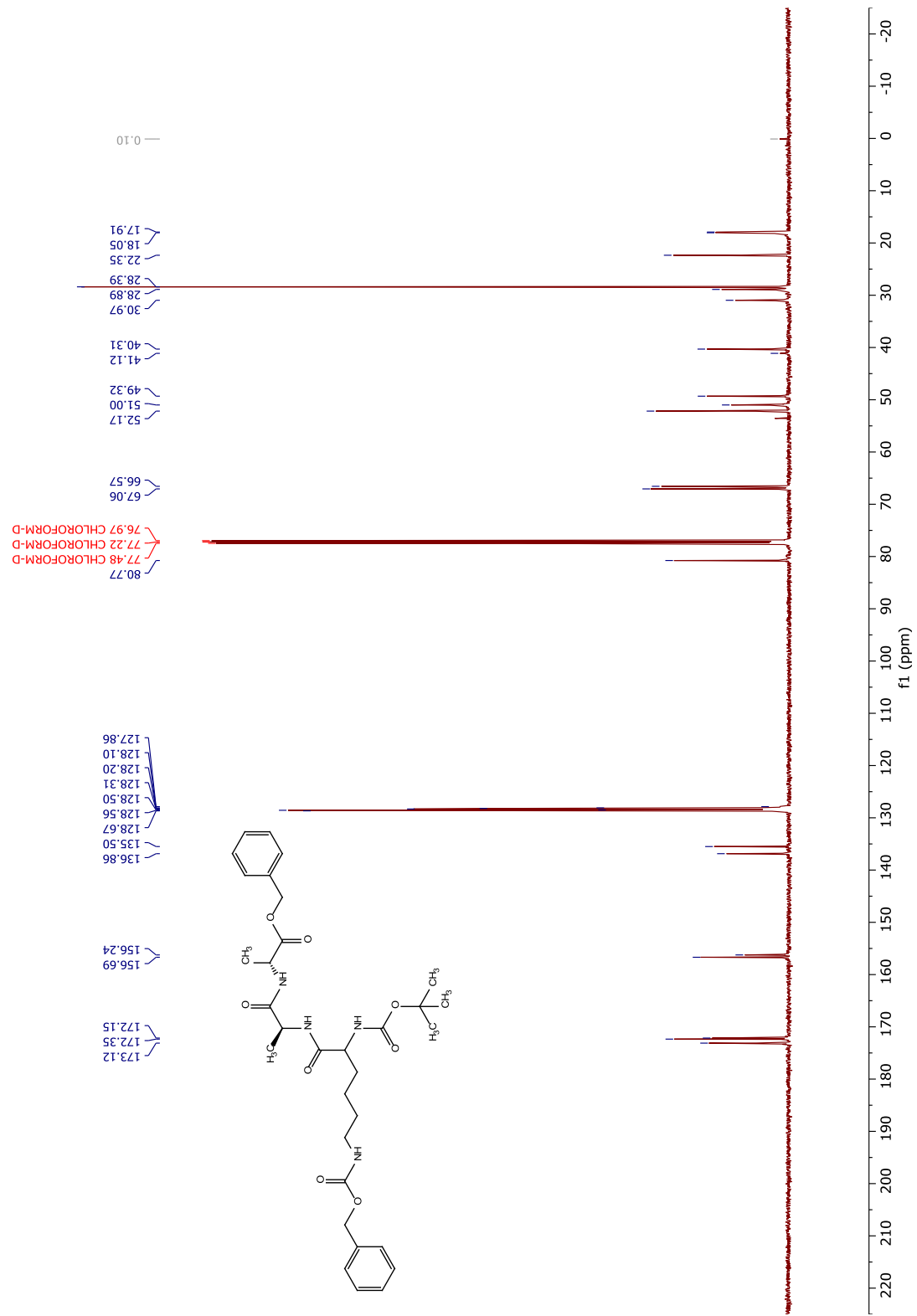


DMSO-D₆

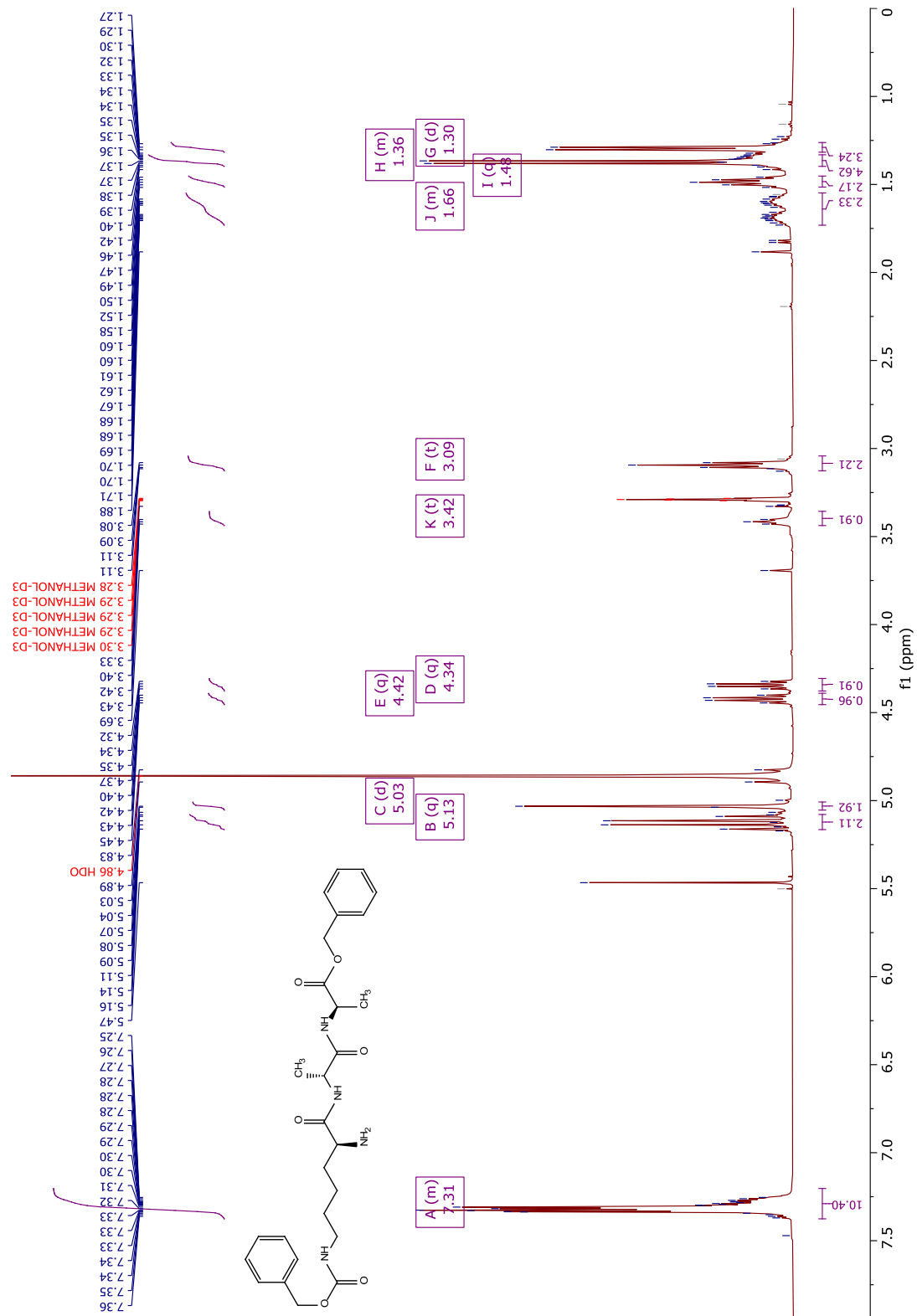




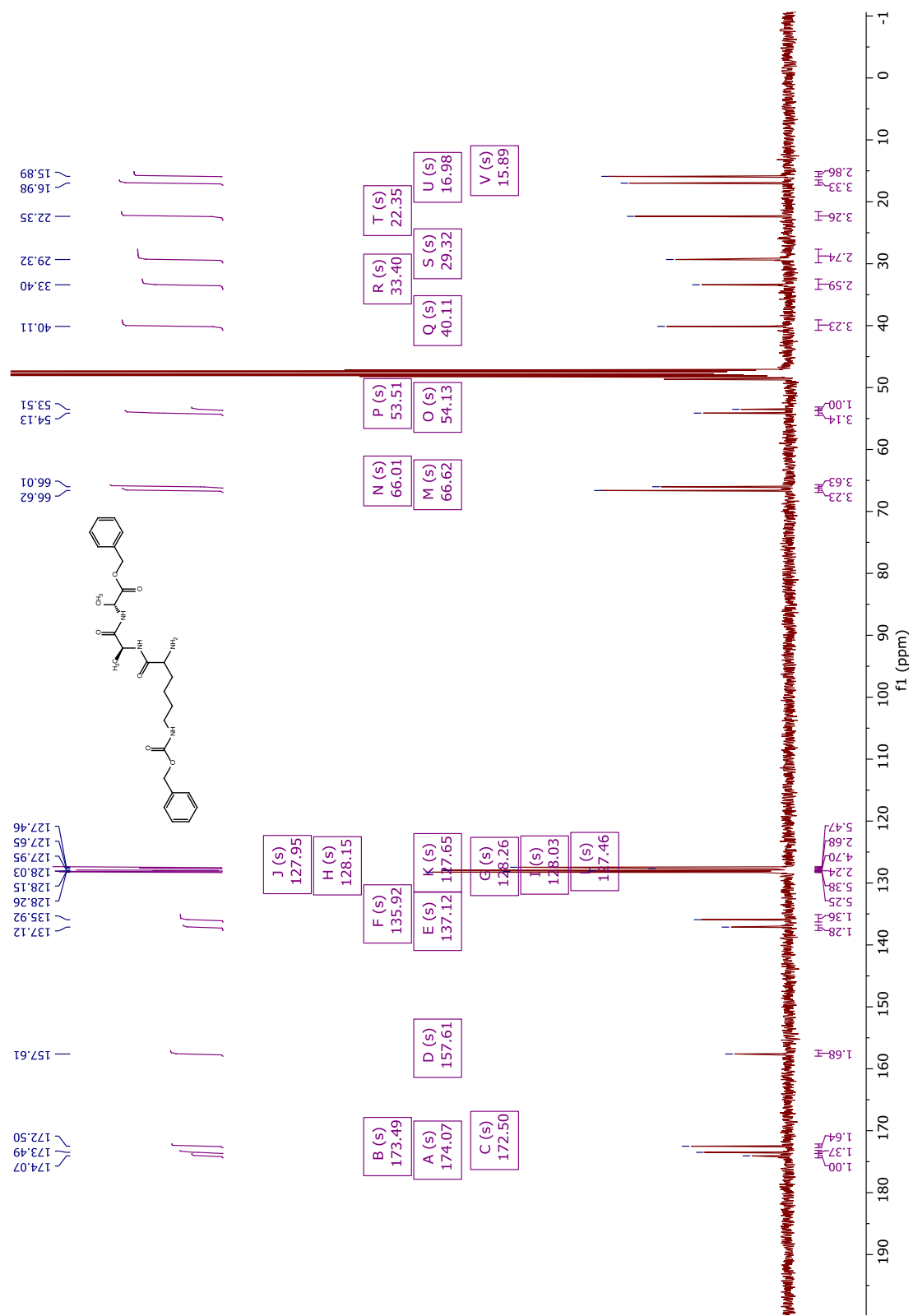
CDCl₃



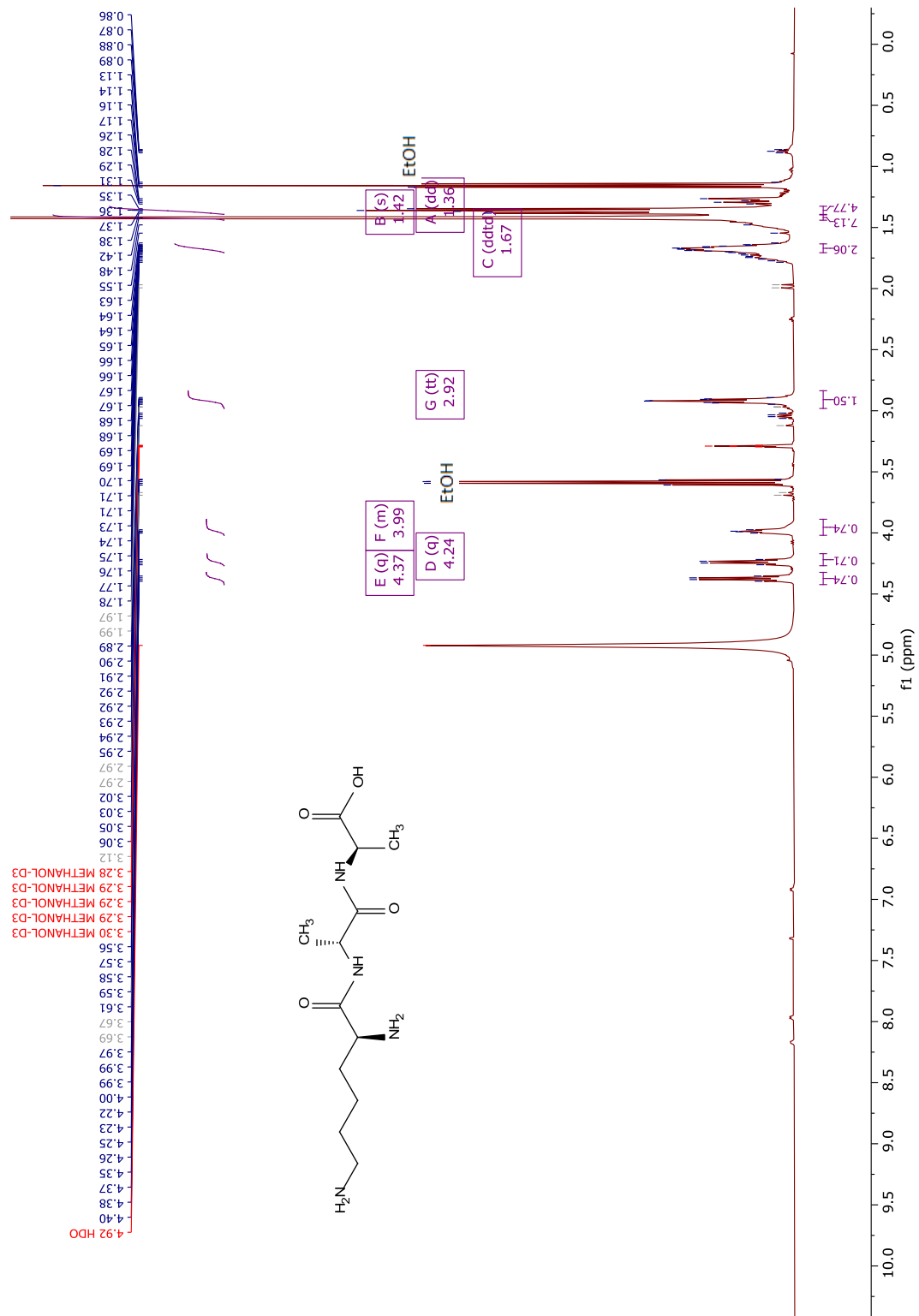
CD₃OD



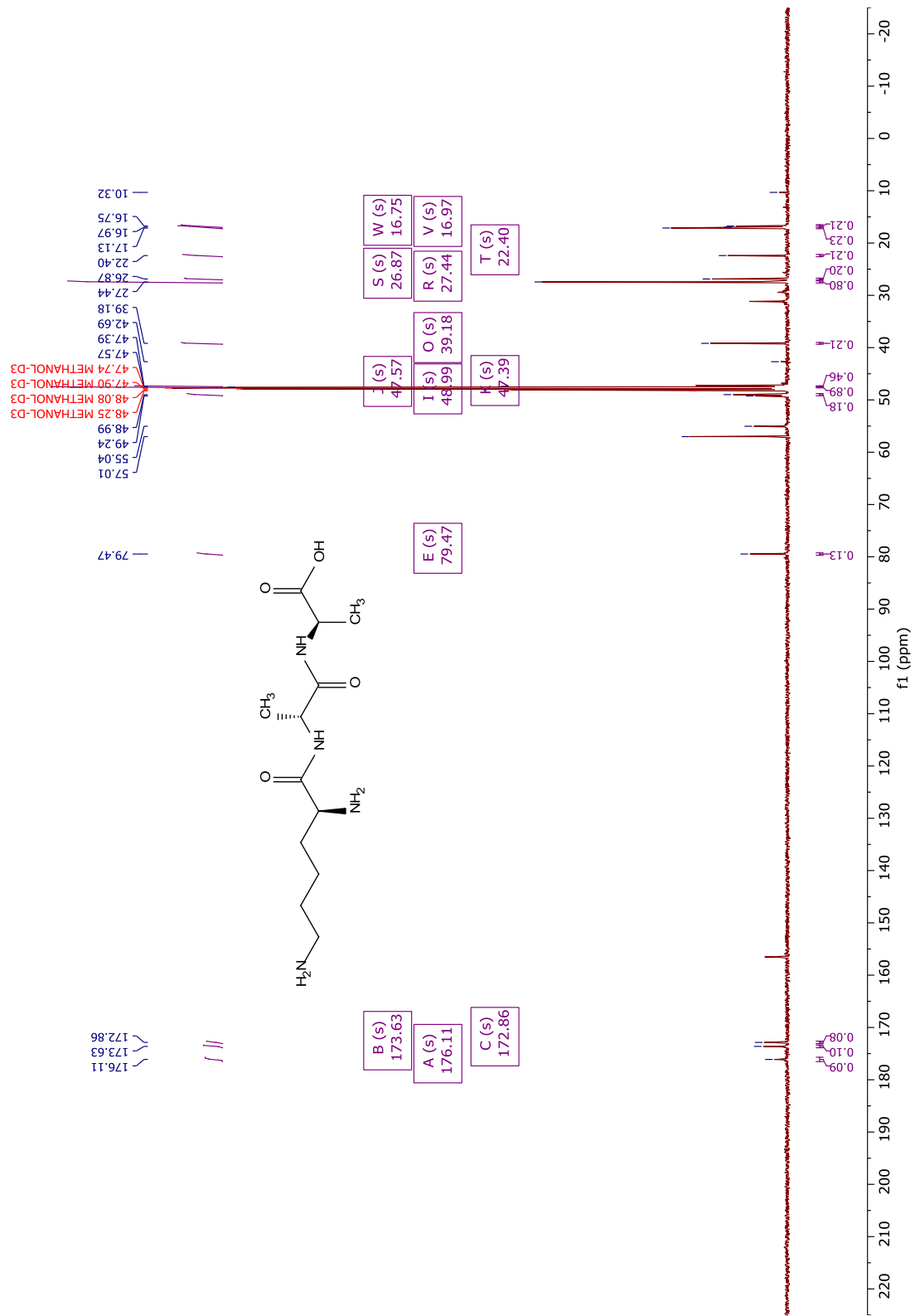
CD₃OD

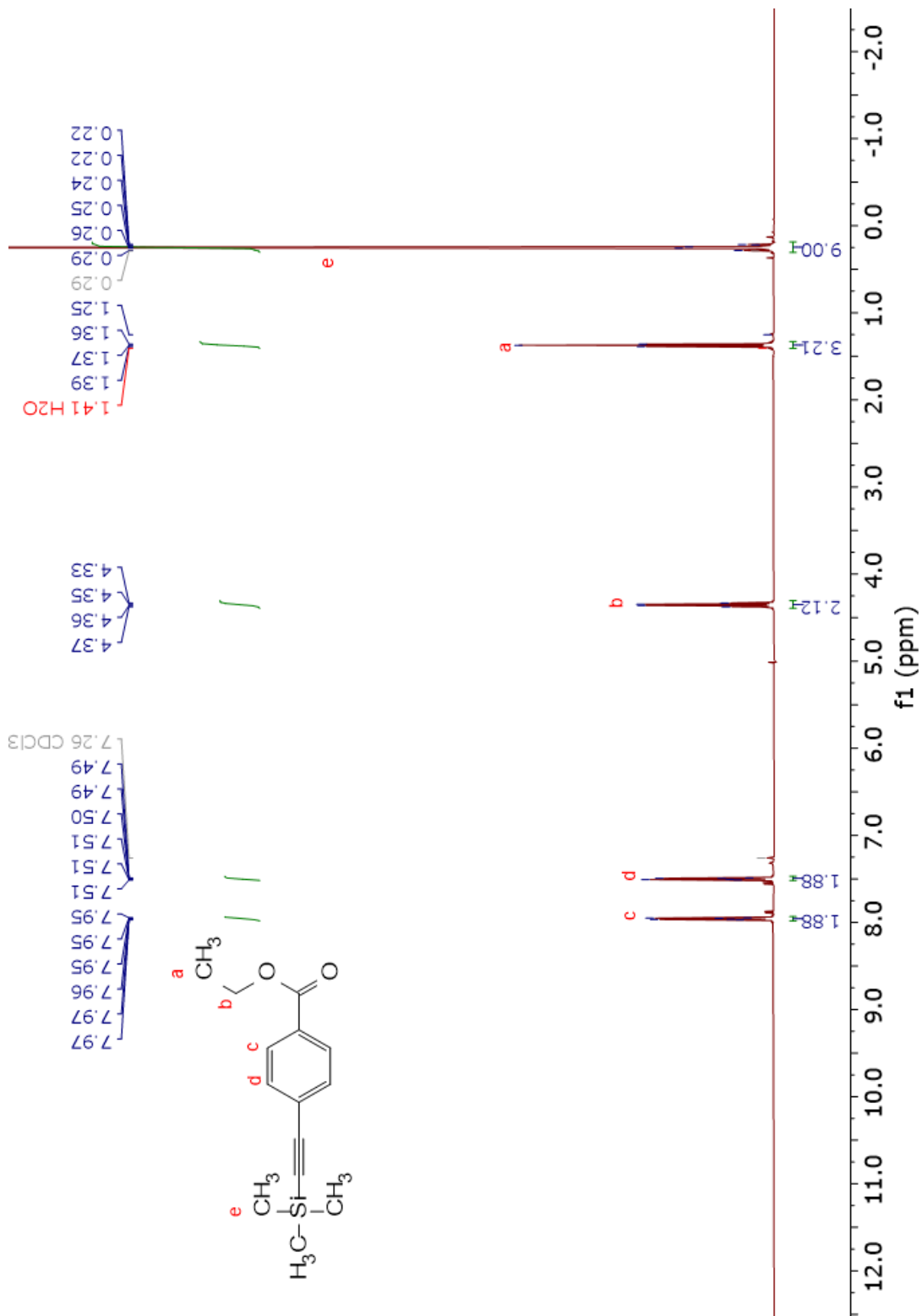


CD₃OD



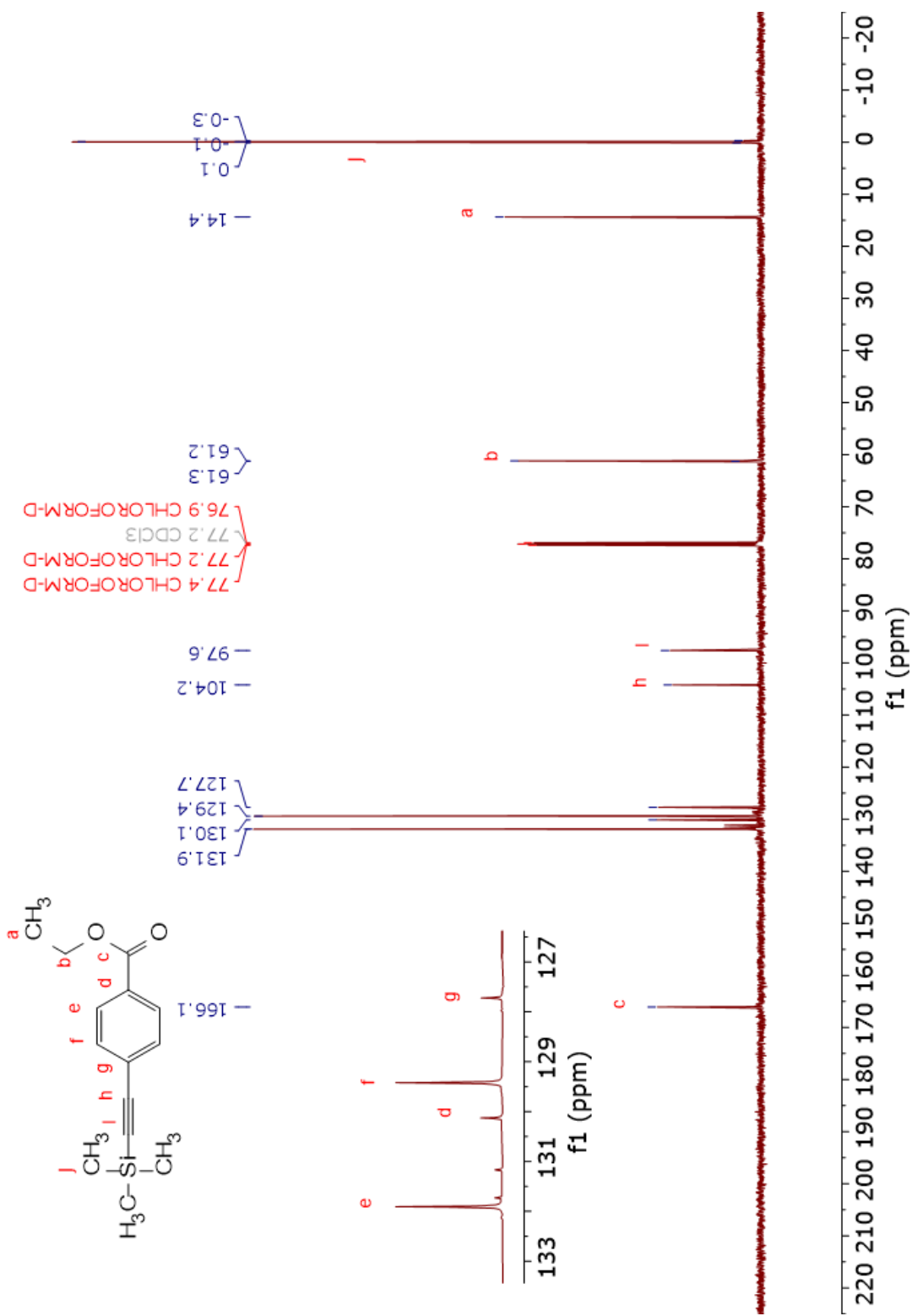
CD₃OD

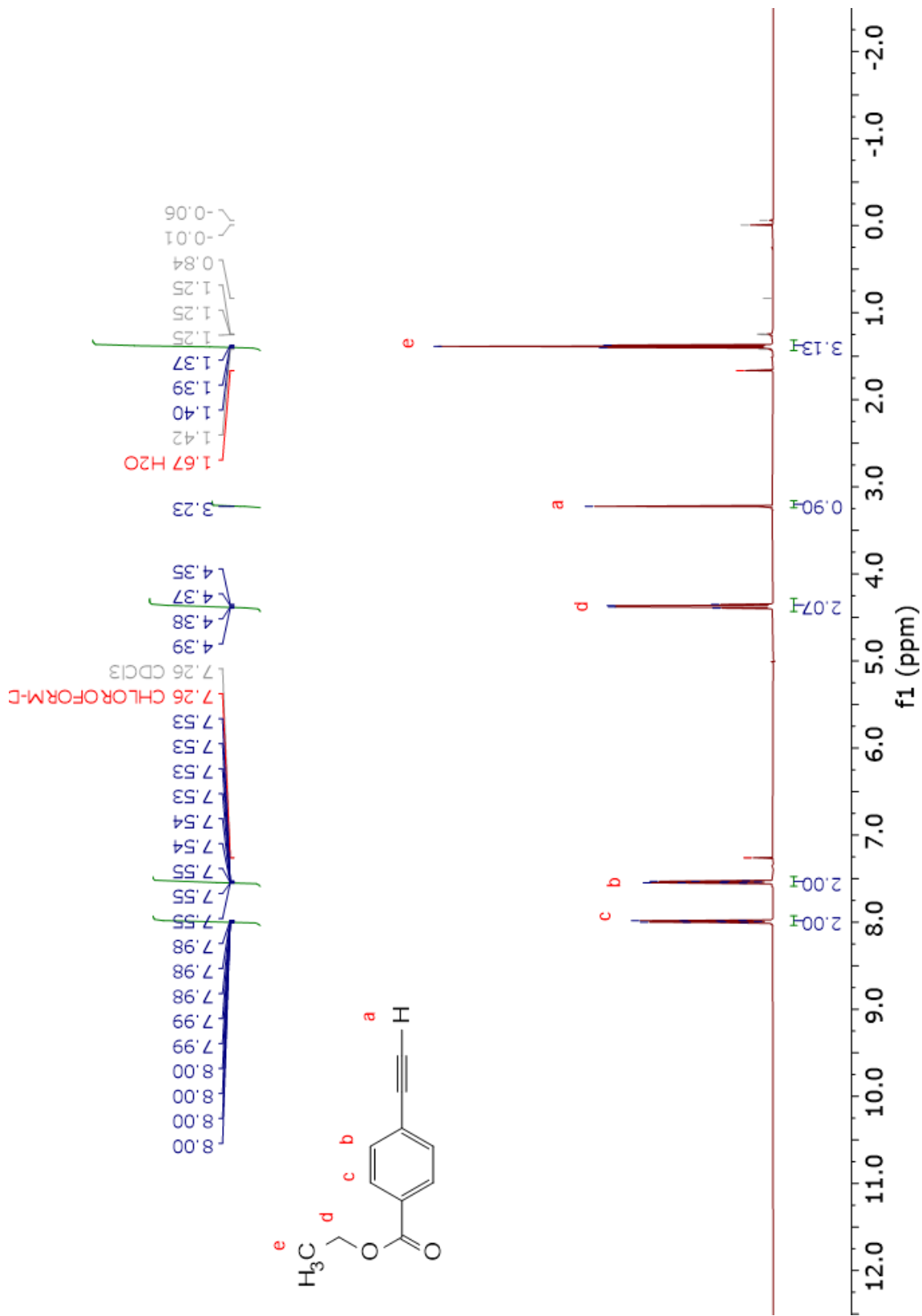




CDCl₃

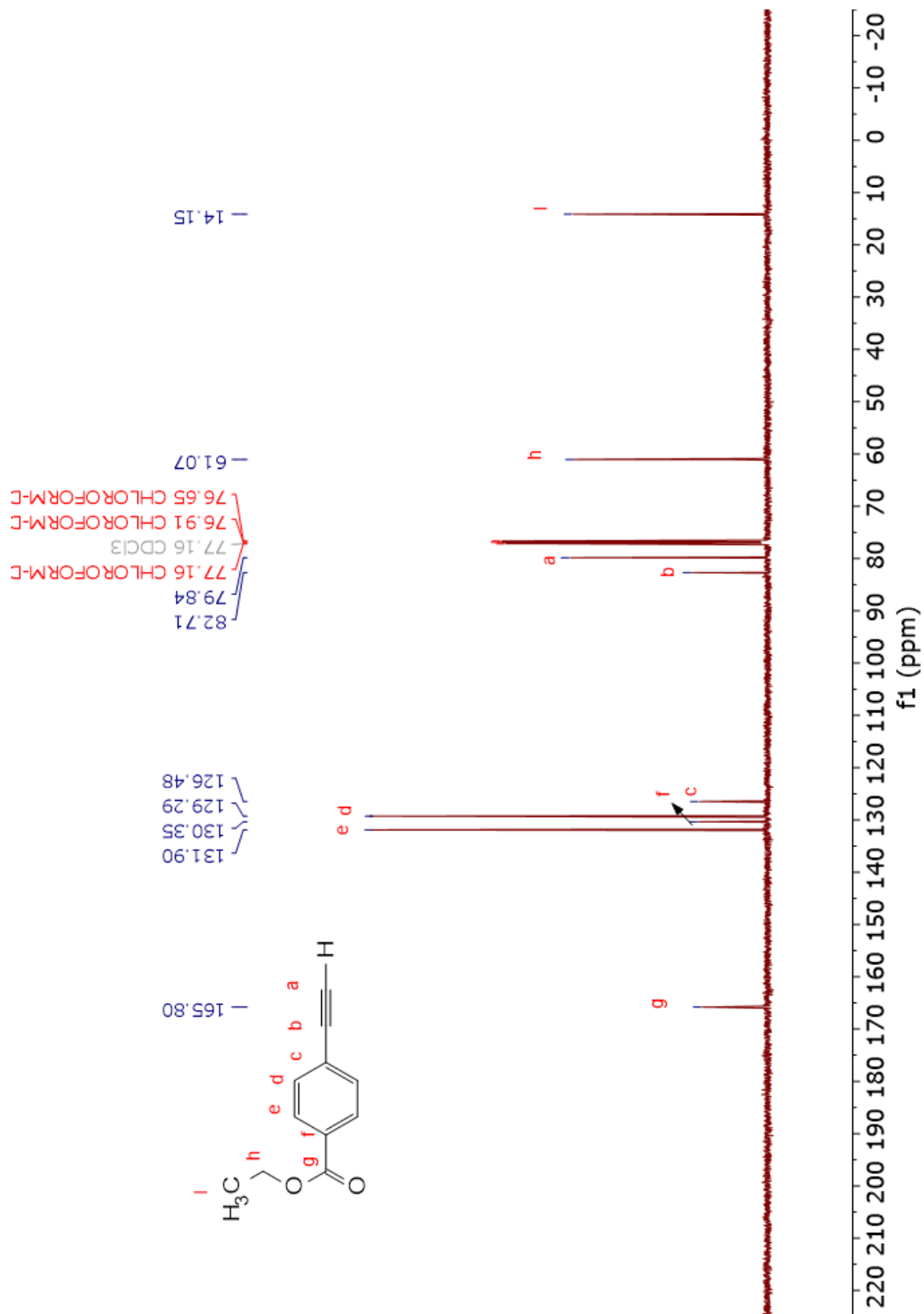
CDCl₃



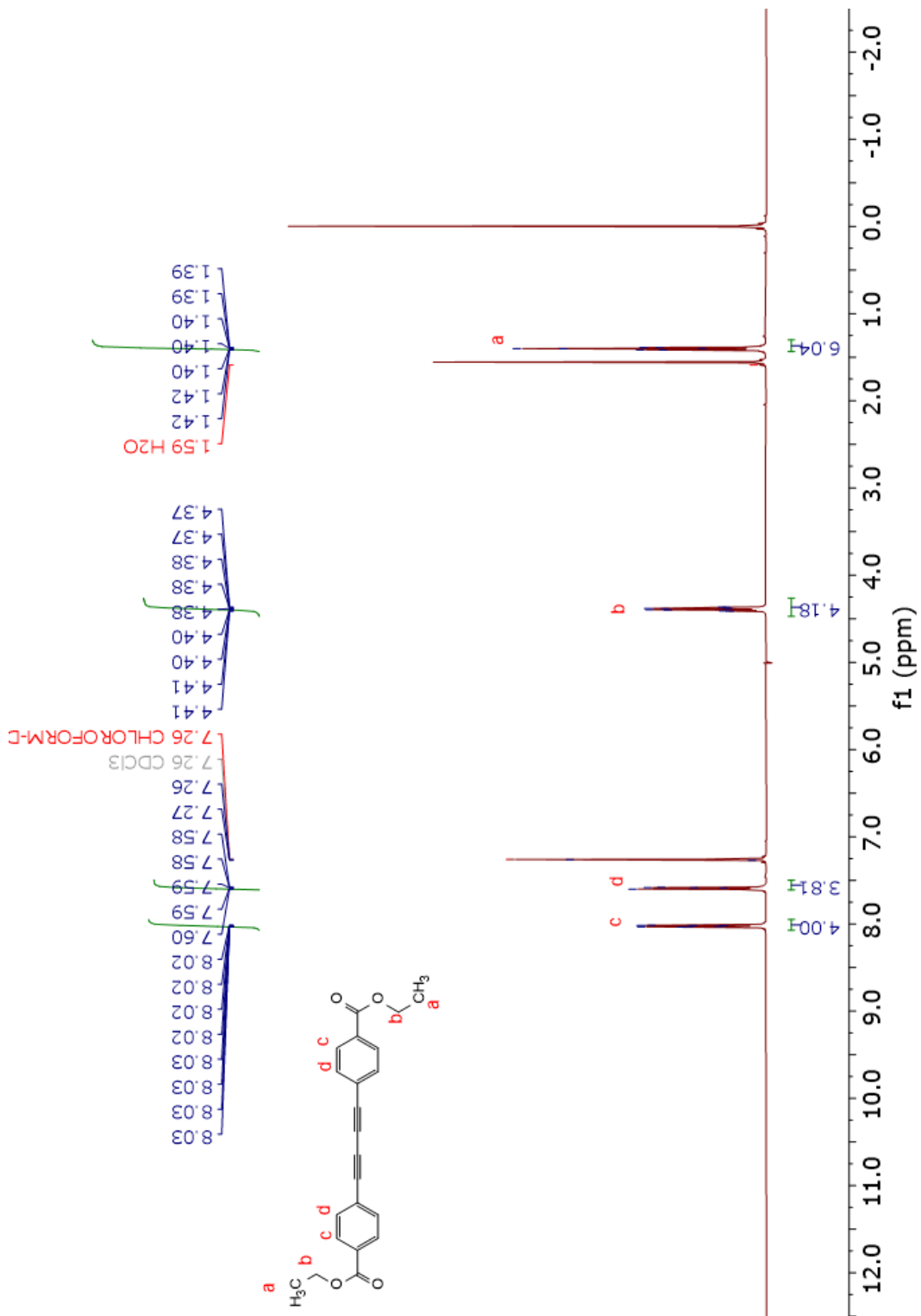


CDCl₃

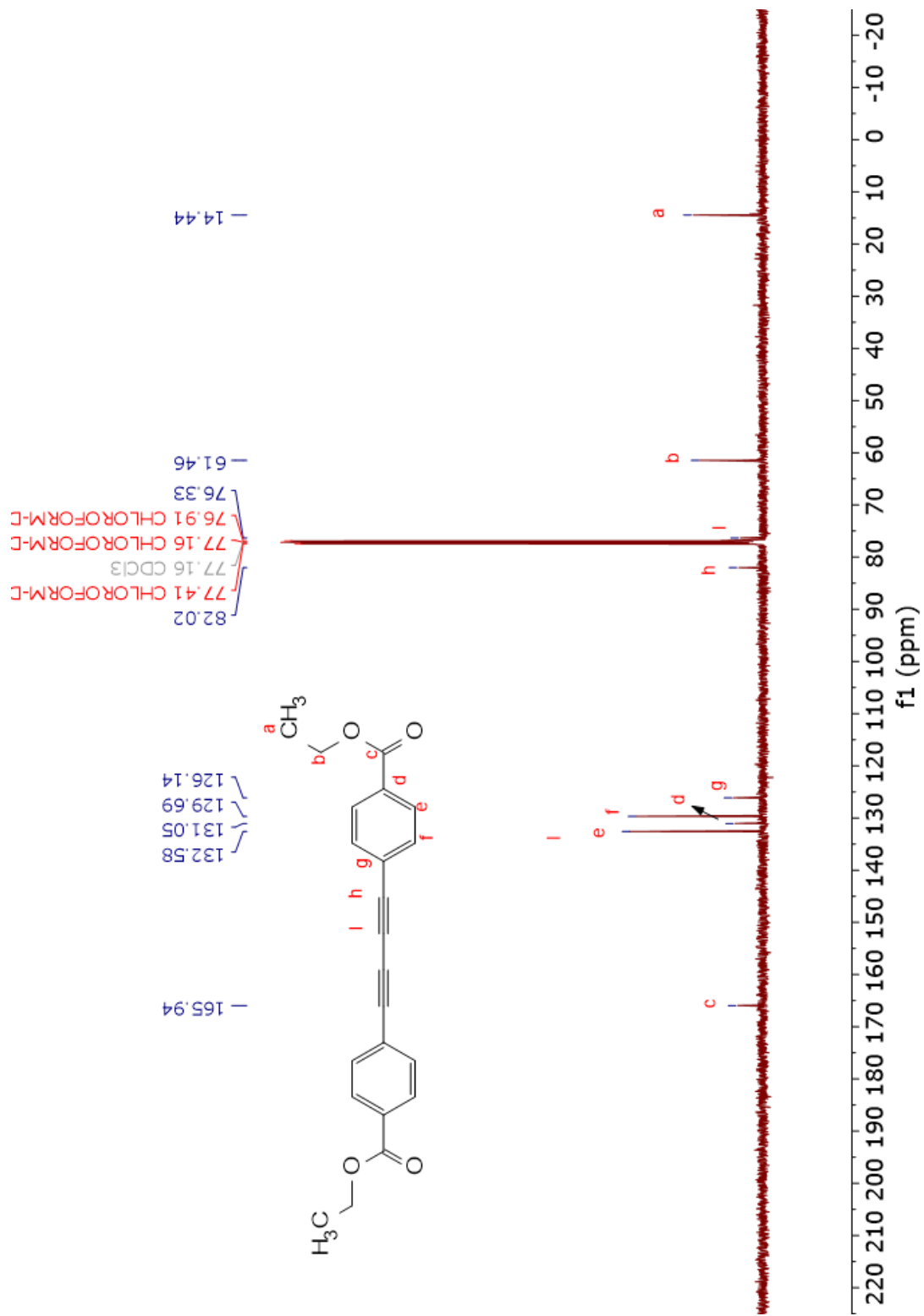
CDCl₃

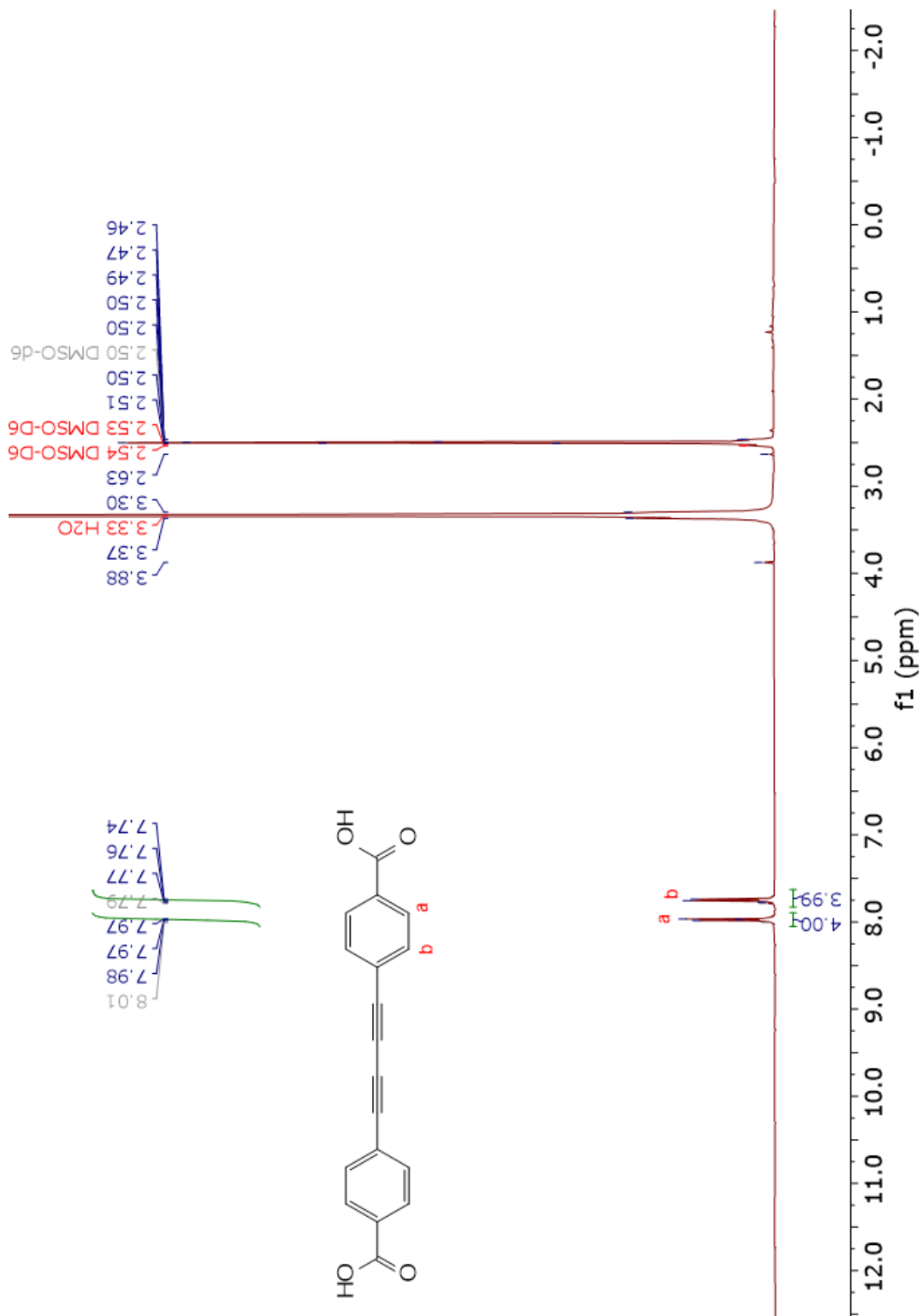


CDCl₃

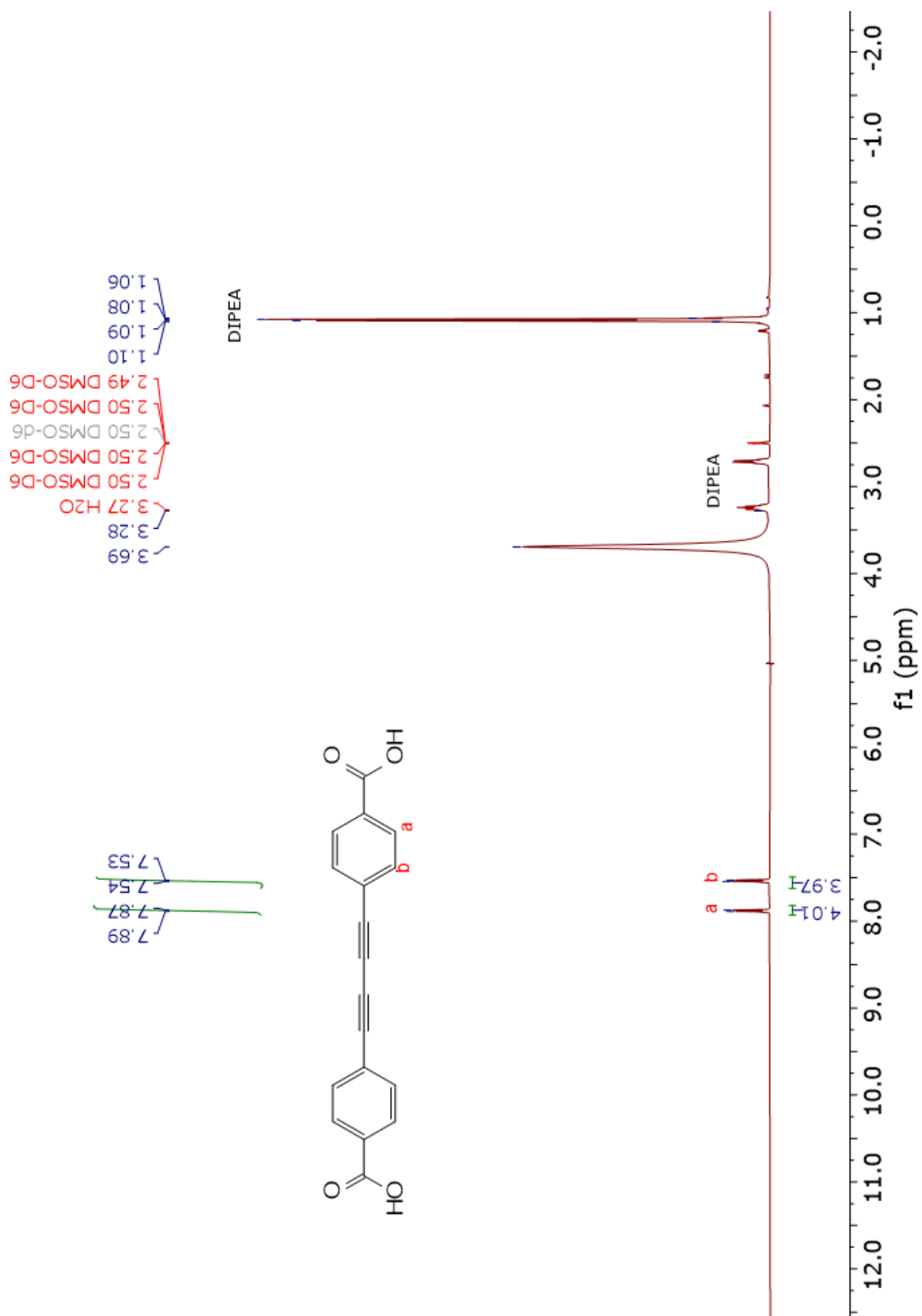


CDCl₃

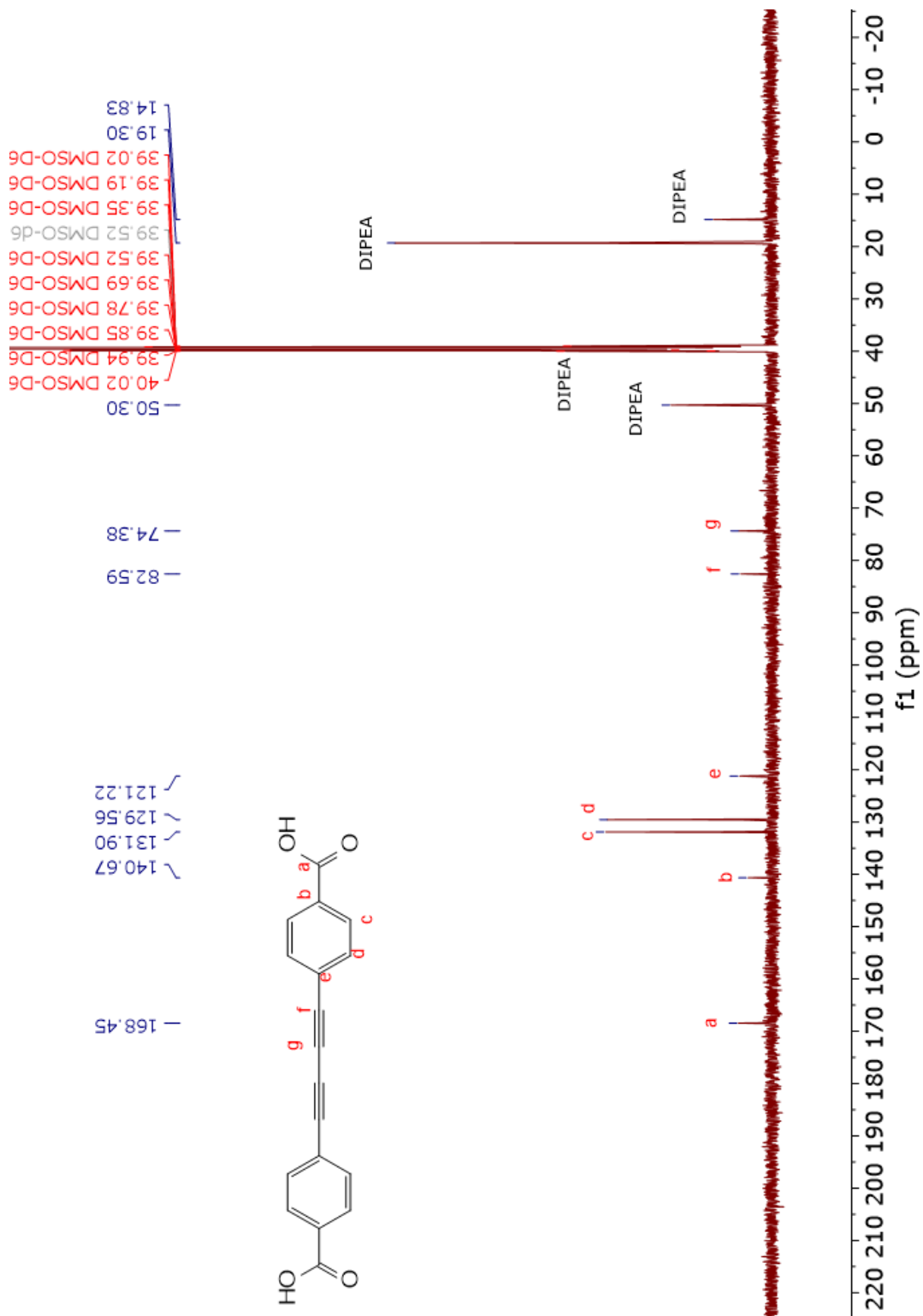




DMSO-d₆

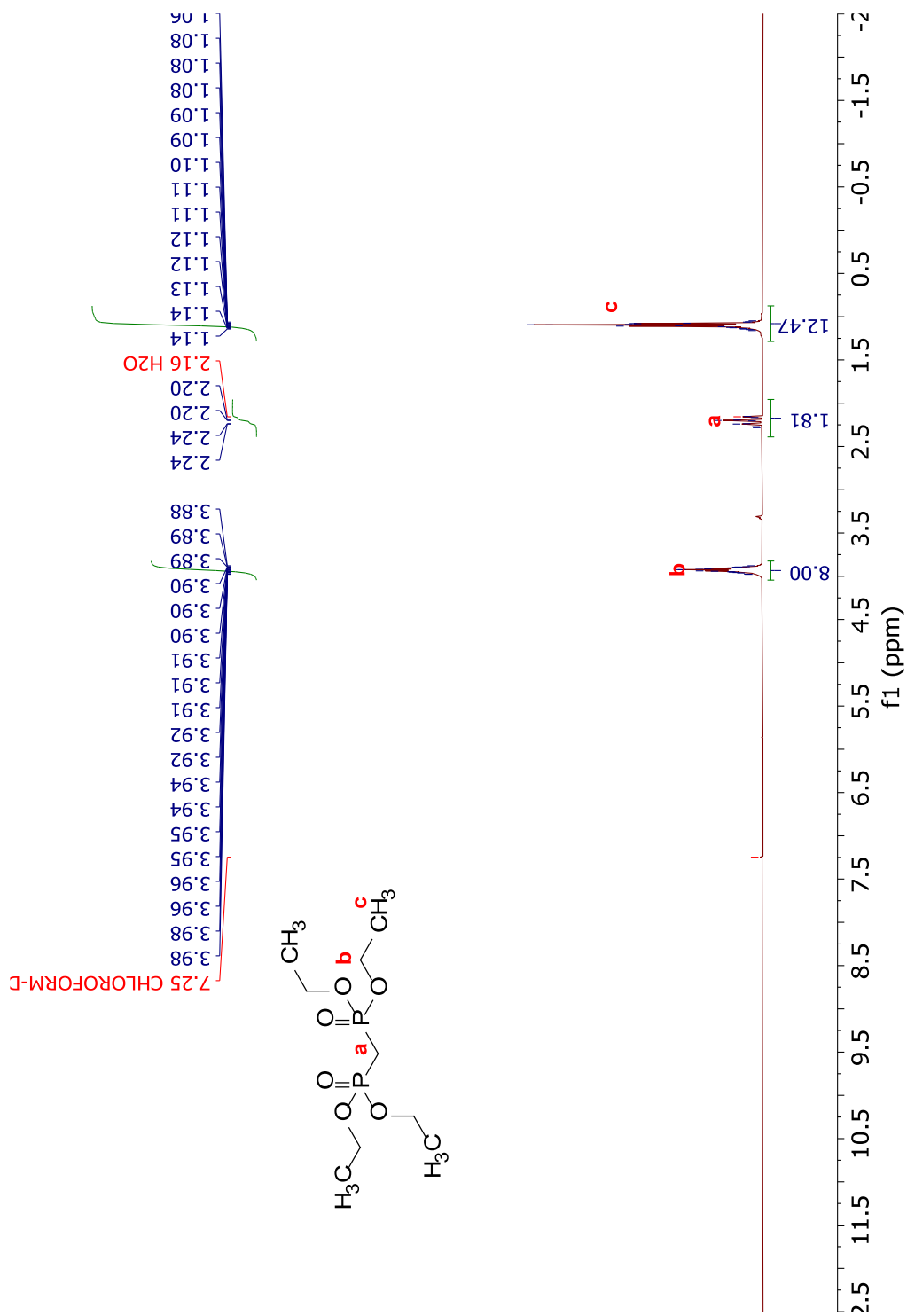


with DIPEA in DMSO-d₆



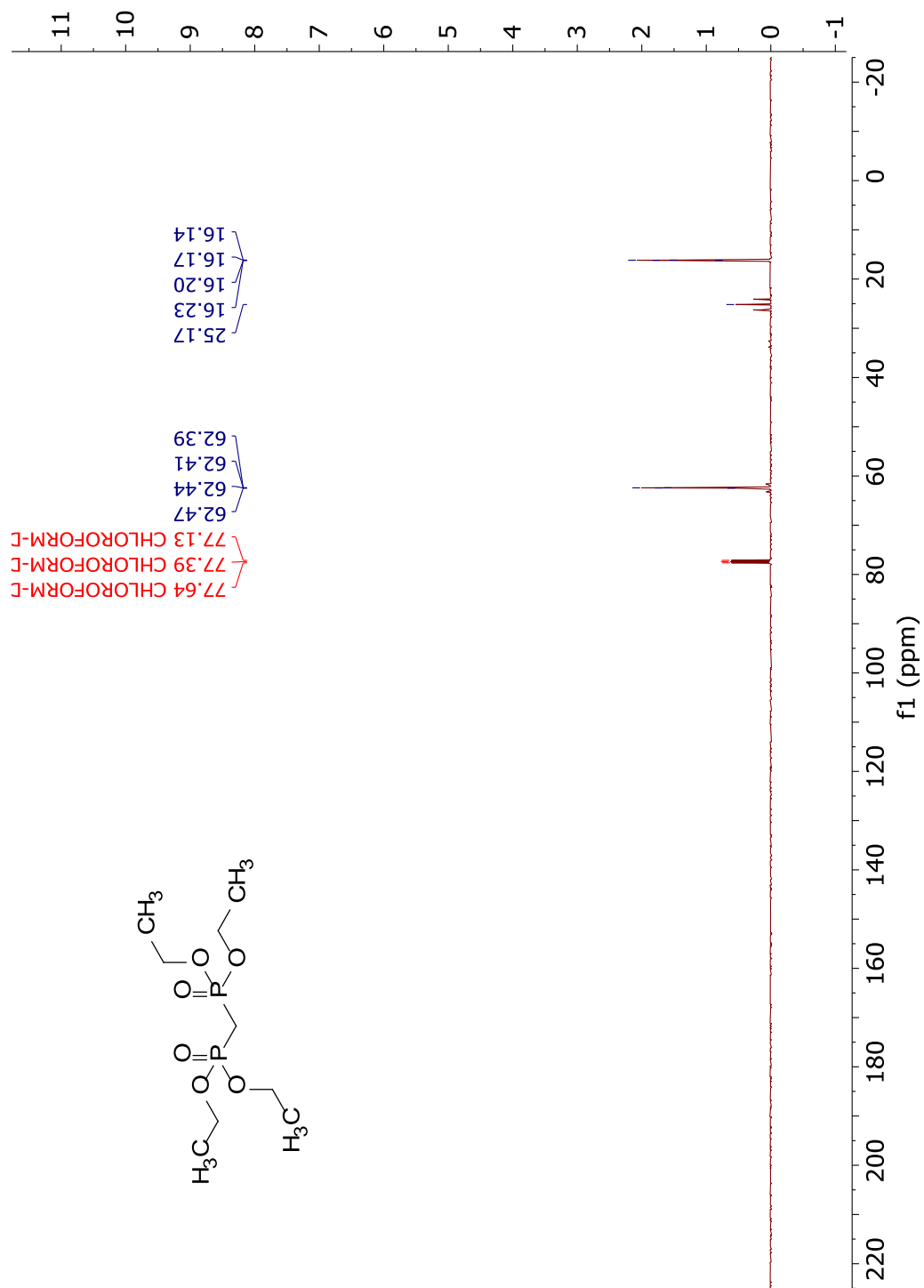
with DIPEA in DMSO-d₆

NMR and other characterization data



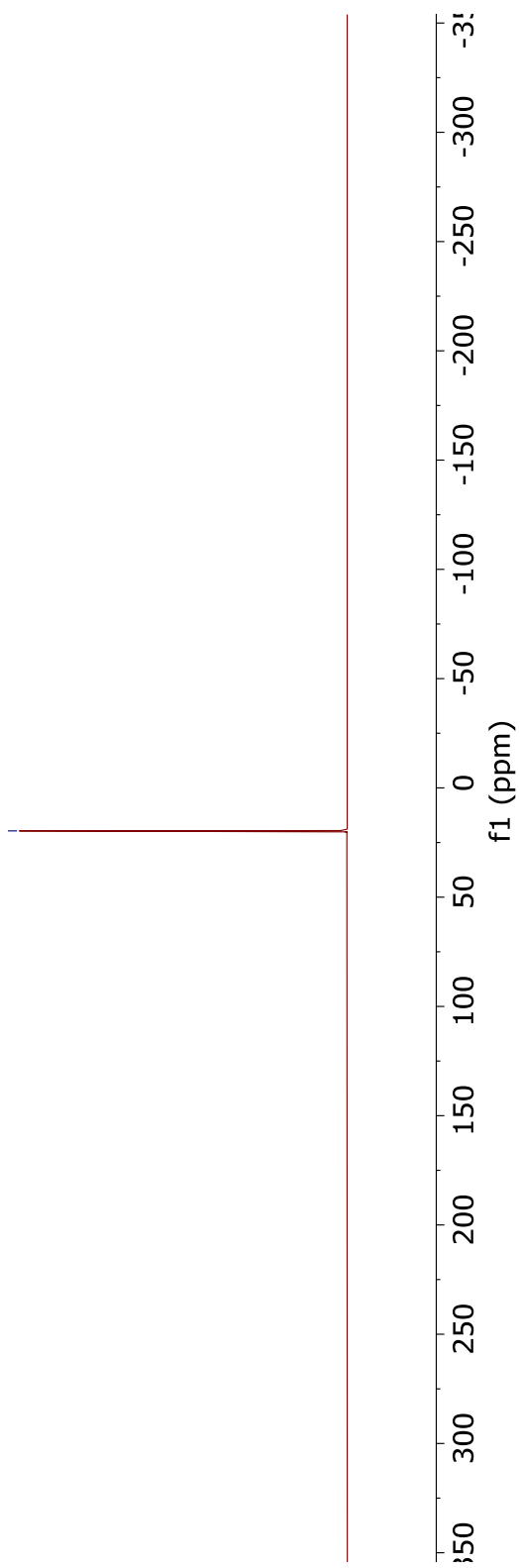
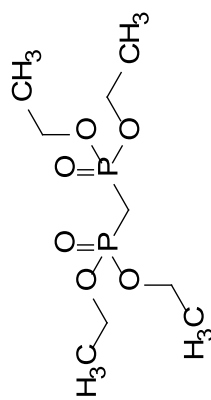
CDCl₃

CDCl₃



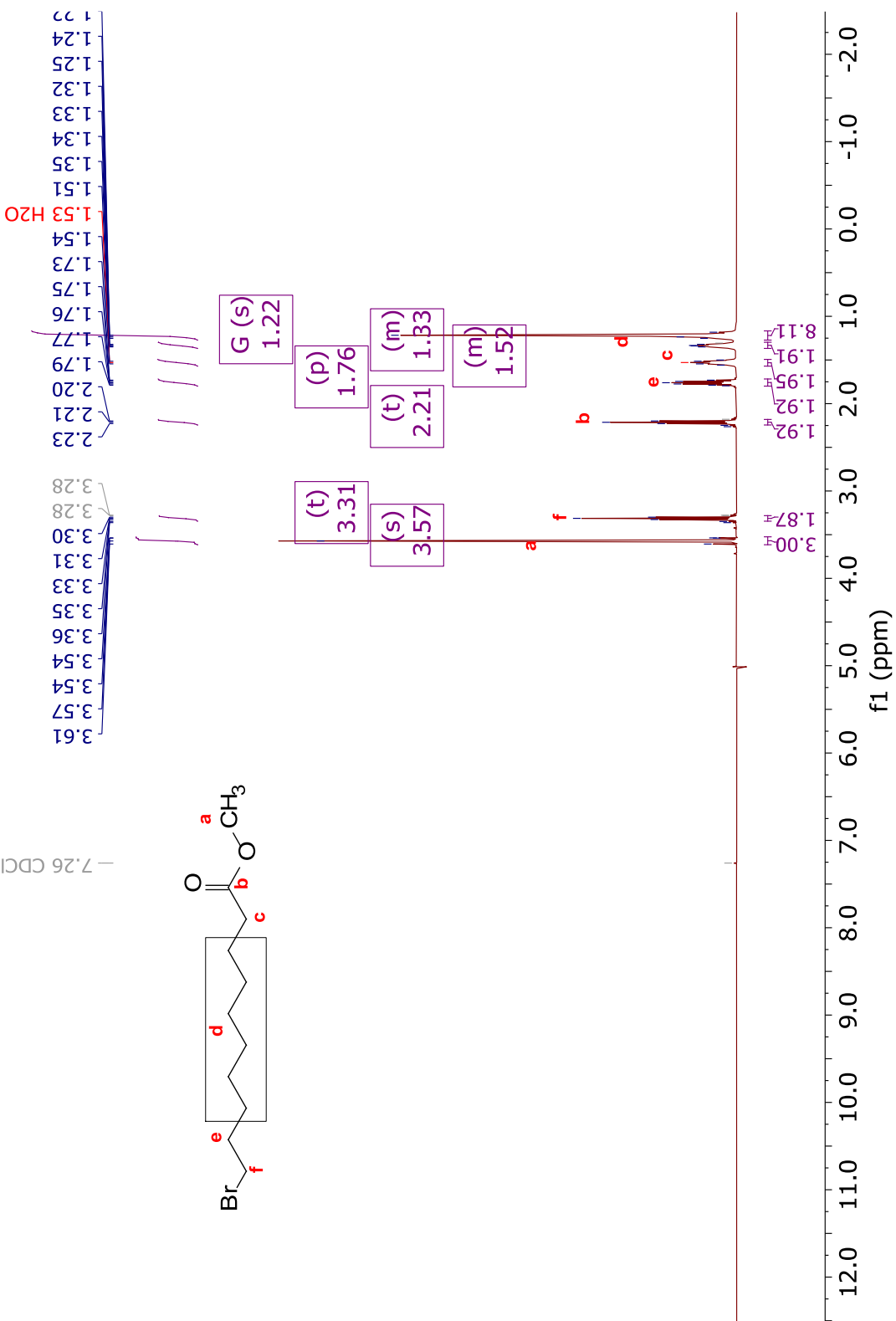
CDCl₃

— 19.68



CDCl₃

-7.26 CDCl₃

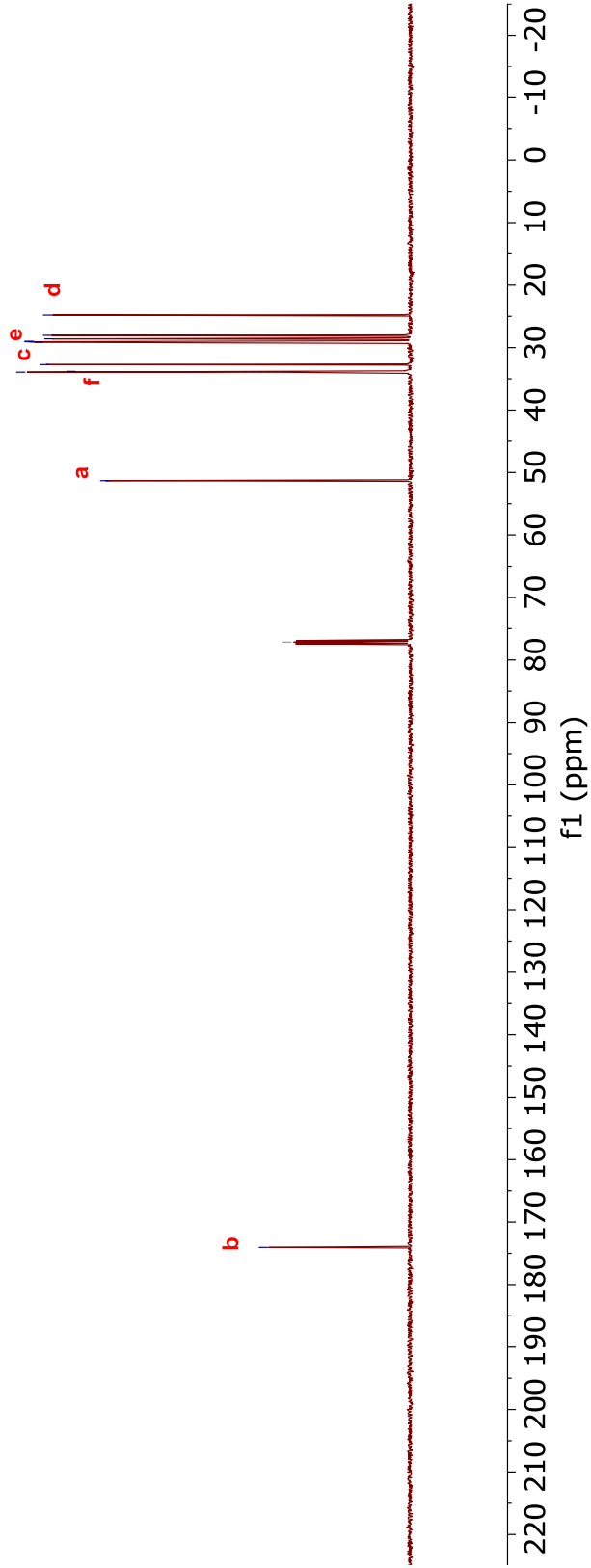
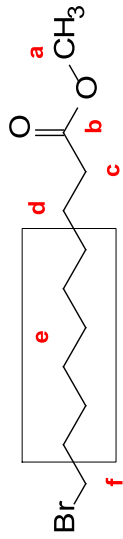


CDCl₃

— 174.04

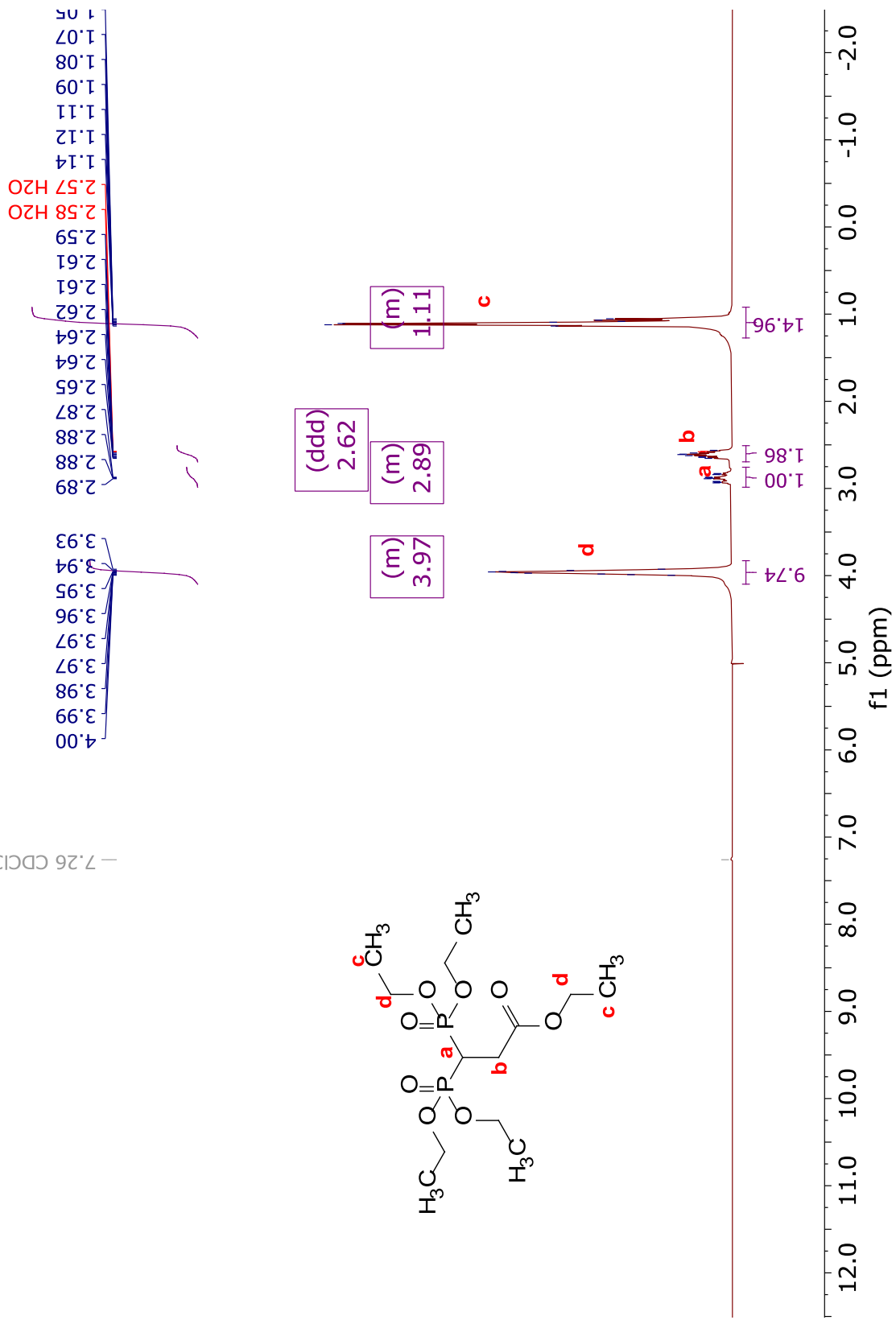
— 51.30
— 33.94
— 33.81
— 32.72
— 29.14
— 29.06
— 28.99
— 28.60
— 28.04
— 24.82

— 77.16 CDCl₃

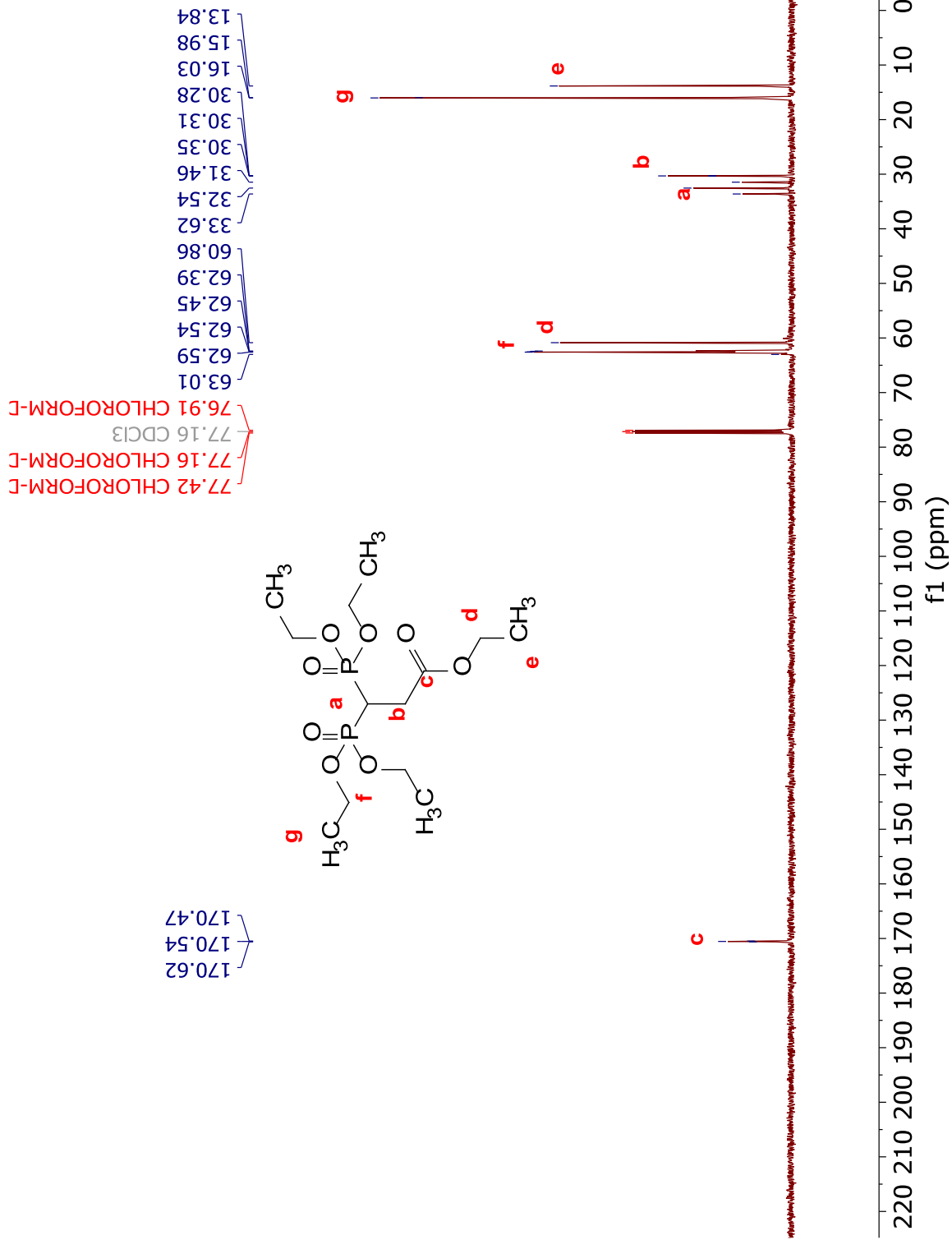


CDCl₃

- 7.26 CDCl₃

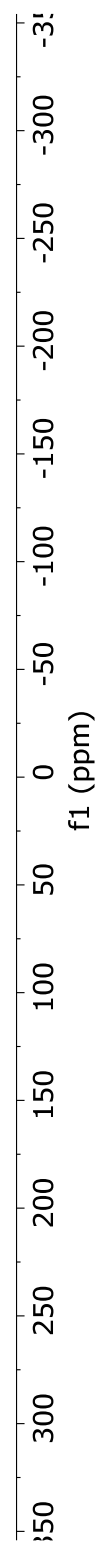
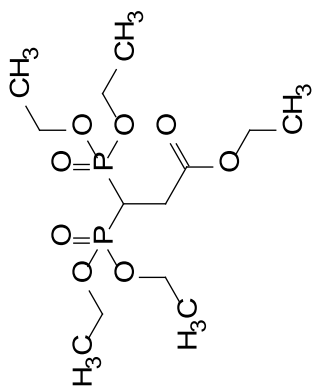


CDCl₃

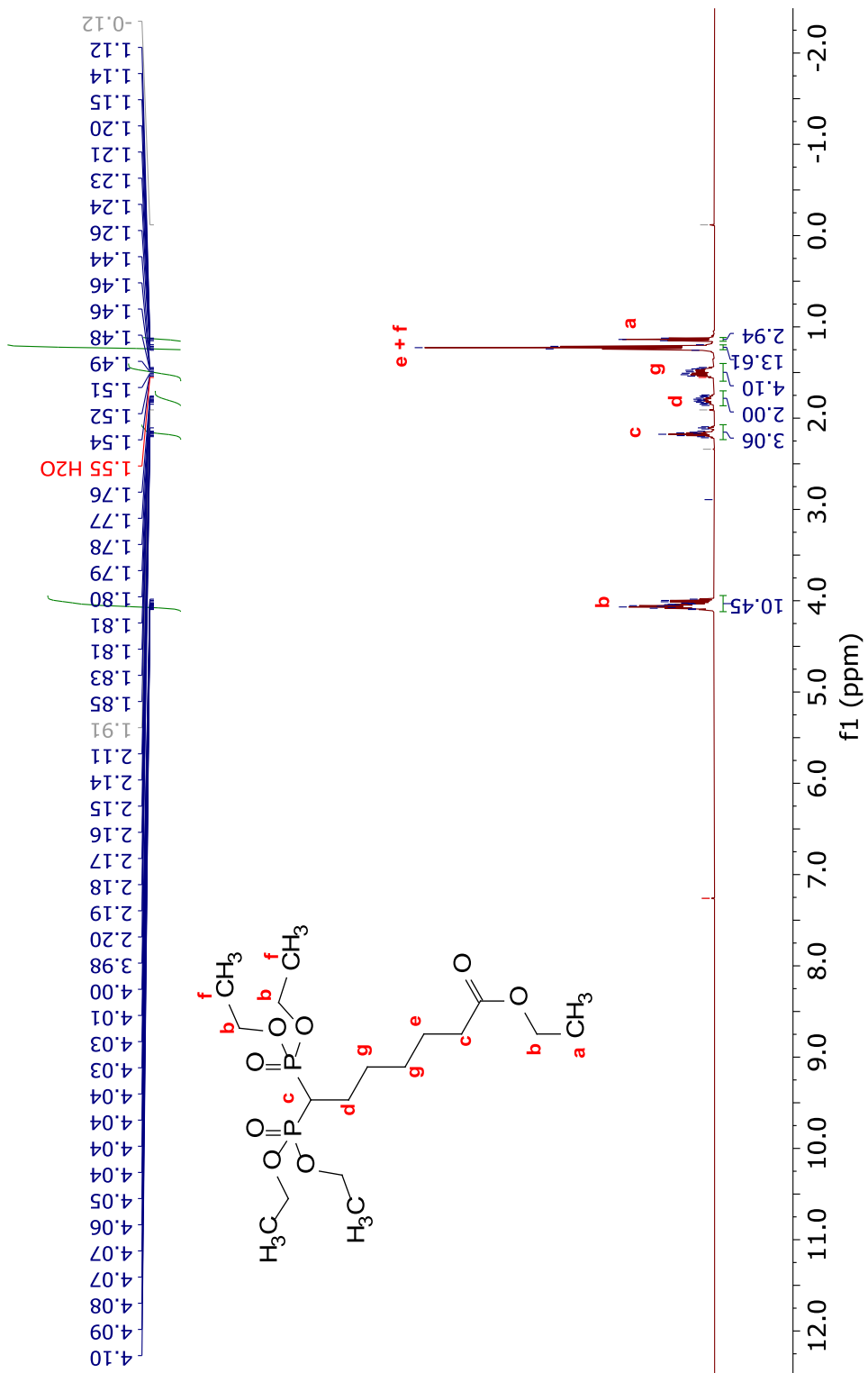


CDCl₃

23.24
22.68
22.13

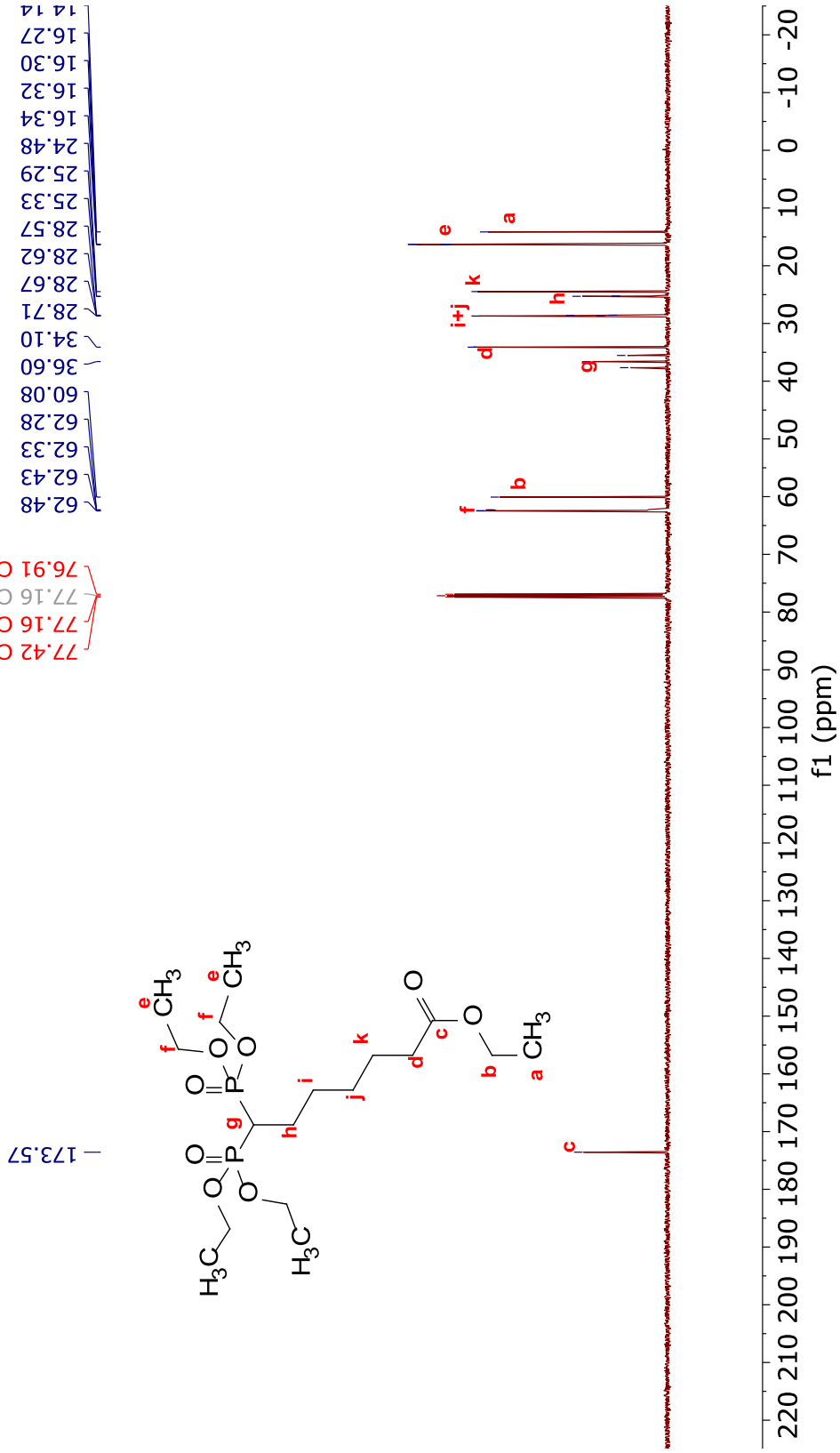


CDCl₃



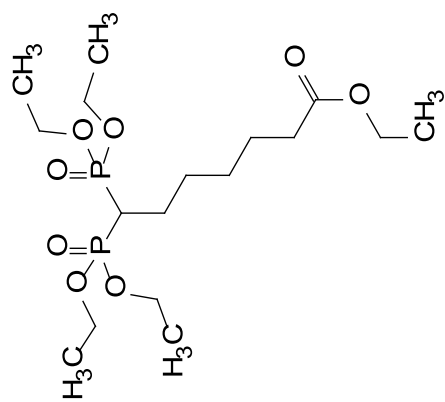
CDCl₃

77.42 CHLOROFORM-D
77.16 CHLOROFORM-D
77.16 CDCl₃
76.91 CHLOROFORM-D

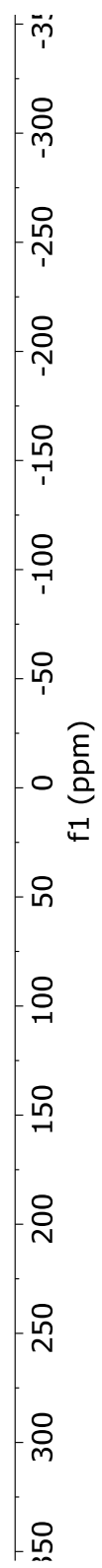


CDCl₃

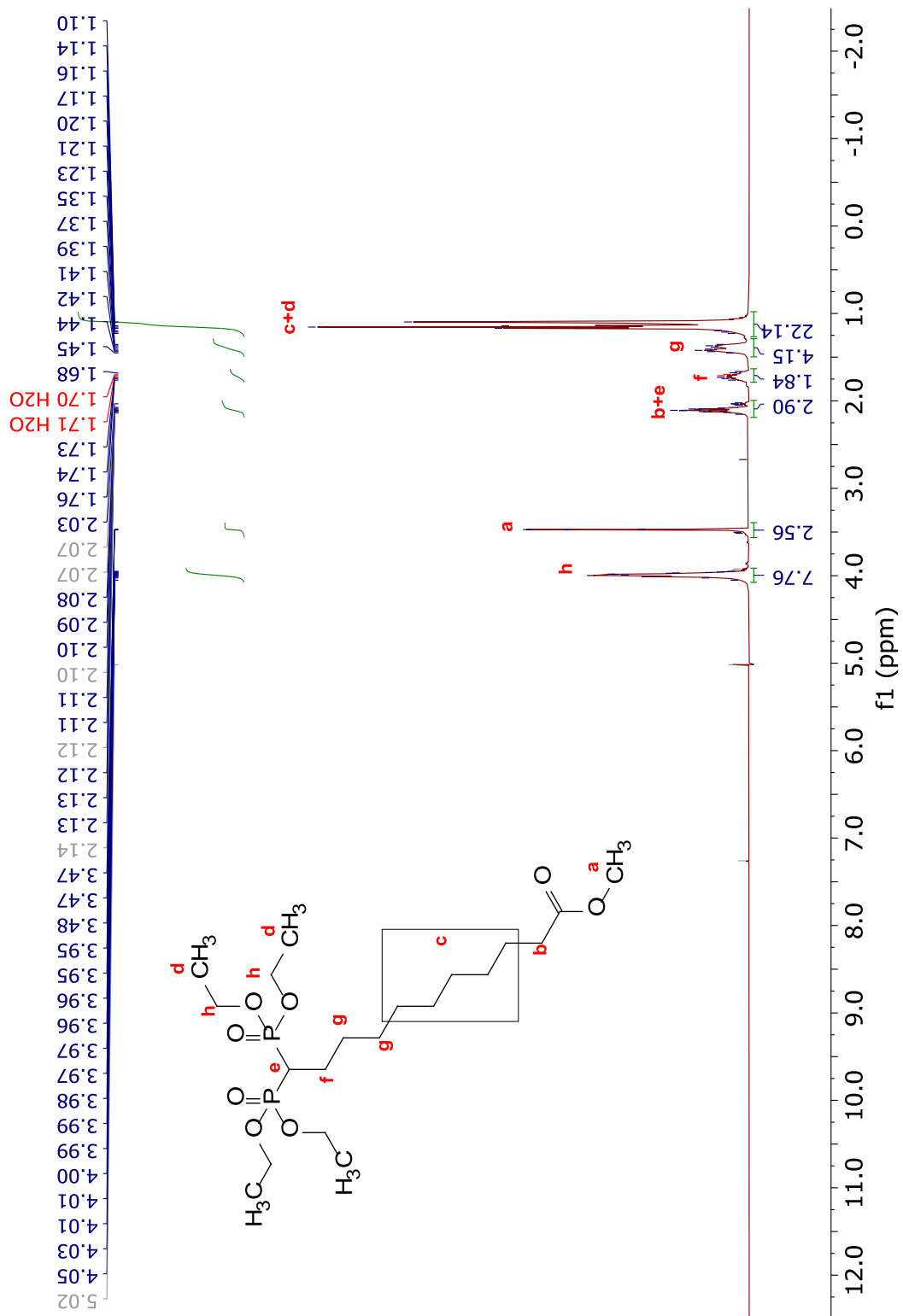
24.96
24.42
23.87



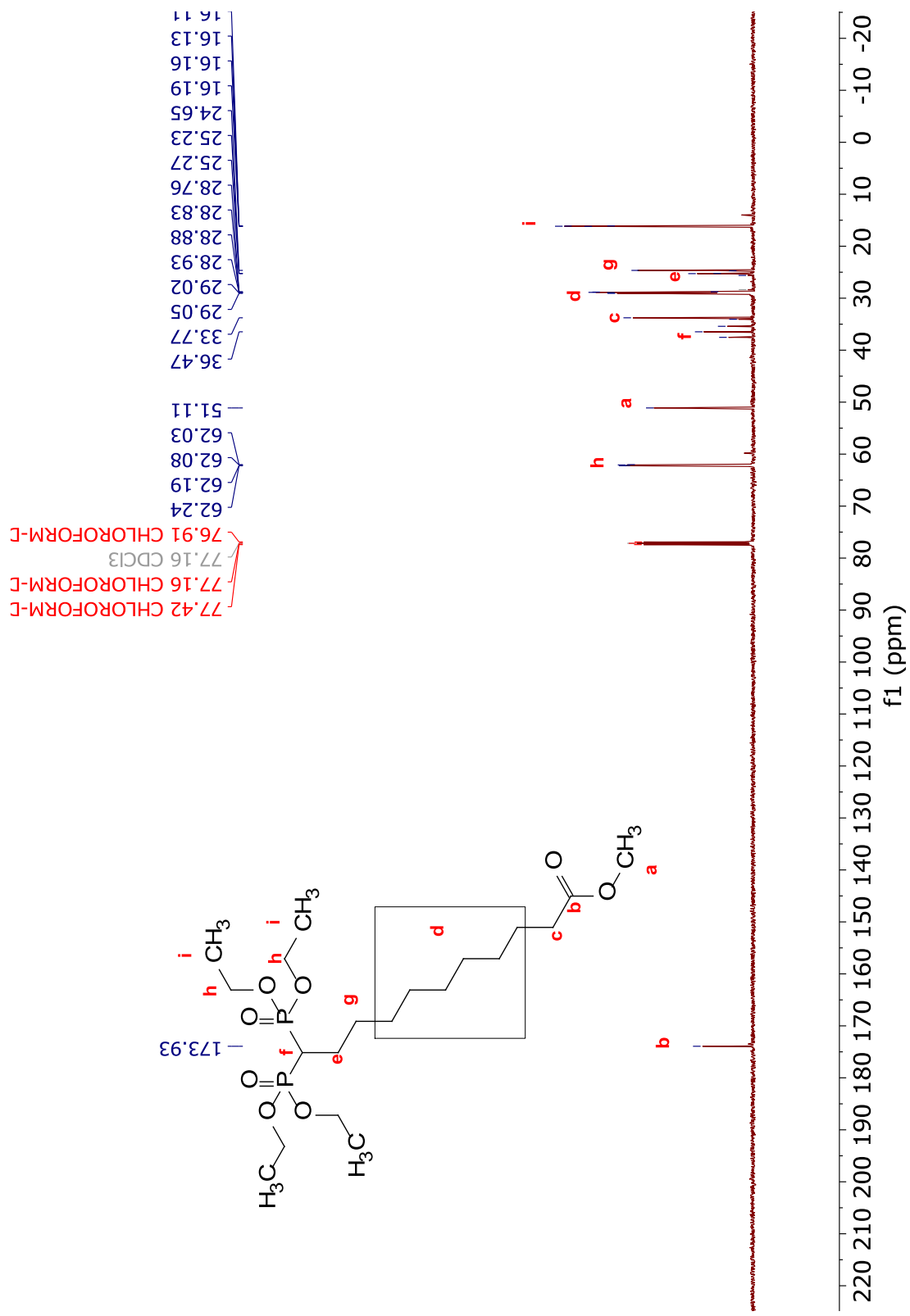
148



CDCl₃

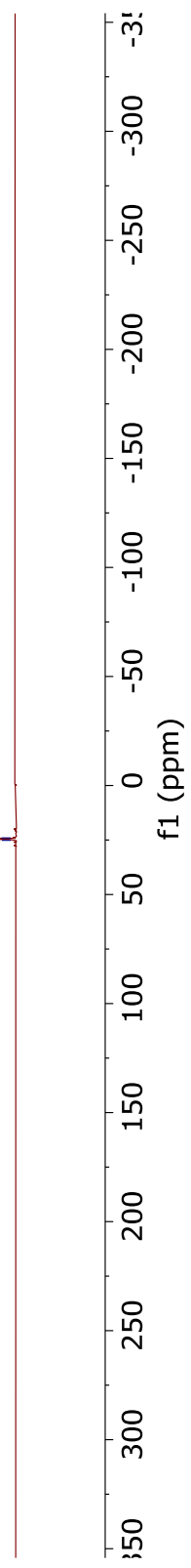
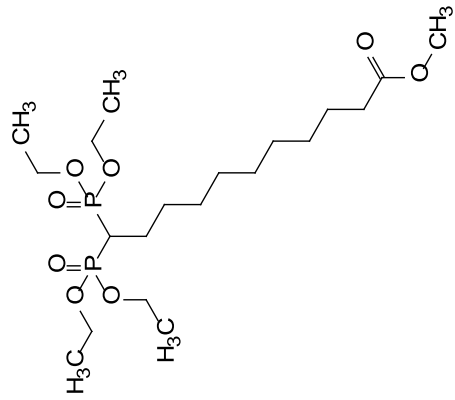


CDCl3

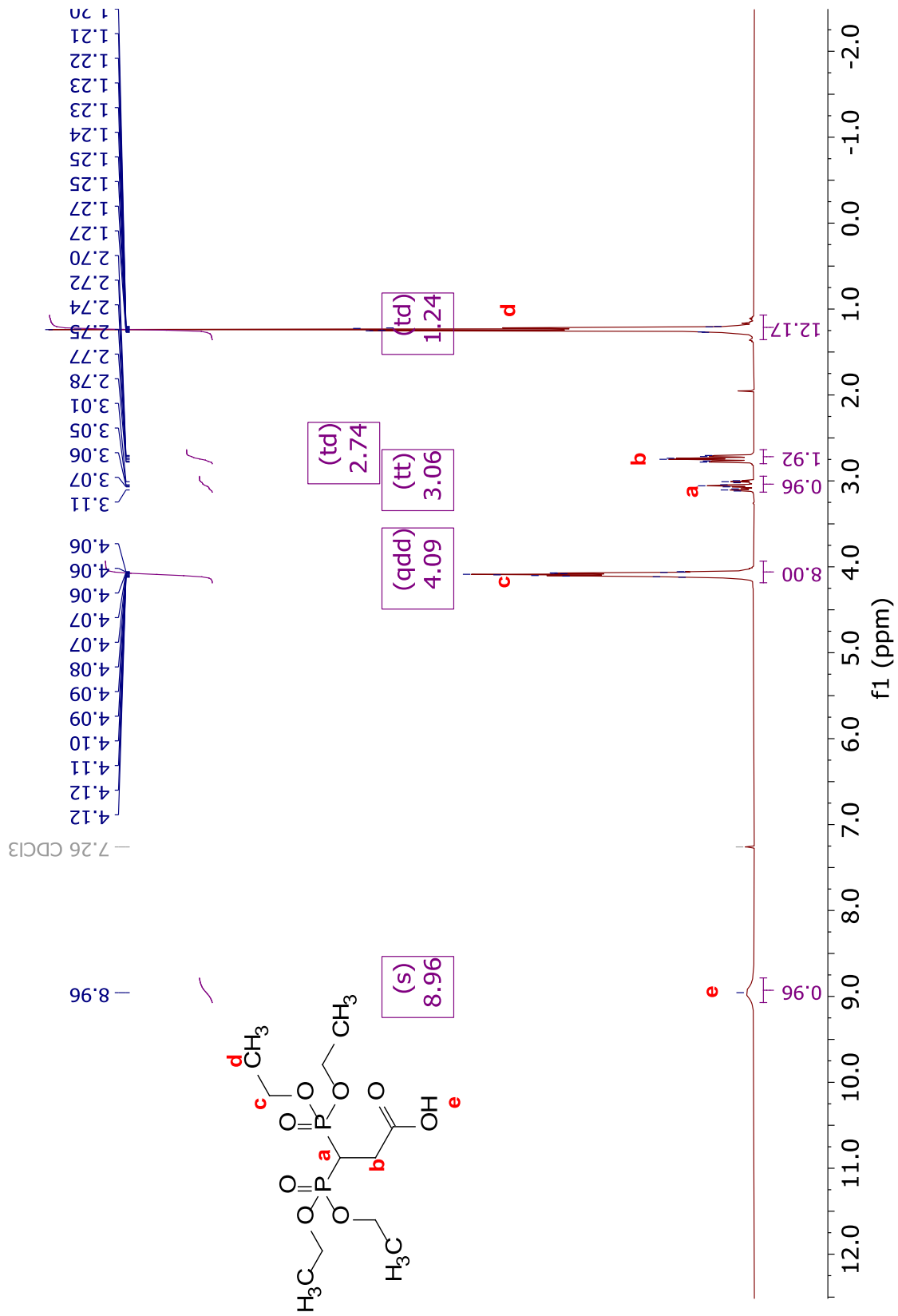


CDCl₃

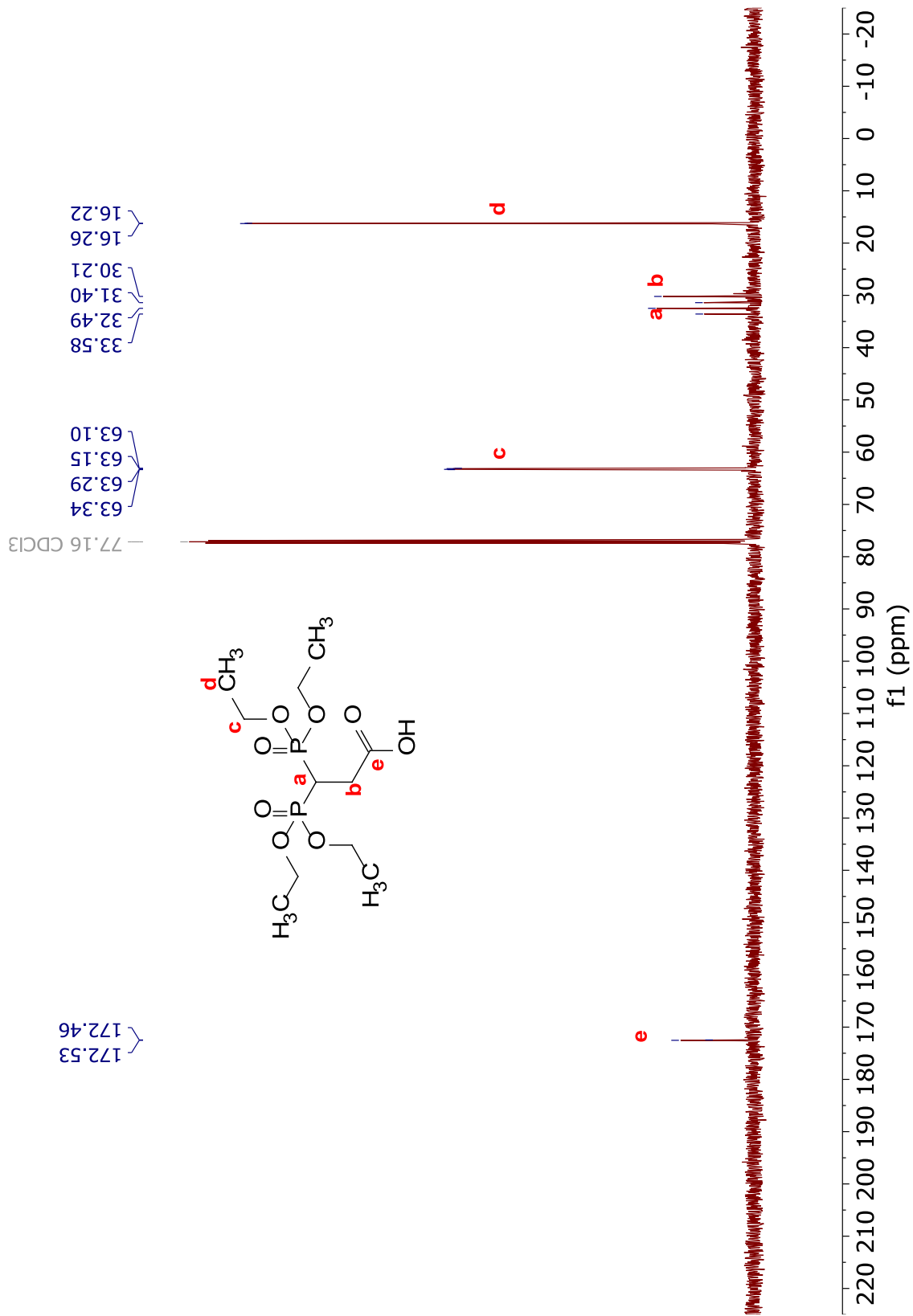
25.13
24.59
24.04



CDCl₃

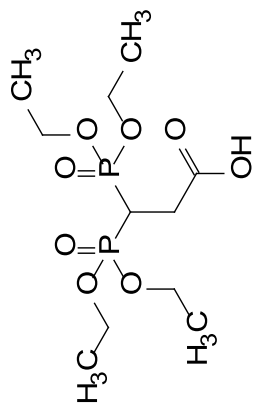


CDCl₃

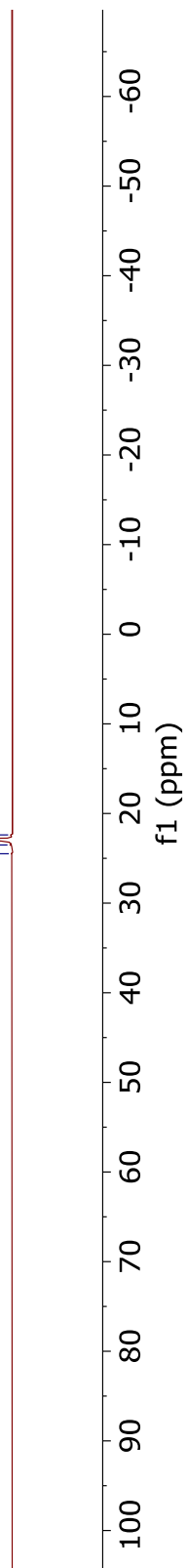


CDCl₃

24.49
23.51
22.95
22.39

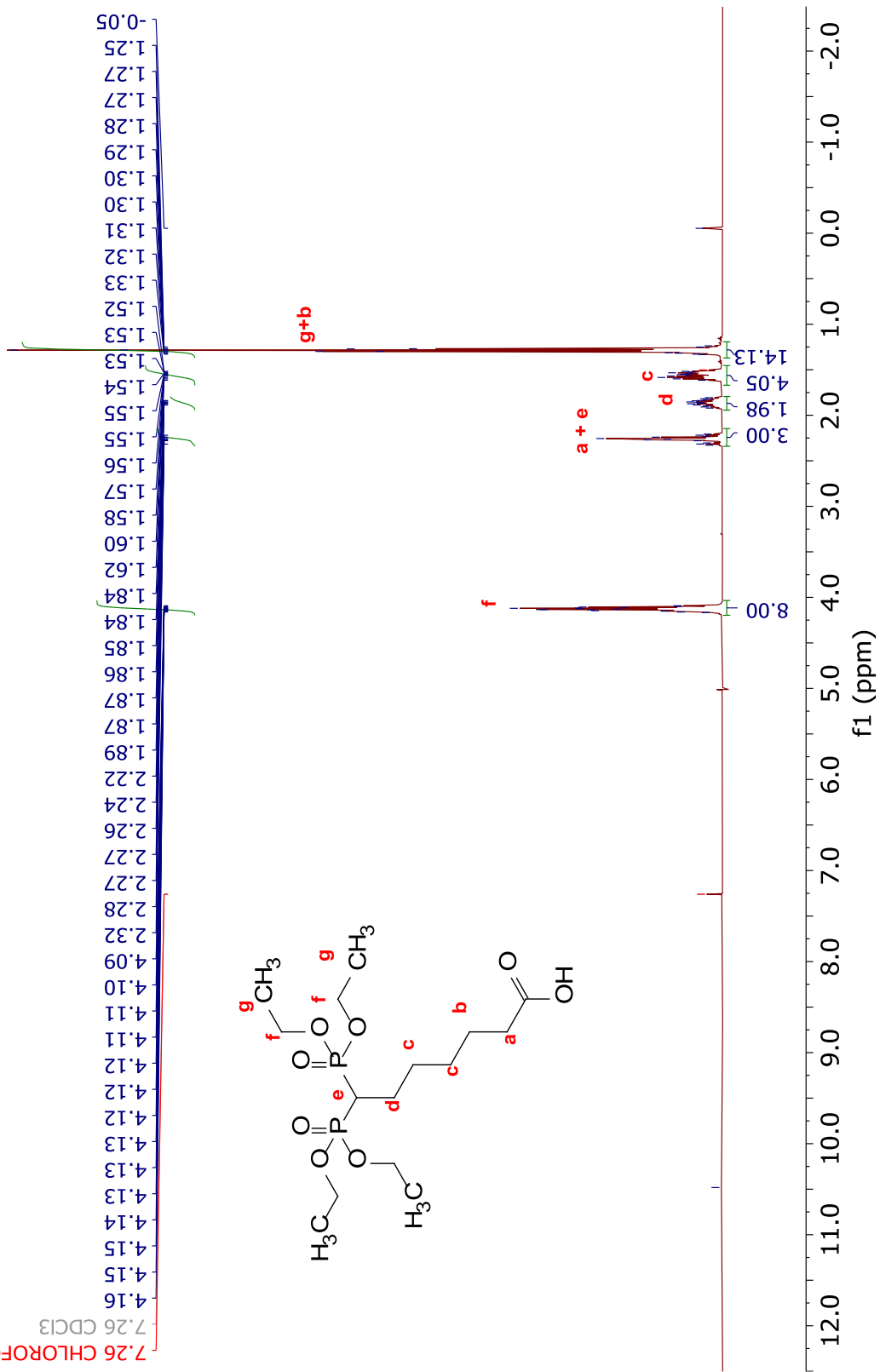


6a

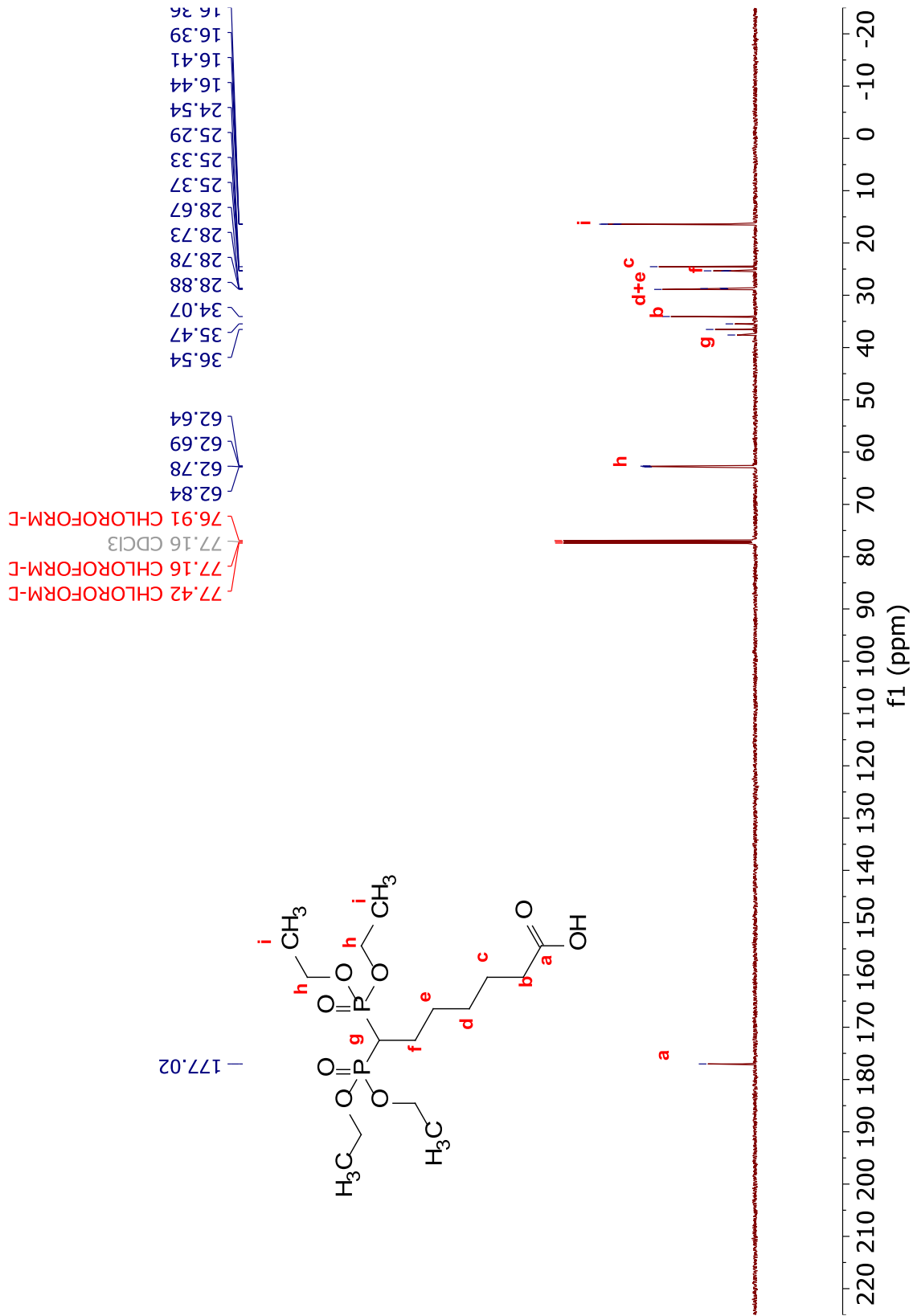


CDCl₃

7.26 CHLOROFORM-D

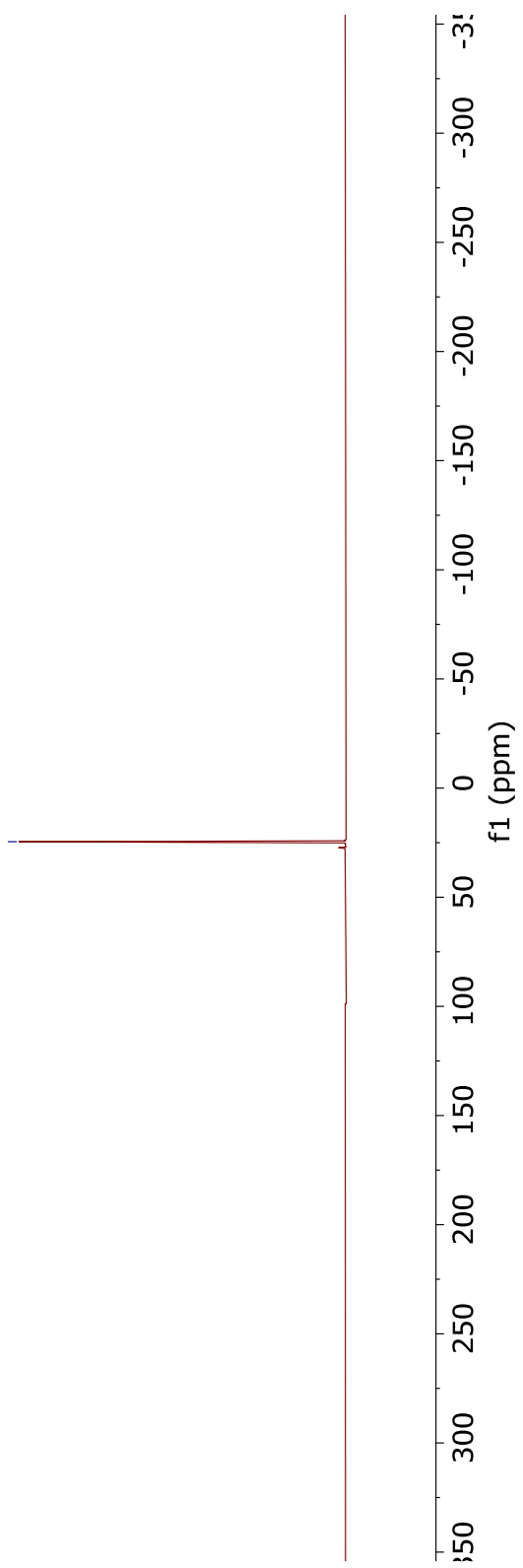
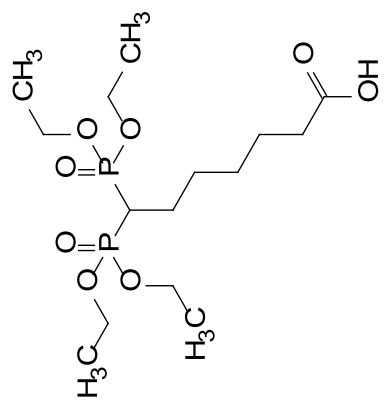


CDCl₃

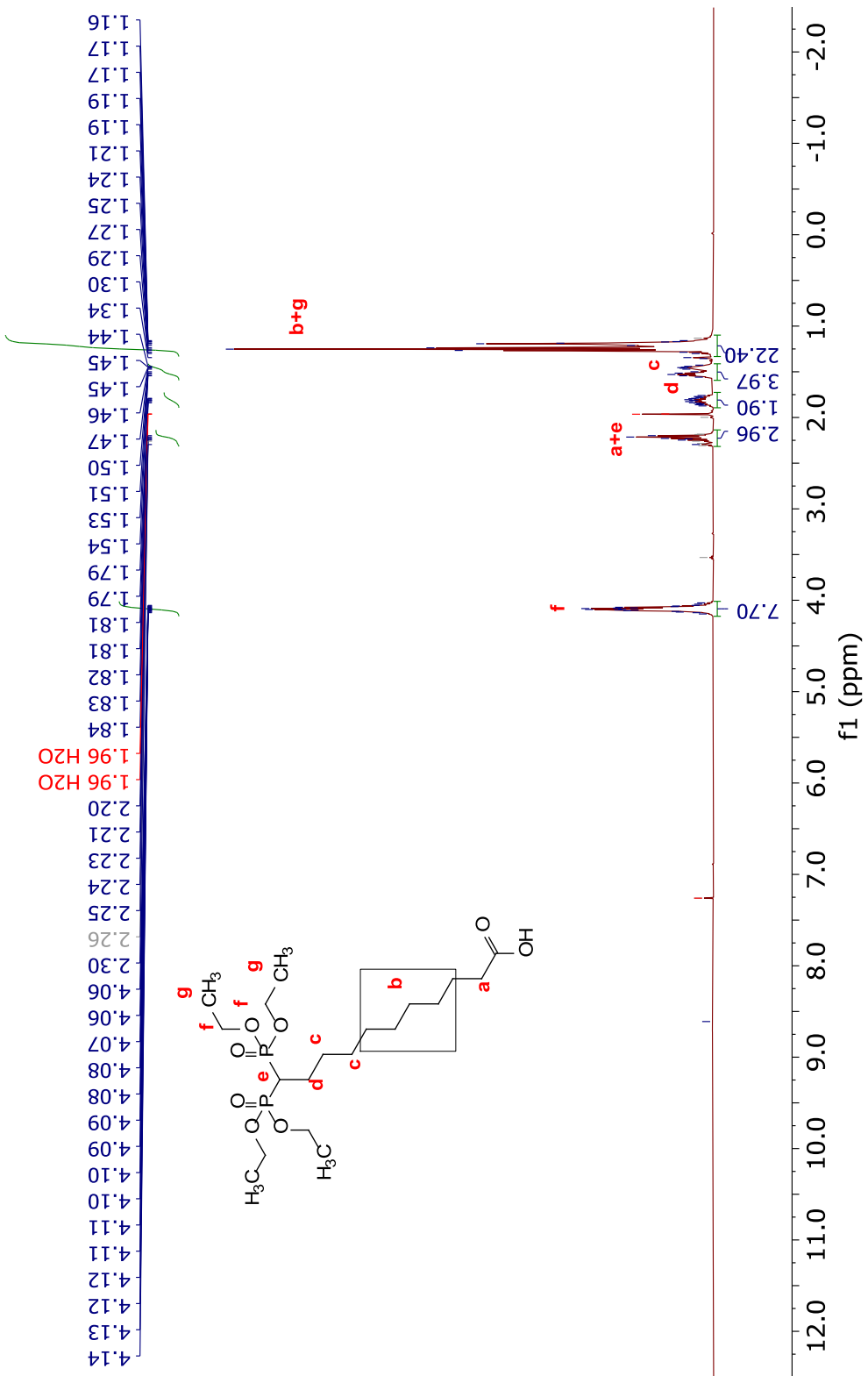


CDCl₃

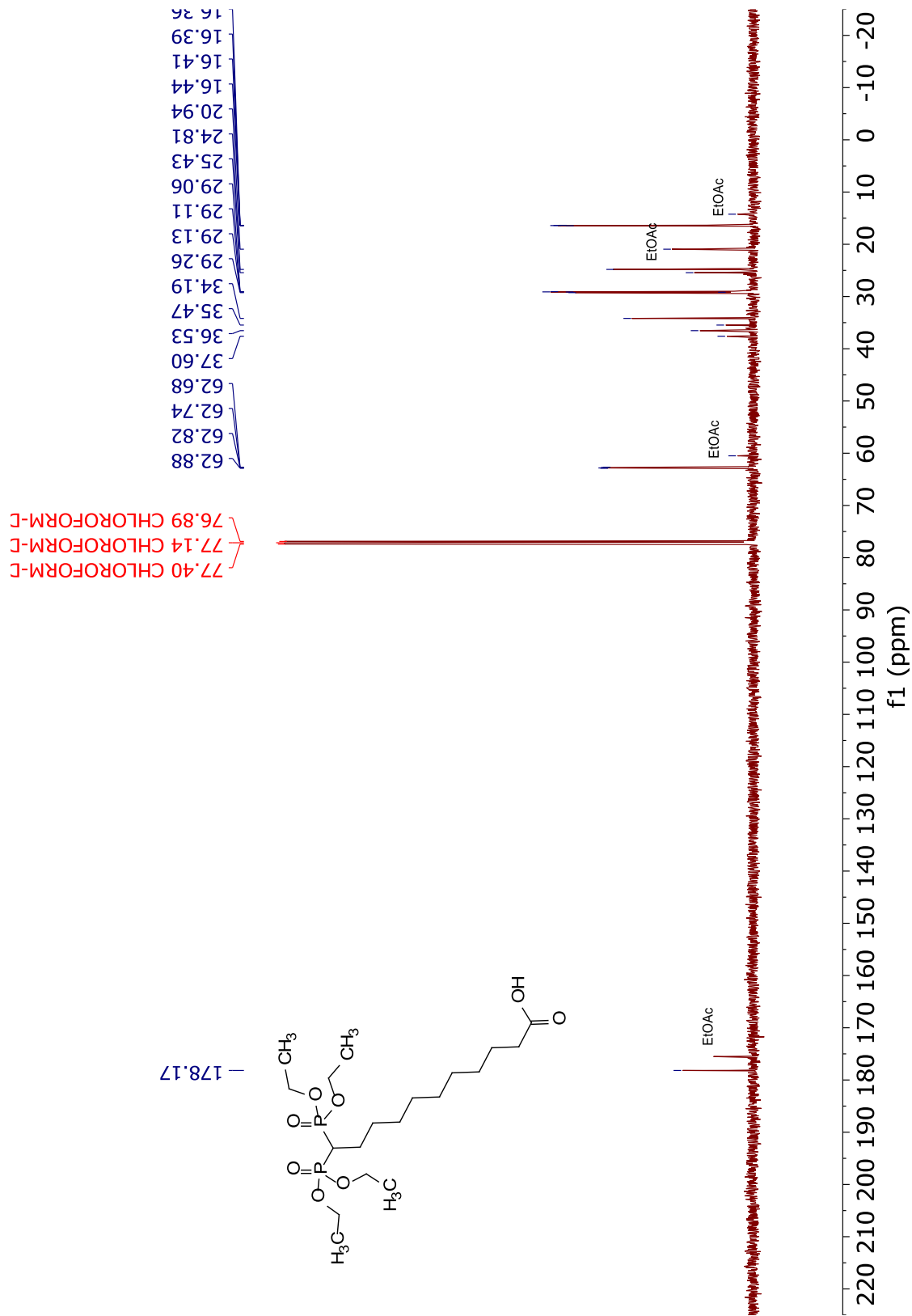
-24.57



CDCl₃

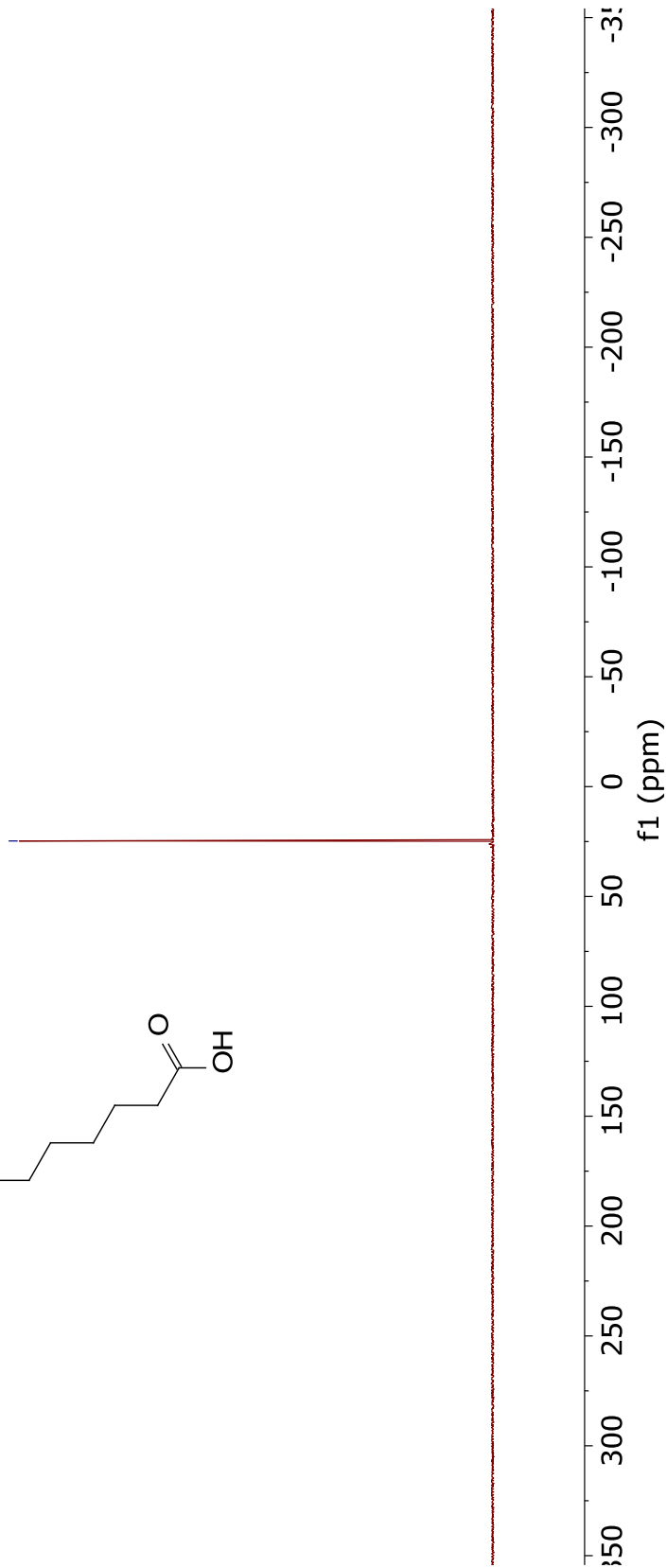
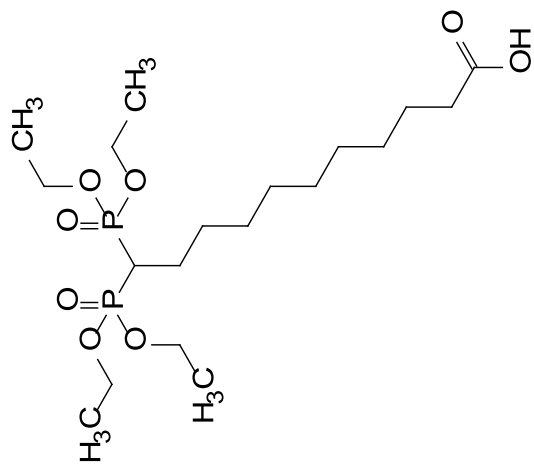


CDCl3

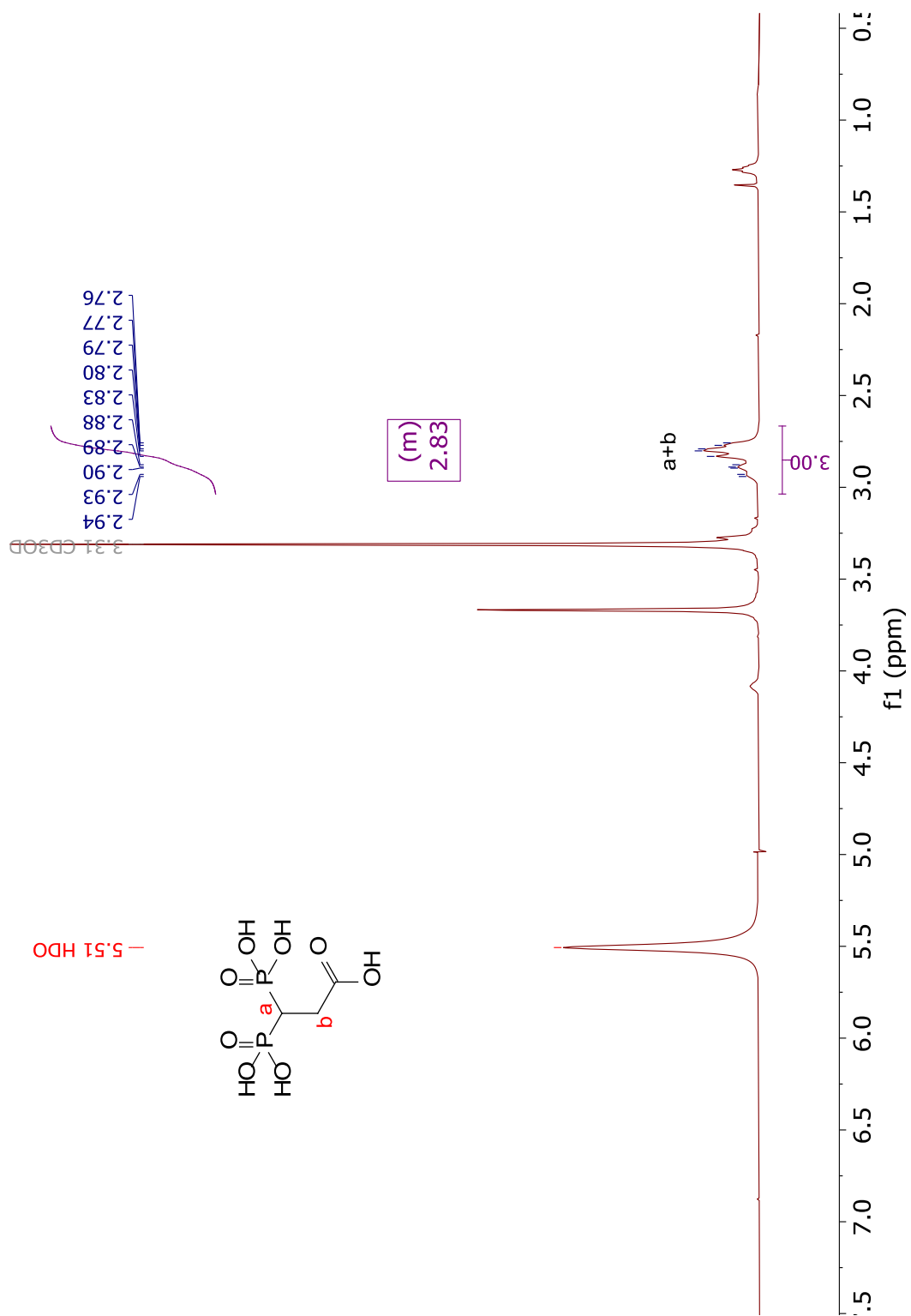


CDCl₃

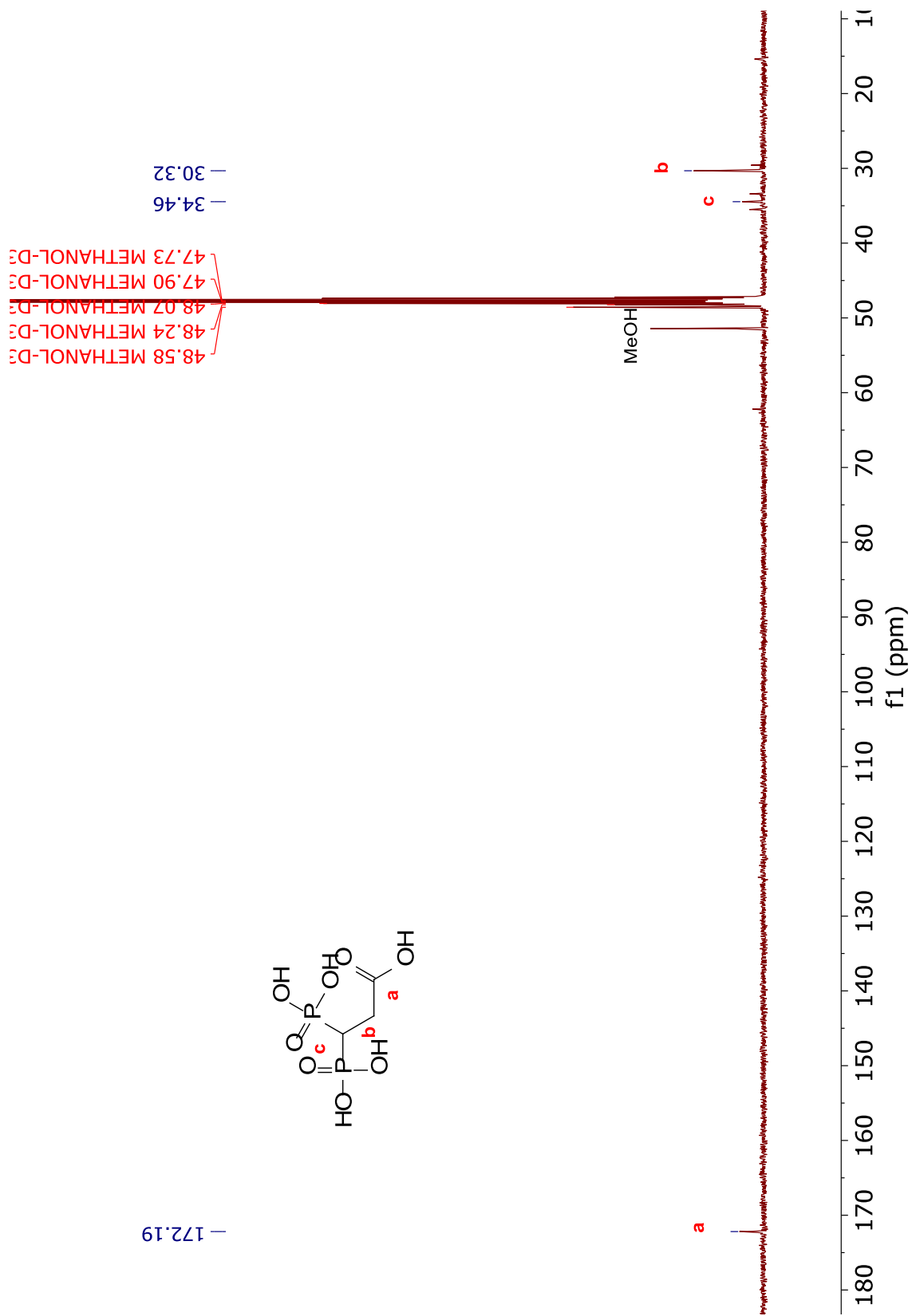
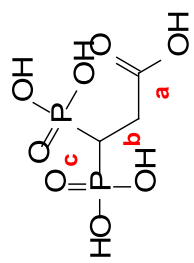
- 24.74



CD3OD

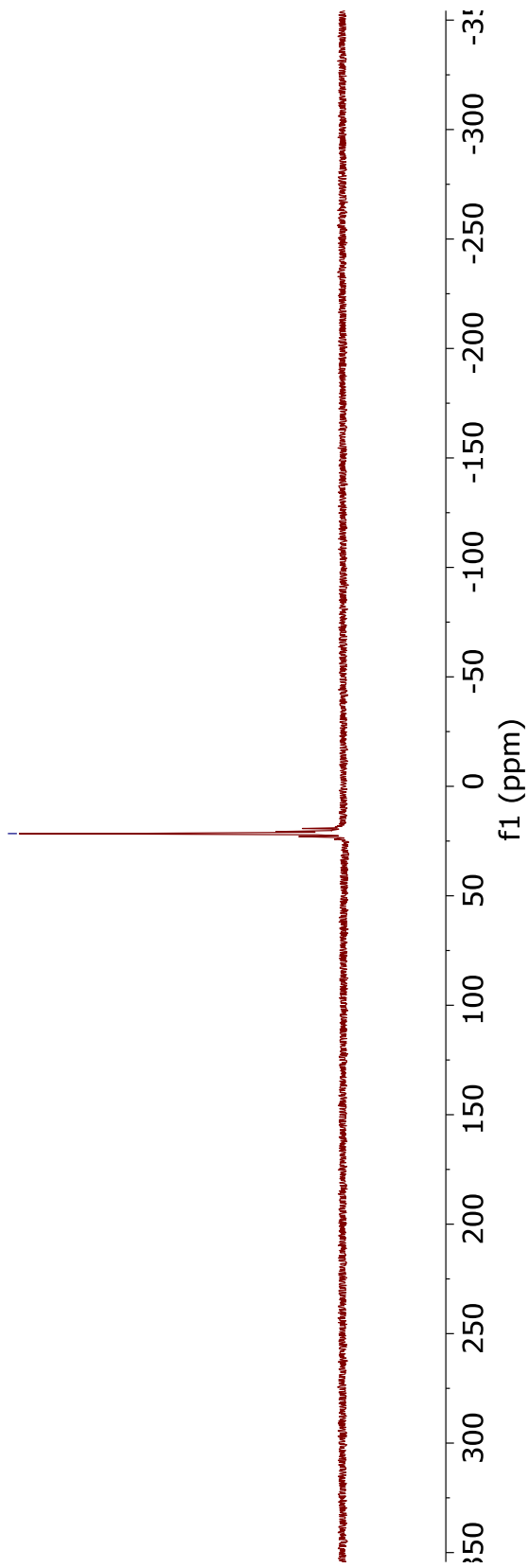
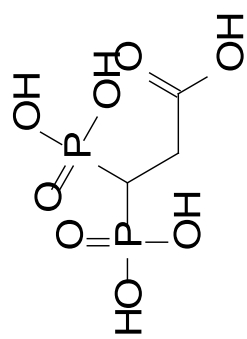


CD3OD

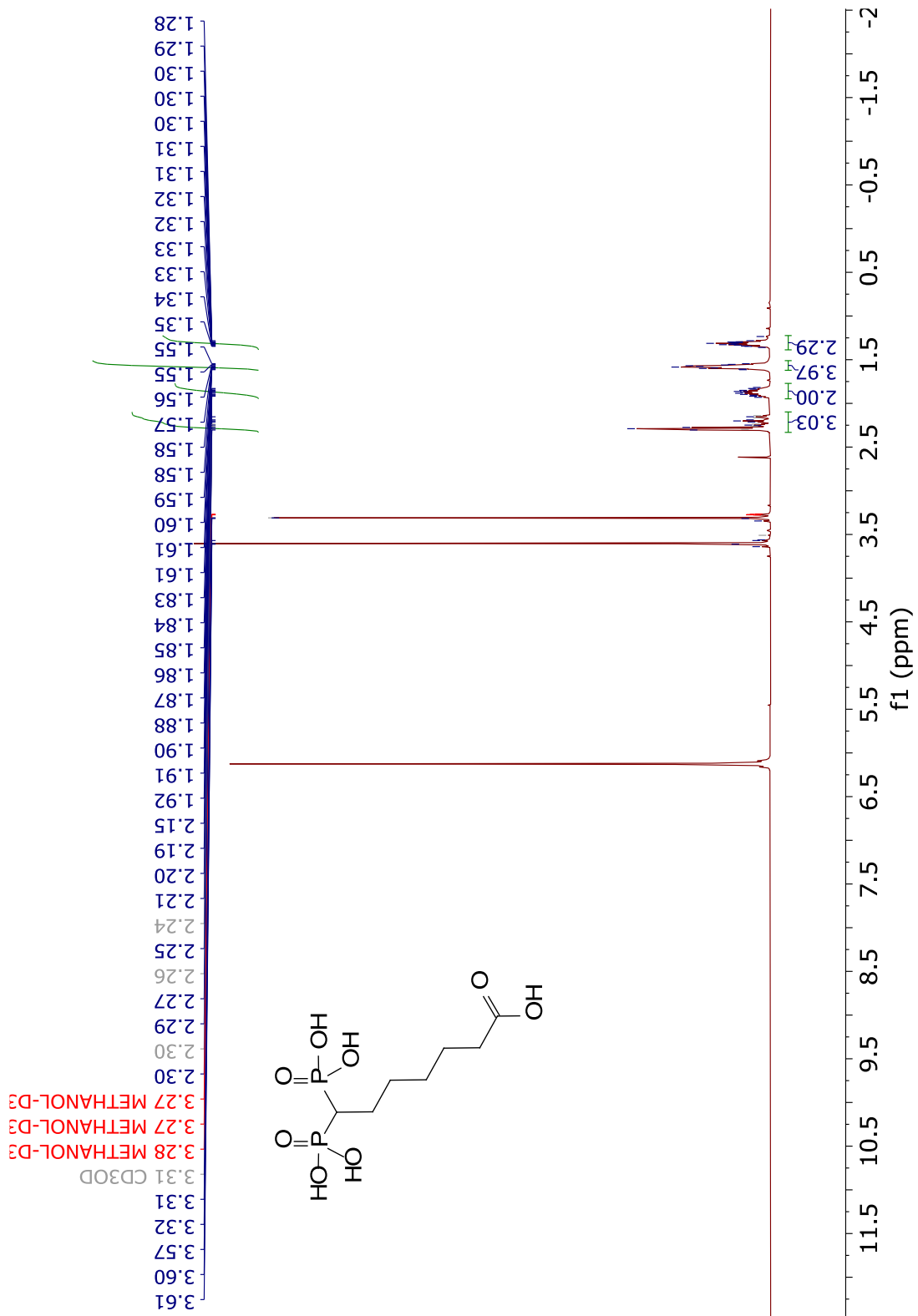


CD30D

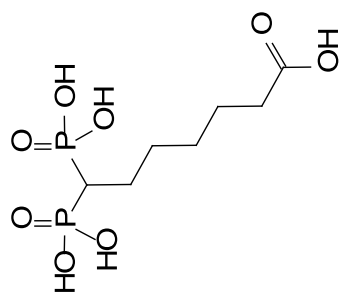
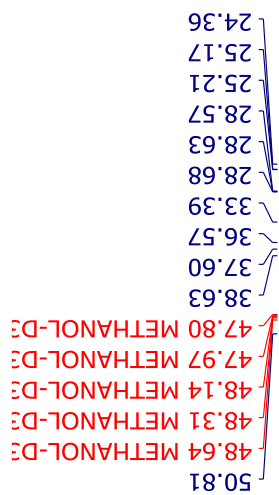
— 21.59



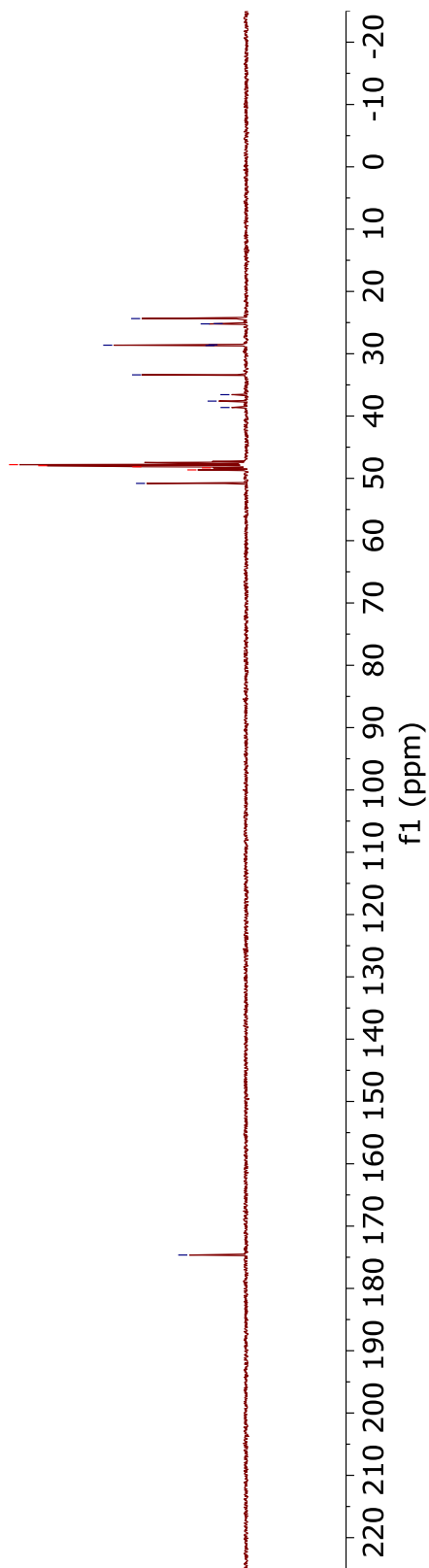
CD3OD



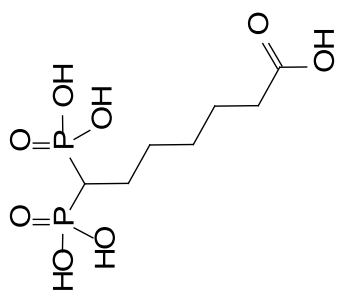
CD3OD



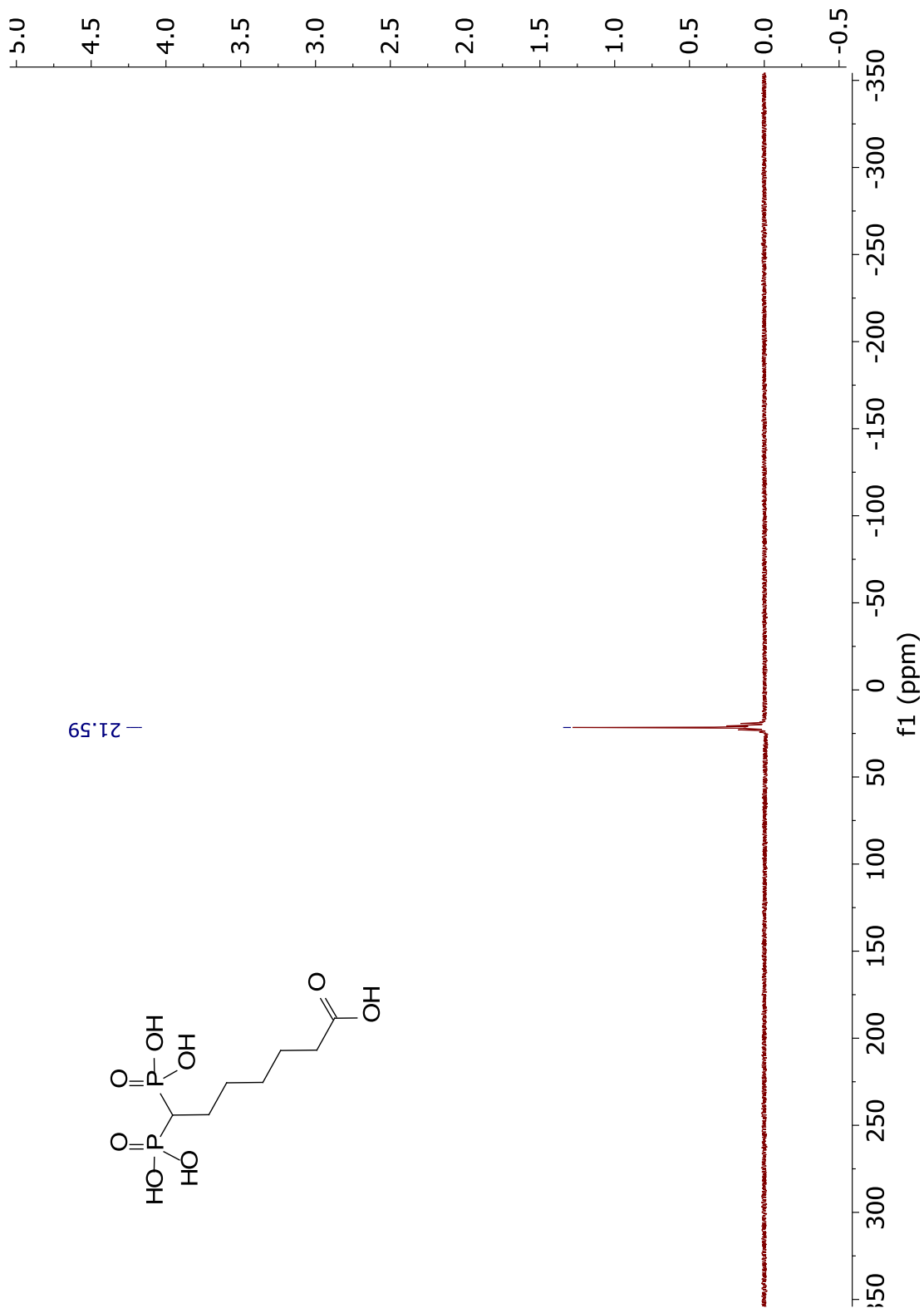
-174.64

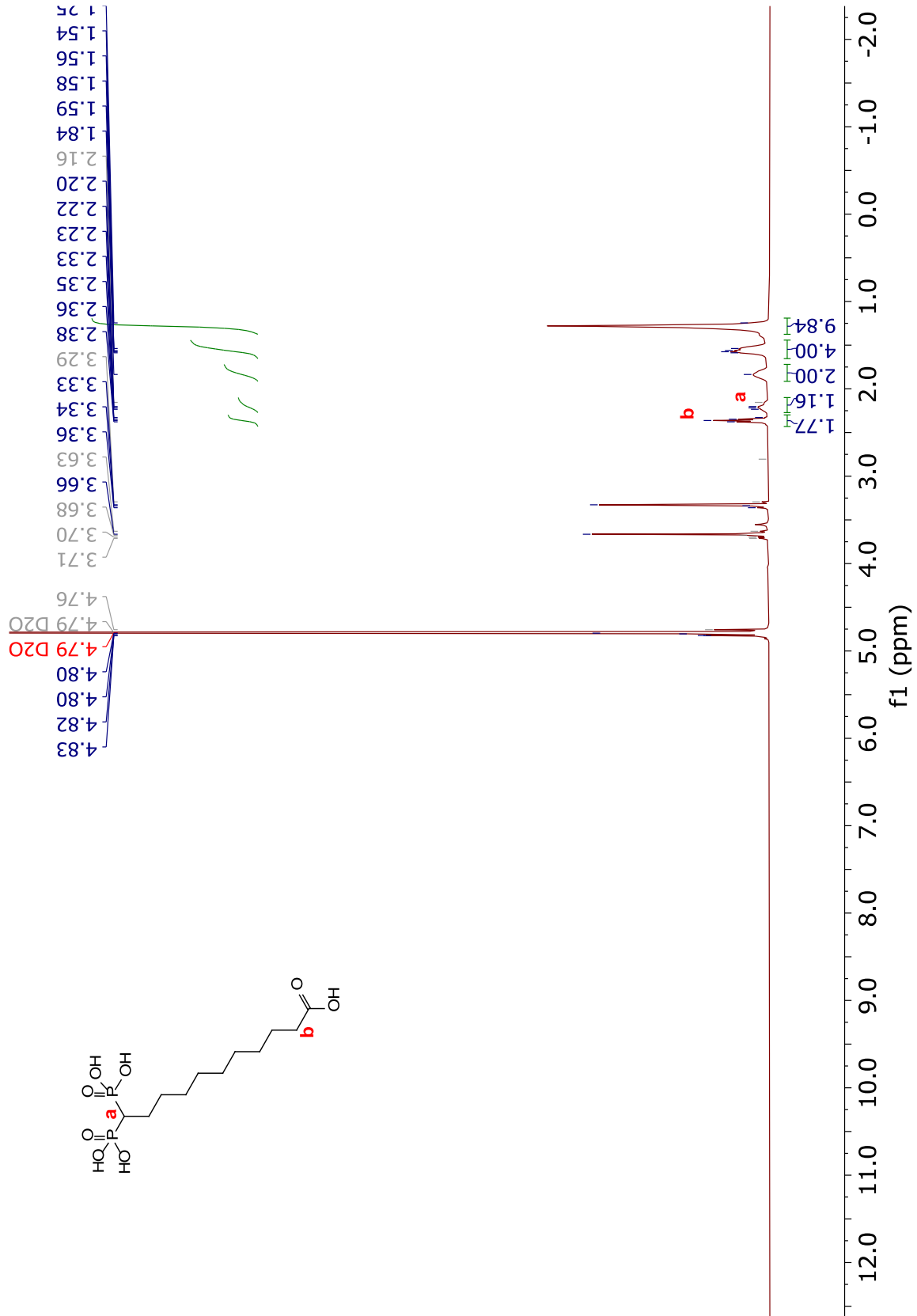


CD3OD



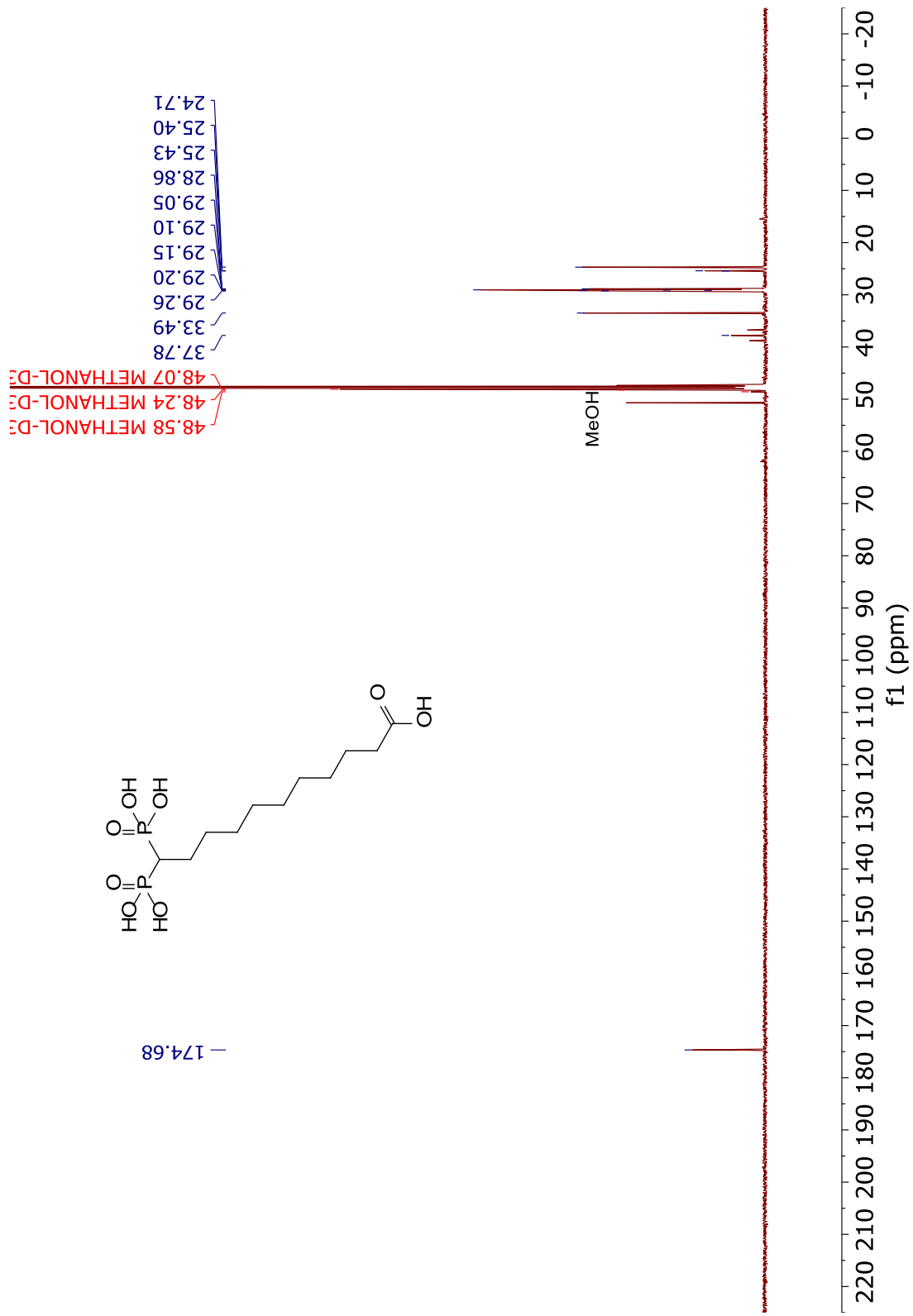
— 21.59





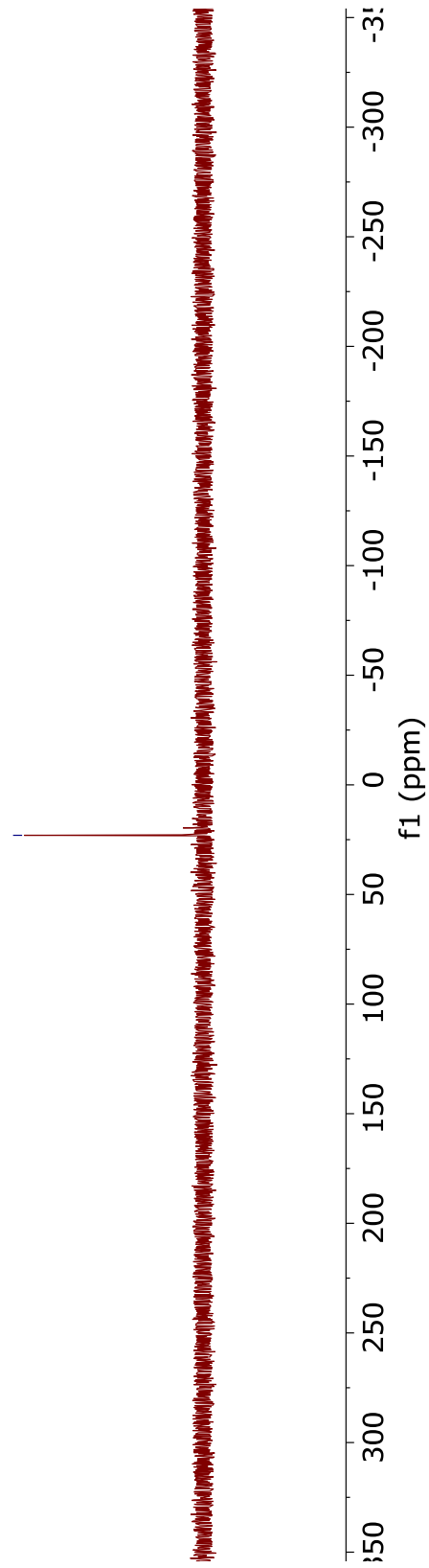
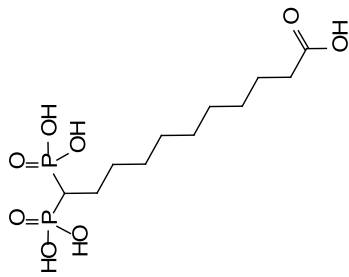
D2O

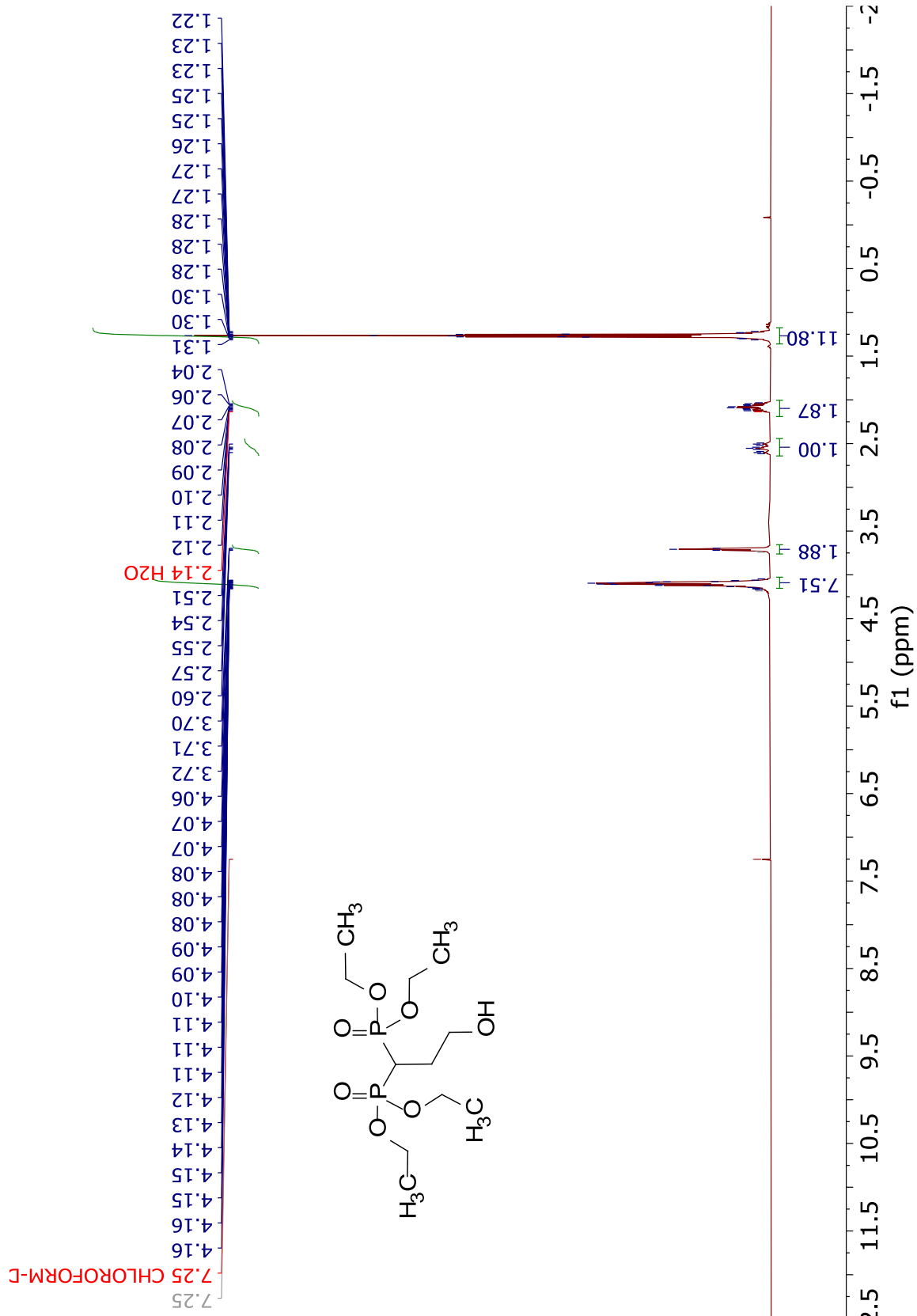
CDCl3



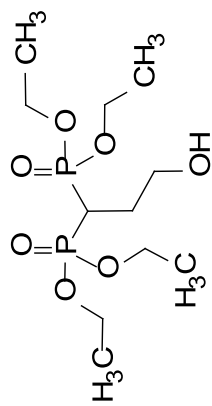
D2O

— 23.01



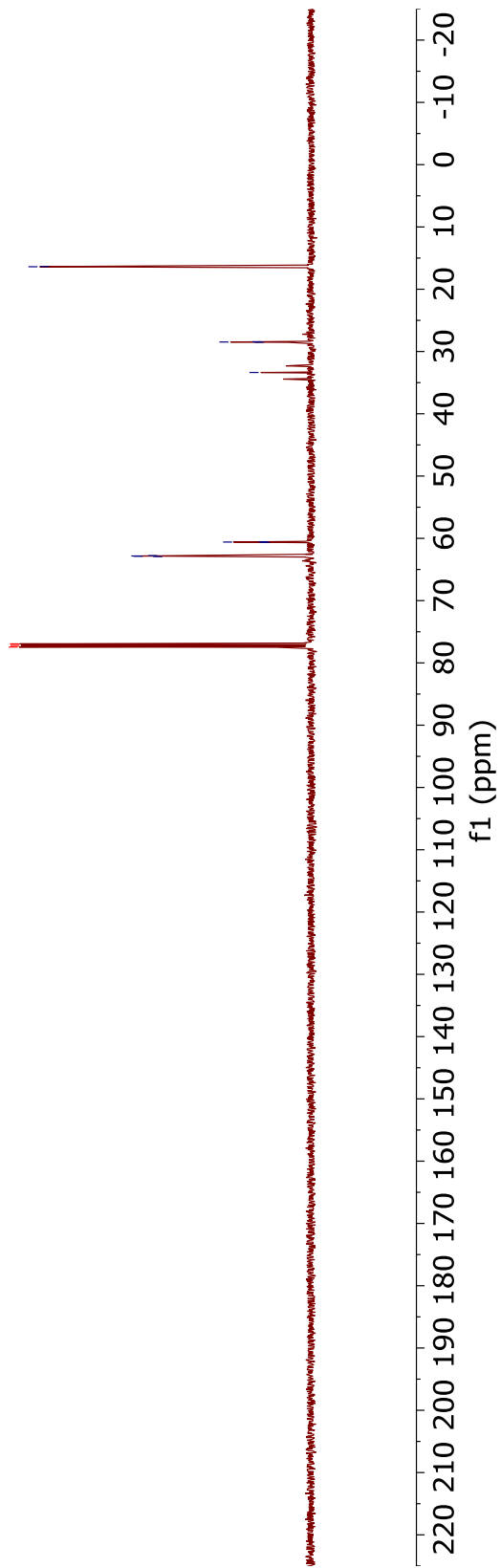


CDCl₃



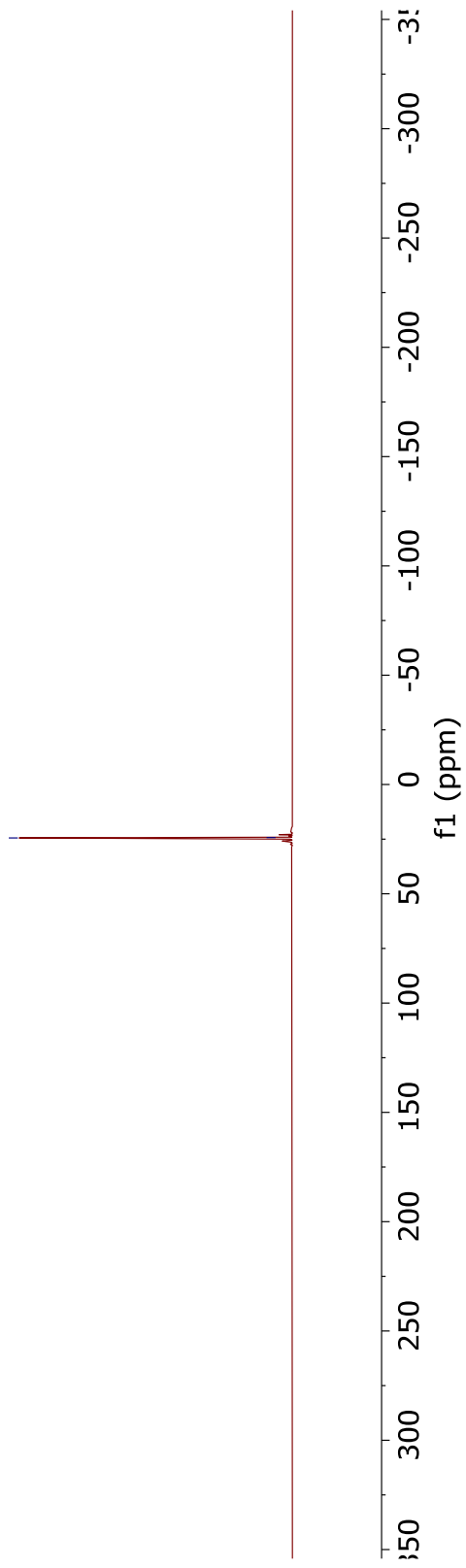
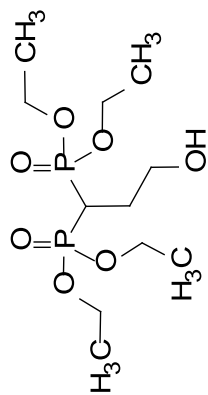
77.45 CHLOROFORM-D
77.20 CHLOROFORM-D
76.94 CHLOROFORM-D
62.92
62.87
62.83
62.78
60.65
60.59
60.54
33.37
28.52
28.48
28.44
16.39
16.35

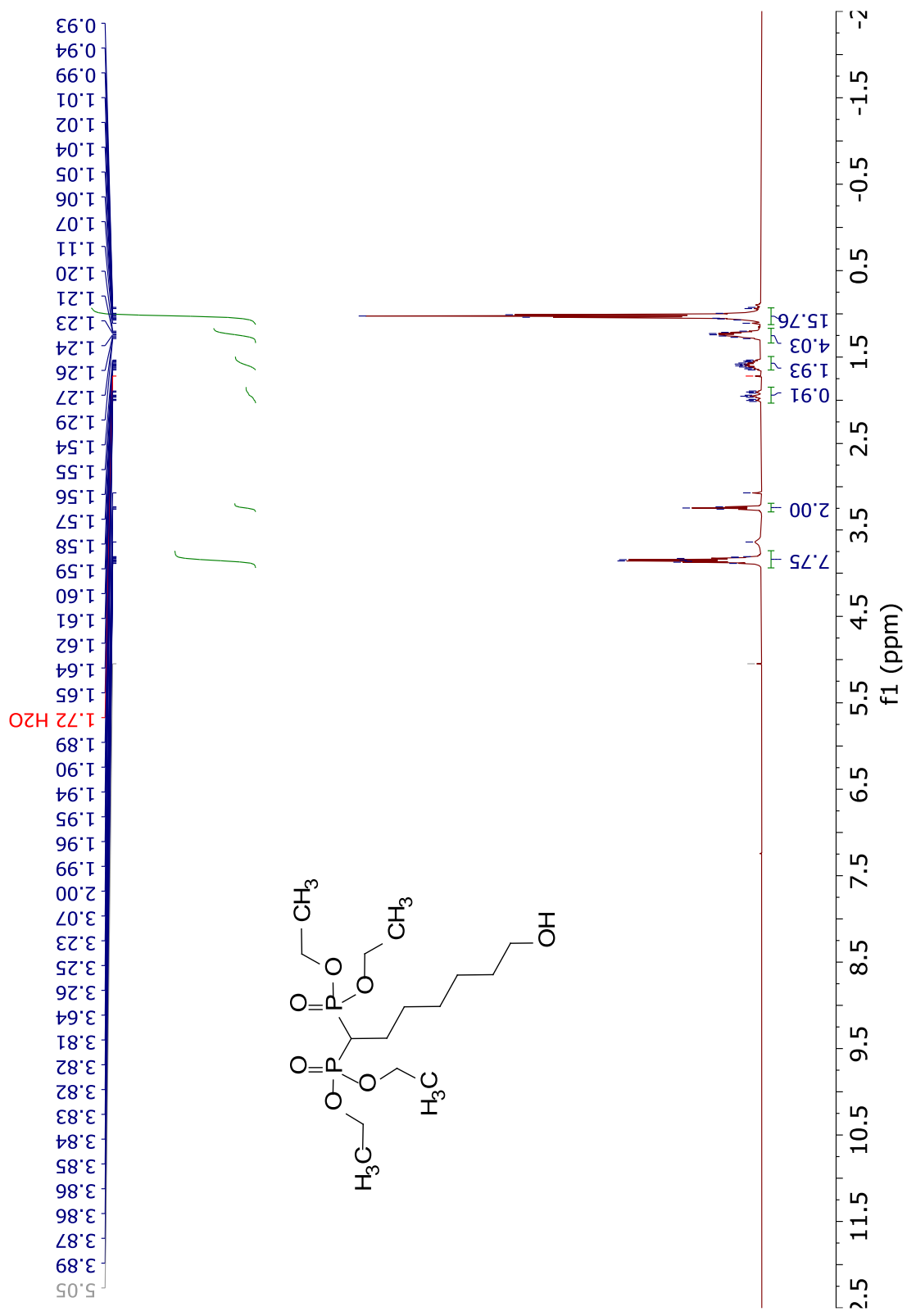
171



CDCl₃

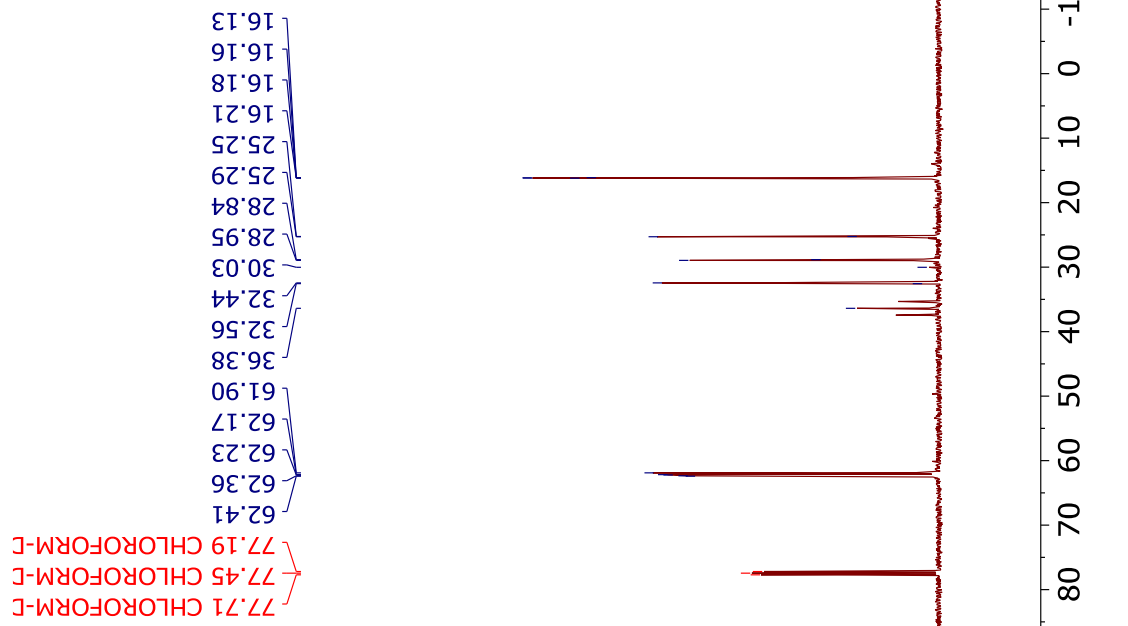
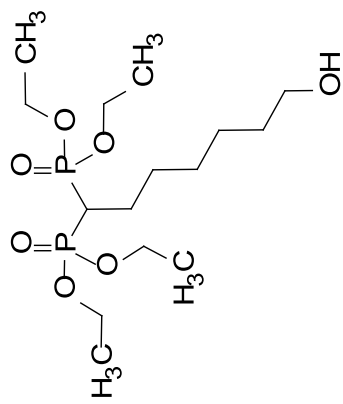
24.45
24.29





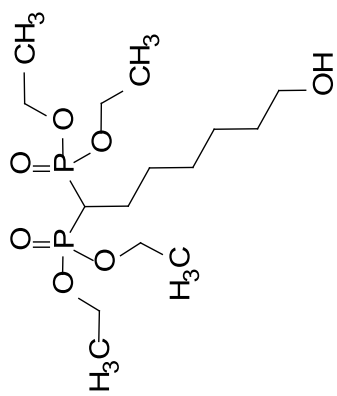
CDCl₃

CDCl₃

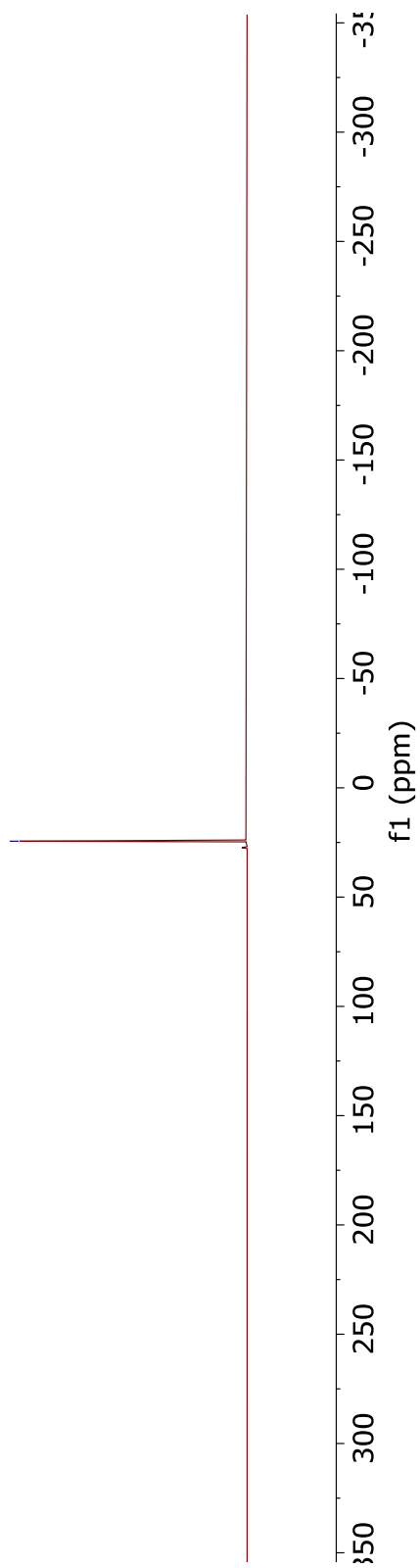


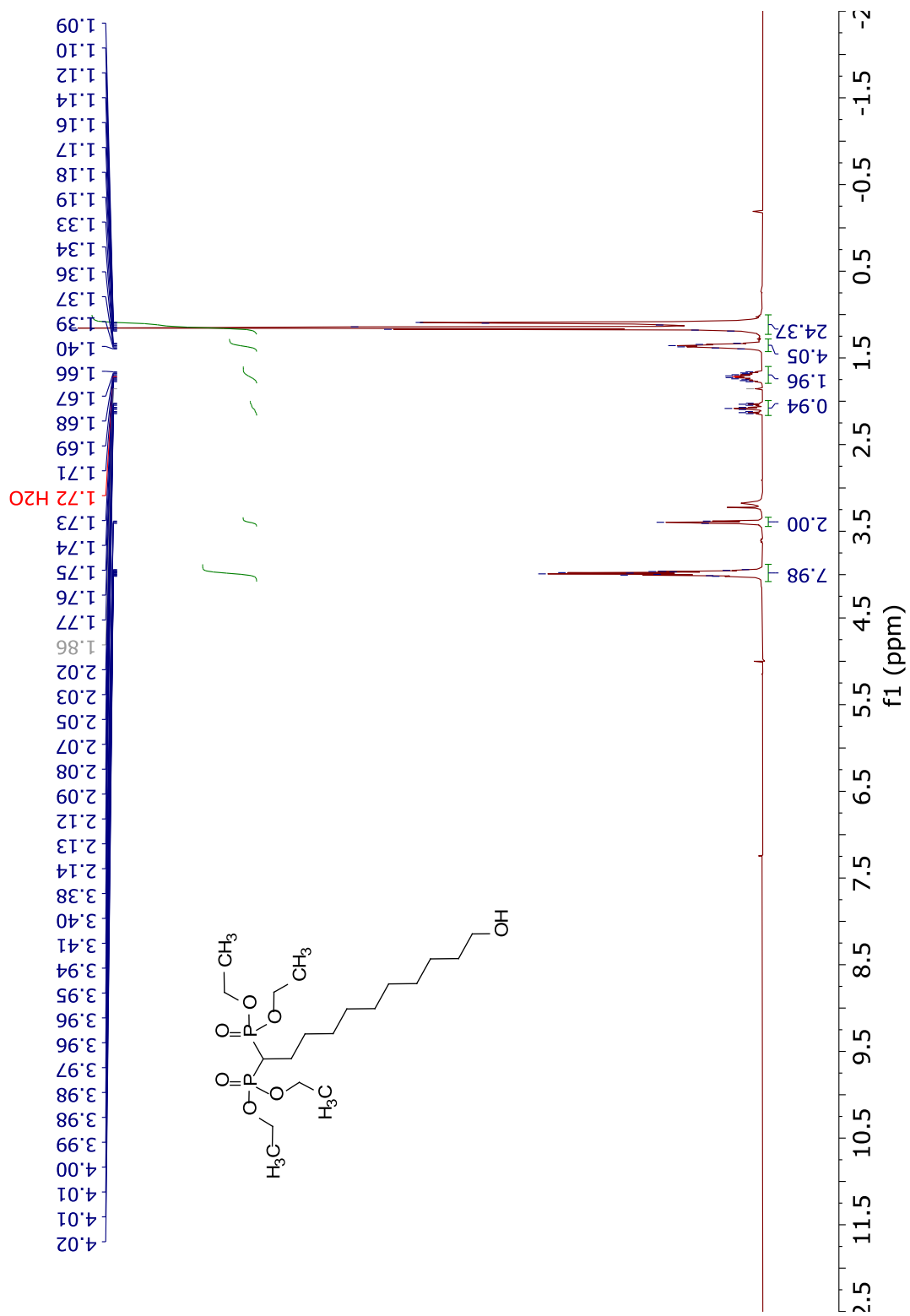
CDCl₃

— 24.42



175

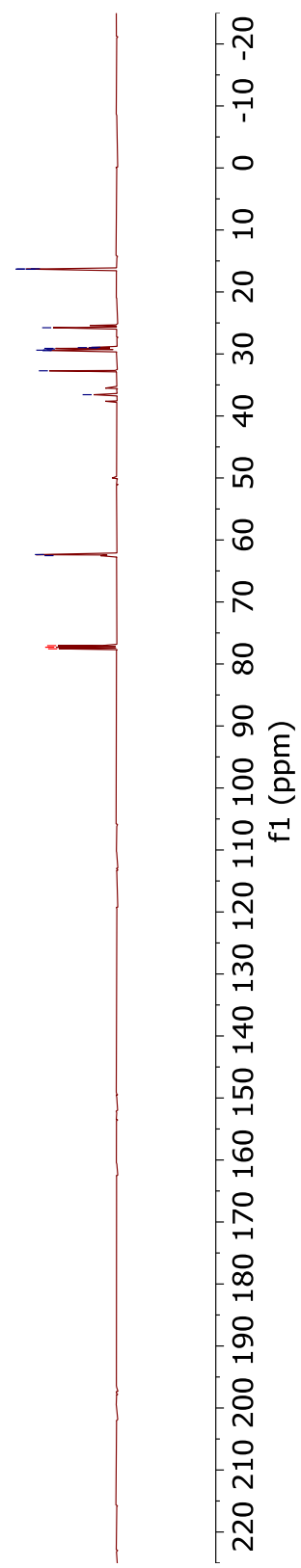
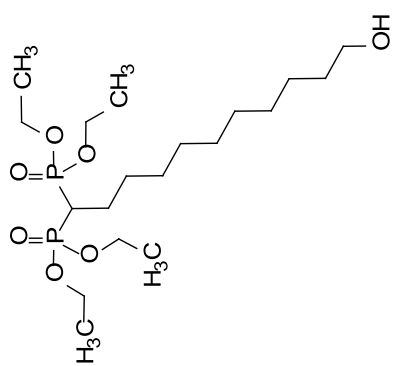




CDCl₃

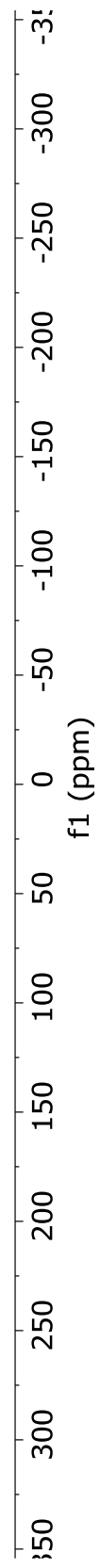
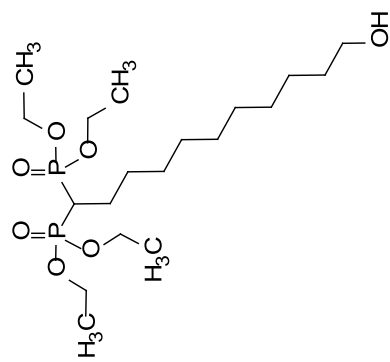
CDCl₃

77.56 CHLORFORM-D
77.30 CHLORFORM-D
77.05 CHLORFORM-D
62.53
62.35
36.57
32.72
29.46
29.39
29.35
29.20
29.10
29.03
28.98
28.92
25.77
16.34
16.32
16.29
16.27

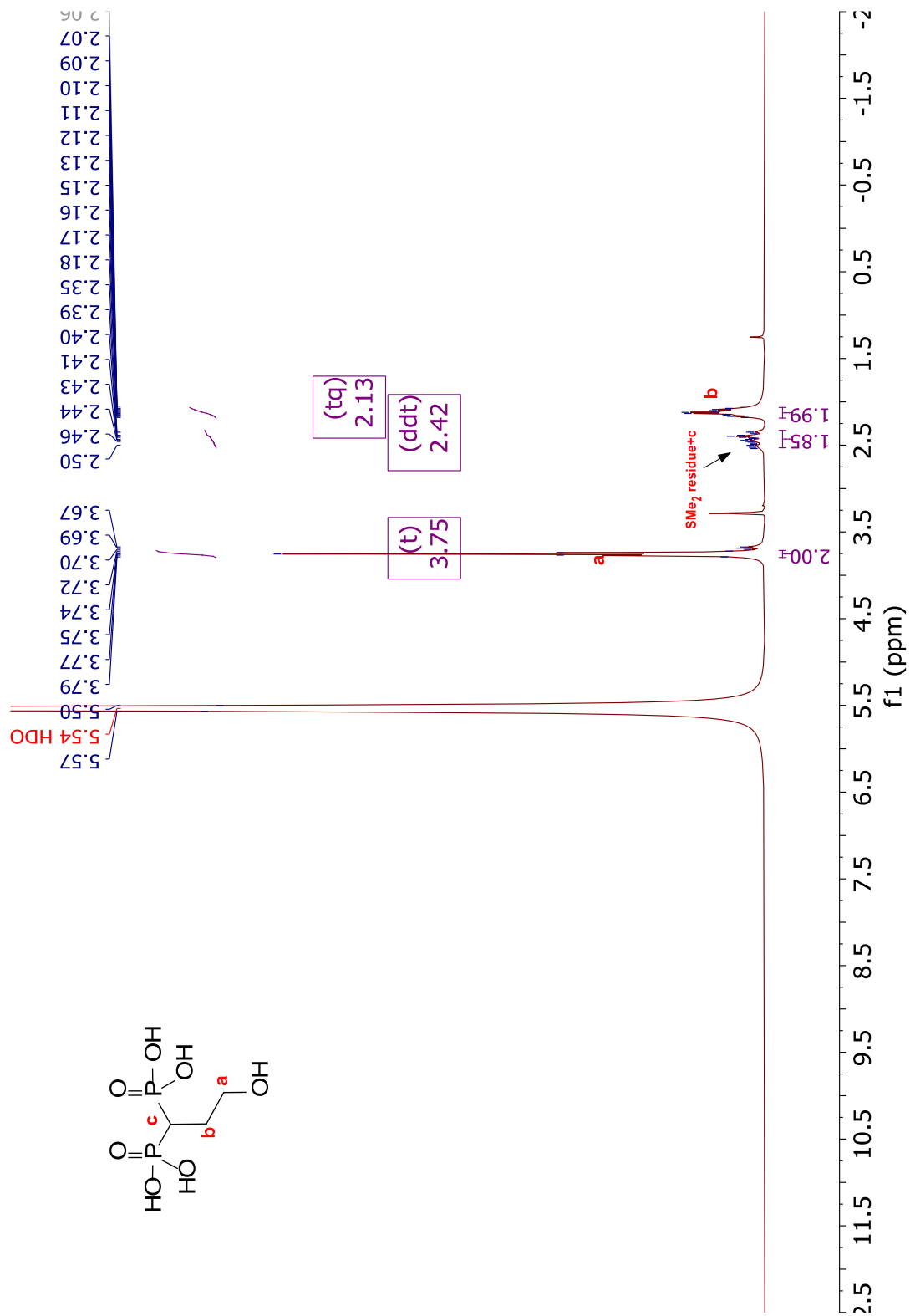


CDCl₃

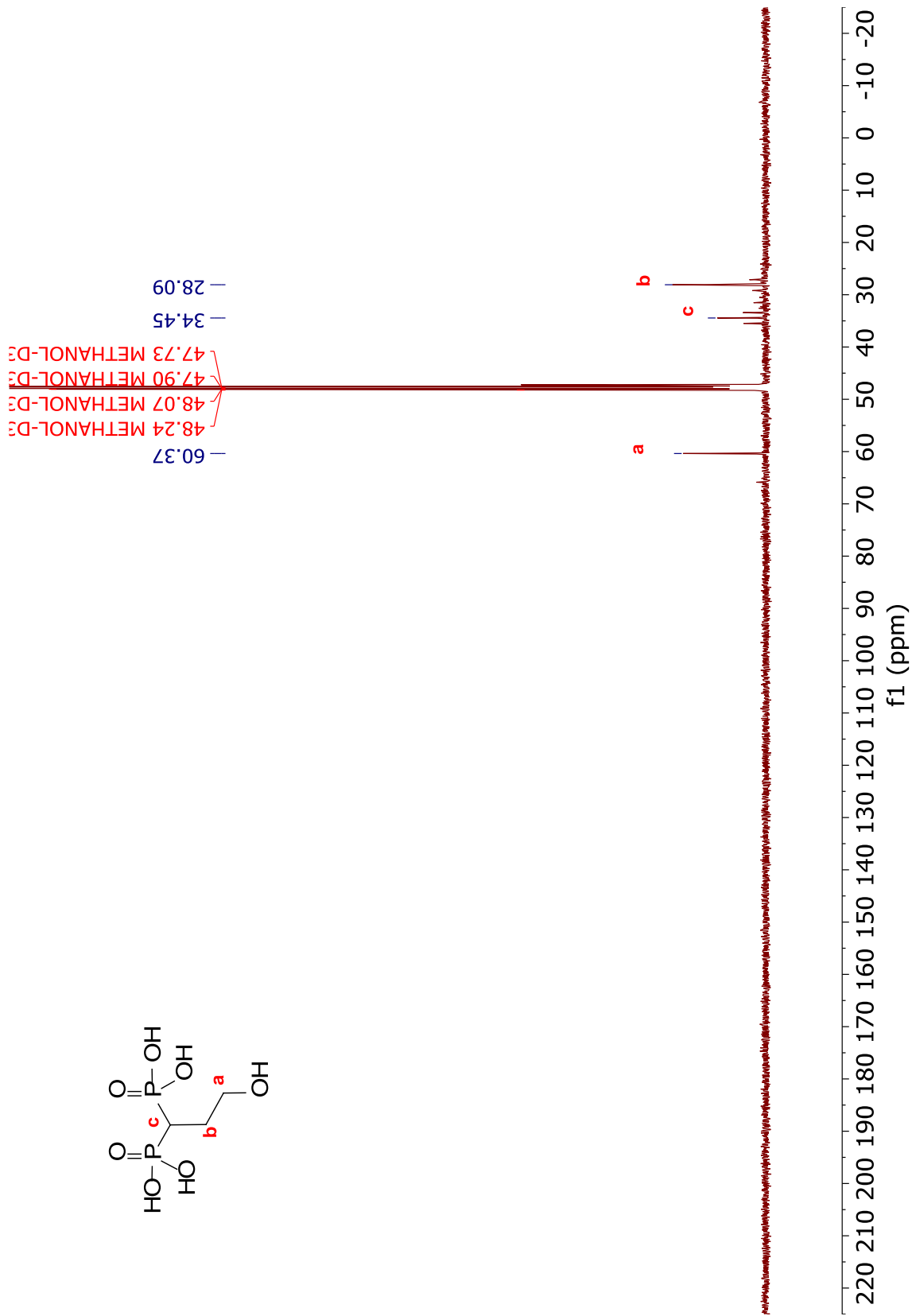
24.61
24.53



CD3OD

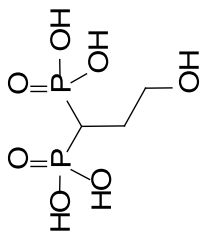


CD3OD

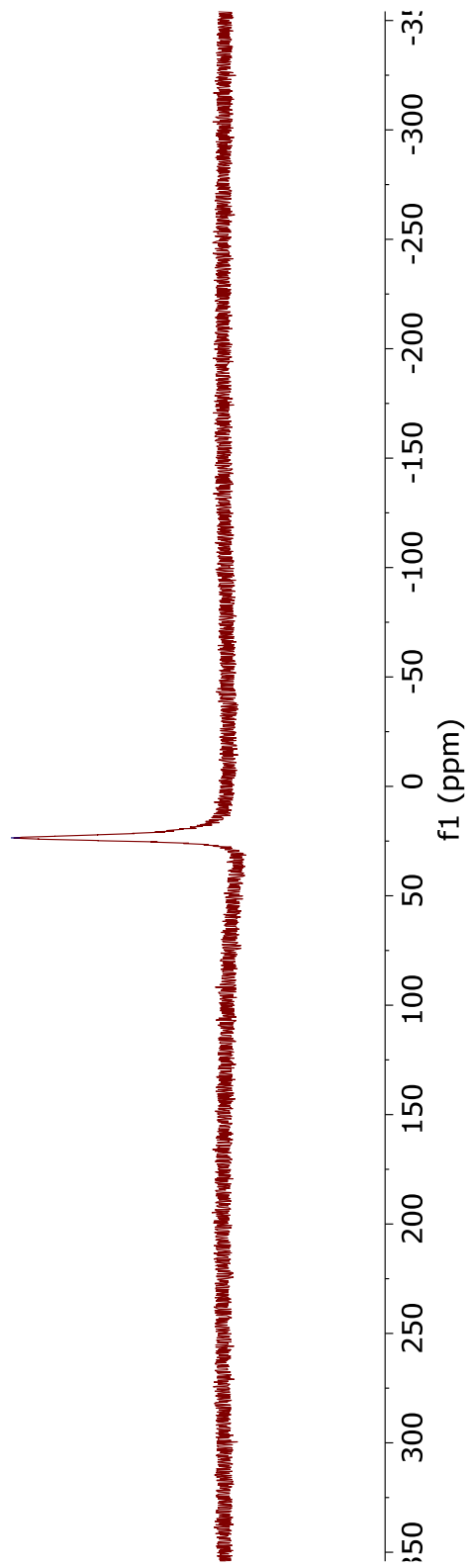


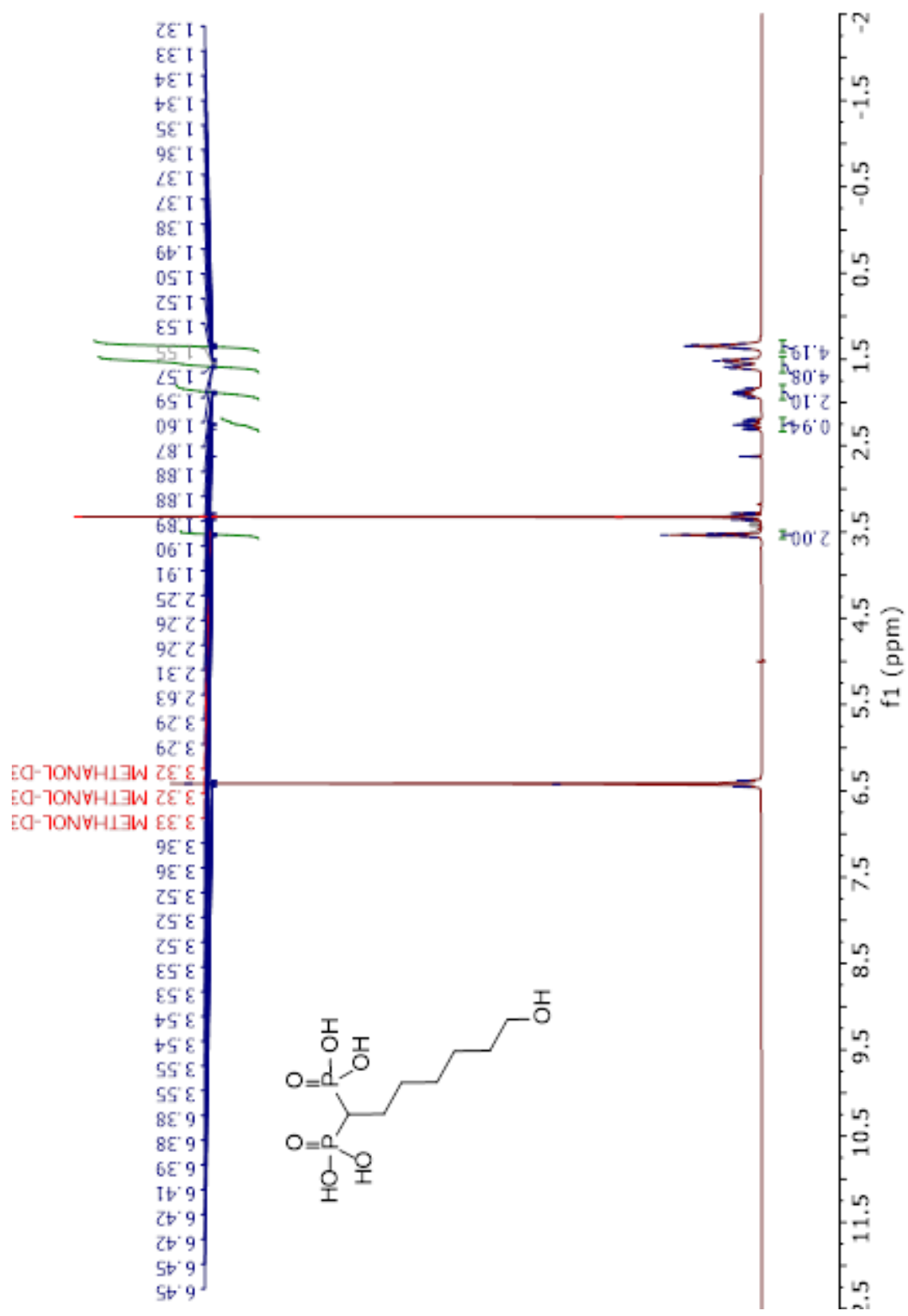
CD3OD

-23.52



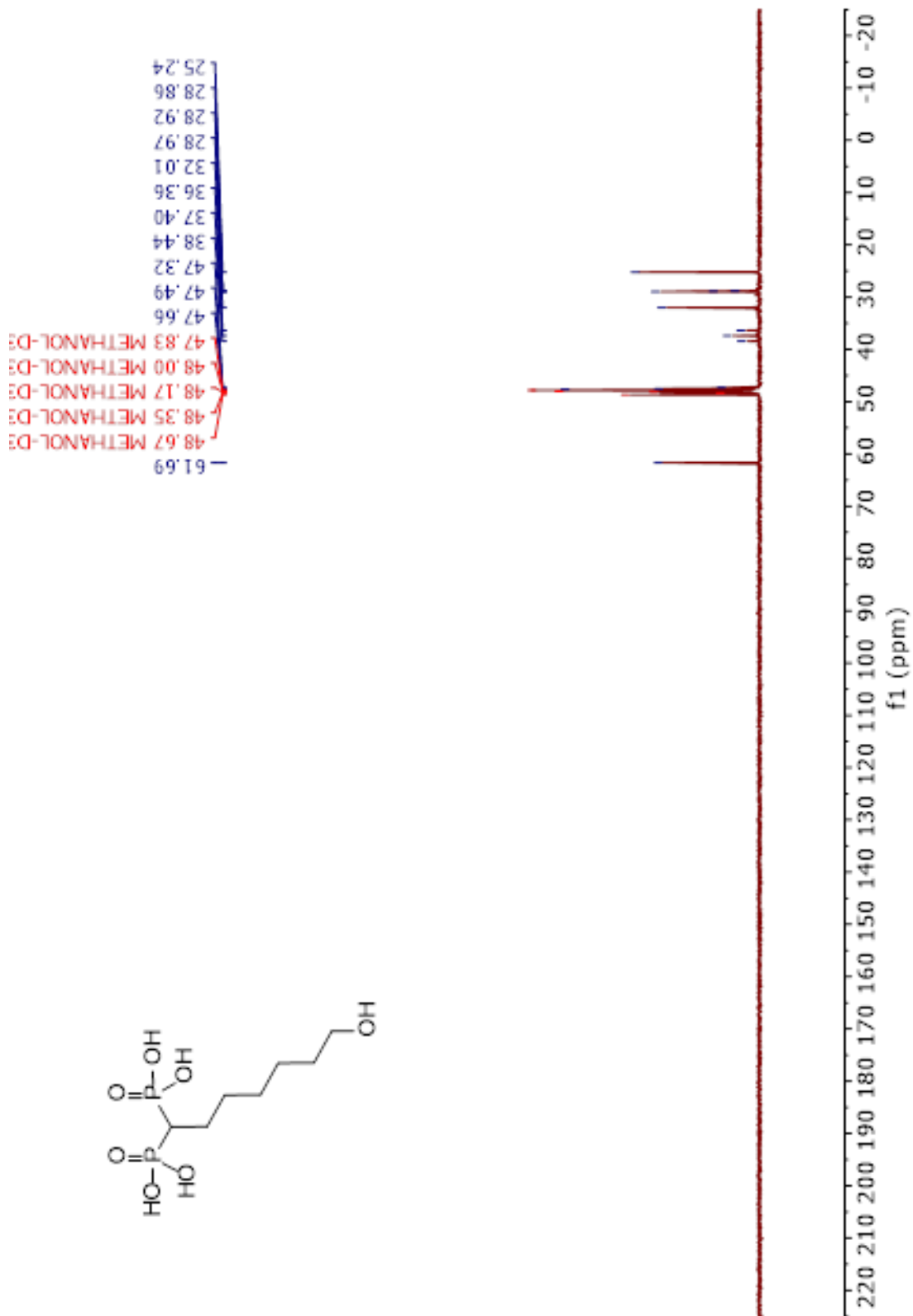
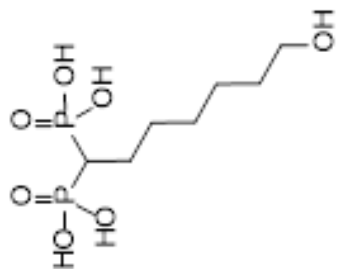
181



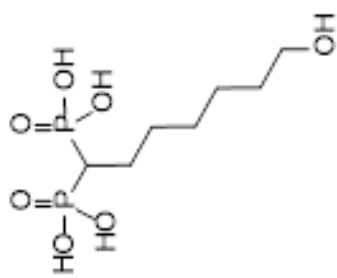


CD3OD

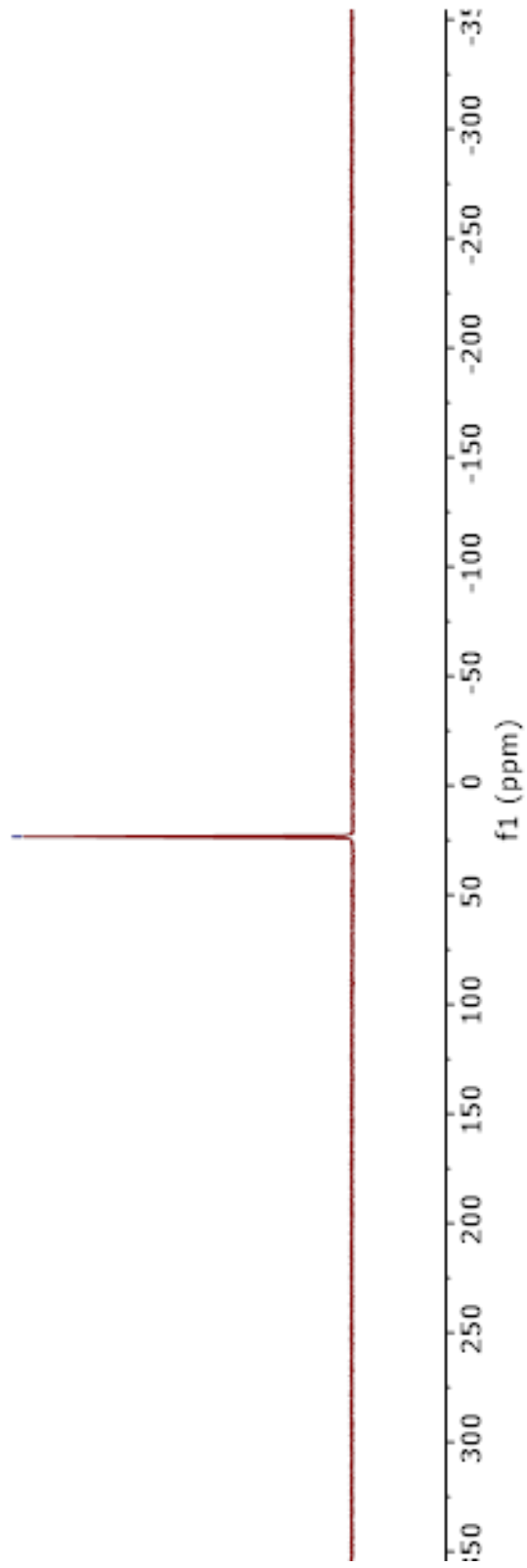
CD3OD



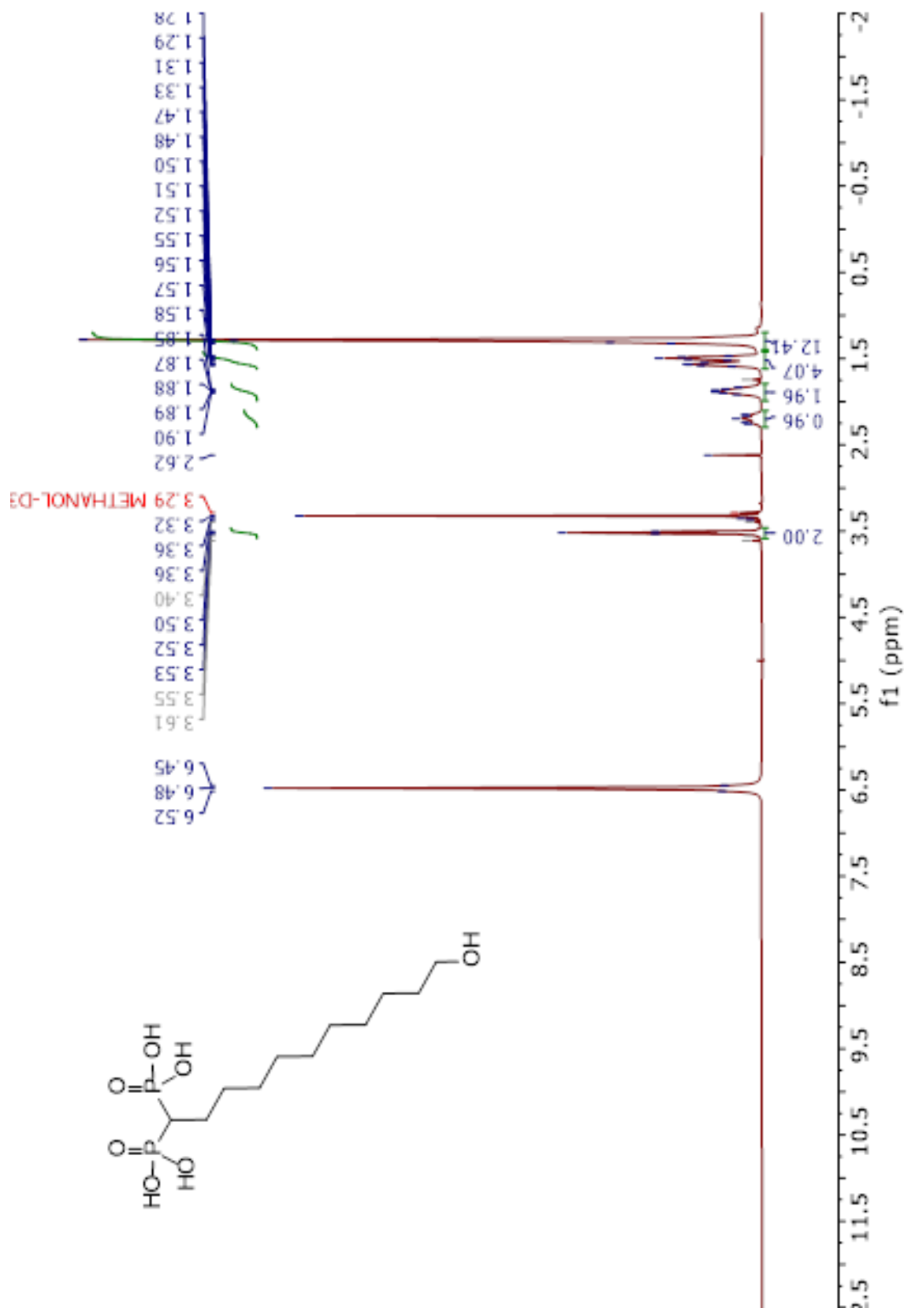
CD3OD



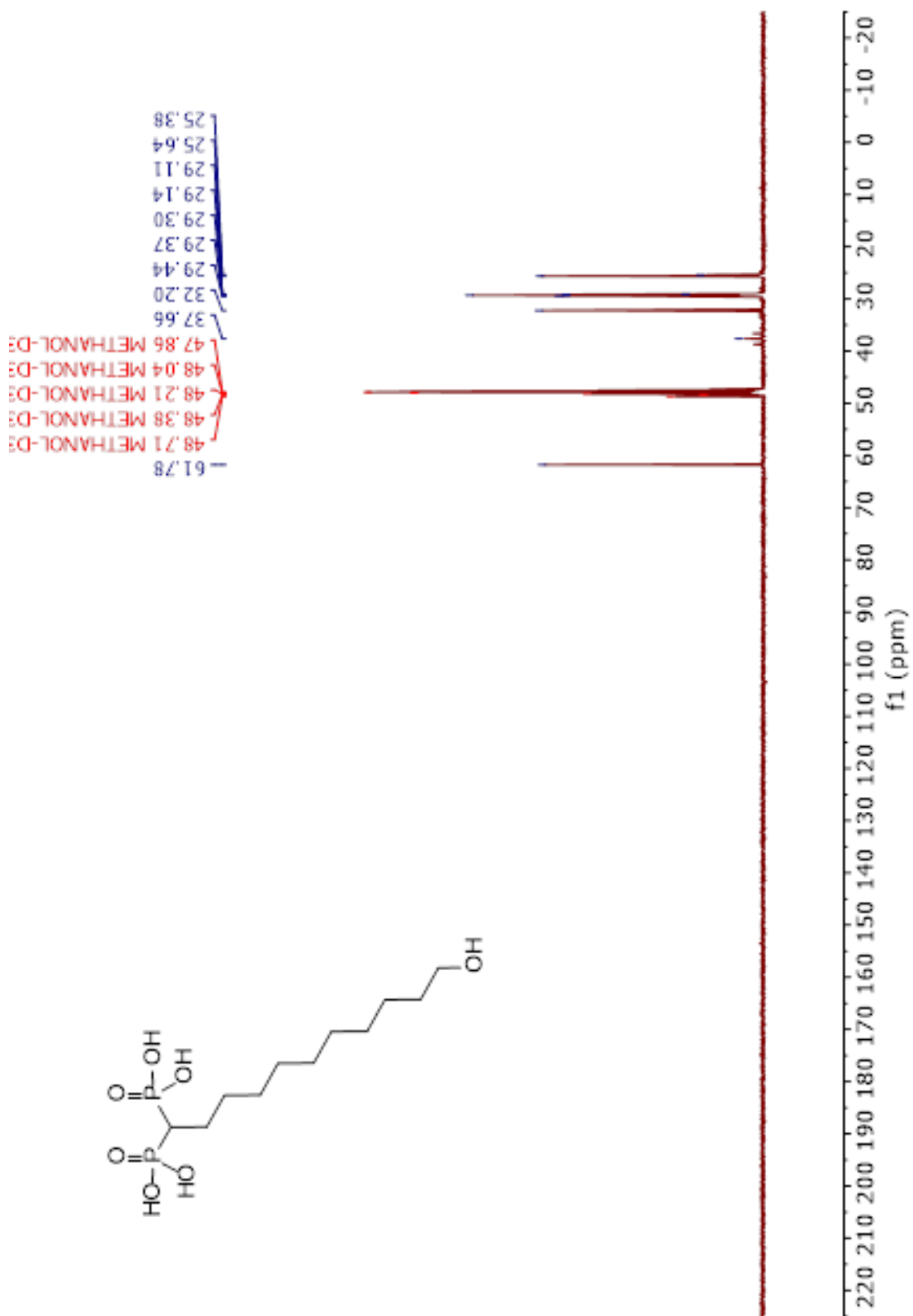
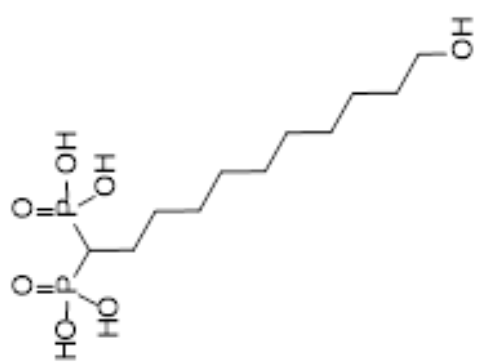
-23.41



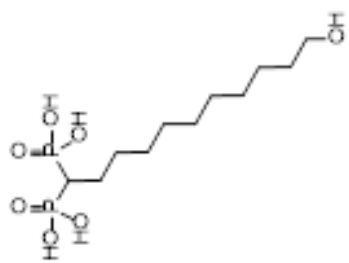
CD3OD



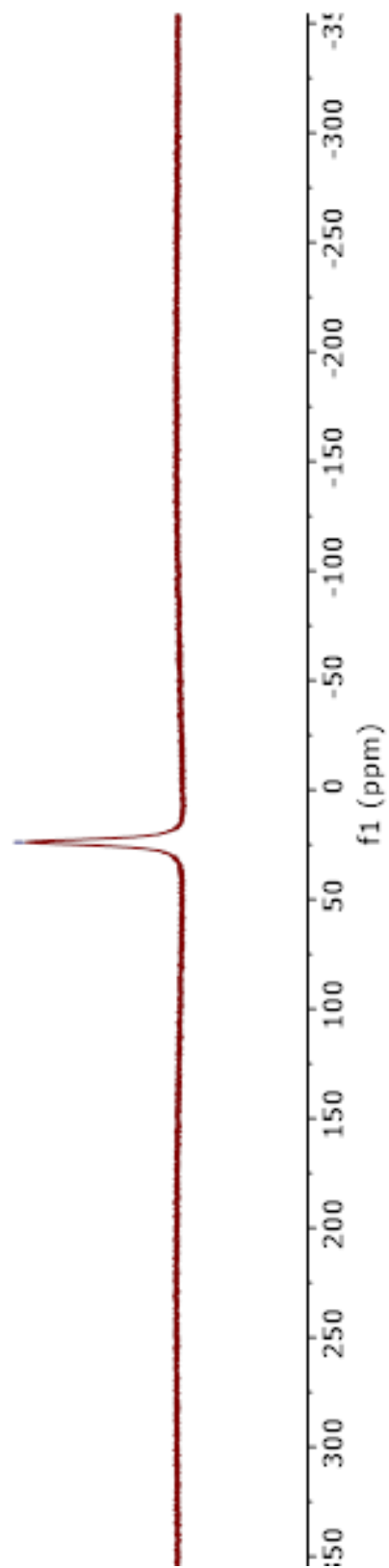
CD3OD

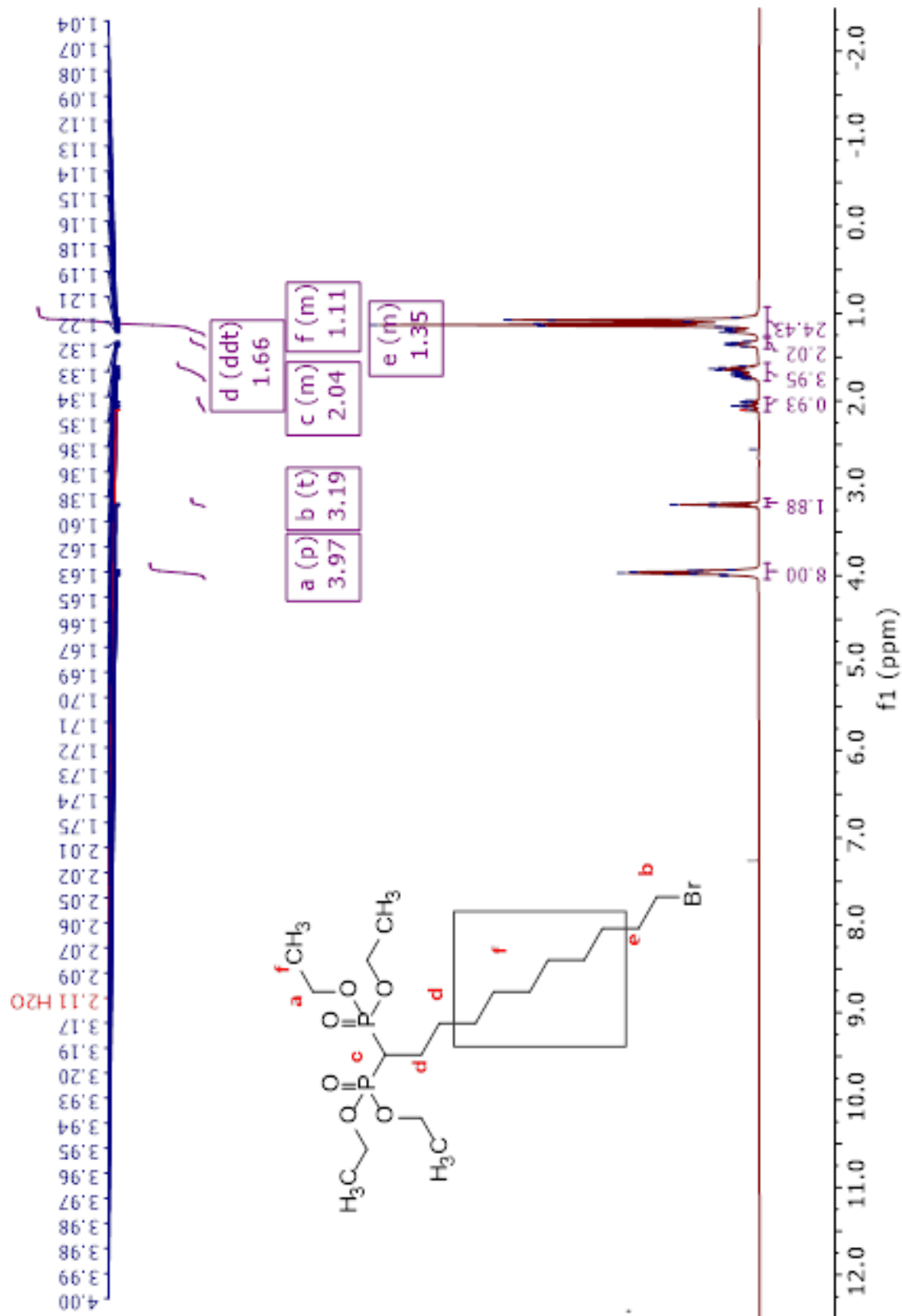


- 23.86



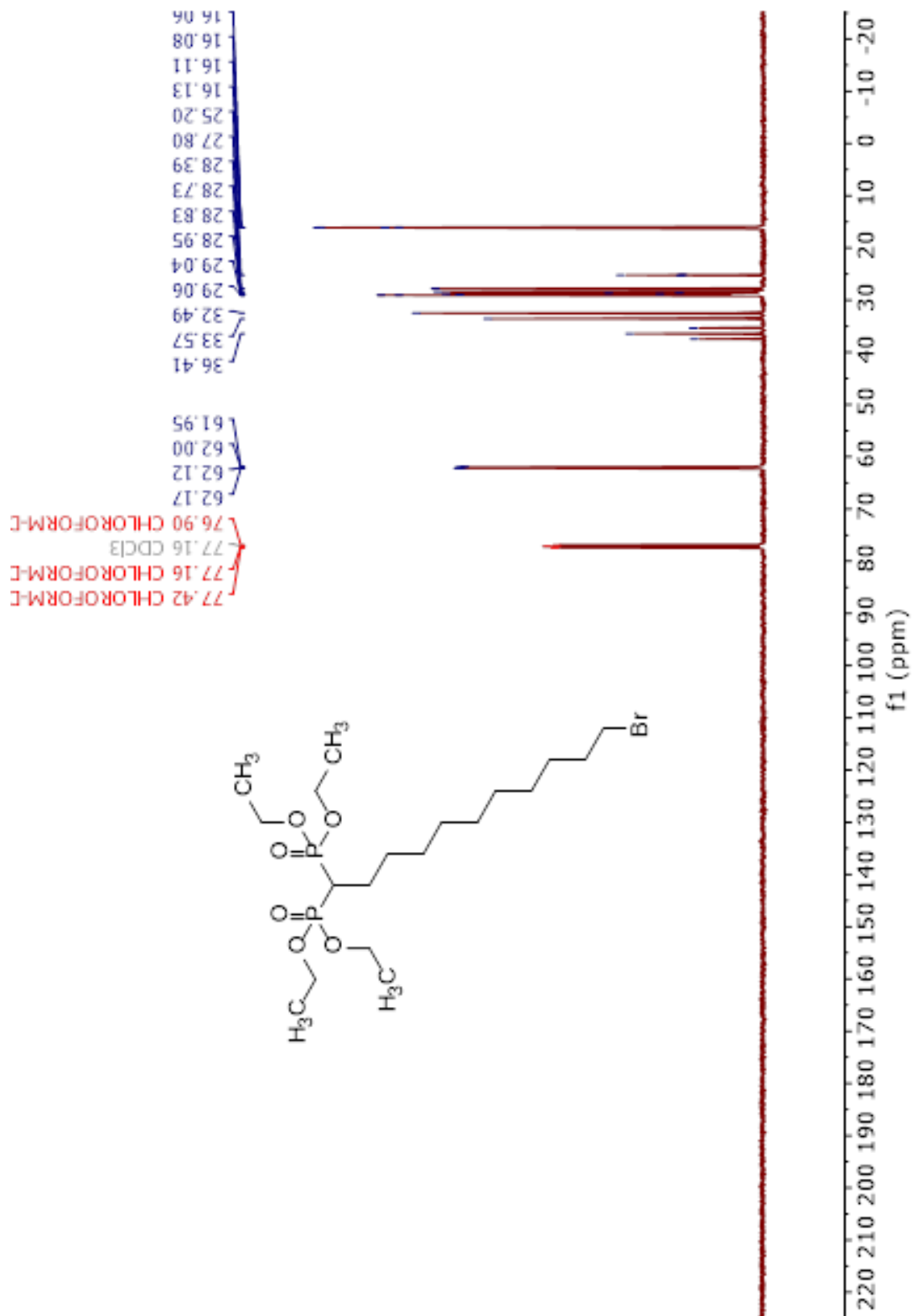
CD3OD





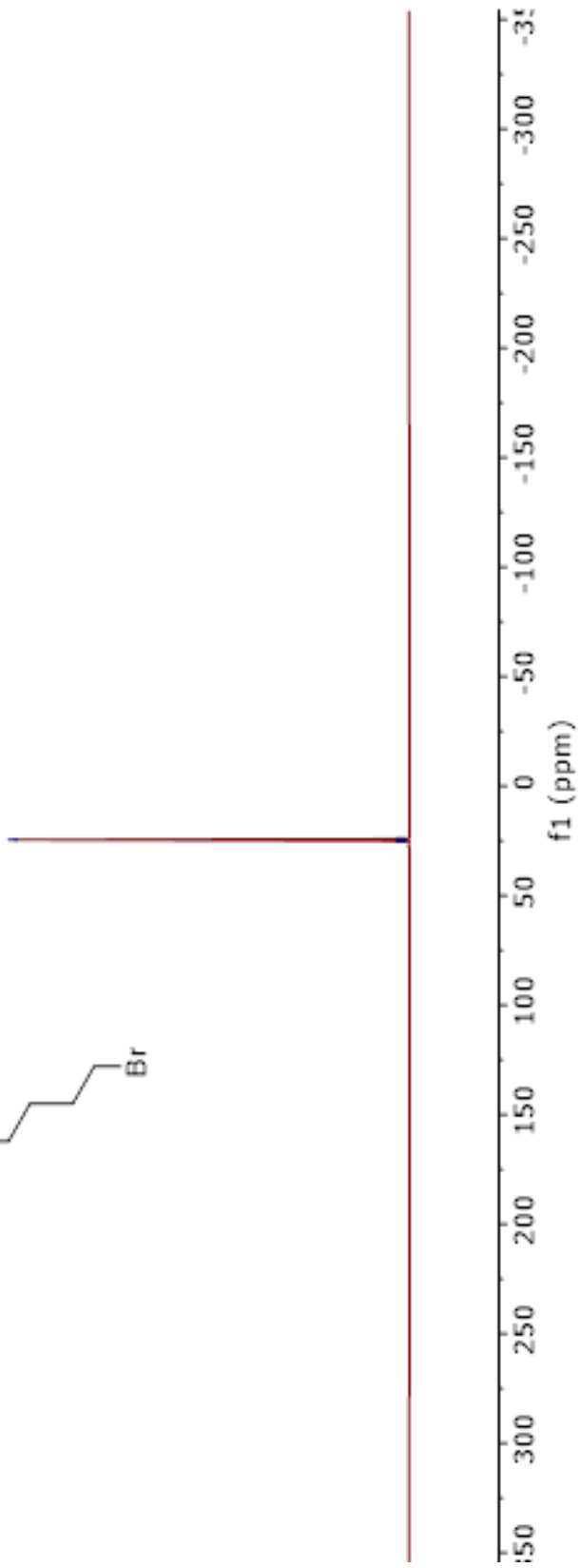
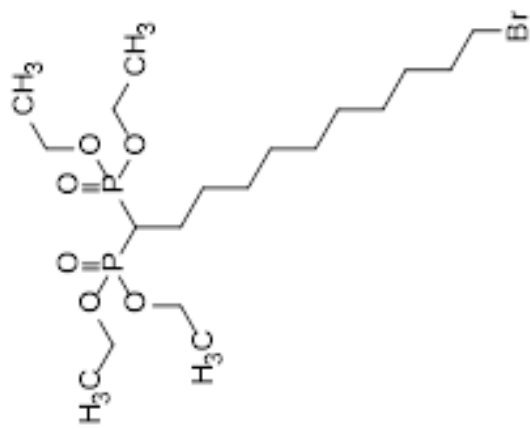
CDCl₃

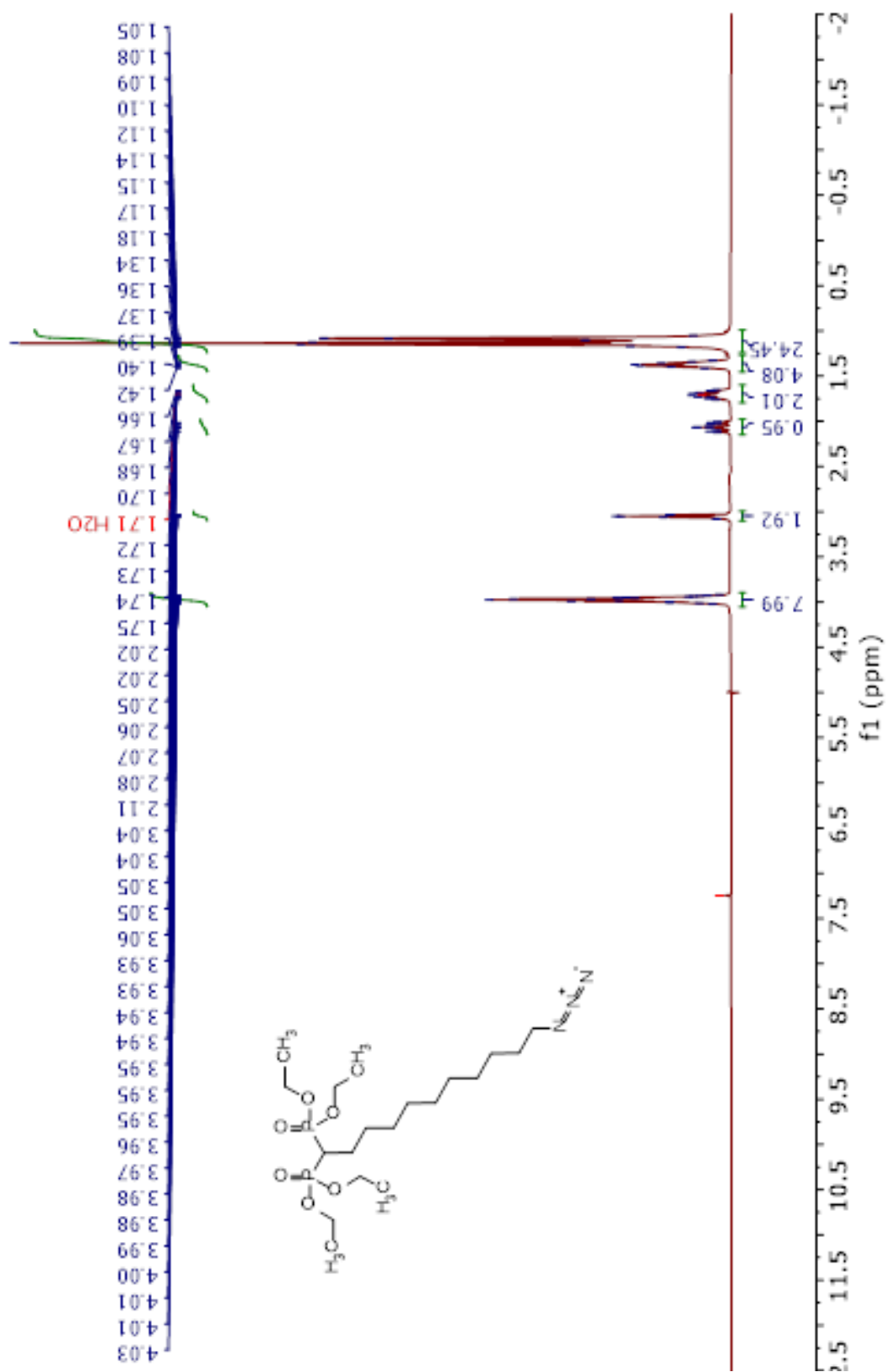
CDCl₃



CDCl₃

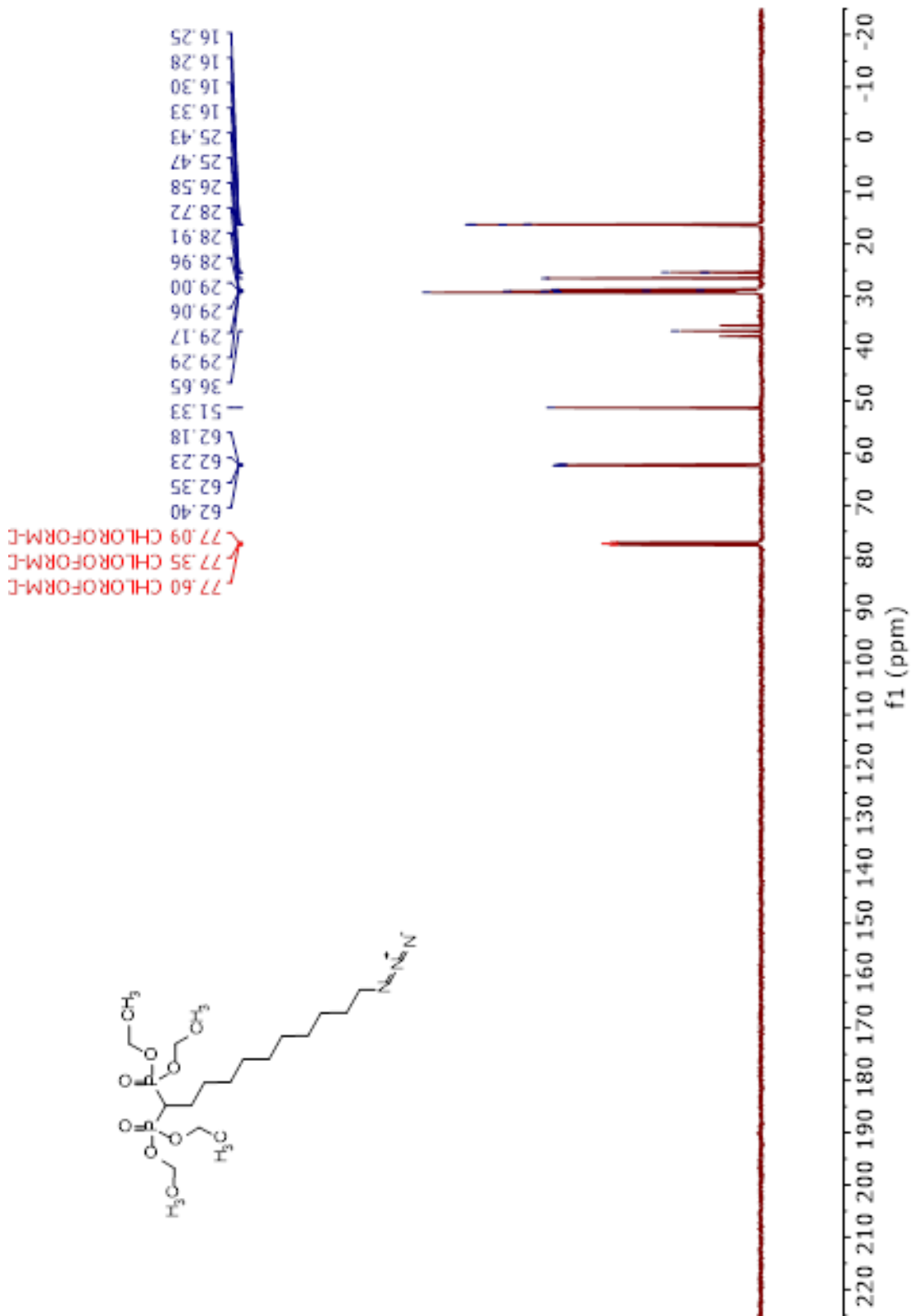
25.10
24.78
24.55
24.00





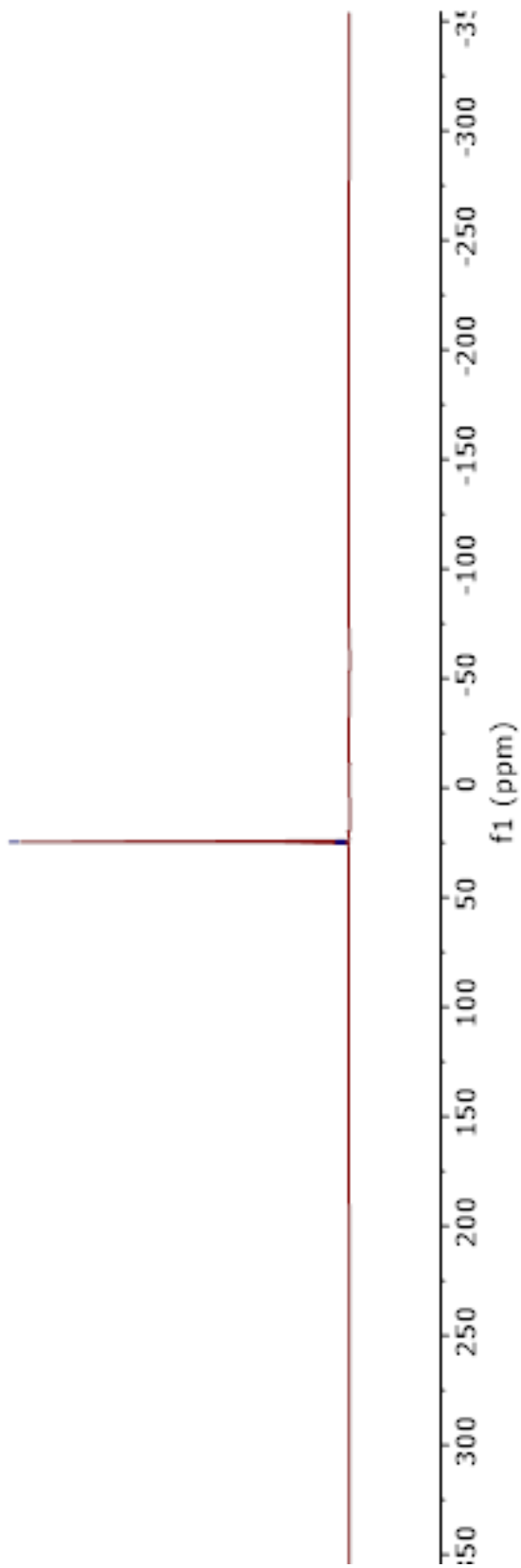
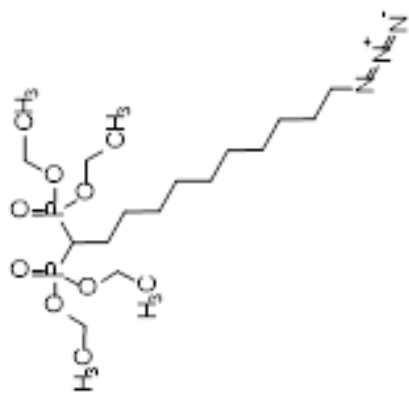
CDCl₃

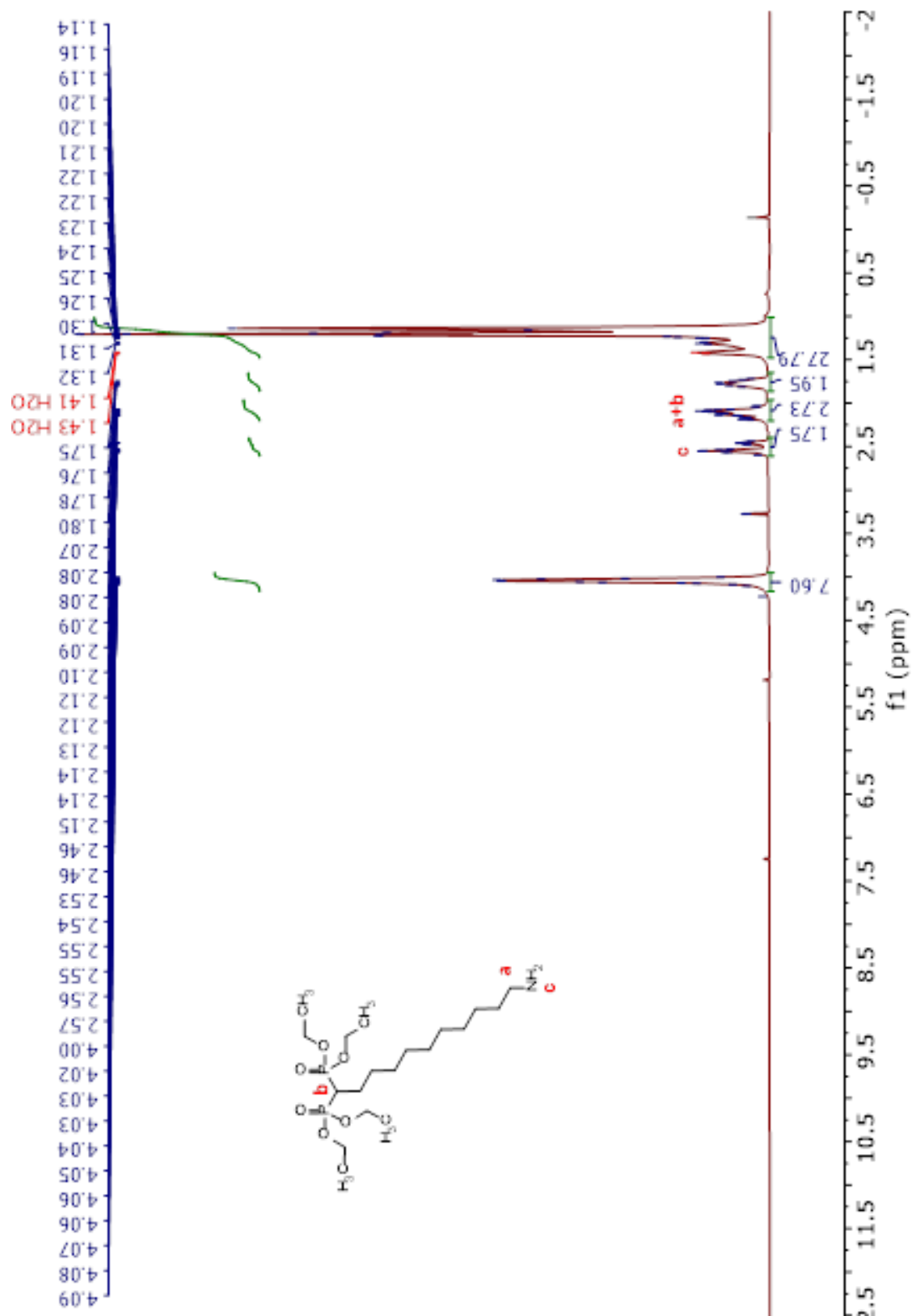
CDCl₃



CDCl₃

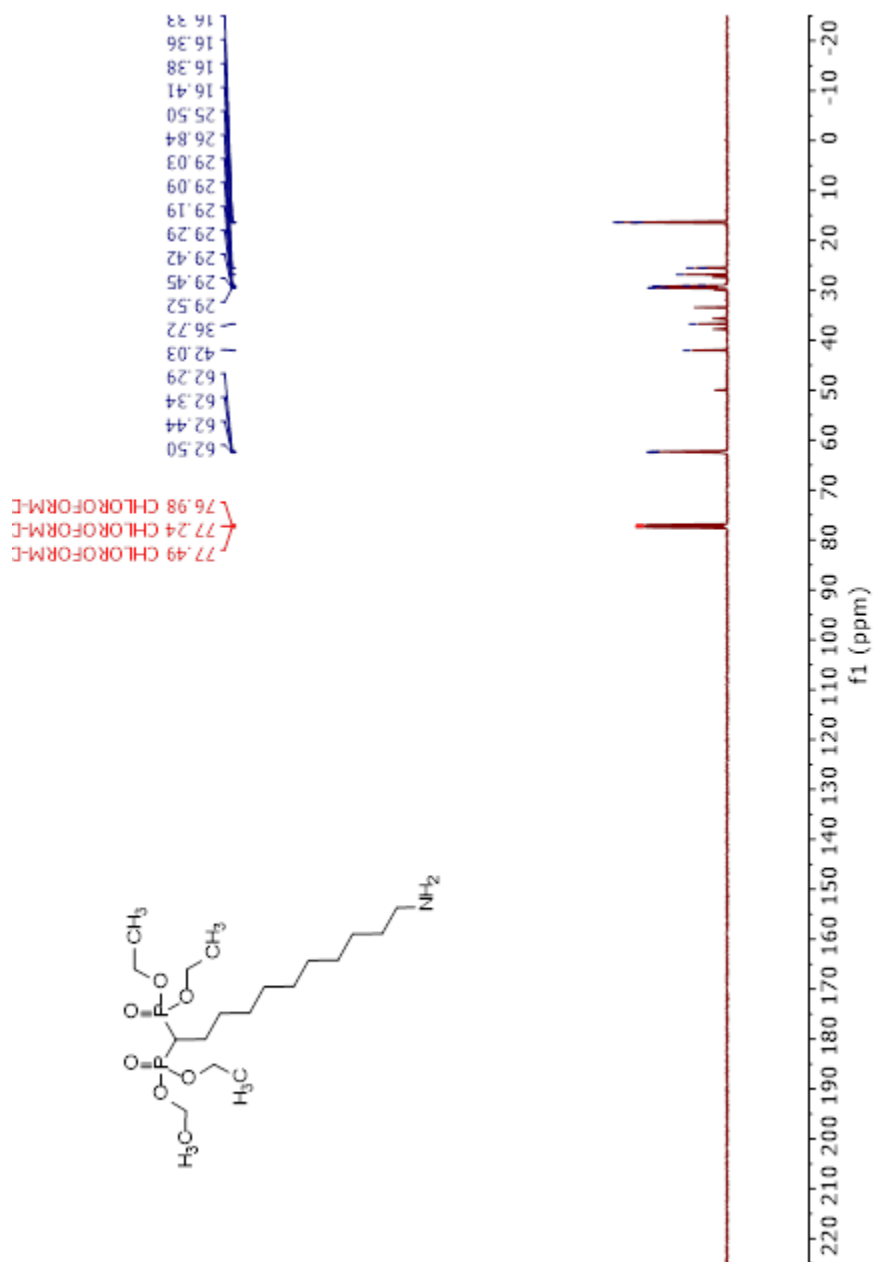
25.25
24.70
24.15





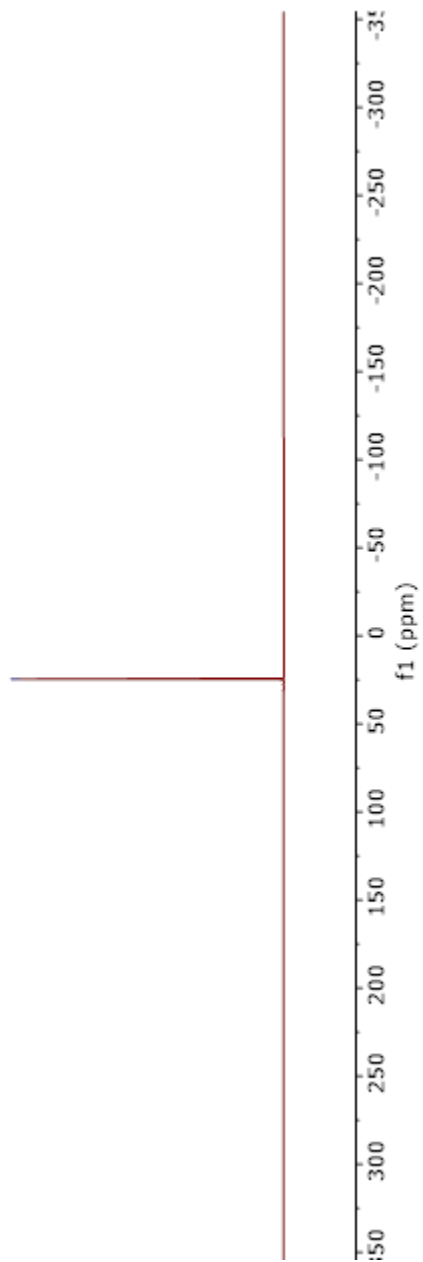
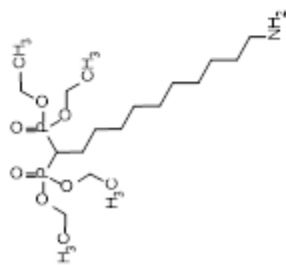
CDCl₃

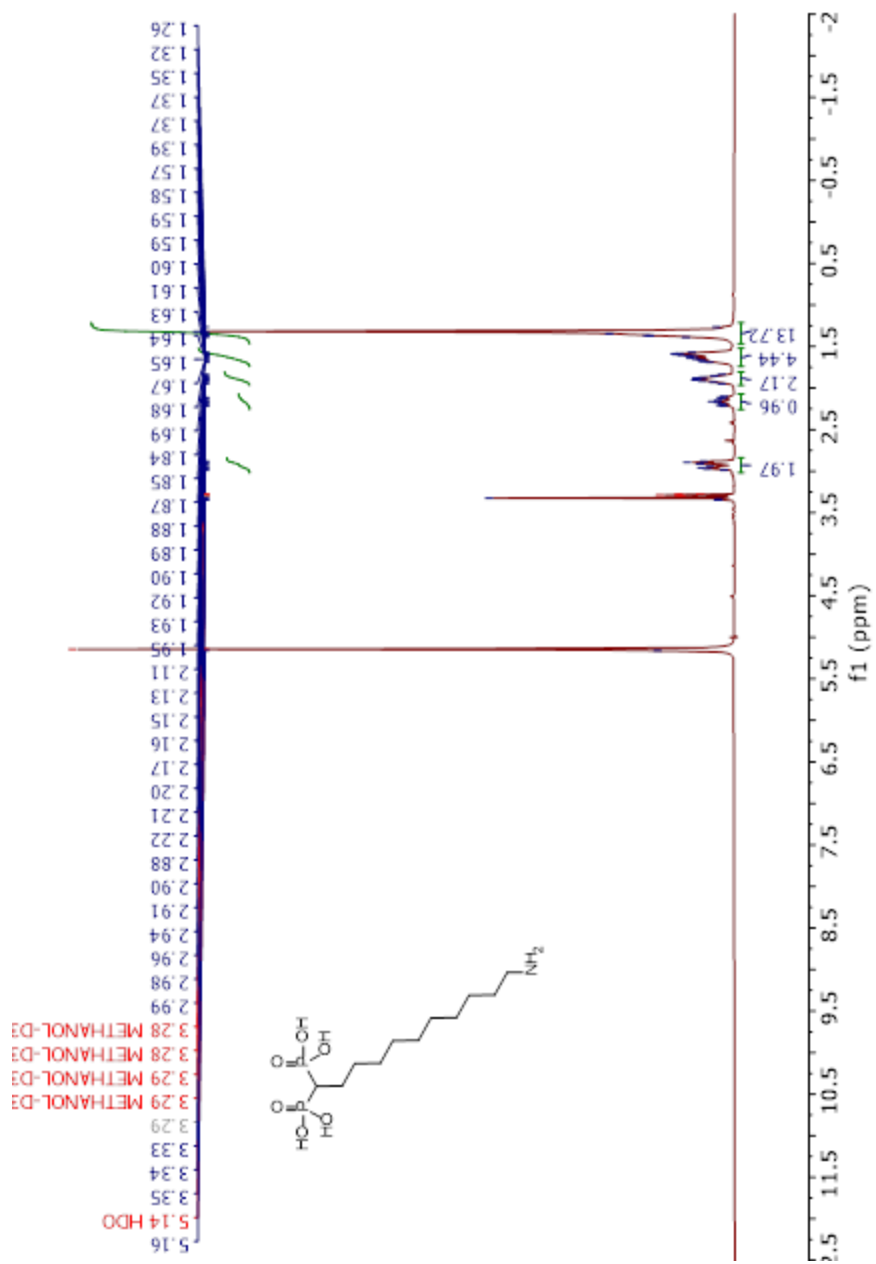
CDCl₃



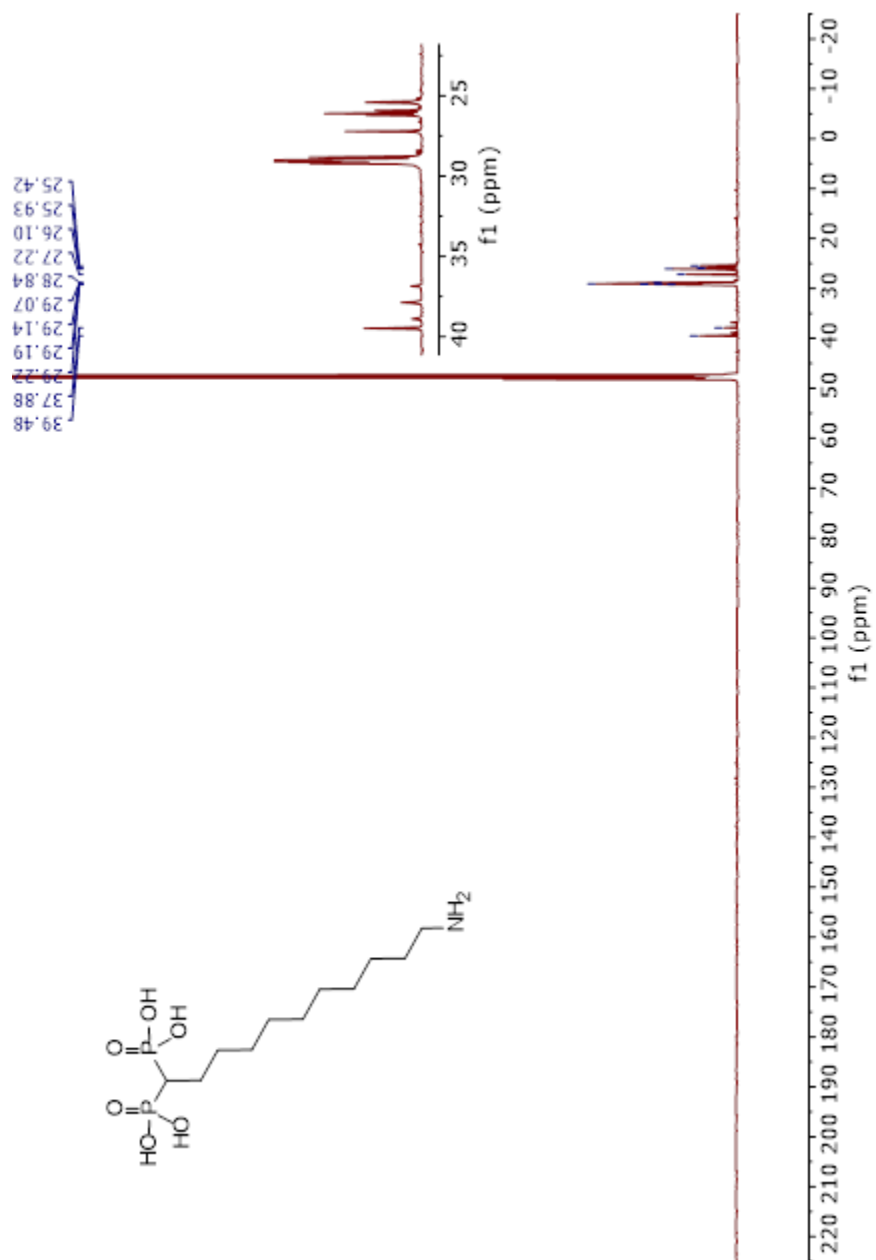
CDCl₃

-24.67





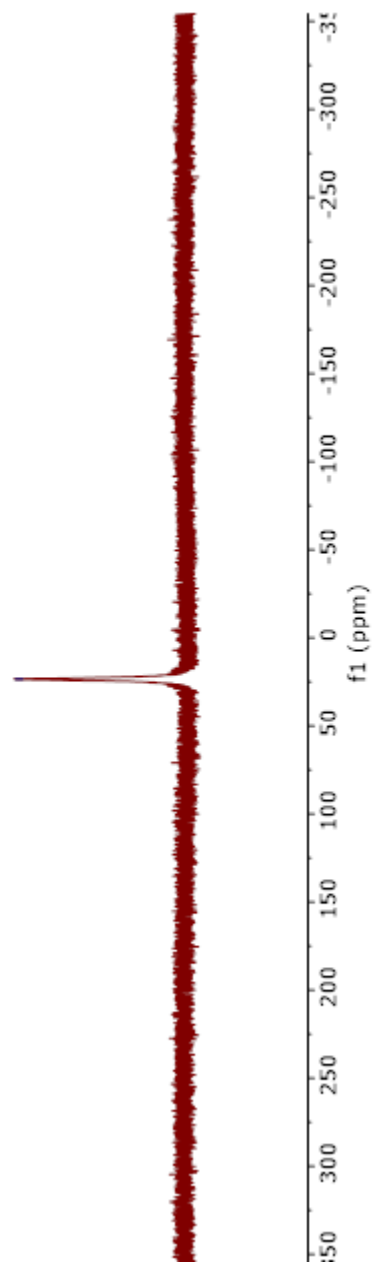
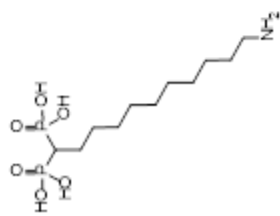
CD3OD

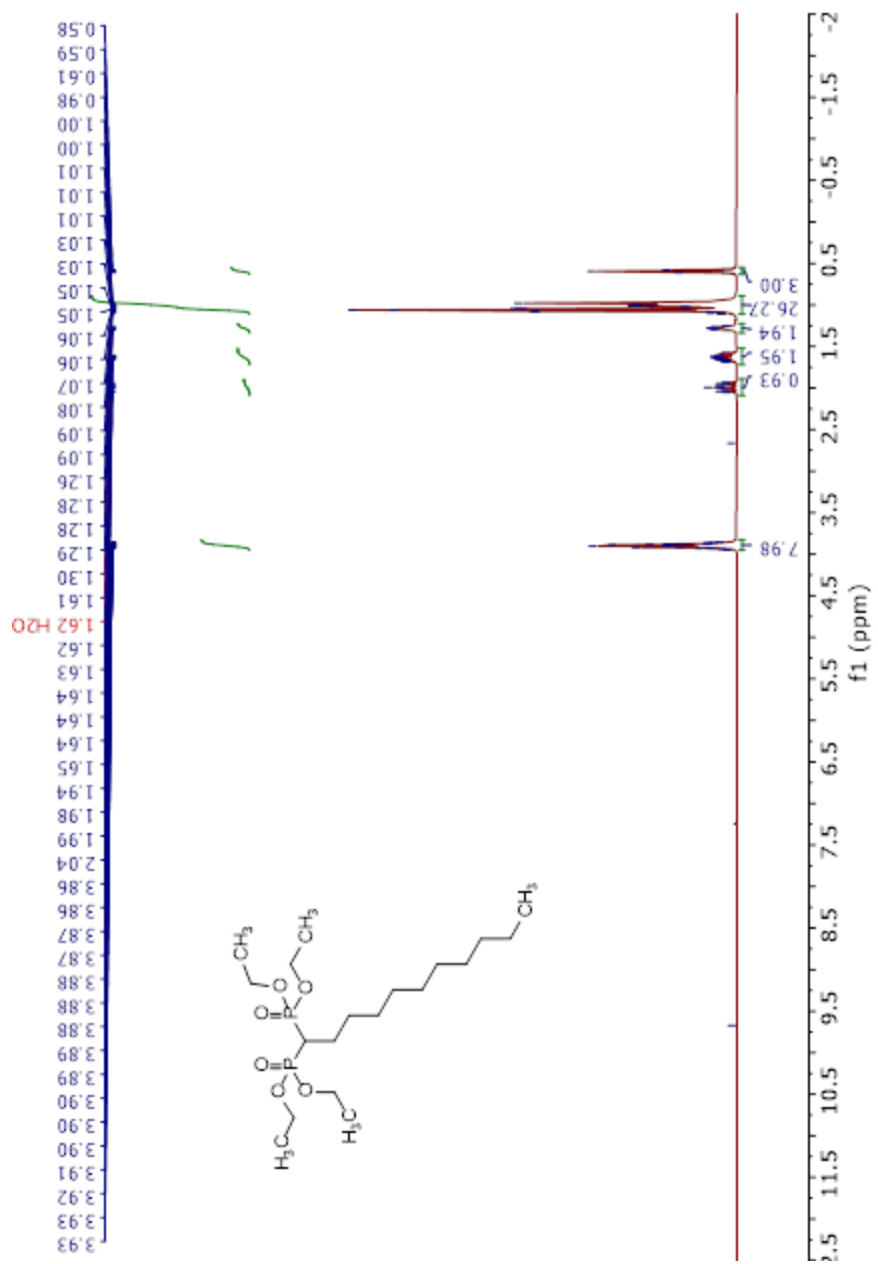


CD3OD

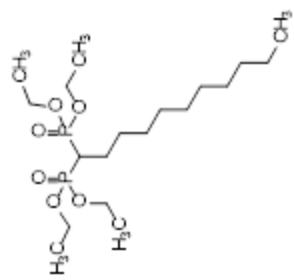
CD3OD

-23.55

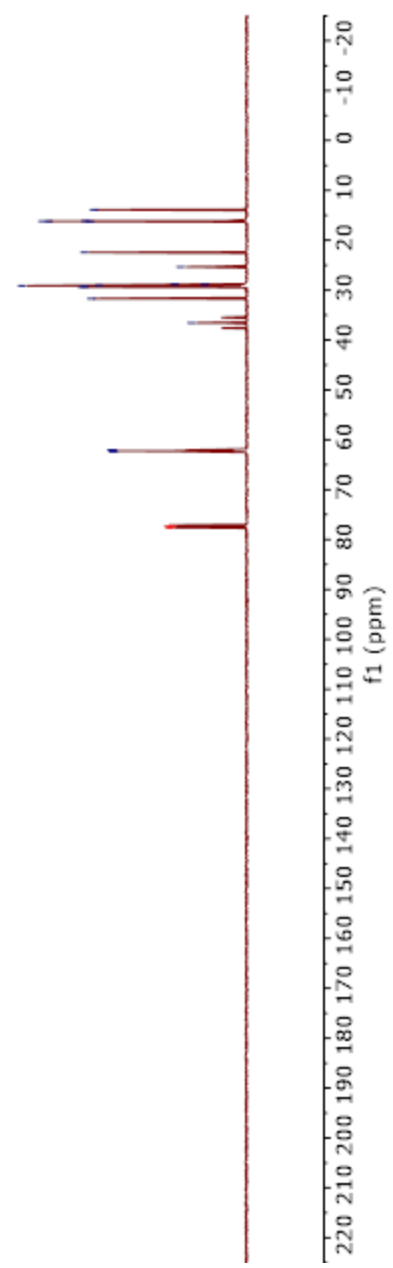




CDCl₃

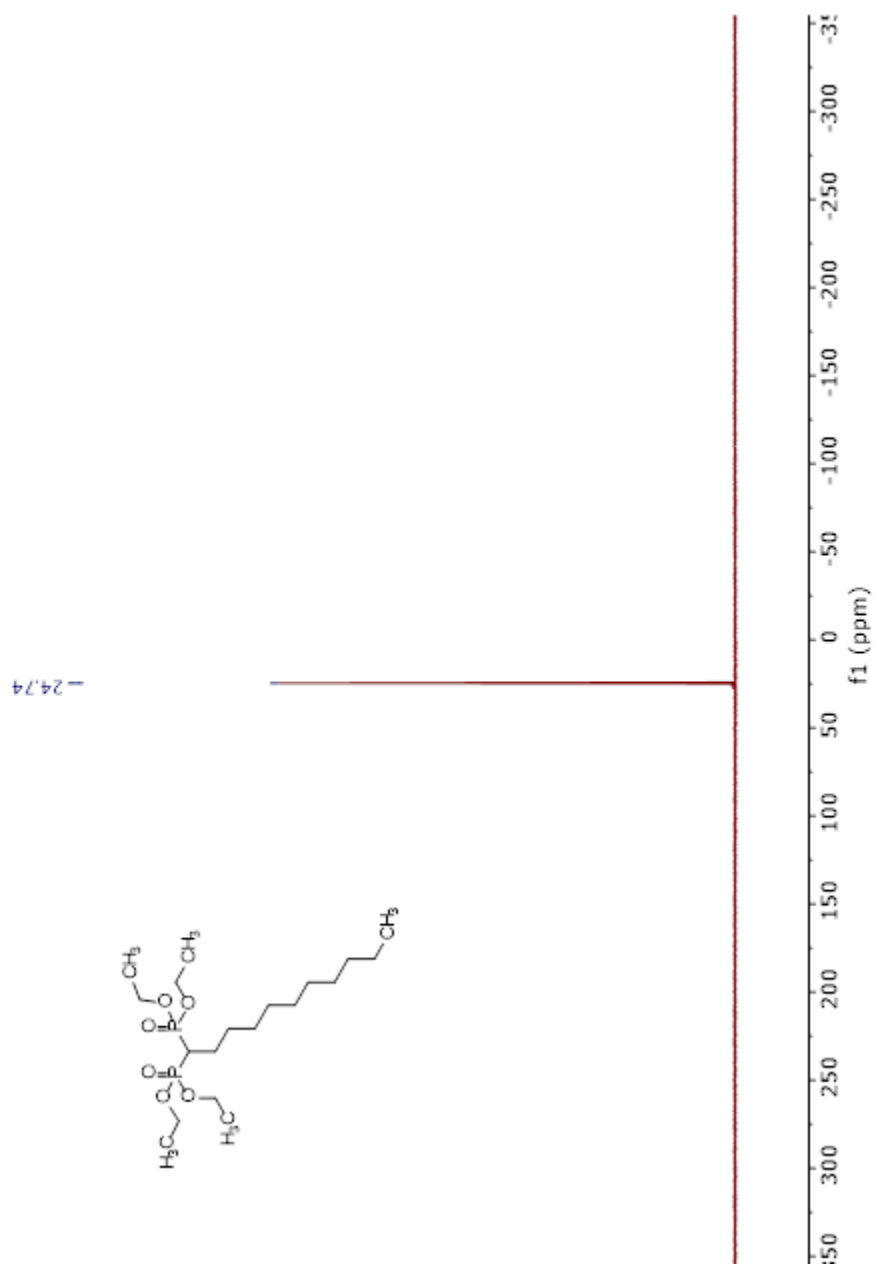


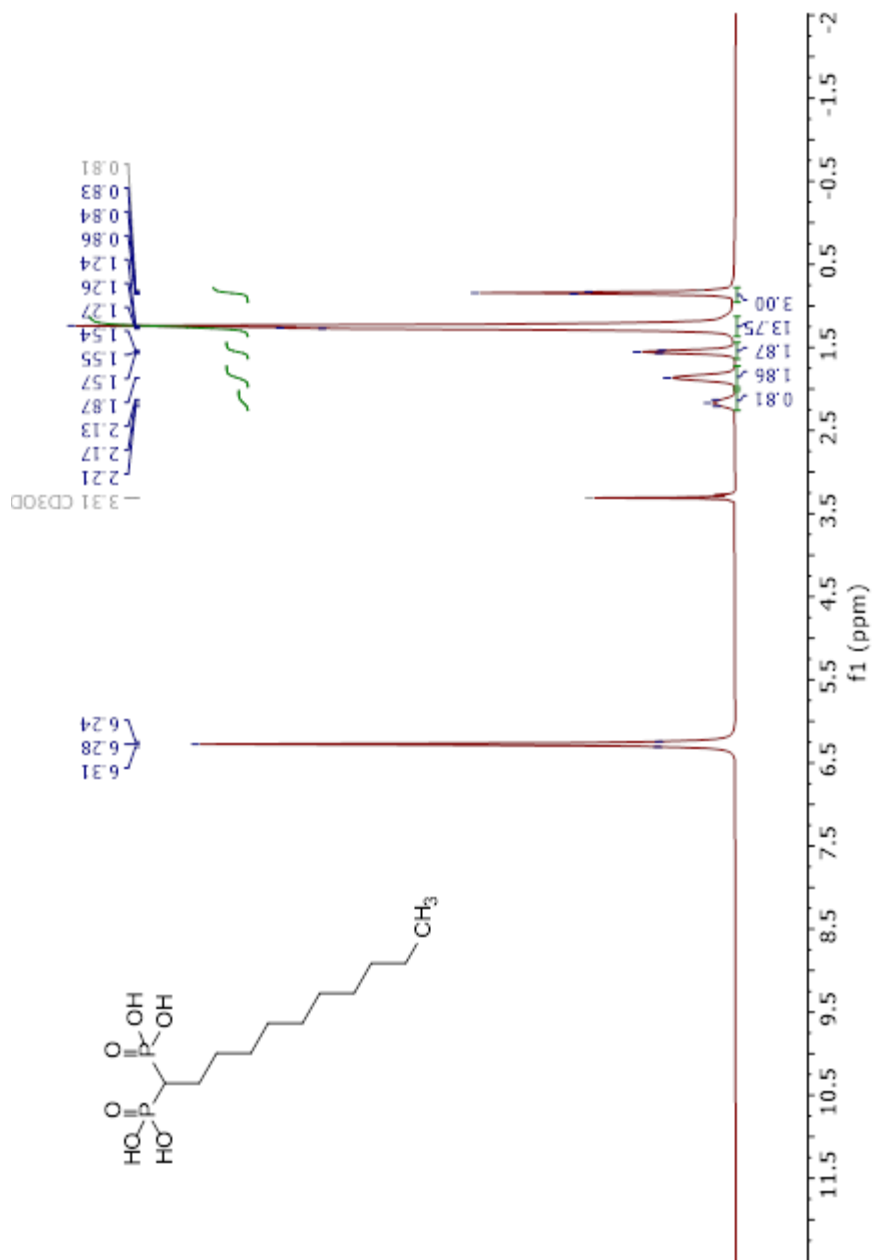
77.64 CHLOROFORM-E
 77.38 CHLOROFORM-E
 77.12 CHLOROFORM-E
 62.31
 62.25
 62.15
 62.10
 36.56
 31.70
 29.37
 29.34
 29.11
 29.02
 28.92
 28.87
 25.34
 22.46
 16.23
 16.20
 16.17
 16.15
 13.87



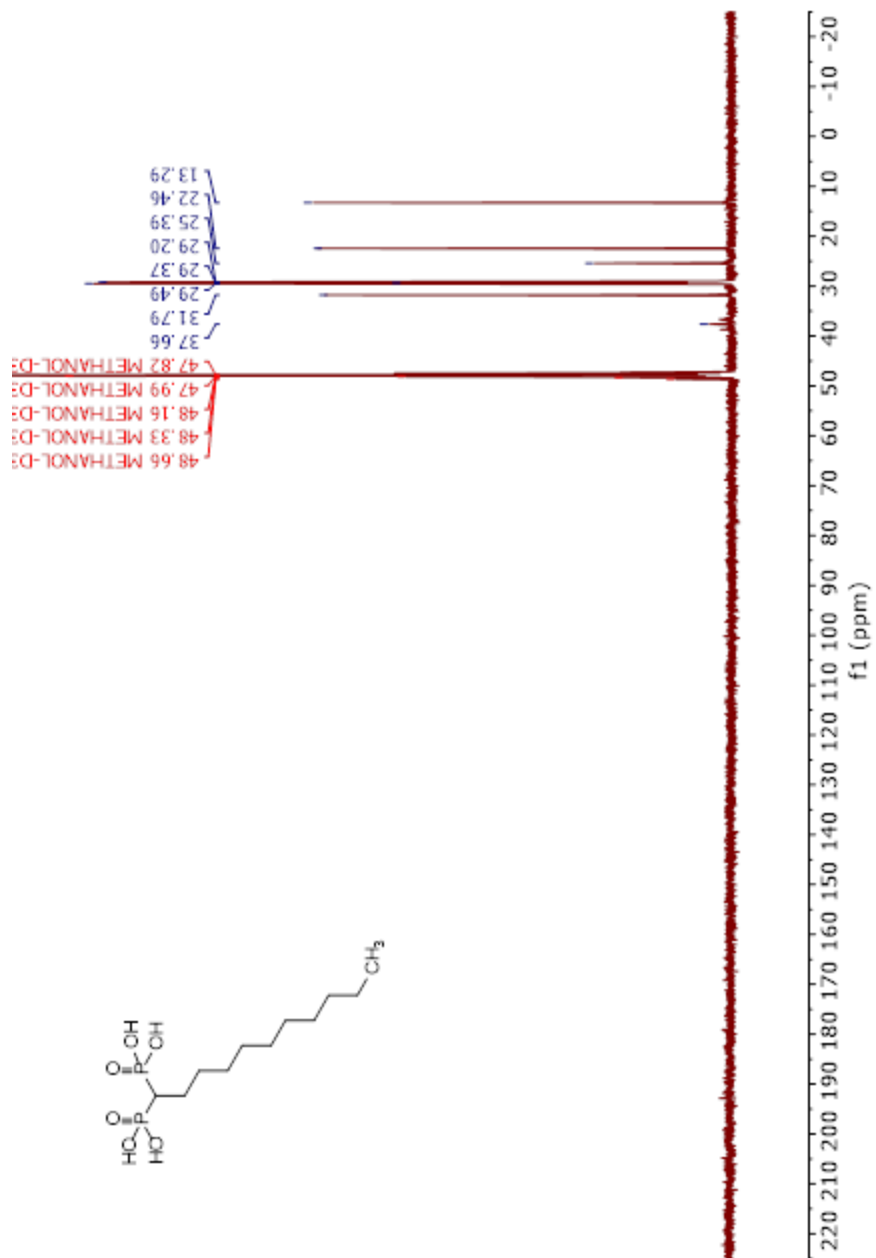
CDCl3

CDCl₃



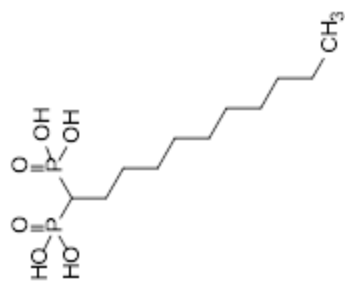


CD3OD

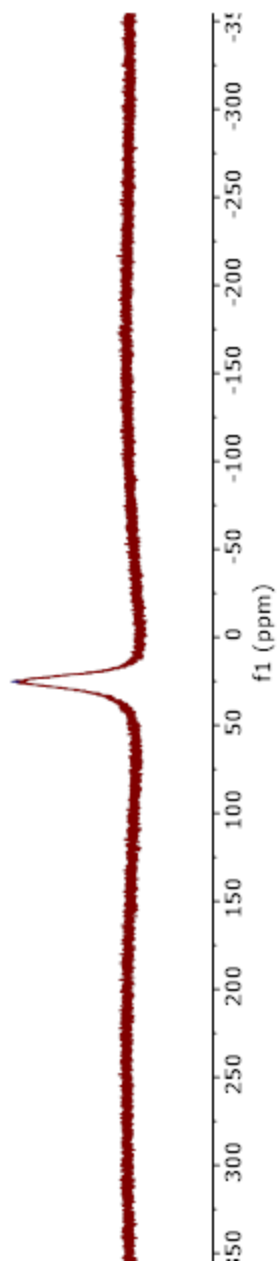


CD3OD

CD3OD



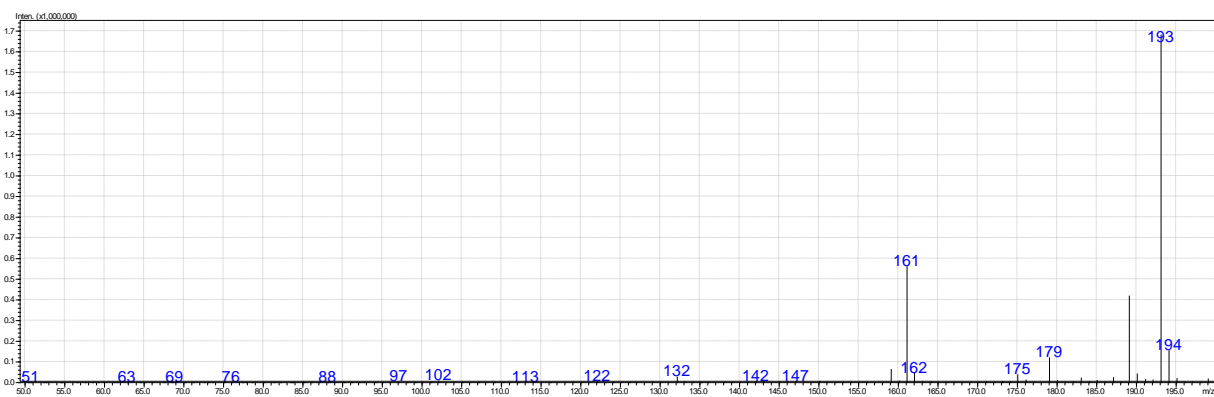
-25.05



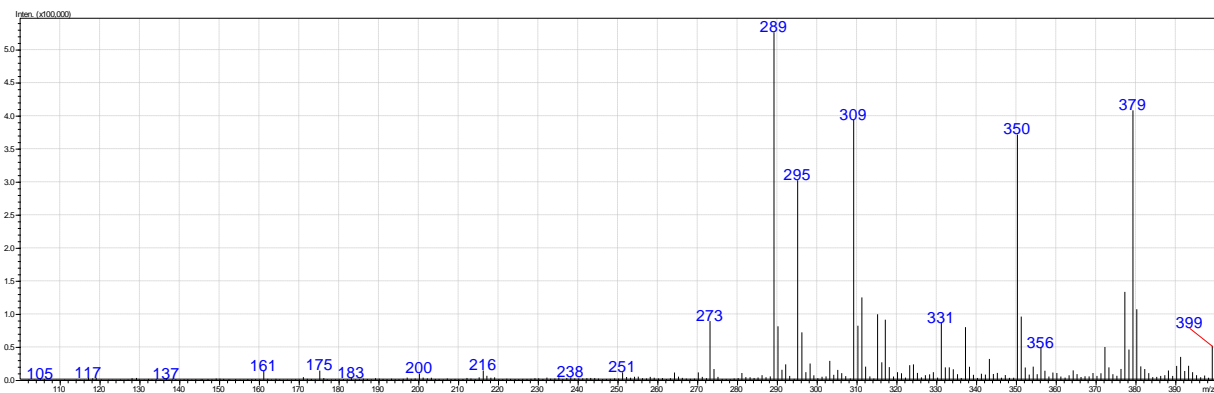
Mass spec

LC/MS and HRMS

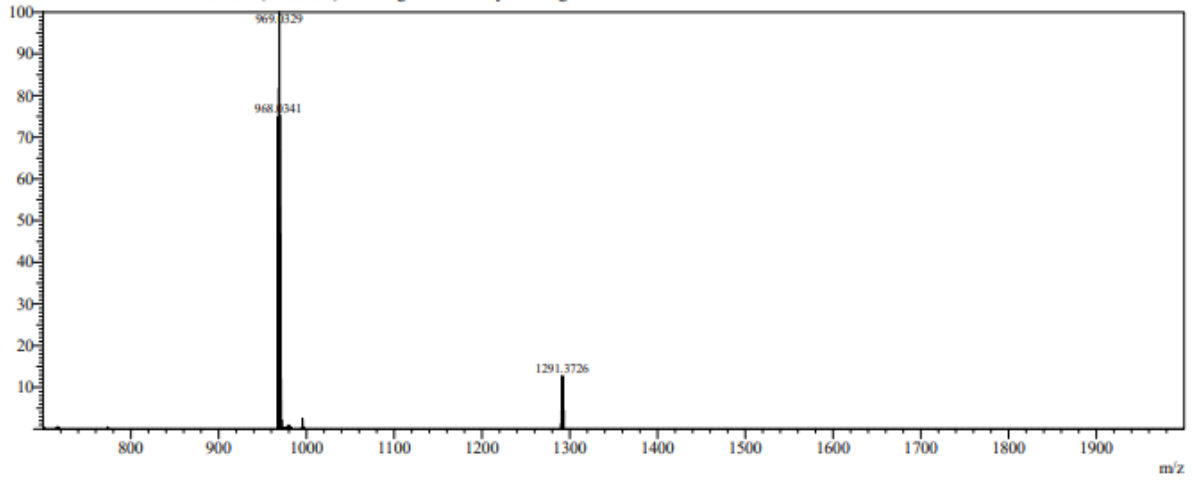
Compound 13



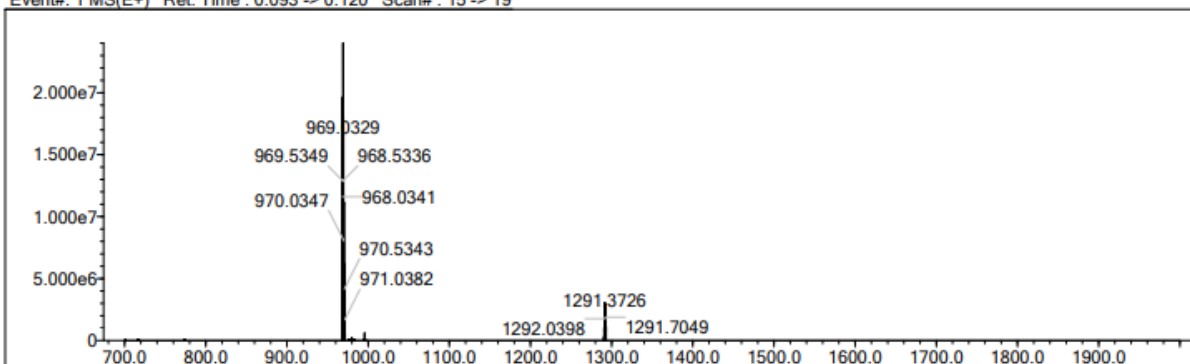
Compound 17



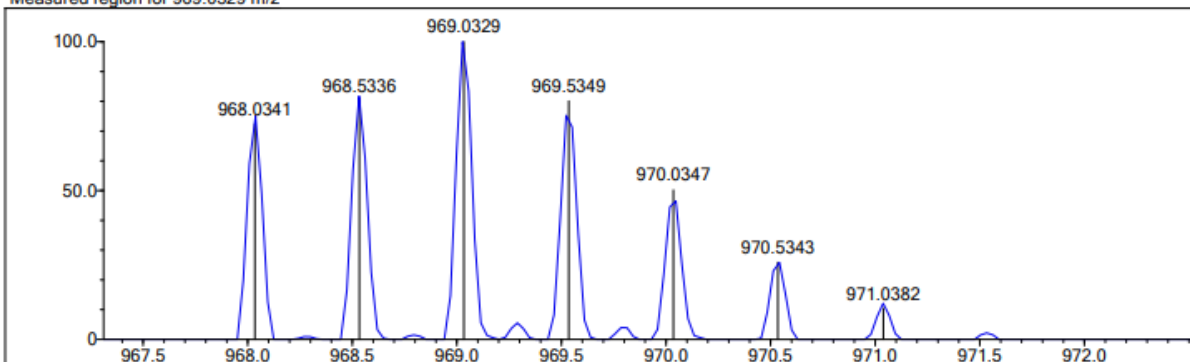
PCDA-vancomycin



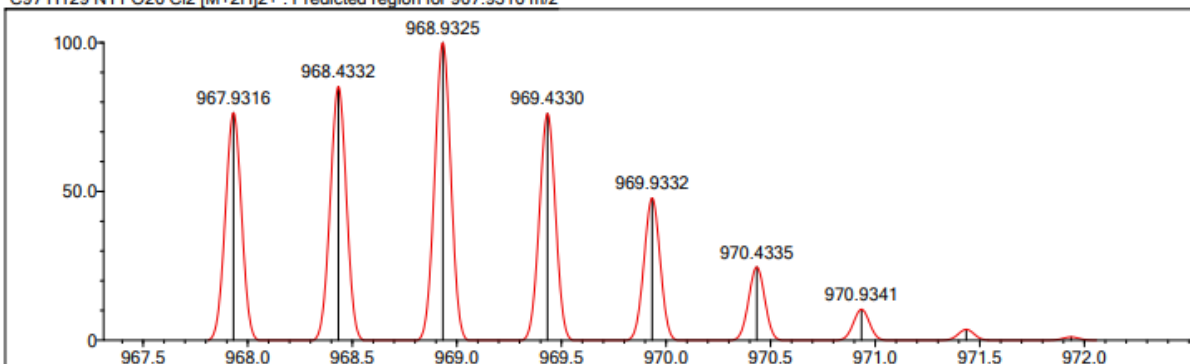
Event#: 1 MS(E+) Ret. Time : 0.093 -> 0.120 Scan#: 15 -> 19



Measured region for 969.0329 m/z



C97 H129 N11 O26 Cl2 [M+2H]2+ : Predicted region for 967.9316 m/z



References

- (1) Klausberger, M.; Leneva, I. A.; Egorov, A.; Strobl, F.; Ghorbanpour, S. M.; Falynskova, I. N.; Poddubikov, A. V.; Makhmudova, N. R.; Krokhin, A.; Svitich, O. A. Off-target effects of an insect cell-expressed influenza HA-pseudotyped Gag-VLP preparation in limiting postinfluenza *Staphylococcus aureus* infections. *Vaccine* **2020**, *38* (4), 859-867.
- (2) Tong, S. Y.; Davis, J. S.; Eichenberger, E.; Holland, T. L.; Fowler Jr, V. G. *Staphylococcus aureus* infections: epidemiology, pathophysiology, clinical manifestations, and management. *Clin. Microbiol. Rev.* **2015**, *28* (3), 603-661.
- (3) Manna, S.; Baindara, P.; Mandal, S. M. Molecular pathogenesis of secondary bacterial infection associated to viral infections including SARS-CoV-2. *J. Infect. Public Health.* **2020**, *13* (10), 1397-1404.
- (4) Miller, L. S.; Fowler Jr, V. G.; Shukla, S. K.; Rose, W. E.; Proctor, R. A. Development of a vaccine against *Staphylococcus aureus* invasive infections: Evidence based on human immunity, genetics and bacterial evasion mechanisms. *FEMS Microbiol. Rev.* **2020**, *44* (1), 123-153.
- (5) Farsimadan, M.; Motamedifar, M. Bacterial infection of the male reproductive system causing infertility. *J. Reprod. Immunol.* **2020**, *142*, 103183.
- (6) Haydar, S. O.; Naqid, I. A Study of Bacterial Vaginosis and Associated Risk Factors among Married Women in Zakho City, Kurdistan Region, Iraq. *J. Life Sci. Res.* **2022**, *3* (02), 33-39.
- (7) Duan, T. Analysis of Microbiological and Clinical Characteristics of Bacterial Infection

- in Patients with Pulmonary Infection. *Comput. Intell. Neurosci.* **2022**, 2022.
- (8) Cassandra, W. The drug-resistant bacteria that pose the greatest health threats. *Nature* **2017**, *543*, 15.
- (9) Kourtis, A. P.; Hatfield, K.; Baggs, J.; Mu, Y.; See, I.; Epton, E.; Nadle, J.; Kainer, M. A.; Dumyati, G.; Petit, S. Vital signs: epidemiology and recent trends in methicillin-resistant and in methicillin-susceptible *Staphylococcus aureus* bloodstream infections—United States. *Morb Mortal Wkly Rep.* **2019**, *68* (9), 214.
- (10) Rungelrath, V.; DeLeo, F. R. *Staphylococcus aureus*, antibiotic resistance, and the interaction with human neutrophils. *Antioxid Redox Signal.* **2021**, *34* (6), 452-470.
- (11) Hameed, S.; Xie, L.; Ying, Y. Conventional and emerging detection techniques for pathogenic bacteria in food science: A review. *Trends Food Sci Technol.* **2018**, *81*, 61-73.
- (12) Fournier, P.-E.; Dubourg, G.; Raoult, D. Clinical detection and characterization of bacterial pathogens in the genomics era. *Genome medicine* **2014**, *6* (11), 1-15.
- (13) Zhang, N.; Wang, L.; Deng, X.; Liang, R.; Su, M.; He, C.; Hu, L.; Su, Y.; Ren, J.; Yu, F. Recent advances in the detection of respiratory virus infection in humans. *J. Med. Virol.* **2020**, *92* (4), 408-417.
- (14) Berns, E.; Barrett, C.; Gardezi, M.; Spake, C.; Glasser, J.; Antoci, V.; Born, C. T.; Garcia, D. R. Current clinical methods for detection of peri-prosthetic joint infection. *Surg. Infect.* **2020**, *21* (8), 645-653.
- (15) Parekh, J. N.; Soni, P.; Meena, M. K.; Tandel, C. K.; Radhakrishanan, G. A New Device and Technology for Detecting Bacterial Infection and its Gram Type in Diabetic Foot Ulcer. *Indian J. Surg.* **2022**, 1-6.

- (16) Ji, E.-K.; Ahn, D.-J.; Kim, J.-M. The fluorescent polydiacetylene liposome. *Bull. Korean Chem. Soc.* **2003**, *24* (5), 667-670.
- (17) Baughman, R. Solid-state synthesis of large polymer single crystals. *J. Polym. Sci., Polym. Phys. Ed.* **1974**, *12* (8), 1511-1535.
- (18) Mino, N.; Tamura, H.; Ogawa, K. Photoreactivity of 10, 12-pentacosadiynoic acid monolayers and color transitions of the polymerized monolayers on an aqueous subphase. *Langmuir* **1992**, *8* (2), 594-598.
- (19) Spagnoli, S.; Briand, E.; Vickridge, I.; Fave, J.-L.; Schott, M. Method for determining the polymer content in nonsoluble polydiacetylene films: application to pentacosadiynoic acid. *Langmuir* **2017**, *33* (6), 1419-1426.
- (20) Wang, D.-E.; Gao, X.; You, S.; Chen, M.; Ren, L.; Sun, W.; Yang, H.; Xu, H. Aptamer-functionalized polydiacetylene liposomes act as a fluorescent sensor for sensitive detection of MUC1 and targeted imaging of cancer cells. *Sens. Actuators B Chem.* **2020**, *309*, 127778.
- (21) Shim, H. Y.; Lee, S. H.; Ahn, D. J.; Ahn, K.-D.; Kim, J.-M. Micropatterning of diacetylenic liposomes on glass surfaces. *Mater. Sci. Eng. C.* **2004**, *24* (1-2), 157-161.
- (22) Kim, C.; Lee, K. Polydiacetylene (PDA) liposome-based immunosensor for the detection of exosomes. *Biomacromolecules* **2019**, *20* (9), 3392-3398.
- (23) Tang, J.; Weston, M.; Kuchel, R. P.; Lisi, F.; Liang, K.; Chandrawati, R. Fabrication of polydiacetylene particles using a solvent injection method. *Mat. Adv.* **2020**, *1* (6), 1745-1752.
- (24) Bhattacharjee, A.; Sabino, R. M.; Gangwish, J.; Manivasagam, V. K.; James, S.;

- Popat, K. C.; Reynolds, M.; Li, Y. V. A novel colorimetric biosensor for detecting SARS-CoV-2 by utilizing the interaction between nucleocapsid antibody and spike proteins. *In vitro models* **2022**, 1-7.
- (25) Prainito, C. D.; Eshun, G.; Osonga, F. J.; Isika, D.; Centeno, C.; Sadik, O. A. Colorimetric Detection of the SARS-CoV-2 Virus (COVID-19) in Artificial Saliva Using Polydiacetylene Paper Strips. *Biosensors* **2022**, 12 (10), 804.
- (26) Hussain, S.; Deb, R.; Suklabaidya, S.; Bhattacharjee, D.; Hussain, S. A. Polydiacetylene a unique material to design biosensors. *Mater. Today: Proc.* **2022**.
- (27) Bhattacharjee, A.; Clark, R.; Gentry-Weeks, C.; Li, Y. V. A novel receptor-free polydiacetylene nanofiber biosensor for detecting E. coli via colorimetric changes. *Mat. Adv.* **2020**, 1 (9), 3387-3397.
- (28) Qian, X.; Städler, B. Polydiacetylene-Based Biosensors for the Detection of Viruses and Related Biomolecules. *Adv. Funct. Mater.* **2020**, 30 (49), 2004605.
- (29) Kim, C.; Hong, C.; Lee, K. Structures and strategies for enhanced sensitivity of polydiacetylene (PDA) based biosensor platforms. *Biosens. Bioelectron.* **2021**, 181, 113120.
- (30) Lebègue, E.; Farre, C.; Jose, C.; Saulnier, J.; Lagarde, F.; Chevalier, Y.; Chaix, C.; Jaffrezic-Renault, N. Responsive polydiacetylene vesicles for biosensing microorganisms. *Sensors* **2018**, 18 (2), 599.
- (31) Charych, D. H.; Nagy, J. O.; Spevak, W.; Bednarski, M. D. Direct colorimetric detection of a receptor-ligand interaction by a polymerized bilayer assembly. *Science* **1993**, 261 (5121), 585-588.
- (32) Zhou, J.; Duan, M.; Huang, D.; Shao, H.; Zhou, Y.; Fan, Y. Label-free visible

- colorimetric biosensor for detection of multiple pathogenic bacteria based on engineered polydiacetylene liposomes. *J. Colloid Interface Sci.* **2022**, *606*, 1684-1694.
- (33) Alam, A. M.; Yapor, J. P.; Reynolds, M. M.; Li, Y. V. Study of polydiacetylene-poly (ethylene oxide) electrospun fibers used as biosensors. *Materials* **2016**, *9* (3), 202.
- (34) de Oliveira, T. V.; de FF Soares, N.; de Andrade, N. J.; Silva, D. J.; Medeiros, E. A. A.; Badaró, A. T. Application of PCDA/SPH/CHO/Lysine vesicles to detect pathogenic bacteria in chicken. *Food chem.* **2015**, *172*, 428-432.
- (35) dos Santos Pires, A. C.; Soares, N. d. F. F.; da Silva, L. H. M.; da Silva, M. d. C. H.; De Almeida, M. V.; Le Hyaric, M.; de Andrade, N. J.; Soares, R. F.; Mageste, A. B.; Reis, S. G. A colorimetric biosensor for the detection of foodborne bacteria. *Sens. Actuators B Chem.* **2011**, *153* (1), 17-23.
- (36) Kim, K.-W.; Choi, H.; Lee, G. S.; Ahn, D. J.; Oh, M.-K. Effect of phospholipid insertion on arrayed polydiacetylene biosensors. *Colloids Surf B Biointerfaces.* **2008**, *66* (2), 213-217.
- (37) de Oliveira, T. V.; de FF Soares, N.; Silva, D. J.; de Andrade, N. J.; Medeiros, E. A. A.; Badaró, A. T. Development of PDA/Phospholipids/Lysine vesicles to detect pathogenic bacteria. *Sens. Actuators B Chem.* **2013**, *188*, 385-392.
- (38) Zhang, Y.; Dawson, P. L.; Hanks, T. W.; Northcutt, J. K.; Tzeng, T.-R.; Pennington, W. T. Detecting and correlating bacterial populations to visual color change of polydiacetylene-coated filters. *Talanta* **2021**, *221*, 121482.
- (39) Jung, Y. K.; Park, H. G.; Kim, J.-M. Polydiacetylene (PDA)-based colorimetric

- detection of biotin–streptavidin interactions. *Biosensors and Bioelectronics* **2006**, *21* (8), 1536-1544.
- (40) Hansen, L.; Sørensen, S. The use of whole-cell biosensors to detect and quantify compounds or conditions affecting biological systems. *Microb. Ecol.* **2001**, *42* (4), 483-494.
- (41) Sørensen, S. J.; Burmølle, M.; Hansen, L. H. Making bio-sense of toxicity: new developments in whole-cell biosensors. *Curr. Opin. Biotechnol.* **2006**, *17* (1), 11-16.
- (42) Levine, D. P. Vancomycin: a history. *Clin. Infect. Dis.* **2006**, *42* (Supplement_1), S5-S12.
- (43) Marsot, A.; Boulamery, A.; Bruguerolle, B.; Simon, N. Vancomycin. *Clin. Pharmacokinet.* **2012**, *51* (1), 1-13.
- (44) Schäfer, M.; Schneider, T. R.; Sheldrick, G. M. Crystal structure of vancomycin. *Structure* **1996**, *4* (12), 1509-1515.
- (45) Goldman, R. C.; Baizman, E. R.; Longley, C. B.; Branstrom, A. A. Chlorobiphenyl-desleucyl-vancomycin inhibits the transglycosylation process required for peptidoglycan synthesis in bacteria in the absence of dipeptide binding. *FEMS Microbiol. Lett.* **2000**, *183* (2), 209-214.
- (46) Song, S.; Ha, K.; Guk, K.; Hwang, S.-G.; Choi, J. M.; Kang, T.; Bae, P.; Jung, J.; Lim, E.-K. Colorimetric detection of influenza A (H1N1) virus by a peptide-functionalized polydiacetylene (PEP-PDA) nanosensor. *RSC Adv.* **2016**, *6* (54), 48566-48570.
- (47) Jung, Y. K.; Park, H. G. Colorimetric polydiacetylene (PDA) liposome-based assay

- for rapid and simple detection of GST-fusion protein. *Sens. Actuators B Chem.* **2019**, 278, 190-195.
- (48) Mishra, N. M.; Briers, Y.; Lamberigts, C.; Steenackers, H.; Robijns, S.; Landuyt, B.; Vanderleyden, J.; Schoofs, L.; Lavigne, R.; Luyten, W. Evaluation of the antibacterial and antibiofilm activities of novel CRAMP–vancomycin conjugates with diverse linkers. *Org. Biomol. Chem.* **2015**, 13 (27), 7477-7486.
- (49) Jeong, J. P.; Cho, E.; Lee, S. C.; Kim, T.; Song, B.; Lee, I. S.; Jung, S. Detection of Foot-and-Mouth Disease Virus Using a Polydiacetylene Immunosensor on Solid-Liquid Phase. *Macromol. Mater. Eng.* **2018**, 303 (6), 1700640.
- (50) Jannah, F.; Kim, J.-H.; Lee, J.-W.; Kim, J.-M.; Kim, J.-M.; Lee, H. Immobilized polydiacetylene lipid vesicles on polydimethylsiloxane micropillars as a surfactin-based label-free bacterial sensor platform. *Front. Mater. Sci.* **2018**, 5, 57.
- (51) Trachtenberg, A.; Malka, O.; Kootery, K. P.; Beglaryan, S.; Malferrari, D.; Galletti, P.; Prati, S.; Mazzeo, R.; Tagliavini, E.; Jelinek, R. Colorimetric analysis of painting materials using polymer-supported polydiacetylene films. *New J. Chem.* **2016**, 40 (11), 9054-9059.
- (52) Kim, H.; Afsari, H. S.; Cho, W. High-throughput fluorescence assay for membrane-protein interaction. *J. Lipid Res.* **2013**, 54 (12), 3531-3538.
- (53) Diegelmann, S. R.; Hartman, N.; Markovic, N.; Tovar, J. D. Synthesis and alignment of discrete polydiacetylene-peptide nanostructures. *J. Am. Chem. Soc.* **2012**, 134 (4), 2028-2031.
- (54) Hsu, L.; Cvetanovich, G. L.; Stupp, S. I. Peptide amphiphile nanofibers with

- conjugated polydiacetylene backbones in their core. *J. Am. Chem. Soc.* **2008**, *130* (12), 3892-3899.
- (55) Fang, F.; Meng, F.; Luo, L. Recent advances on polydiacetylene-based smart materials for biomedical applications. *Mater. Chem. Front.* **2020**, *4* (4), 1089-1104.
- (56) van den Heuvel, M.; Löwik, D. W.; van Hest, J. C. Effect of the diacetylene position on the chromatic properties of polydiacetylenes from self-assembled peptide amphiphiles. *Biomacromolecules* **2010**, *11* (6), 1676-1683.
- (57) Ramakers, B. E.; van den Heuvel, M.; Tsihchlis i Spithas, N.; Brinkhuis, R. P.; van Hest, J. C.; Löwik, D. W. Polymerization-induced color changes of polydiacetylene-containing liposomes and peptide amphiphile fibers. *Langmuir* **2012**, *28* (4), 2049-2055.
- (58) Kim, T. H.; Lee, B. Y.; Jaworski, J.; Yokoyama, K.; Chung, W.-J.; Wang, E.; Hong, S.; Majumdar, A.; Lee, S.-W. Selective and sensitive TNT sensors using biomimetic polydiacetylene-coated CNT-FETs. *ACS nano* **2011**, *5* (4), 2824-2830.
- (59) Jaworski, J.; Yokoyama, K.; Zueger, C.; Chung, W.-J.; Lee, S.-W.; Majumdar, A. Polydiacetylene incorporated with peptide receptors for the detection of trinitrotoluene explosives. *Langmuir* **2011**, *27* (6), 3180-3187.
- (60) de Samaniego, M. S. S.; Miller, A. F. Two-dimensional polymerization of a polydiacetylene functionalized amphiphilic peptide at the air–water interface. *Colloids Surf. A Physicochem. Eng. Asp.* **2008**, *321* (1-3), 271-274.
- (61) Lv, N.; Yin, X.; Yang, Z.; Ma, T.; Qin, H.; Xiong, B.; Jiang, H.; Zhu, J. Electrostatically Controlled ex Situ and in Situ Polymerization of Diacetylene-Containing Peptide Amphiphiles in Living Cells. *Macro Lett.* **2022**, *11* (2), 223-229.

- (62) Wu, J.; Zawistowski, A.; Ehrmann, M.; Yi, T.; Schmuck, C. Peptide functionalized polydiacetylene liposomes act as a fluorescent turn-on sensor for bacterial lipopolysaccharide. *J. Am. Chem. Soc.* **2011**, *133* (25), 9720-9723.
- (63) Ramenskaya, G.; Shikh, E.; Arzamastsev, A.; Kukes, V. Molecular-biological problems of drug design and mechanism of drug action-Pharmacokinetic study of the new domestic hypodermic form of naltrexone: Prodetoxon depot tablets. *Pharm. Chem. J.* **2005**, *39* (1), 1-3.
- (64) Alharthi, S.; Alavi, S. E.; Moyle, P. M.; Ziora, Z. M. Sortase A (SrtA) inhibitors as an alternative treatment for superbug infections. *Drug Discov. Today* **2021**, *26* (9), 2164-2172.
- (65) Hou, X.; Wang, M.; Wen, Y.; Ni, T.; Guan, X.; Lan, L.; Zhang, N.; Zhang, A.; Yang, C.-G. Quinone skeleton as a new class of irreversible inhibitors against *Staphylococcus aureus* sortase A. *Bioorg. Med. Chem. Lett.* **2018**, *28* (10), 1864-1869.
- (66) Jaudzems, K.; Kurbatska, V.; Jēkabsons, A.; Bobrovs, R.; Rudevica, Z.; Leonchiks, A. Targeting bacterial Sortase A with covalent inhibitors: 27 new starting points for structure-based hit-to-lead optimization. *ACS Infect. Dis.* **2019**, *6* (2), 186-194.
- (67) Wang, J.; Li, H.; Pan, J.; Dong, J.; Zhou, X.; Niu, X.; Deng, X. Oligopeptide targeting sortase a as potential anti-infective therapy for *Staphylococcus aureus*. *Front. Microbiol.* **2018**, *9*, 245.
- (68) Zhang, L.; Yuan, Y.-Z.; Tian, X.-H.; Sun, J.-Y. A thermally reversible supramolecular system based on biphenyl polydiacetylene. *Chin. Chem. Lett.* **2015**, *26* (9), 1133-1136.

- (69) Tovar, J. D. Supramolecular construction of optoelectronic biomaterials. *Acc. Chem. Res.* **2013**, *46* (7), 1527-1537.
- (70) Kuo, Y.-L.; Tseng, C.-Y.; Tseng, C.-W.; Chu, K.-T.; Liu, Y.-C.; Chiang, M.-H.; Saeki, A.; Tao, Y.-T.; Chen, H.-H. Polymerization of columnar mesogens tethered with diacetylenic side chains. *ACS Appl. Polym. Mater.* **2019**, *2* (2), 248-255.
- (71) Maurya, G. P.; Verma, D.; Sinha, A.; Brunsveld, L.; Haridas, V. Hydrophobicity Directed Chiral Self-Assembly and Aggregation-Induced Emission: Diacetylene-Cored Pseudopeptide Chiral Dopants. *Angew. Chem., Int. Ed. Engl.* **2022**, *61* (42), e202209806.
- (72) Arakawa, Y.; Nakajima, S.; Kang, S.; Konishi, G.-i.; Watanabe, J. Synthesis and evaluation of high-birefringence polymethacrylate having a diphenyl-diacetylene LC moiety in the side chain. *J. Mater. Chem.* **2012**, *22* (29), 14346-14348.
- (73) Néabo, J. R. o.; Tohondjona, K. s. I. S.; Morin, J.-F. Topochemical polymerization of a diarylbutadiyne derivative in the gel and solid states. *Org. Lett.* **2011**, *13* (6), 1358-1361.
- (74) Sarkar, A.; Okada, S.; Matsuzawa, H.; Matsuda, H.; Nakanishi, H. Novel polydiacetylenes for optical materials: beyond the conventional polydiacetylenes. *J. Mater. Chem.* **2000**, *10* (4), 819-828.
- (75) Matsuo, H.; Okada, S.; Nakanishi, H.; Matsuda, H.; Takaragi, S. Solid-state polymerization of monomers possessing two diphenylbutadiyne moieties with amido groups to form ladder polymers. *Polym. J.* **2002**, *34* (11), 825-834.
- (76) Chan, Y.-H.; Lin, J.-T. s.; Chen, I.-W. P.; Chen, C.-h. Monolayers of

- diphenyldiacetylene derivatives: Tuning molecular tilt angles and photopolymerization efficiency via electrodeposited Ag interlayer on Au. *J. Phys. Chem. B.* **2005**, *109* (41), 19161-19168.
- (77) Gong, Y.; Liu, J. Sequential Sonogashira and Glaser coupling reactions: facile access to 1, 4-disubstituted 1, 3-butadiynes from arylbromide. *Tetrahedron Lett.* **2016**, *57* (20), 2143-2146.
- (78) Stewart, L.; Lu, W.; Wei, Z.-W.; Ila, D.; Padilla, C.; Zhou, H.-C. A zirconium metal–organic framework with an exceptionally high volumetric surface area. *Dalton Trans.* **2017**, *46* (41), 14270-14276.
- (79) Chen, W. Self-assembling Peptides: From Fundamental Design to Therapeutic Applications. The University of Texas at Arlington, 2022.
- (80) Bassioni, G. A study towards “greener” construction. *Appl. Energy* **2012**, *93*, 132-137.
- (81) Environment, E. C. D. G. f. Guidance Document for EPER Implementation. 2000.
- (82) Sivakrishna, A.; Adesina, A.; Awoyera, P.; Kumar, K. R. Green concrete: A review of recent developments. *Mater. Today: Proceedings* **2020**, *27*, 54-58.
- (83) Survey, G. *Mineral Commodity Summaries: 2012*; Government Printing Office, 2012.
- (84) Müller, N.; Harnisch, J. A blueprint for a climate friendly cement industry. *Gland: WWF Lafarge conservation partnership* **2008**.
- (85) Imbabi, M. S.; Carrigan, C.; McKenna, S. Trends and developments in green cement and concrete technology. *Int. J. Sustain. Built Environ.* **2012**, *1* (2), 194-216.
- (86) Combes, C.; Miao, B.; Bareille, R.; Rey, C. Preparation, physical–chemical

- characterisation and cytocompatibility of calcium carbonate cements. *Biomaterials* **2006**, 27 (9), 1945-1954.
- (87) Constantz, B. R.; Ison, I. C.; Fulmer, M. T.; Poser, R. D.; Smith, S. T.; VanWagoner, M.; Ross, J.; Goldstein, S. A.; Jupiter, J. B.; Rosenthal, D. I. Skeletal repair by in situ formation of the mineral phase of bone. *Science* **1995**, 267 (5205), 1796-1799.
- (88) Khairoun, I.; Boltong, M.; Driessens, F.; Planell, J. Effect of calcium carbonate on the compliance of an apatitic calcium phosphate bone cement. *Biomaterials* **1997**, 18 (23), 1535-1539.
- (89) Brečević, L.; Nielsen, A. E. Solubility of amorphous calcium carbonate. *J. Cryst. Growth* **1989**, 98 (3), 504-510.
- (90) Burton, W.-K.; Cabrera, N.; Frank, F. The growth of crystals and the equilibrium structure of their surfaces. *Philos. Trans. A Math. Phys. Eng. Sci.* **1951**, 243 (866), 299-358.
- (91) Faatz, M.; Gröhn, F.; Wegner, G. Amorphous calcium carbonate: synthesis and potential intermediate in biomineralization. *Adv. Mater.* **2004**, 16 (12), 996-1000.
- (92) Wang, S. S.; Picker, A.; Cölfen, H.; Xu, A. W. Heterostructured calcium carbonate microspheres with calcite equatorial loops and vaterite spherical cores. *Angew. Chem., Int. Ed. Engl.* **2013**, 52 (24), 6317-6321.
- (93) Kurland, R. J. Binding of Ca²⁺ and Mg²⁺ to phosphatidylserine vesicles: Different effects on P-31 NMR shifts and relaxation times. *Biochem. Biophys. Res. Commun.* **1979**, 88 (3), 927-932.
- (94) Zou, Z.; Bertinetti, L.; Politi, Y.; Fratzl, P.; Habraken, W. J. Control of polymorph

- selection in amorphous calcium carbonate crystallization by poly (aspartic acid):
Two different mechanisms. *Small* **2017**, *13* (21), 1603100.
- (95) Huang, Z.; Zhang, G. Biomimetic synthesis of aragonite nanorod aggregates with unusual morphologies using a novel template of natural fibrous proteins at ambient condition. *Cryst. Growth Des.* **2012**, *12* (4), 1816-1822.
- (96) Politi, Y.; Mahamid, J.; Goldberg, H.; Weiner, S.; Addadi, L. Asprich mollusk shell protein: in vitro experiments aimed at elucidating function in CaCO₃ crystallization. *CrystEngComm* **2007**, *9* (12), 1171-1177.
- (97) Weiner, S. Aspartic acid-rich proteins: major components of the soluble organic matrix of mollusk shells. *Calcif. Tissue Int.* **1979**, *29* (1), 163-167.
- (98) Tsukamoto, D.; Sarashina, I.; Endo, K. Structure and expression of an unusually acidic matrix protein of pearl oyster shells. *Biochem. Biophys. Res. Commun.* **2004**, *320* (4), 1175-1180.
- (99) Veis, A.; Perry, A. The phosphoprotein of the dentin matrix. *Biochemistry* **1967**, *6* (8), 2409-2416.
- (100) Marin, F.; Amons, R.; Guichard, N.; Stigter, M.; Hecker, A.; Luquet, G.; Layrolle, P.; Alcaraz, G.; Riondet, C.; Westbroek, P. Caspartin and calprismismin, two proteins of the shell calcitic prisms of the Mediterranean fan mussel *Pinna nobilis*. *J. Biol. Chem.* **2005**, *280* (40), 33895-33908.
- (101) Addadi, L.; Joester, D.; Nudelman, F.; Weiner, S. Mollusk shell formation: a source of new concepts for understanding biomineralization processes. *Eur. J. Chem.* **2006**, *12* (4), 980-987.
- (102) Tambutté, S.; Holcomb, M.; Ferrier-Pagès, C.; Reynaud, S.; Tambutté, É.; Zoccola,

- D.; Allemand, D. Coral biomineralization: From the gene to the environment. *J. Exp. Mar. Biol. Ecol.* **2011**, *408* (1-2), 58-78.
- (103) Tong, H.; Ma, W.; Wang, L.; Wan, P.; Hu, J.; Cao, L. Control over the crystal phase, shape, size and aggregation of calcium carbonate via a L-aspartic acid inducing process. *Biomaterials* **2004**, *25* (17), 3923-3929.
- (104) Tobler, D.; Blanco, J. R.; Dideriksen, K.; Sand, K.; Bovet, N.; Benning, L. G.; Stipp, S. The effect of aspartic acid and glycine on amorphous calcium carbonate (ACC) structure, stability and crystallization. *Procedia Environ. Sci.* **2014**, *10*, 143-148.
- (105) Clarkson, J. R.; Price, T. J.; Adams, C. J. Role of metastable phases in the spontaneous precipitation of calcium carbonate. *J. Chem. Soc., Faraday trans.* **1992**, *88* (2), 243-249.
- (106) Sawada, K. The mechanisms of crystallization and transformation of calcium carbonates. *Pure Appl. Chem.* **1997**, *69* (5), 921-928.
- (107) Xu, A. W.; Yu, Q.; Dong, W. F.; Antonietti, M.; Cölfen, H. Stable amorphous CaCO₃ microparticles with hollow spherical superstructures stabilized by phytic acid. *Adv. Mater.* **2005**, *17* (18), 2217-2221.
- (108) Muñoz, J. A.; Valiente, M. Determination of phytic acid in urine by inductively coupled plasma mass spectrometry. *Anal. Chem.* **2003**, *75* (22), 6374-6378.
- (109) Leadbetter, M. R.; Brown, R. W.; McKenna, M. M. Process for the preparation of tetraethyl methylenebisphosphonate. Google Patents: 1997.
- (110) Zhao, Y.; Truhlar, D. G. The M06 suite of density functionals for main group thermochemistry, thermochemical kinetics, noncovalent interactions, excited states, and transition elements: two new functionals and systematic testing of four

- M06-class functionals and 12 other functionals. *Theor. Chem. Acc.* **2008**, *120* (1), 215-241.
- (111) Frisch, M.; Trucks, G.; Schlegel, H. Gaussian 09, Revision A. 02. Wallingford, CT: Gaussian, Inc.; 2009. *Google Scholar*.
- (112) Lambrakos, S. G.; Huang, L.; Massa, L.; Shabaev, A. *Calculation of IR Spectra Using Density Functional Theory for Nerve-Agent-Sorbent Binding*; NAVAL RESEARCH LAB WASHINGTON DC WASHINGTON United States, 2019.
- (113) Hall, R. J.; Davidson, M. M.; Burton, N. A.; Hillier, I. H. Combined density functional, self-consistent reaction field model of solvation. *J. Phys. Chem.* **1995**, *99* (3), 921-924.
- (114) Liu, T.; Romanova, S.; Wang, S.; Hyun, M. A.; Zhang, C.; Cohen, S. M.; Singh, R. K.; Bronich, T. K. Alendronate-modified polymeric micelles for the treatment of breast cancer bone metastasis. *Mol. Pharm.* **2019**, *16* (7), 2872-2883.
- (115) Demadis, K. D.; Katarachia, S. D. Metal-phosphonate chemistry: synthesis, crystal structure of calcium-amino tris-(methylene phosphonate) and inhibition of CaCO₃ *Phosphorus Sulfur Silicon Relat. Elem.* **2004**, *179* (3), 627-648.
- (116) Kim, J.-M.; Lee, J.-S.; Choi, H.; Sohn, D.; Ahn, D. J. Rational design and in-situ FTIR analyses of colorimetrically reversible polydiacetylene supramolecules. *Macromolecules* **2005**, *38* (22), 9366-9376.
- (117) Phonchai, N.; Khanantong, C.; Kielar, F.; Traiphol, R.; Traiphol, N. Enhancing thermal and chemical sensitivity of polydiacetylene colorimetric sensors: The opposite effect of zinc oxide nanoparticles. *Colloids Surf. A Physicochem. Eng. Asp.* **2020**, *589*, 124459.

- (118) Yuan, Z.; Hanks, T. W. A reversible colorimetric and fluorescent polydiacetylene vesicle sensor platform. *Polymer* **2008**, *49* (23), 5023-5026.
- (119) Dong, W.; Lin, G.; Wang, H.; Lu, W. New dendritic polydiacetylene sensor with good reversible thermochromic ability in aqueous solution and solid film. *ACS Appl. Mater. Interfaces* **2017**, *9* (13), 11918-11923.
- (120) Sun, X.; Chen, T.; Huang, S.; Li, L.; Peng, H. Chromatic polydiacetylene with novel sensitivity. *Chem. Soc. Rev.* **2010**, *39* (11), 4244-4257.
- (121) Chen, X.; Yoon, J. A thermally reversible temperature sensor based on polydiacetylene: Synthesis and thermochromic properties. *Dyes Pigm.* **2011**, *89* (3), 194-198.
- (122) Qian, X.; Städler, B. Recent developments in polydiacetylene-based sensors. *Chem. Mater.* **2019**, *31* (4), 1196-1222.
- (123) Yun, D.; Jeong, D.; Cho, E.; Jung, S. Colorimetric detection of some highly hydrophobic flavonoids using polydiacetylene liposomes containing pentacosyl-10, 12-diylnoyl succinoglycan monomers. *Plos One* **2015**, *10* (11), e0143454.
- (124) David Nelson, A.; Shiveshwarkar, P.; Lim, B.; Rojas, G.; Abure, I.; Shrestha, A.; Jaworski, J. Tuning the Surface Charge of Self-Assembled Polydiacetylene Vesicles to Control Aggregation and Cell Binding. *Biosensors* **2020**, *10* (10), 132.
- (125) Bolchi, C.; Bavo, F.; Pallavicini, M. One-step preparation of enantiopure l-or d-amino acid benzyl esters avoiding the use of banned solvents. *J. Amino Acids* **2017**, *49* (5), 965-974.
- (126) Kieboom, A.; De Kreuk, J.; Van Bekkum, H. Substituent effects in the

- hydrogenolysis of benzyl alcohol derivatives over palladium. *J. Catal.* **1971**, *20* (1), 58-66.
- (127) Houghton, T. J.; Tanaka, K. S. E.; Kang, T.; Dietrich, E.; Lafontaine, Y.; Delorme, D.; Ferreira, S. S.; Viens, F.; Arhin, F. F.; Sarmiento, I.; et al. Linking Bisphosphonates to the Free Amino Groups in Fluoroquinolones: Preparation of Osteotropic Prodrugs for the Prevention of Osteomyelitis. *J. Med. Chem.* **2008**, research-article. DOI: 10.1021/jm801007z.
- (128) Keniche, A.; Mezrai, A.; Mulengi, J. K. Synthesis of a Novel Class of Phosphonoaziridines as Interesting Antibacterial Agents. *Open Conf. Proc J.* **2011**, *2* (1).
- (129) Álvarez, C.; Pérez, M.; Zúñiga, A.; Gómez, G.; Fall, Y. Synthesis of enantiomerically pure 2, 5-disubstituted 3-oxygenated tetrahydrofurans. *Synthesis* **2010**, *2010* (22), 3883-3890.
- (130) Chen, C.; Li, Y.; Yu, X.; Jiang, Q.; Xu, X.; Yang, Q.; Qian, Z. Bone-targeting melphalan prodrug with tumor-microenvironment sensitivity: Synthesis, in vitro and in vivo evaluation. *Chin. Chem. Lett.* **2018**, *29* (11), 1609-1612.
- (131) Chen, W.; Hazoor, S.; Madigan, R.; Adones, A. A.; Chintapula, U. K.; Nguyen, K. T.; Tang, L.; Foss Jr, F. W.; Dong, H. Alkaline-responsive polydiacetylene-peptide hydrogel for pH-sensing and on-demand antimicrobial release. *Mater. Today Adv.* **2022**, *16*, 100288.

(132) Urbina, F.; Zorn, K. M.; Brunner, D.; Ekins, S. Comparing the Pfizer Central Nervous System Multiparameter Optimization Calculator and a BBB Machine Learning Model. *ACS Chem. Neurosci.* **2021**, *12* (12), 2247-2253.

Biographical Information

Shan Hazoor was born in Lahore, Pakistan. It is second largest city of Pakistan and is considered 14th most populated city in the world with population about 11.13 million. In 2015, he graduated with BS (hons) in chemistry from Forman Christian College University (FCCU) Lahore. In 2017, he moved to University of Texas at Arlington (UTA), where he finished his Master's (MS) in organic chemistry in 2019 under Dr. Foss's supervision. In 2019, he started his Ph.D. program at UTA in organic chemistry in the same lab. The focus of his graduate research was synthesis of biosensing and biomimetic molecules to detect infective species and for calcium carbonate precipitation respectively.